

Advances

in Clinical and Experimental Medicine

MONTHLY ISSN 1899-5276 (PRINT) ISSN 2451-2680 (ONLINE)

www.advances.umed.wroc.pl

2021, Vol. 30, No. 7 (July)

Impact Factor (IF) – 1.727
Ministry of Science and Higher Education – 40 pts.
Index Copernicus (ICV) – 152.95 pts



WROCLAW
MEDICAL UNIVERSITY

Advances
in Clinical and Experimental
Medicine



Advances in Clinical and Experimental Medicine

ISSN 1899-5276 (PRINT)

ISSN 2451-2680 (ONLINE)

www.advances.umed.wroc.pl

MONTHLY 2021
Vol. 30, No. 7
(July)

Advances in Clinical and Experimental Medicine (*Adv Clin Exp Med*) publishes high quality original articles, research-in-progress, research letters and systematic reviews and meta-analyses of recognized scientists that deal with all clinical and experimental medicine.

Editorial Office

ul. Marcinkowskiego 2–6
50-368 Wrocław, Poland
Tel.: +48 71 784 11 36
E-mail: redakcja@umed.wroc.pl

Publisher

Wrocław Medical University
Wybrzeże L. Pasteura 1
50-367 Wrocław, Poland

© Copyright by Wrocław Medical University,
Wrocław 2021

Online edition is the original version
of the journal

Editor-in-Chief

Prof. Donata Kurpas

Deputy Editor

Prof. Wojciech Kosmala

Managing Editor

Paulina Piątkowska

Scientific Committee

Prof. Sabine Bährer-Kohler
Prof. Antonio Cano
Prof. Breno Diniz
Prof. Erwan Donal
Prof. Chris Fox
Prof. Naomi Hachiya
Prof. Carol Holland
Prof. Markku Kurkinen
Prof. Christos Lionis

Section Editors

Basic Sciences

Dr. Anna Lebedeva
Dr. Mateusz Olbromski
Dr. Maciej Sobczyński

Biochemistry

Prof. Małgorzata Krzystek-Korpacka

Clinical Anatomy, Legal Medicine,

Innovative Technologies

Prof. Rafael Boscolo-Berto

Dentistry

Prof. Marzena Dominiak
Prof. Tomasz Gedrange
Prof. Jamil Shibli

Statistical Editors

Wojciech Bombała, MSc
Katarzyna Giniewicz, MSc Eng.
Anna Kopszak, MSc
Dr. Krzysztof Kujawa

Manuscript editing

Marek Misiak, Paulina Piątkowska

Prof. Raimundo Mateos

Prof. Zbigniew W. Ras
Prof. Jerzy W. Rozenblit
Prof. Silvina Santana
Prof. James Sharman
Prof. Jamil Shibli
Prof. Michal Toborek
Prof. László Vécsei
Prof. Cristiana Vitale

Dermatology

Prof. Jacek Szepietowski

Emergency Medicine, Innovative Technologies

Prof. Jacek Smereka

Gynecology and Obstetrics

Prof. Olimpia Sipak-Szmigiel

Histology and Embryology

Prof. Marzena Podhorska-Okolów

Internal Medicine

Angiology

Dr. Angelika Chachaj

Cardiology

Prof. Wojciech Kosmala
Dr. Daniel Morris

Endocrinology

Prof. Marek Bolanowski

Gastroenterology

Assoc. Prof. Katarzyna Neubauer

Hematology

Prof. Dariusz Wołowicz

Nephrology and Transplantology

Assoc. Prof. Dorota Kamińska

Assoc. Prof. Krzysztof Letachowicz

Pulmonology

Prof. Elżbieta Radzikowska

Microbiology

Prof. Marzenna Bartoszewicz

Assoc. Prof. Adam Junka

Molecular Biology

Dr. Monika Bielecka

Prof. Jolanta Saczko

Dr. Marta Sochocka

Neurology

Assoc. Prof. Magdalena Koszewicz

Assoc. Prof. Anna Pokryszko-Dragan

Dr. Masaru Tanaka

Oncology

Dr. Marcin Jędryka

Prof. Lucyna Kępka

Gynecological Oncology

Dr. Marcin Jędryka

Ophthalmology

Prof. Marta Misiuk-Hojło

Orthopedics

Prof. Paweł Reichert

Otolaryngology

Assoc. Prof. Tomasz Zatoński

Pediatrics

Pediatrics, Metabolic Pediatrics, Clinical Genetics, Neonatology, Rare Disorders

Prof. Robert Śmigiel

Pediatric Nephrology

Prof. Katarzyna Kiliś-Pstrusińska

Pediatric Oncology and Hematology

Assoc. Prof. Marek Ussowicz

Pharmaceutical Sciences

Assoc. Prof. Maria Kepinska

Prof. Adam Matkowski

Pharmacoeconomics, Rheumatology

Dr. Sylwia Szafraniec-Buryło

Psychiatry

Prof. Istvan Boksay

Prof. Jerzy Leszek

Public Health

Prof. Monika Sawhney

Prof. Izabella Uchmanowicz

Qualitative Studies, Quality of Care

Prof. Ludmiła Marcinowicz

Rehabilitation

Prof. Jakub Taradaj

Surgery

Assoc. Prof. Mariusz Chabowski

Prof. Renata Taboła

Telemedicine, Geriatrics, Multimorbidity

Assoc. Prof. Maria Magdalena

Bujnowska-Fedak

Editorial Policy

Advances in Clinical and Experimental Medicine (Adv Clin Exp Med) is an independent multidisciplinary forum for exchange of scientific and clinical information, publishing original research and news encompassing all aspects of medicine, including molecular biology, biochemistry, genetics, biotechnology and other areas. During the review process, the Editorial Board conforms to the "Uniform Requirements for Manuscripts Submitted to Biomedical Journals: Writing and Editing for Biomedical Publication" approved by the International Committee of Medical Journal Editors (www.ICMJE.org/). The journal publishes (in English only) original papers and reviews. Short works considered original, novel and significant are given priority. Experimental studies must include a statement that the experimental protocol and informed consent procedure were in compliance with the Helsinki Convention and were approved by an ethics committee.

For all subscription-related queries please contact our Editorial Office:

redakcja@umed.wroc.pl

For more information visit the journal's website:

www.advances.umed.wroc.pl

Pursuant to the ordinance No. 134/XV R/2017 of the Rector of Wrocław Medical University (as of December 28, 2017) from January 1, 2018 authors are required to pay a fee amounting to 700 euros for each manuscript accepted for publication in the journal Advances in Clinical and Experimental Medicine.

Indexed in: MEDLINE, Science Citation Index Expanded, Journal Citation Reports/Science Edition, Scopus, EMBASE/Excerpta Medica, Ulrich's™ International Periodicals Directory, Index Copernicus

Typographic design: Piotr Gil, Monika Kołęda

DTP: Wydawnictwo UMW

Cover: Monika Kołęda

Printing and binding: Soft Vision Mariusz Rajski

Contents

Editorials

- 653 Markku Kurkinen
Alzheimer's trials: A cul-de-sac with no end in sight

Original papers

- 655 Martin Floer, Mareike Clausen, Tobias Meister, Richard Vollenberg, Dominik Bettenworth, Phil-Robin Tepas
Soluble syndecan-1 as marker of intestinal inflammation: A preliminary study and evaluation of a new panel of biomarkers for non-invasive prediction of active ulcerative colitis
- 661 Li Tong, Jinglin Cheng, Heping Zuo, Jingrong Li
MicroRNA-197 promotes proliferation and inhibits apoptosis of gallbladder cancer cells by targeting insulin-like growth factor-binding protein 3
- 673 Yi Qiao, Jie Chen
Investigating the inflammatory cascade effect of basophil activation in children with allergic rhinitis or asthma, via the IgE-FcεRI-NF-κB signaling pathway
- 681 Beata Wyrębek, Renata Górka, Katarzyna Gawron, Małgorzata Nędzi-Góra, Bartłomiej Górski, Paweł Plakwicz
Periodontal condition of mandibular incisors treated with modified Kazanjian vestibuloplasty compared to untreated sites: A prospective study
- 691 Yongbo Wang, Yue Wang, Chunna Ren, Haicun Wang, Yang Zhang, Yunxia Xiu
Upregulation of centromere protein K is crucial for lung adenocarcinoma cell viability and invasion
- 701 Zijun Zhao, Li Ma, Yishuai Li, Qi Zhang, Ying Wang, Yanlei Tai, Qiujuan Wang
MiR-124 protects against cognitive dysfunction induced by sevoflurane anesthesia in vivo and in vitro through targeting calpain small subunit 1 via NF-κB signaling pathway
- 711 Weiting Chen, Zhongen Shen, Shuiqi Cai, Long Chen, Dabin Wang
FGF21 promotes wound healing of rat brain microvascular endothelial cells through facilitating TNF-α-mediated VEGFA and ERK1/2 signaling pathway
- 721 Xiaojie Li, Dapeng Liao, Gang Sun, HanWen Chu
Notch pathway activation promotes the differentiation of beagle dog periodontal ligament stem cells to Schwann cells
- 727 Hongwei Lei, Jingbin Shi, Yun Teng, Chenghui Song, Lijuan Zou, Fuxiu Ye, Haichen Zhang
Baicalein modulates the radiosensitivity of cervical cancer cells in vitro via miR-183 and the JAK2/STAT3 signaling pathway

Reviews

- 737 Szymon Urban, Mikołaj Błaziak, Jan Biegus, Robert Zymlński
Ultrafiltration in acute heart failure: Current knowledge and fields for further research
- 747 Agata Czarnywojtek, Alicja Ochmańska, Małgorzata Zgorzalewicz-Stachowiak, Nadia Sawicka-Gutaj, Beata Matyjaszek-Matuszek, Magdalena Woźniak, Marek Ruchała
Influence of SARS-CoV-2 infection on thyroid gland function: The current knowledge

Research-in-progress

- 757 Maciej Dejneka, Helena Moreira, Sylwia Płaczowska, Piotr Morasiewicz, Ewa Barg, Jarosław Witkowski, Paweł Reichert
Analysis and comparison of autologous platelet-rich plasma preparation systems used in the treatment of enthesopathies: A preliminary study
- 765 Julia Rudno-Rudzińska, Wojciech Kielan, Maciej Guziński, Julita Kulbacka
Effects of calcium electroporation, electrochemotherapy, and irreversible electroporation on quality of life and progression-free survival in patients with pancreatic cancer: IREC clinical study

Alzheimer's trials: A cul-de-sac with no end in sight

Markku Kurkinen^{D,F}

NeuroActiva™, Inc., San Jose, USA

A – research concept and design; B – collection and/or assembly of data; C – data analysis and interpretation;
D – writing the article; E – critical revision of the article; F – final approval of the article

Advances in Clinical and Experimental Medicine, ISSN 1899–5276 (print), ISSN 2451–2680 (online)

Adv Clin Exp Med. 2021;30(7):653–654

Address for correspondence

Markku Kurkinen
E-mail: markku@genetics.wayne.edu

Funding sources

None declared

Conflict of interest

None declared

Acknowledgements

I thank Manuel Graeber, Anna Thuring, Jack de la Torre and Lloyd Tran for their interest and comments.

Received on June 21, 2021

Accepted on June 28, 2021

Published online on July 27, 2021

Cite as

Markku Kurkinen. Alzheimer's trials: A cul-de-sac with no end in sight. *Adv Clin Exp Med*. 2021;30(7):653–654. doi:10.17219/acem/139501

DOI

10.17219/acem/139501

Copyright

© 2021 by Wrocław Medical University
This is an article distributed under the terms of the Creative Commons Attribution 3.0 Unported (CC BY 3.0) (<https://creativecommons.org/licenses/by/3.0/>)

Key words: Alzheimer's disease, clinical trials, drug discovery, EAAT2

Understanding and treatment of disease go hand in hand. A case in point, the topic of this Editorial, is Alzheimer's disease (AD), a most devastating disorder of the human mind and the major cause of dementia. Despite decades of research efforts in academia and the drug industry, and hundreds of clinical trials, we have no cure, no prevention and no treatment for AD. Why is that? The short answer is that we do not understand AD – its origin and disease mechanisms.

The long answer is as follows. In the early 1900s, when Alois Alzheimer and many others described amyloid plaques and neurofibrillary tangles in the postmortem brains of senile people, they did not propose any cause or effect. Do the plaques and tangles cause dementia, or does dementia cause the plaques and tangles? Indeed, in 1911 Alzheimer wrote: "There is then no tenable reason to consider these cases as caused by a specific disease process."¹ The amyloid hypothesis proposes A β peptide accumulation and amyloid formation in the brain cause AD. The hypothesis has almost singularly guided AD research and clinical trials ever since it was formulated 30 years ago.² Yet, several facts, and experimental studies, are against the hypothesis.^{3–8} All AD trials, hundreds of them over the years, whether with β - or γ -secretase inhibitors to reduce A β peptides production or with anti-A β antibodies to clear amyloid from the brain, have failed to stop or slow cognitive decline or improve daily living of AD patients. Similarly, in preventive trials in cognitively unimpaired people at high risk of developing AD, due to the *APOE4* gene or elevated PET scan-determined brain amyloid, reducing A β peptide production and amyloid did not prevent or slow cognitive decline. The most definitive evidence against the hypothesis, however, comes from the recent preventive trials in cognitively unimpaired people carrying the presenilin *PS1* mutation E280A, which causes AD at age 45. Trials with the anti-A β antibodies solanezumab or ganterumab failed to prevent or slow cognitive decline. Even worse, the preventive trials and treatment methods intended to help often harmed many study participants volunteering for the trials by causing serious health problems, including enhanced cognitive decline.

If these AD trials and failures do not prove the amyloid hypothesis wrong, then what does? And if these trials and errors do not ring the bell and call for a major change in AD research, and question the rationales of AD research policy making, then what does?

It is fair to say the absence of disease-modifying treatments for AD today is due to the amyloid hypothesis, a misguided hypothesis of AD etiology, which

has dominated research, drug development and clinical trials for 30 years. In 2014, when Jack de la Torre was writing in *The New England Journal of Medicine*: “[...] when is a dead hypothesis really dead?”, he was commenting on the failed trials in AD patients with the anti-A β antibodies solanezumab and bapineuzumab.⁹ However, the hypothesis is not dead yet, as exemplified by the recent resurrection of clinical trials with aducanumab.¹⁰ On June 7, 2021, the US Food and Drug Administration (FDA) approved the use of aducanumab (Aduhelm™) to treat AD.¹¹

In 1991, Swash et al. wrote: “Recent advances in Alzheimer’s disease imply a need for adequate clinical trials of new treatments which require careful design.”¹² Today, recent advances in AD research have investigated astrocytes, synaptic function and glutamate signaling. In neurotransmission, synaptic glutamate signaling is regulated by the glutamate transporter EAAT2 expressed on astrocytes (which cover the synapses). As soon as glutamate signaling starts, it is stopped within 1 ms by EAAT2, which binds and removes glutamate from the synapses. This prevents excessive glutamate signaling, which can lead to synapse loss and neuron cell death, the early signs of developing AD. In mouse models of AD, increasing EAAT2 expression slows disease progression, whereas decreasing EAAT2 expression enhances disease progression. Human postmortem AD brains have less EAAT2. These observations, and many other studies, indicate EAAT2 as a promising target in drug discovery and clinical development for novel therapies in AD and other neurological and psychiatric diseases.^{13–15}

ORCID iDs

Markku Kurkinen  <https://orcid.org/0000-0002-4483-5101>

References

1. Förstl H, Levy R. On certain peculiar diseases of old age. *Hist Psychiatr.* 1991;2(5 Pt 1):74–99. doi:10.1177/0957154X9100200505
2. Selkoe DJ, Hardy J. The amyloid hypothesis of Alzheimer’s disease at 25 years. *EMBO Mol Med.* 2016;8(6):595–608. doi:10.15252/emmm.201606210
3. Sun L, Zhou R, Yang G, Shi Y. Analysis of 138 pathogenic mutations in presenilin-1 on the in vitro production of A β 42 and A β 40 peptides by γ -secretase. *Proc Natl Acad Sci U S A.* 2016;114(4):E476–E485. doi:10.1073/pnas.1618657114
4. Kurkinen M. The amyloid hypothesis is too good to be true. *Alzheimers Dement Cogn Neurol.* 2017;1:1–9. doi:10.15761/ADCN.1000106
5. Egan MF, Mukai Y, Boss T, et al. Further analyses of the safety of verubecestat in the phase 3 EPOCH trial of mild-to-moderate Alzheimer’s disease. *Alzheimers Res Ther.* 2019;11(1):68. doi:10.1186/s13195-019-0520-1
6. Yiannopoulou KG, Anastasiou AI, Zachariou V, Pelidou SH. Reasons for failed clinical trials of disease-modifying-treatments for Alzheimer’s disease and their contribution in recent research. *Biomedicines.* 2019;7(4):97. doi:10.3390/biomedicines7040097
7. Tian Hui Kwan A, Arfaie S, Therriault J, Rosa-Neto P, Gauthier S. Lessons learnt from the second generation of anti-amyloid monoclonal antibody clinical trials. *Dement Geriatr Cogn Disord.* 2020;49(4):334–348. doi:10.1159/000511506
8. Kolata G. An Alzheimer’s Treatment Fails: ‘We Don’t Have Anything Now’. *The New York Times.* February 10, 2020. nytimes.com/2020/02/10/health/alzheimers-amyloid-drug.html? searchResultPosition=1. Accessed February 10, 2020.
9. de la Torre JC. Phase 3 trials of solanezumab and bapineuzumab for Alzheimer’s disease. *N Engl J Med.* 2014;370(15):1459–1460. doi:10.1056/NEJMc1402193
10. Schneider L. A resurrection of aducanumab for Alzheimer’s disease. *Lancet Neurol.* 2020;19(2):111–112. doi:10.1016/S1474-4422(19)30480-6
11. U.S. Food and Drug Administration. FDA Grants Accelerated Approval for Alzheimer’s Drug. https://www.fda.gov/news-events/press-announcements/fda-grants-accelerated-approval-alzheimers-drug?utm_medium=email&utm_source=govdelivery. Accessed June 7, 2021.
12. Swash M, Brooks DN, Day NE, Frith CD, Levy R, Warlov CP. Clinical trials in Alzheimer’s disease. *J Neurol Neurosurg Psychiatry.* 1991;54(2):178–181. doi:10.1136/jnnp.54.2.178
13. Takahashi K, Foster JB, Lin CL. Glutamate transporter EAAT2: Regulation, function, and potential as a therapeutic target for neurological and psychiatric disease. *Cell Mol Life Sci.* 2015;72(18):3489–3506. doi:10.1007/s00018-015-1937-8
14. Fontana AC. Current approaches to enhance glutamate transporter function and expression. *J Neurochem.* 2015;134(6):982–1007. doi:10.1111/jnc.13200
15. Kurkinen M. Astrocyte glutamate transporter EAAT2 in Alzheimer dementia. In: Pavlovic ZM, ed. *Glutamate and Neuropsychiatric Disorders – Current and Emerging Treatments.* Basingstoke, UK: Springer Nature; 2021.

Soluble syndecan-1 as marker of intestinal inflammation: A preliminary study and evaluation of a new panel of biomarkers for non-invasive prediction of active ulcerative colitis

Martin Floer^{1,A–F}, Mareike Clausen^{2,A–F}, Tobias Meister^{1,A–F},
Richard Vollenberg^{3,A–F}, *Dominik Bettenworth^{3,A–F}, *Phil-Robin Tepassee^{3,A–F}

¹ Department of Medicine 1, Klinikum Ibbenbüren, Germany

² Department of Medicine, Evangelisches Krankenhaus Weende, Göttingen, Germany

³ University Hospital Münster, Department of Medicine B for Gastroenterology, Hepatology, Endocrinology and Clinical Infectiology, Germany

A – research concept and design; B – collection and/or assembly of data; C – data analysis and interpretation;

D – writing the article; E – critical revision of the article; F – final approval of the article

Advances in Clinical and Experimental Medicine, ISSN 1899–5276 (print), ISSN 2451–2680 (online)

Adv Clin Exp Med. 2021;30(7):655–660

Address for correspondence

Martin Floer
E-mail: martinfloer@web.de

Funding sources

HELIOS research grant No. HRC-ID 061939.

Conflict of interest

This study was supported by a HELIOS research grant (HRC-ID 061939). Helios GmbH was not involved in study design, data collection or interpretation, or publication of this study. This study was an investigator-initiated trial.

Acknowledgements

We would like to thank Lydia Rosenbaum, MHSoc for her valuable help as a native speaker.

*Dominik Bettenworth and Phil-Robin Tepassee contributed equally to this work.

Received on March 2, 2021

Reviewed on May 4, 2021

Accepted on June 16, 2021

Published online on July 20, 2021

Cite as

Floer M, Clausen M, Meister T, Vollenberg R, Bettenworth D, Tepassee PR. Soluble syndecan-1 as marker of intestinal inflammation: A preliminary study and evaluation of a new panel of biomarkers for non-invasive prediction of active ulcerative colitis. *Adv Clin Exp Med.* 2021;30(7):655–660. doi:10.17219/acem/139040

DOI

10.17219/acem/139040

Copyright

© 2021 by Wrocław Medical University

This is an article distributed under the terms of the Creative Commons Attribution 3.0 Unported (CC BY 3.0) (<https://creativecommons.org/licenses/by/3.0/>)

Abstract

Background. Syndecan-1 (Sdc1) is a heparin sulfate proteoglycan expressed in intestinal epithelium, which plays a crucial role in inflammation and epithelial repair. Sdc1-knockout mice have a deteriorated course of dextran sulfate sodium-induced colitis as compared to controls. Syndecan-1 is also shed into the serum during inflammation of the epithelium. We hypothesized that an increased serum level of soluble Sdc1 is a biomarker of intestinal inflammation in ulcerative colitis (UC).

Objectives. To evaluate serum soluble Sdc1 as a biomarker of intestinal inflammation in UC.

Materials and methods. This is a proof-of-concept study. Patients were recruited by the University Hospital Münster and HELIOS Albert Schweitzer Klinik Northeim (Germany). Blood samples were collected from UC patients actively suffering from this condition and those in remission. The levels of Sdc1 were measured with Diaclone CD 138 ELISA kit (Diaclone Research, Besançon, France) and routine clinical data were collected (C-reactive protein (CRP) levels, calprotectin in stool samples). Data were analyzed using SPSS software.

Results. Soluble Sdc1 levels were significantly elevated in the active UC group as compared to the inactive UC group (94.5 ± 68.1 ng/mL compared to 28.3 ± 12.6 ng/mL, $p = 0.0020$). The levels of Sdc1 also significantly correlated with the severity of UC as measured with the Mayo score ($p = 0.0248$). Receiver operating characteristic (ROC) analysis showed a good correlation of Sdc1 with an endoscopic Mayo score ≥ 2 , with a value of 0.7747 (95% confidence interval (95% CI) = 0.5775–0.9718). A cutoff value of 37.1 ng/mL of Sdc1 showed a sensitivity of 78% and a specificity of 77%. A panel of biomarkers including CRP, hemoglobin, hematocrit, and Sdc1 was able to precisely predict active UC with an area under the curve (AUC) = 0.9395 (95% CI = 0.8509–1.0000).

Conclusions. Serum soluble Sdc1 correlates significantly with mucosa inflammation and Mayo score in UC. Clinical trials No. NCT 02333526.

Key words: inflammatory bowel disease, biomarker, CD138, syndecan-1, ulcerative colitis

Background

Syndecan-1 (CD138, Sdc1) is a heparin sulfate proteoglycan that plays an important role in inflammation and wound healing.^{1,2} Physiologically, there is a high concentration of Sdc1 in the intestinal epithelium. Sdc1-knockout mice exhibit impaired wound healing of the skin and show a higher mortality rate in an experimental model of colitis induced with dextran sulfate sodium.^{3,4} Likewise, in ulcerative colitis (UC) patients, a lack of Sdc1 has been observed in histological specimens of ulcers.^{5,6} In addition, a shedding of Sdc1 into the bloodstream during inflammation has been observed.^{7,8} Furthermore, Sdc1 has been shown to play a role in autoimmune diseases like psoriasis.⁹

Guidelines recommend that the therapeutic aim of UC treatment should be both clinical and endoscopic remission.^{10,11} In particular, the therapeutic goal is to achieve mucosal healing.¹² Therefore, it would be advantageous to identify non-invasive assessments, such as biomarkers or a panel of biomarkers, that indicate endoscopic remission. Presently, C-reactive protein (CRP), sedimentation rate and stool calprotectin are established biomarkers for intestinal inflammation, but none of these markers are specific to inflammatory bowel disease (IBD),¹³ nor are any of these markers used as an alternative to endoscopic remission.¹⁴ For example, stool calprotectin is most frequently used in studies of IBD, but the cutoff levels have been difficult to determine.¹⁵ Other fecal markers like lactoferrin have not proven to be superior to stool calprotectin.¹⁴ C-reactive protein is a long-standing marker for inflammation in general, but its ability to distinguish between mucosal healing and moderate-to-severe colitis is controversial due to poor accuracy and the use of different cutoff values.¹⁵ Cytokines and downstream proteins have been evaluated as markers for UC, but they also have not been shown to be superior to stool calprotectin in its ability to distinguish between active and inactive colitis.¹⁶ A wide range of markers connected to the immune response has also been evaluated.¹⁴ However, none have proven superior if used as a single marker for active UC. A relatively new approach is to evaluate biomarker panels for the detection of mucosal healing. For example, Hosomi et al. evaluated a combination of presepsin and CRP for Crohn's disease activity, which showed a sensitivity of nearly 100%.¹⁷ Therefore, identifying biomarkers specific to IBD is worthy of investigation.

Objectives

Based on previous research, we considered the possibility that soluble Sdc1 levels in blood serum may correlate with the presence of colonic inflammation in UC and may be useful as a specific biomarker. Thus, the aim of this study was to examine the correlation between Sdc1 levels and the presence of inflammation with respect to disease activity, medication and other biomarkers of inflammation.

Materials and methods

Study design

This study was designed as proof of concept study. We hypothesized that Sdc1 is a suitable indicator of intestinal inflammation. The main outcome parameter was serum soluble Sdc1 levels from blood samples collected during routine outpatient visits from patients diagnosed with UC.

Setting

This study was performed in accordance with the Declaration of Helsinki. The trial involved human participants, was approved by the local ethics committee at the University of Göttingen, Germany (approval No. 25/8/14) and was registered (Clinical trials No. NCT 02333526).

The study was conducted at the Helios Albert-Schweitzer-Hospital in Northeim, Germany and the University Hospital in Münster, Germany from 2015 to 2018. Routine outpatient visits were used to recruit patients, and all participants signed informed consent for blood collection and data storage. All data were collected in a Microsoft Excel table (Microsoft Office 2013; Microsoft Corp., Redmond, USA), immediately anonymized and processed according to the European Union law. A follow-up examination was not performed.

Participants

Patients older than 18 years with a history of UC and signed informed consent were considered eligible for the study. Exclusion criteria included a history of Crohn's disease, infectious intestinal disease, an age under 18 years, pregnancy, and lack of informed consent.

Variables

Secondary parameters were age, sex, active UC, UC in remission, Mayo score for UC, extent of UC, medication, leucocyte count, CRP, thrombocyte count, hemoglobin, hematocrit, and fecal calprotectin.

Data sources and management

All blood samples were collected according to good clinical practice. The samples were labeled with a code and brought to the laboratory. Samples were centrifuged at 3000 × g for 10 min and serum was obtained. The serum samples were stored at -70°C until processing. A commercially available enzyme-linked immunosorbent assay (ELISA) kit was used to measure soluble Sdc1 (Diaclone Research, Besançon, France). Material that was not used was discarded.

To avoid bias, all patients with UC had their diagnosis confirmed by endoscopy and histologic examination of gut specimens.

Study size

As this was a proof of concept study, the patients were divided into 2 groups: 13 patients with UC and a Mayo score <2, and 14 patients with UC and a Mayo score ≥2. Patient recruitment was considered complete after attaining a strong and significant signal for our main outcome parameter, and when statistical power 1-beta surpassed 0.8 (80%).

Quantitative variables

We chose the endoscopic Mayo score for the discrimination of active and inactive UC as this methodology has been well established in literature. Patients with a Mayo score <2 (inactive or mild disease) were considered as inactive, while patients with a Mayo score ≥2 (moderate-to-severe) were considered as active. A Mayo score of 2 was chosen due to the significant signal of Sdc1 detected using an unpaired t-test.

Statistical analyses

Statistical analyses were performed using IBM SPSS Statistics for Windows, v. 27 (IBM Corp., Armonk, USA). Values are displayed as mean and standard deviation (SD), or n. To test for significance, unpaired t-tests (to compare means) or Pearson's χ^2 tests (to compare n in contingency tables) were used, and an alpha level of a $p < 0.05$ was considered significant. To examine the correlation between the complete Mayo score and Sdc1, the Kruskal–Wallis test was used, and a $p < 0.05$ was considered statistically significant. To examine the correlations of CRP and stool calprotectin with Sdc1, bivariate correlation (Pearson's r) was used. A receiver operator characteristic (ROC) curve analysis was performed to check for the discrimination threshold of Sdc1 (discrimination of colonoscopic Mayo score <2 compared to ≥2). Points on the ROC curve nearest the upper left corner were chosen for cutoff values as this resulted in optimal sensitivity and specificity. Logistic regression analysis was performed to determinate the regression coefficients of CRP, hemoglobin, hematocrit, and Sdc1 since these parameters were proven to be significant in t-test analyses. Based on these data, a model (see results) was created to improve the prediction of active UC. This model was again analyzed using ROC curve analysis.

Results

Twenty-seven patients with UC were eligible for this study and provided informed consent. All of the recruited patients were included. Among these, 13 were considered inactive and 14 were considered active, as indicated by the Mayo score. For those with active UC, the distribution of colonic inflammation was as follows: 50% pancolitis, 31.5% left-sided UC, 12.5% ulcerative proctitis, and 6% right-sided UC.

Blood was drawn and samples underwent Sdc1 analysis. As outlined above, 2 groups were differentiated based on a Mayo score <2 and ≥2. In these 2 groups, no significant differences in age, duration of disease, gender, mesalazine usage, comorbidities, tumor necrosis factor (TNF) blocker usage, and azathioprine usage were observed. It was found that drugs like vedolizumab, steroids or other immunomodulatory drugs were used more often in the active UC group than in the inactive UC group. Significant differences were also found between the active and inactive UC groups in the level of CRP, leucocyte count, hemoglobin, hematocrit level, and fecal calprotectin.

The Sdc1 was also significantly elevated in the active UC group as compared to the inactive UC group (94.5243 ±68.0518 ng/mL compared to 28.3423 ±12.5921 ng/mL, $p = 0.0020$; Table 1). The Kruskal–Wallis test showed a significant correlation between Sdc1 values and the extent of UC as measured with the complete Mayo score (degrees of freedom (df) = 8, $p = 0.0248$; Fig. 1). In addition, ROC analysis showed an area under curve (AUC) of 0.7747 (95% confidence interval (95% CI) = 0.5775–0.9718; Fig. 1), indicating a pretty good correlation of Sdc1 with the activity of UC (according to the endoscopic Mayo score). As a result of the ROC analysis, it was determined that a cutoff value of 37.1 ng/mL of Sdc1 was associated with a sensitivity of 78% and a specificity of 77%.

Based on these data, we were able to model a panel of biomarkers for improved prediction of active UC. First, we performed a logistic regression analysis identifying CRP, hemoglobin, hematocrit, and soluble Sdc1 as parameters for the prediction of active colitis as defined with an endoscopic Mayo score of 2 or above. Next, we calculated the x -value where

$$x = 4.078 * [\text{CRP [mg/dL]}] - 1.961 * [\text{hemoglobin [g/dL]}] + 0.466 * [\text{hematocrit [%]}] + 0.040 * [\text{Sdc1 [ng/mL]}] + 2.900.$$

The probability (P) that the patients suffers from active UC was estimated using x in this mathematical term (1):

$$P = \frac{1}{1 + e^x} \quad (1)$$

ROC analysis of this predictive model revealed an AUC of 0.9395 (95% CI = 0.8509–1.0000; Fig. 1).

Finally, a significant correlation between Sdc1 and CRP was observed ($r = 0.6061$, $p = 0.0008$). The correlation between Sdc1 and fecal calprotectin was positive but non-significant ($r = 0.3381$, $p = 0.2001$).

Discussion

Our data suggest that soluble Sdc1 is a marker of activity for UC, indicating the possibility of a strong biomarker signal that should be validated in a larger multicenter study. It is known that level of Sdc1 can be influenced by other non-inflammatory states. For example, acute exercise

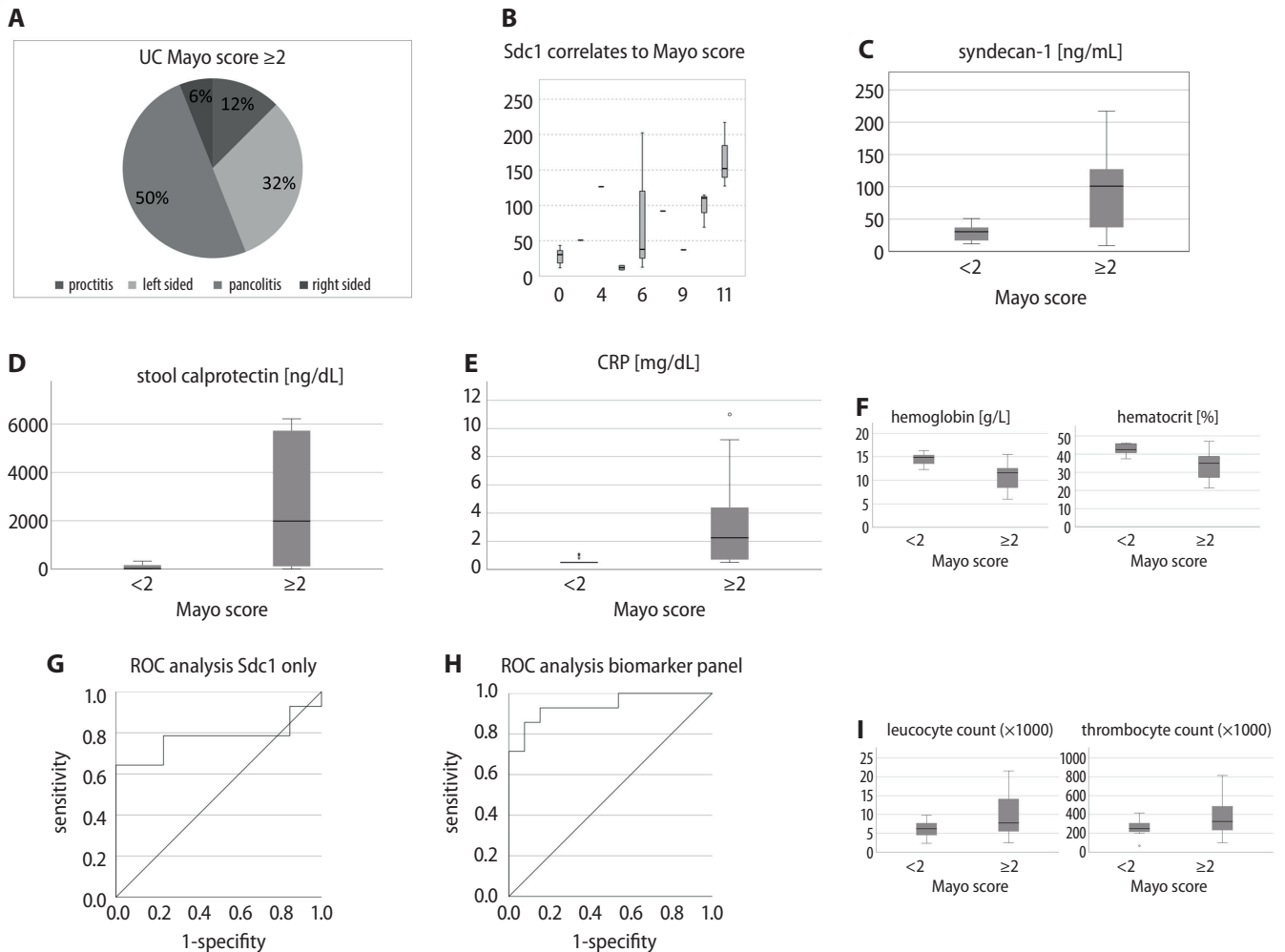


Fig. 1. A. Ulcerative colitis infestation pattern; B. Kruskal–Wallis diagram: positive correlation of Sdc1 with the complete Mayo score ($p = 0.0248$); C. Sdc1 is elevated in active UC, $p = 0.002$; D. Stool calprotectin is elevated in UC ($p = 0.0179$); E. CRP is higher in active UC ($p = 0.0080$); F. Hemoglobin and hematocrit are significantly altered as compared to inactive UC (for p-values see Table 1); G. Receiver operation characteristic for Sdc1 only. X-axis is 1-specificity, Y-axis is sensitivity. AUC is 0.7747 (95% CI = 0.5775–0.9718). Best discriminative cutoff value is 37.1 ng/mL Sdc1 (sensitivity of 78% and a specificity of 77%); H. Receiver operation characteristic for a biomarker panel including Sdc1, CRP, hematocrit, and hemoglobin. X-axis is 1-specificity, Y-axis is sensitivity. This panel enables sharp discrimination of inactive and active UC beyond a Mayo score of 2; AUC is 0.9395 (95% CI = 0.8509–1.0000); I. Leucocyte and thrombocyte count. Leucocyte count is significantly higher in active UC ($p = 0.0429$). A nonsignificant elevation of the thrombocyte count in active UC was observed

is able to raise Sdc1.¹⁸ The Sdc1 is also elevated after trauma, especially after polytrauma, where it is a quantitative marker of endotheliopathy.¹⁹ In arterial hypertension, elevated Sdc1 levels are also observed.²⁰ Furthermore, Sdc1 is a biomarker for sepsis and sepsis survival after abdominal surgery.²¹ Previous studies have also associated Sdc1 with breast cancer. For example, Sdc1 levels correlate with the tumor size of breast cancers.²² Aside from the different roles of Sdc1 in human biology, the role of Sdc1 in IBD is apparent. In UC, the amelioration of intestinal inflammation and neutrophil migration is well described.²³ Soluble Sdc1 is elevated in IBD,²⁴ which is also confirmed by our results. In contrast to the abovementioned publication, we found a higher level of Sdc1 in active UC. Other forms of IBD, such as Crohn's disease²⁵ and acute colonic diverticulitis,²⁶ are also associated with elevated soluble Sdc1 levels. Additionally, Sdc1 levels are elevated in acute neuromyelitis optica²⁷ and in children with celiac disease.²⁸

All of these conditions suggest that Sdc1 alone is likely insufficient as a biomarker for colon inflammation.²⁹ Therefore, we established a biomarker panel to include CRP, hemoglobin, hematocrit, and Sdc1, all of which can be easily obtained from patient blood samples. Our calculations revealed that active UC, as defined by an endoscopic Mayo score ≥ 2 , can be identified using this panel. The accuracy of this panel (93%) exceeds that of stool calprotectin (89%),³⁰ which is the best-established marker for UC activity to date. Stool calprotectin serves as a good marker to discriminate severe UC from mild-to-moderate UC,³¹ but its ability to detect mucosal healing is less sensitive (sensitivity is only 79%).³² Stidham et al. described a neuronal network evaluation of UC videos that was able to predict the endoscopic Mayo score with an accuracy of 96%, as compared to human review which had an accuracy of 89%.³³ Therefore, our panel has the potential to be as good as the human eye to predict active UC.

Table 1. Demographic data, comorbidities, medication, and results

Parameter	UC Mayo score <2	UC Mayo score ≥2	p-value	df
n	13	14	n/a	
Age [years] ±SD	44.69 ±16.849	38.86 ±13.722	0.3316 (t-test)	25
Patients with comorbidities, n	7	6	0.5680 (χ ² test)	1
Arterial hypertension, n	3	1	0.2442 (χ ² test)	1
PSC, n	2	3	0.6862 (χ ² test)	1
Other comorbidities, n	3	3	0.9180 (χ ² test)	1
Duration of disease [years] ±SD	15.23 ±13.755	19.71 ±12.035	0.0849 (t-test)	25
Female, n	7	6	0.5679 (χ ² test)	1
Mesalazin, n	7	6	0.5680 (χ ² test)	1
TNF blocker, n	6	4	0.3445 (χ ² test)	1
Azathioprin, n	3	2	0.5568 (χ ² test)	1
Other medication, n	0	3	0.0766 (χ ² test)	1
CRP [mg/dL] ±SD	0.608 ±0.2139	3.386 ±3.4678	0.0080 (t-test)	25
Leucocyte count [×1000/μL] ±SD	6.2531 ±2.2982	10.3171 ±6.4863	0.0426 (t-test)	25
Thrombocyte count [×1000/μL] ±SD	255.62 ±85.243	375 ±202.951	0.0607 (t-test)	25
Hemoglobin [g/L] ±SD	14.508 ±1.2945	10.936 ±2.9209	0.0004 (t-test)	25
Hematocrit [%] ±SD	42.792 ±3.0674	33.993 ±7.7225	0.0007 (t-test)	25
Stool calprotectin [ng/mL] ±SD	86.75 ±118.705	2734.38 ±2792.978	0.0179 (t-test)	14*
Sdc1 [ng/mL] ±SD	28.3423 ±12.5921	94.5243 ±68.0518	0.0020 (t-test)	25

All values as mean and standard deviation (SD) or n. Bold digits denote significant result ($p < 0.05$); *stool calprotectin was not available in all cases; PSC – primary sclerosing cholangitis; TNF – tumor necrosis factor; CRP – C-reactive protein; Sdc1 – syndecan-1; n/a – not applicable; df – degrees of freedom.

Our results prove to be very important as they demonstrate a non-invasive way to identify a treat to target strategy (especially mucosal healing) in UC that is coupled with a better disease management outcome. Therefore, non-invasive detection of active UC using blood sample would be of value.³⁴ The Sdc1, as part of a biomarker panel, has the potential to be a simple non-invasive way for disease management. Treatment could then be modified or individually dosed without repeated endoscopy.

Limitations

Our study has some important limitations. There were nonsignificant differences between both groups regarding comorbidities, duration of disease and age, which might have contributed to our results. We also cannot exclude that use of a TNF blocker like infliximab influenced the results, as these agents likely downregulate Sdc1 in UC.³⁵ In addition, only 2 centers contributed to this study. Our post hoc power analysis showed an effect size of $d = 1.37$ and a 1-beta error of 0.88, which means that the power of this study was sufficient to draw conclusions. Nevertheless, due to the low numbers of patients included and study centers, we fear that the data available here cannot be generalized. However, we do think that we accomplished a proof of principle. It is possible that disruptive factors may also have influenced our results (e.g., inflammation of other origins, undetected cancer or trauma before blood collection). Additionally, we were

not able to correlate our data to histology patterns as described using the Riley score.

Conclusions

Finally, we would like to suggest validating the presented panel of biomarkers in a larger cohort of patients. As previously described, the traditional panel with the inclusion of Sdc1 might be useful for treat-to-target strategies in UC.

ORCID iDs

Martin Floer  <https://orcid.org/0000-0002-8572-9372>
 Mareike Clausen  <https://orcid.org/0000-0001-9038-7664>
 Tobias Meister  <https://orcid.org/0000-0002-7664-8108>
 Richard Vollenberg  <https://orcid.org/0000-0003-3208-7924>
 Dominik Bettenworth  <https://orcid.org/0000-0002-1435-4825>
 Phil-Robin Tepassee  <https://orcid.org/0000-0002-2757-4755>

References

- Principi M, Day R, Marangi S, et al. Differential immunohistochemical expression of syndecan-1 and tumor necrosis factor alpha in colonic mucosa of patients with Crohn's disease. *Immunopharmacol Immunotoxicol.* 2006;28(2):185–195. doi:10.1080/08923970600815048
- Day R, Forbes A. Heparin, cell adhesion, and pathogenesis of inflammatory bowel disease. *Lancet.* 1999;354(9172):62–65. doi:10.1016/S0140-6736(98)09267-8
- Götte M. Syndecans in inflammation. *FASEB J.* 2003;17(6):575–591. doi:10.1096/fj.02-0739rev
- Floer M, Götte M, Wild MK, et al. Enoxaparin improves the course of dextran sodium sulfate-induced colitis in syndecan-1-deficient mice. *Am J Pathol.* 2010;176(1):146–157. doi:10.2353/ajpath.2010.080639

5. Zhang S, Qing Q, Wang Q, et al. Syndecan-1 and heparanase: Potential markers for activity evaluation and differential diagnosis of Crohn's disease. *Inflamm Bowel Dis.* 2013;19(5):1025–1033. doi:10.1097/MIB.0b013e318280298f
6. Bartlett AH, Hayashida K, Park PW. Molecular and cellular mechanisms of syndecans in tissue injury and inflammation. *Mol Cells.* 2007;24(2):153–166. PMID:17978567
7. Ierardi E, Giorgio F, Zotti M, et al. Infliximab therapy downregulation of basic fibroblast growth factor/syndecan-1 link: A possible molecular pathway of mucosal healing in ulcerative colitis. *J Clin Pathol.* 2011;64(11):968–972. doi:10.1136/jcp.2010.086892
8. Manon-Jensen T, Itoh Y, Couchman JR. Proteoglycans in health and disease: The multiple roles of syndecan shedding. *FEBS J.* 2010;277(19):3876–3889. doi:10.1111/j.1742-4658.2010.07798.x
9. Tomas D, Vucić M, Situm M, Kruslin B. The expression of syndecan-1 in psoriatic epidermis. *Arch Dermatol Res.* 2008;300(7):393–395. doi:10.1007/s00403-008-0848-z
10. Feuerstein JD, Isaacs KL, Schneider Y, et al. AGA clinical practice guidelines on the management of moderate to severe ulcerative colitis. *Gastroenterology.* 2020;158(5):1450–1461. doi:10.1053/j.gastro.2020.01.006
11. Harbord M, Eliakim R, Bettenworth D, et al. Third European Evidence-based Consensus on Diagnosis and Management of Ulcerative Colitis. Part 2: Current Management [published correction appears in *J Crohns Colitis.* 2017;11(12):1512]. *J Crohns Colitis.* 2017;11(7):769–784. doi:10.1093/ecco-jcc/jjx009
12. Neurath MF, Travis SP. Mucosal healing in inflammatory bowel diseases: A systematic review. *Gut.* 2012;61(11):1619–1635. doi:10.1136/gutjnl-2012-302830
13. Laserna-Mendieta EJ, Lucendo AJ. Faecal calprotectin in inflammatory bowel diseases: A review focused on meta-analyses and routine usage limitations. *Clin Chem Lab Med.* 2019;57(9):1295–1307. doi:10.1515/cclm-2018-1063
14. Krzystek-Korpaczka M, Kempniński R, Bromke M, Neubauer K. Biochemical biomarkers of mucosal healing for inflammatory bowel disease in adults. *Diagnostics (Basel).* 2020;10(6):367. doi:10.3390/diagnostics10060367
15. Yoon JY, Park SJ, Hong SP, Kim TI, Kim WH, Cheon JH. Correlations of C-reactive protein levels and erythrocyte sedimentation rates with endoscopic activity indices in patients with ulcerative colitis. *Dig Dis Sci.* 2014;59(4):829–837. doi:10.1007/s10620-013-2907-3
16. Rodríguez-Perálvarez ML, García-Sánchez V, Villar-Pastor CM, et al. Role of serum cytokine profile in ulcerative colitis assessment. *Inflamm Bowel Dis.* 2012;18(10):1864–1871. doi:10.1002/ibd.22865
17. Hosomi S, Yamagami H, Itani S, et al. Sepsis markers soluble IL-2 receptor and soluble CD14 subtype as potential biomarkers for complete mucosal healing in patients with inflammatory bowel disease. *J Crohns Colitis.* 2018;12(1):87–95. doi:10.1093/ecco-jcc/jjx124
18. Lee S, Kolset SO, Birkeland KI, Drevon CA, Reine TM. Acute exercise increases syndecan-1 and -4 serum concentrations. *Glycoconj J.* 2019;36(2):113–125. doi:10.1007/s10719-019-09869-z
19. Gonzalez Rodriguez E, Ostrowski SR, Cardenas JC, et al. Syndecan-1: A quantitative marker for the endotheliopathy of trauma. *J Am Coll Surg.* 2017;225(3):419–427. doi:10.1016/j.jamcollsurg.2017.05.012
20. Miftode RS, Șerban IL, Timpau AS, et al. Syndecan-1: A review on its role in heart failure and chronic liver disease patients' assessment. *Cardiol Res Pract.* 2019;2019:4750580. doi:10.1155/2019/4750580
21. Holzmann MS, Winkler MS, Strunden MS, et al. Syndecan-1 as a biomarker for sepsis survival after major abdominal surgery. *Biomark Med.* 2018;12(2):119–127. doi:10.2217/bmm-2017-0231
22. Malek-Hosseini Z, Jelodar S, Talei A, Ghaderi A, Doroudchi M. Elevated syndecan-1 levels in the sera of patients with breast cancer correlate with tumor size. *Breast Cancer.* 2017;24(6):742–747. doi:10.1007/s12282-017-0773-0
23. Zhang Y, Wang Z, Liu J, et al. Cell surface-anchored syndecan-1 ameliorates intestinal inflammation and neutrophil transmigration in ulcerative colitis [published correction appears in *J Cell Mol Med.* 2017;21(4):834]. *J Cell Mol Med.* 2017;21(1):13–25. doi:10.1111/jcmm.12934
24. Yablecovitch D, Stein A, Shabat-Simon M, et al. Soluble syndecan-1 levels are elevated in patients with inflammatory bowel disease. *Dig Dis Sci.* 2015;60(8):2419–2426. doi:10.1007/s10620-015-3589-9
25. Çekiç C, Kırıcı A, Vatanserver S, et al. Serum syndecan-1 levels and its relationship to disease activity in patients with Crohn's disease. *Gastroenterol Res Pract.* 2015;2015:850351. doi:10.1155/2015/850351
26. Tursi A, Elisei W, Giorgetti GM, et al. Expression of basic fibroblastic growth factor, syndecan-1 and tumour necrosis factor α in resected acute colonic diverticulitis. *Colorectal Dis.* 2014;16(3):O98–O103. doi:10.1111/codi.12504
27. Pei S, Zheng D, Wang Z, Hu X, Pan S, Wang H. Elevated soluble syndecan-1 levels in neuromyelitis optica are associated with disease severity. *Cytokine.* 2018;111:140–145. doi:10.1016/j.cyto.2018.08.017
28. Yablecovitch D, Oren A, Ben-Horin S, et al. Soluble syndecan-1: A novel biomarker of small bowel mucosal damage in children with celiac disease. *Dig Dis Sci.* 2017;62(3):755–760. doi:10.1007/s10620-016-4415-8
29. Patterson AM. Soluble syndecan-1: Does this biomarker address a seemingly insoluble problem in inflammatory bowel disease? *Dig Dis Sci.* 2015;60(8):2222–2224. doi:10.1007/s10620-015-3669-x
30. Schoepfer AM, Beglinger C, Straumann A, Trummler M, Renzulli P, Seibold F. Ulcerative colitis: Correlation of the Rachmilewitz endoscopic activity index with fecal calprotectin, clinical activity, C-reactive protein, and blood leukocytes. *Inflamm Bowel Dis.* 2009;15(12):1851–1858. doi:10.1002/ibd.20986
31. Jusué V, Chaparro M, Gisbert JP. Accuracy of fecal calprotectin for the prediction of endoscopic activity in patients with inflammatory bowel disease. *Dig Liver Dis.* 2018;50(4):353–359. doi:10.1016/j.dld.2017.12.022
32. Carlsen K, Riis LB, Elsberg H, et al. The sensitivity of fecal calprotectin in predicting deep remission in ulcerative colitis. *Scand J Gastroenterol.* 2018;53(7):825–830. doi:10.1080/00365521.2018.1482956
33. Stidham RW, Liu W, Bishu S, et al. Performance of a deep learning model vs human reviewers in grading endoscopic disease severity of patients with ulcerative colitis [published correction appears in *JAMA Netw Open.* 2020;3(1):e1920585]. *JAMA Netw Open.* 2019;2(5):e193963. doi:10.1001/jamanetworkopen.2019.3963
34. Colombel JF, D'haens G, Lee WJ, Petersson J, Panaccione R. Outcomes and strategies to support a treat-to-target approach in inflammatory bowel disease: A systematic review. *J Crohns Colitis.* 2020;14(2):254–266. doi:10.1093/ecco-jcc/jjz131
35. Ierardi E, Giorgio F, Zotti M, et al. Infliximab therapy downregulation of basic fibroblast growth factor/syndecan-1 link: A possible molecular pathway of mucosal healing in ulcerative colitis. *J Clin Pathol.* 2011;64(11):968–972. doi:10.1136/jcp.2010.086892

MicroRNA-197 promotes proliferation and inhibits apoptosis of gallbladder cancer cells by targeting insulin-like growth factor-binding protein 3

Li Tong^{A,D}, Jinglin Cheng^{A,C}, Heping Zuo^B, Jingrong Li^C

The Second Affiliated Hospital of Anhui Medical University, Hefei, China

A – research concept and design; B – collection and/or assembly of data; C – data analysis and interpretation; D – writing the article; E – critical revision of the article; F – final approval of the article

Advances in Clinical and Experimental Medicine, ISSN 1899–5276 (print), ISSN 2451–2680 (online)

Adv Clin Exp Med. 2021;30(7):661–672

Address for correspondence

Jinglin Cheng
E-mail: ChengJingLin082828@163.com

Funding sources

None declared

Conflict of interest

None declared

Acknowledgements

We would like to acknowledge the reviewers for their helpful comments on this paper.

Received on August 28, 2020

Reviewed on January 11, 2021

Accepted on March 24, 2021

Published online on June 11, 2021

Cite as

Tong L, Cheng J, Zuo H, Li J. MicroRNA-197 promotes proliferation and inhibits apoptosis of gallbladder cancer cells by targeting insulin-like growth factor-binding protein 3. *Adv Clin Exp Med.* 2021;30(7):661–672. doi:10.17219/acem/134833

DOI

10.17219/acem/134833

Copyright

© 2021 by Wrocław Medical University
This is an article distributed under the terms of the Creative Commons Attribution 3.0 Unported (CC BY 3.0) (<https://creativecommons.org/licenses/by/3.0/>)

Abstract

Background. Gallbladder cancer (GBC) is one of the common malignant tumors of the biliary tract. There is no report that miR-197 is involved in GBC.

Objectives. The relationship between miR-197 expression and survival time of GBC patients was analyzed. Furthermore, the role and mechanism of miR-197 in GBC was explored.

Materials and methods. A total of 39 GBC patients (21 males, 18 females; average age 56.1 ± 8.5 years) were included from December 2013 to November 2014. All patients were admitted to our hospital for surgical treatment (excluding patients with preoperative chemotherapy). The expression of miR-197 in GBC tissues was examined, and the relationship between miR-197 and patient survival time was analyzed. Cell Counting Kit-8 (CCK-8) and colony formation assays were used to detect cell proliferation. Flow cytometry and TUNEL staining were used to detect apoptosis. Expressions of proteins related with proliferation and apoptosis were detected. The target of miR-197 was predicted through bioinformatics website and verified using the dual luciferase reporter gene assay. The target gene was interfered to so that the effect of miR-197 on the regulation of GBC cell proliferation and apoptosis could be observed.

Results. MiR-197 was highly expressed in GBC tissues, and the expression was closely related to the poor prognosis of GBC. Downregulation of miR-197 inhibited the proliferation and promoted the apoptosis of GBC cells; it also decreased the expressions of proliferation-related proteins p-ERK1/2 and p-AKT, and increased that of apoptosis pathway-related proteins Bax/Bcl-2 and c-caspase-3. The upregulation of miR-197 induced an opposite trend. MiR-197 directly regulated *IGFBP3*.

Conclusions. Our study proved that the expression of miR-197 is closely related to the poor prognosis of GBC. The miR-197–*IGFBP3* axis regulates the proliferation and apoptosis of GBC cells. Downregulation of miR-197 inhibited the proliferation and promoted the apoptosis of GBC cells, indicating potential therapeutic effects.

Key words: apoptosis, proliferation, gallbladder carcinoma, *IGFBP3*, miR-197

Background

Gallbladder cancer (GBC) is the most common malignant tumor of the biliary tract, and ranked 6th among all digestive system cancers by incidence.¹ It is highly malignant and prone to both recur and metastasize, with a five-year survival rate between 5% and 15%.^{2,3} Therefore, it is crucial to clarify the pathogenesis of GBC. It is derived from the gallbladder mucosa, and studies have shown that the occurrence and development of GBC are closely related to the activation of the proliferation and inhibition of apoptosis pathways.⁴ At present, surgical resection remains an effective method to treat GBC; however, due to the poor prognosis of GBC most patients do not have the opportunity to undergo radical resection.⁵ Therefore, further research focusing on the molecular mechanism is urgently needed to develop more effective therapeutic approaches for GBC treatment.

Recent studies have shown that microRNAs (miRs) are integrally involved in the onset and development of tumors. The miRs function as critical regulators of cancer occurrence, proliferation and apoptosis and certain miRs; namely, miR-20a, miR-182 and miR-155 have been described as potential GBC biomarkers.⁶ Furthermore, recent literature has revealed that miR-197 has various patterns of expression and effects in different tumors. For example, miR-197 is downregulated in osteosarcoma, colorectal cancer and breast cancer, while being upregulated in lung, ovarian and pancreatic cancer, and hepatocellular carcinoma.⁷ Through bioinformatics analysis, we found that miR-197 was significantly upregulated in GBC tissues,⁸ but the mechanism remains unclear.

Objectives

This study intends to explore the underlying mechanism of miR-197 in regulating GBC.

Materials and methods

Clinical samples

A total of 39 GBC patients from The Second Affiliated Hospital of Anhui Medical University, Hefei, China, were included from December 2013 to November 2014, with an average age of 56.1 ± 8.5 years (21 males and 18 females). All patients were admitted to our hospital for surgical treatment (patients with preoperative chemotherapy were excluded). The overall survival (OS) time of patients was followed for up to 5 years. Tumor samples and adjacent normal tissue biopsies were taken during the operation. This study was approved by the institutional Ethics Committee and all patients gave informed consent prior to undergoing any procedure.

This study was approved by Ethics Committee of The Second Affiliated Hospital of Anhui Medical University. All patients provided written informed consent.

Differential expression analysis of microarray data in GBC

The GBC expression microarray, GSE104165, which contains 40 GBC and 8 normal gallbladder tissue samples, was extracted from the Gene Expression Omnibus (GEO) database (<https://www.ncbi.nlm.nih.gov/geo/>).⁸ Differential expression analyses were performed using the R language “limma” package (<https://www.r-project.org/>), with log fold change (FC) >2 and p-value <0.05 regarded as the threshold of differentially expressed genes.

Cell culture

Human gallbladder epithelial cells (HGBEC) and 5 gallbladder cancer cell lines (GBC-SD, EH-GB1, NOZ, SGC-996, and MZ-CHA-1; purchased from the Cell Bank of Shanghai Institute of Biochemistry and Cell Biology, Chinese Academy of Sciences, Shanghai, China) were cultured in Dulbecco's modified Eagle's medium (DMEM; Gibco, Carlsbad, USA) with 10% fetal bovine serum (FBS), 1% penicillin (100 U/L) and streptomycin (100 mg/L) in a 5% CO₂ incubator at 37°C. Sub-culture was performed every 2–3 days.

Cell transfection

The synthetic miR-197 mimic (miR-197) and miR-197 inhibitor (in-miR-197), together with corresponding mimic and inhibitor controls, were purchased from GenePharma Inc. (Shanghai, China). The cells were seeded in six-well plates and transfected with miR-197, in-miR-197 or their negative controls using Lipofectamine[®] 2000 transfection reagent (Invitrogen, Thermo Fisher Scientific, Inc., Waltham, USA), based on the manufacturer's guidelines. Briefly, 100 pmol of mimic or inhibitor was added to the mixture of 250 µL of Opti-MEM (Gibco, Thermo Fisher Scientific, Inc.) and 5 µL of Lipofectamine[®] 2000. The mixture was then added into cells ensuring the final concentration of miR-197, in-miR-197 or corresponding controls is 50 nM, and the culture medium was changed 6 h after transfection. After a 48-hour period, the cells were collected for subsequent experiments.

Insulin-like growth factor binding protein 3 (IGFBP3) siRNA (siIGFBP3) and its corresponding negative control were constructed using GENECHM and siIGFBP3 transfection was performed. In brief, the medium was removed from the six-well plate, and 2 mL of serum-containing medium was added without antibiotics into each well. Then, 100 µL of Opti-MEM[®] (Gibco, Thermo Fisher Scientific, Inc.) + 2000 ng of siIGFBP3 plasmid + 10 µL of transfection reagent was added (Invitrogen, Thermo Fisher Scientific, Inc.) to each well of the plate, the plate was vortexed and incubated at room temperature for 10 min. Next,

the transfection mixture was added to a six-well plate and continued to incubate in a 5% CO₂ incubator. The mixture was added to the cells, and the medium changed after 6 h. After 48 h, the cells were collected for further experiments.

Dual luciferase reporter gene assay

We applied the biological database (http://www.targetscan.org/vert_71/) to confirm the relationship between miR-197 and its putative binding sequence of the *IGFBP3* gene. The outcome indicates that the *IGFBP3* gene is one of the target genes of miR-197. Fragments from *IGFBP3* and flanking sequences on each side were synthesized with a short extension containing cleavage sites for XhoI (5'-end) and NotI (3'-end), while the second fragment, containing mutated binding site sequences, was also synthesized. The 2 constructs were termed as WT (wild-type gene) and MT (mutant genes). The fragments were cloned into the psi-CHECKTM-2 vector (Promega, Madison, USA). Then, 293 T-cells (purchased from Cell Bank of the Shanghai Institute of Biochemistry & Cell Biology) were seeded in a six-well plate (Corning Inc., Corning, USA) at a density of 1 × 10⁵ cells per well, and the wild-type *IGFBP3* UTR or mutant *IGFBP3* UTR plasmids (Hanyin, Shanghai, China) with miR-197 mimic using InvitrogenTM Lipofectamine 2000 (Invitrogen) were transfected according to the manufacturer's instructions. After 24 h of incubation, the luciferase activity of the WT and mutated *IGFBP3* UTR was detected using the dual-luciferase reporter assay system (Promega).

Quantitative real-time PCR

Total RNA was extracted from GBC tissues and cells using an RNA extraction kit (Invitrogen); PrimeScript reverse transcription (RT) kit was applied to reverse-transcribe RNA into cDNA. Fluorescent quantitative polymerase chain reaction (qPCR) was performed with SYBR[®] Premix Ex TaqTM II solution kit using the ABI PRISM[®] 7300 system (Applied Biosystems, Foster City, USA). The primers for real-time PCR (RT-PCR) are shown in Table 1. *U6* was used as the internal reference for miR-197, and *GAPDH* was applied as the endogenous control for mRNA. The data was analyzed using the 2^{-ΔΔCt} method.⁹

Table 1. Primers (mRNA) for real-time PCR

Name	Sequences
miR-197	5'-TTCACCACCTTCTCCACCCAGC-3' (forward)
	5'-TGCACTGGTCCAAGCTCTAACC-3' (reverse)
U6	5'-CTCGCTTCGGCAGCACA-3" (forward)
	5'-AACGCTTCACGAATTTG CGT-3' (reverse)
IGFBP3	5'-GAGGGCGACACTGCTTTTTC-3' (forward)
	5'-CCAGCT CCAGGAAATGCTAG-3' (reverse)
GAPDH	5'-GAAGGTGAAGGTCGGAGTC-3' (forward)
	5'-AAGATGGTATGGGATTTTC-3' (reverse)

Western blotting analysis

SGC-996 and MZ-CHA-1 cells were washed twice with ice-cold PBS, then incubated in lysis buffer (150 mM NaCl, 1% Nonidet P-40, 0.1% SDS, 2 mg/mL of aprotinin, and 1 mM phenylmethylsulfonyl fluoride (PMSF)) for 30 min. The supernatants were centrifuged at 12,000 × g for 15 min at 4°C, and retained for protein extraction. The protein (30 μg) was subjected to sodium dodecyl sulfate salt – polyacrylamide gel electrophoresis (SDS-PAGE 10% (w/v) acrylamide gel) and blotted onto polyvinylidene difluoride (PVDF) membranes, which were washed for 1 h with a blocking solution. The membranes were incubated overnight at 4°C with anti-IGFBP3 (1:1000; ab220429; Abcam Inc., Cambridge, USA), anti-ERK1/2 (1:1000; 9102; Cell Signaling Technology (CST), Beverly, USA), anti-p-ERK1/2 (1:1000; 4370; CST), anti-AKT (1:1000; 4691; CST), anti-p-AKT (1:1000; 4060; CST), and anti-glyceraldehyde-3-phosphate dehydrogenase (GAPDH) (1:2000; ATA29666; Zhongshan Golden Bridge Biotechnology, Beijing, China) antibodies. The next day, membranes were incubated with a secondary anti-rabbit or anti-mouse horseradish peroxidase (HRP)-conjugated antibody (1:1000; Zhongshan Golden Bridge Biotechnology). Finally, the relative expression levels of protein bands were analyzed using ImageJ software (National Institutes of Health, Bethesda, USA).

TdT-mediated dUTP nick-end labeling (TUNEL) staining

Based on the instructions of the Biyuntian TUNEL Apoptosis Detection Kit, genomic DNA was cut, and on the exposed 3'-OH end, a dUTP-GFP base was fixed that could be directly viewed under a microscope. The specific steps were as follows: cells were fixed with 4% paraformaldehyde and then permeabilized with 0.1% Triton X-100 for 2 min. The TUNEL reaction mixture was added to react for 60 min, and then with Converter-POD for 30 min. After washing, the cells were stained in 100 μL of DAPI nuclear staining reagent (Sigma-Aldrich, St. Louis, USA) for 10 min. The stained cells were observed under the Olympus BX-53 fluorescence microscope and the images were captured using a digital camera (Olympus Corp., Tokyo, Japan) with a ×10 magnification. Nine fields per slide were then randomly selected. The number of TUNEL-positive cells was counted and averaged on each field of view. The results were expressed as mean ± standard error of the mean (SEM).

Colony formation assay

The colony formation assay is conducted in a six-well plate in which cells were seeded at a density of 8 × 10² cells/well and cultured for 2 weeks, and then the colonies were

fixed with 4% paraformaldehyde and stained with 0.1% crystal violet (Sigma-Aldrich). The number of colonies was counted, and the experiment was independently repeated 3 times to ensure accuracy.

Flow cytometry

The cells of each group were suspended, collected and washed twice with saline. After that, the cells were fixed with 70% ethanol. Then, 100 μ L of cell suspension was added to a 5-mL culture tube, and subsequently 5 μ L of FITC-labeled Annexin-V (1:20, C1062S; Biotechnology, Shanghai, China) and 5 μ L of propidium iodide (PI) (1:20, C1062S) were added, mixed and incubated in the dark at room temperature for 15 min. After incubation, 400 μ L of 1X binding buffer was added, ensuring precise and accurate movements the whole procedure. Next, cell apoptosis was detected using flow cytometry (BD FACS Canto II; Becton Dickinson, Franklin Lakes, USA).

Cell Counting Kit-8 assay

The transfected cells were seeded into 96-well plates (1×10^3 cells/well) with added Cell Counting Kit-8 (CCK-8; Invitrogen) according to the manufacturer's protocol. Cell proliferation was detected through the optical density (OD) value (570 nm).

Statistical analyses

The IBM SPSS v. 21.0 software (IBM Corp. Armonk, USA) was utilized for data processing. The Kolmogorov–Smirnov test was used to check whether data was distributed normally. Data are presented as mean \pm standard deviation (SD). Comparisons between 2 groups were analyzed using a Student's t-test and comparisons among

multiple groups were analyzed using one-way or two-way analysis of variance (ANOVA), followed by the Tukey's multiple comparisons test. Kaplan–Meier method was used for survival analysis. The p-value was calculated using a two-tailed test and $p < 0.05$ indicated a statistically significant difference.

Results

MiR-197 was highly expressed in GBC tissues

To date, there is no study that focuses on whether miR-197 regulates the occurrence and development of GBC. Through a bioinformatics analysis (<http://www.ncbi.nlm.nih.gov/geo/>), we found that miR-197 was highly expressed in GBC tissues (Fig. 1A). Furthermore, there is a significant upregulation of miR-197 in tumor tissues ($p < 0.05$) when compared to healthy gallbladder tissue (Fig. 1B). Then, according to the median expression of miR-197, the 39 patients examined in this study were categorized into a high (\geq median miR-197 expression; $n = 19$) or low expression group ($<$ median miR-197 expression; $n = 20$), and the baseline characteristics of different groups were compared (Table 2). The results showed that the expression of miR-197 was significantly correlated with T classification, also known as the depth of tumor invasion ($p < 0.05$). Kaplan–Meier analysis showed that the expression of miR-197 was closely related to the poor prognosis of the GBC patients (Fig. 1C). Additionally, compared with normal gallbladder cells (HGBEC), GBC cell lines (EH-GB1, NOZ, SGC-996, and MZ-CHA-1) had higher expression of miR-197 ($p < 0.05$), and of these cell lines, the upregulated expression of miR-197 in SGC-996 and MZ-CHA-1 cells was statistically significant (Fig. 1D).

Table 2. Correlation between clinicopathological characteristics and miR-197 expression in 39 patients with GBC

Characteristics		miR-197 expression (median expression 8.374)		p-value
		low	high	
Age	<56	11 (28.2%)	9 (23.1%)	0.634
	>56	9 (23.1%)	10 (25.6%)	
Gender	male	12 (30.8%)	9 (23.1%)	0.429
	female	8 (20.5%)	10 (25.6%)	
T classification	1–2	14 (35.9%)	6 (15.4%)	0.016
	3–4	6 (15.4%)	13 (33.3%)	
N classification	0	11 (28.2%)	11 (28.2%)	0.855
	1–2	9 (23.1%)	8 (20.5%)	
Distant metastasis	no	10 (25.6%)	9 (23.1%)	0.870
	yes	10 (25.6%)	10 (25.6%)	
Pathologic stage	1–2	9 (23.1%)	10 (25.6%)	0.634
	3–4	11 (28.2%)	9 (23.1%)	

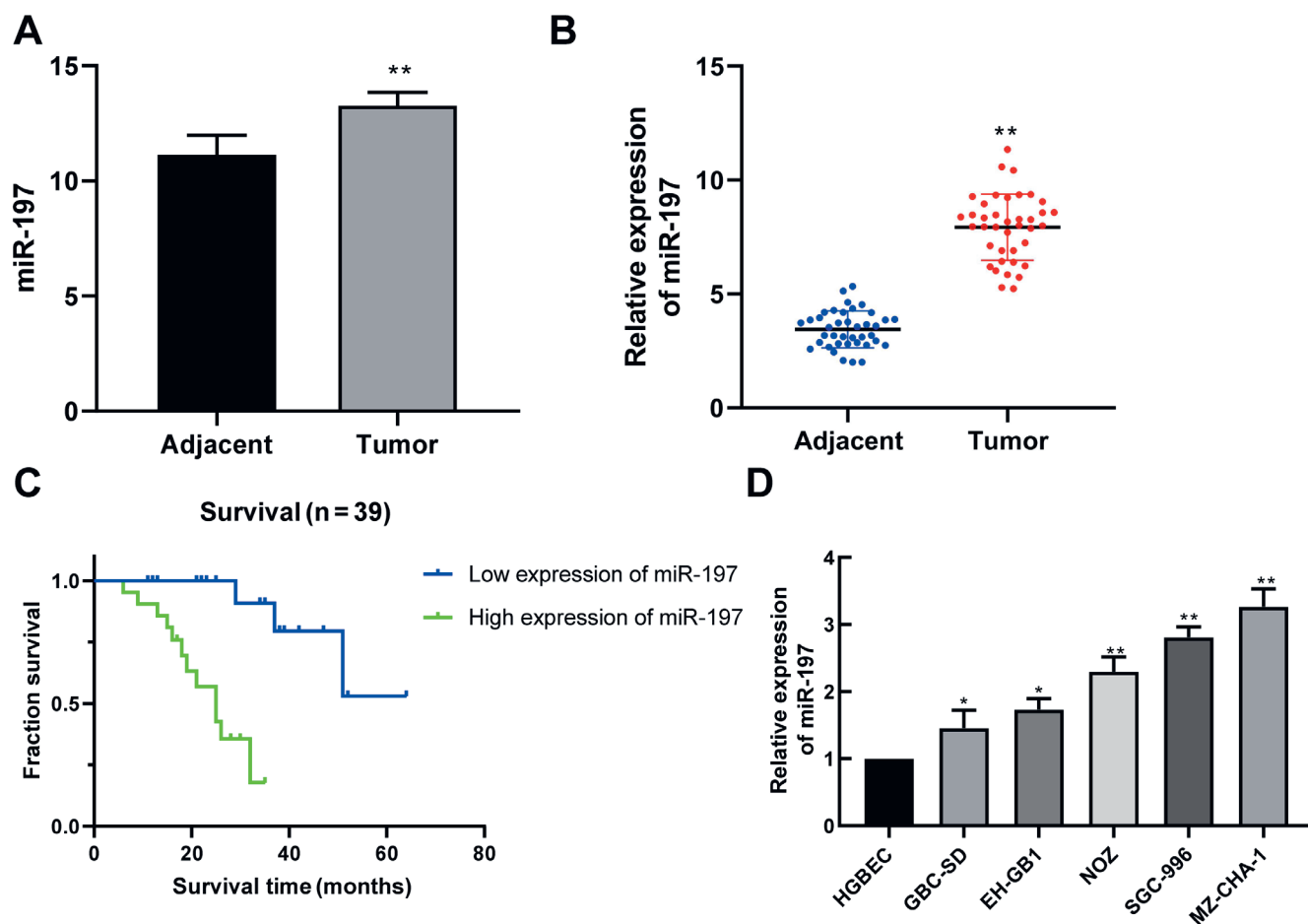


Fig. 1. MiR-197 is highly expressed in GBC tissues and cells. A. Bioinformatics analysis (<http://www.ncbi.nlm.nih.gov/geo/>) of the expression of miR-197 in GBC. **compared with the adjacent group, $p < 0.01$; B. The expression of miR-197 in GBC tissues and adjacent normal tissues was detected using qRT-PCR. U6 was used as endogenous control. **compared with the adjacent group, $p < 0.01$; C. Kaplan–Meier analysis observed the correlation between expression of miR-197 and survival; D. The expression of miR-197 in HGBEC, GBC-SD, EH-GB1, NOZ, SGC-996, and MZ-CHA-1 cell lines was detected using qRT-PCR, and U6 was used as endogenous control. *compared with HGBEC group, $p < 0.05$. Data represent the mean \pm SD (n = 3)

Downregulation of miR-197 impeded cell proliferation and promoted apoptosis of GBC cells

To study the role of miR-197 in GBC cells, the miR-197 inhibitor in-miR-197 was applied to GBC cells, while a random sequence was used as a negative control (in-NC), and transiently transfected into SGC-996 and MZ-CHA-1 cell lines. After 48 h, miR-197 expression was significantly reduced in SGC-996 and MZ-CHA-1 cells (both $p < 0.01$; Fig. 2A). Then, CCK-8 and plate cloning experiments were used to test the effect of miR-197 on cell proliferation. These results demonstrated that in-miR-197 significantly inhibited cell proliferation compared with cells in the in-NC group (Fig. 2B), with a concomitant significant reduction in the number of clones (both $p < 0.01$; Fig. 2C). We then observed reduced miR-197 in SGC-996 and MZ-CHA-1 cells resulted in a significant increase in both the apoptosis rate (both $p < 0.01$; Fig. 2D), and the number of TUNEL-positive cells (both $p < 0.01$; Fig. 2E). The above results showed that downregulation of miR-197 inhibited GBC cell proliferation and promoted apoptosis.

MiR-197 regulated the expressions of proliferation pathway and apoptosis pathway-related proteins

As mentioned above, downregulation of miR-197 inhibited the proliferation of GBC cells and promoted apoptosis. This prompted us to explore the regulatory role of miR-197 in proliferation/apoptosis signaling pathways. It was demonstrated that miR-197 was significantly elevated in MZ-CHA-1 cells after transfection with miR-197 (Supplementary Fig. 6A), causing a subsequent upregulation of p-ERK1/2, p-AKT and Bcl-2, and downregulated the expression of c-caspase-3 and Bax (Fig. 3A–C). Inhibition of miR-197 with in-miR-197 significantly downregulated the expression of p-ERK1/2, p-AKT and Bcl-2, and upregulated the expression of c-caspase-3 and Bax (Fig. 3A,B,D). From the data above, it is reasonable to conclude that upregulation of miR-197 stimulated ERK and AKT pathways, and inhibited the Bax/Bcl-2 and caspase-3 pathways, while downregulation of miR-197 showed the opposite effect.

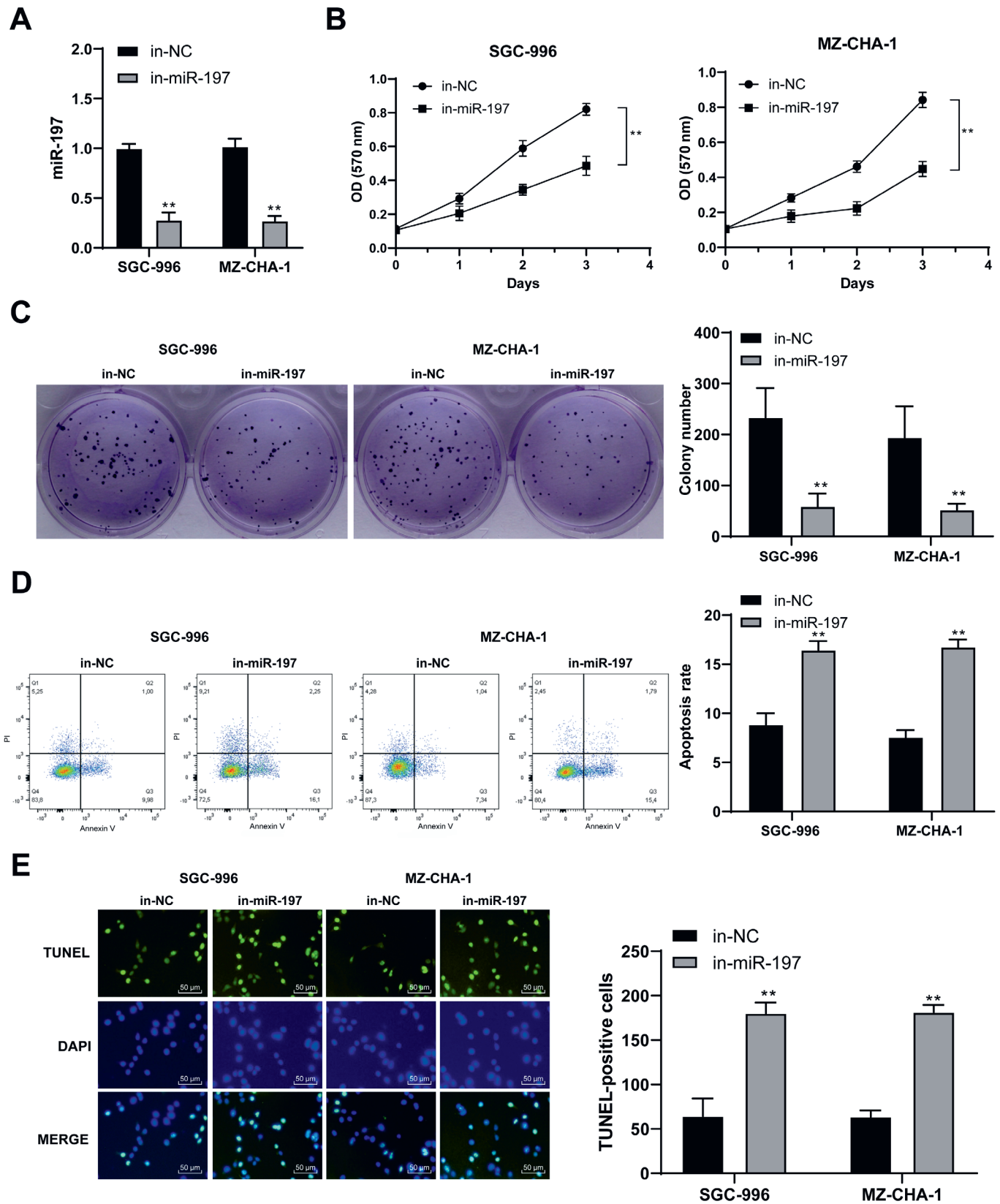


Fig. 2. Downregulation of miR-197 impedes cell proliferation and promotes apoptosis in GBC cells. SGC-996 and MZ-CHA-1 cells were transfected with in-miR-197. A. MiR-197 expression was detected using qRT-PCR; B. OD value (at 570 nm) was detected on day 1–5; C. Cloning number was counted; D. Apoptosis rate was observed with flow cytometry; E. Apoptosis-positive cells were observed using TUNEL experiment. Data represent the mean \pm SD ($n = 3$)

*compared with in-NC, $p < 0.05$, **compared with in-NC, $p < 0.01$.

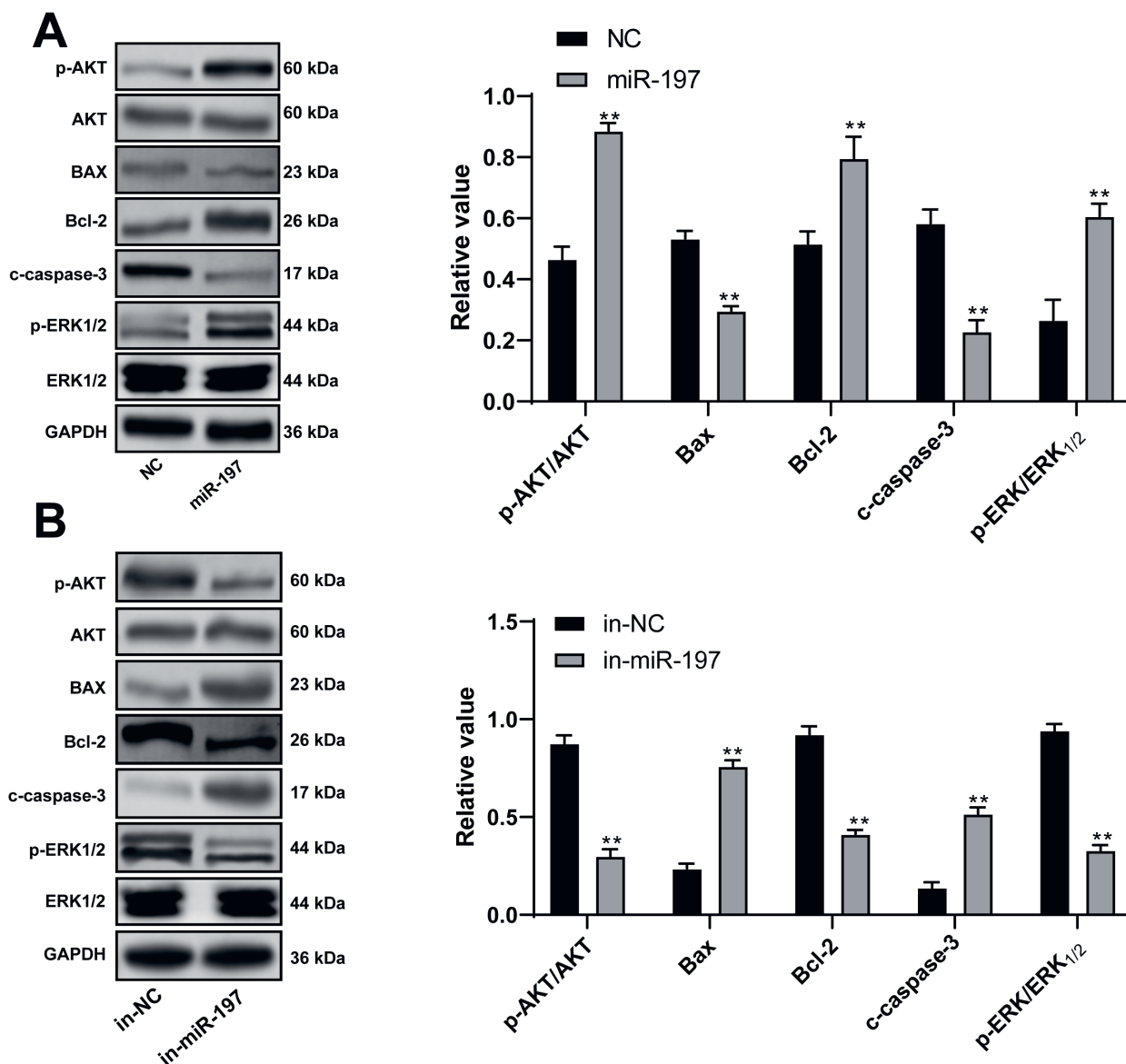


Fig. 3. MiR-197 regulates the expression of proliferation pathway proteins p-ERK1/2 and p-AKT and apoptosis pathway proteins Bax/Bcl-2 and c-caspase-3. A and B. MZ-CHA-1 cells were transfected with miR-197/in-miR-197, and western blotting analysis was used to detect the expression of p-ERK1/2 (42KD), p-AKT (60KD), Bax (21KD), Bcl-2 (26KD), and c-caspase-3 (17KD); C and D. Statistical analysis. Data represent the mean \pm SD (n = 3)

*compared with NC/in-NC, $p < 0.05$.

MiR-197 inhibited the expression of *IGFBP3*

MiRNA regulates cell proliferation and apoptosis by regulating its downstream target genes. Therefore, we predicted which mRNA may be targeted by miR-197 using an online database (http://www.targets can.org/vert_71/) to further explore the mechanism of miR-197 regulation of GBC cell proliferation and apoptosis. The predicted results revealed that the *IGFBP3* gene, which is closely related to tumor proliferation, is one of the target genes of miR-197. The binding sites of *IGFBP3* mRNA and miR-197 are shown in Fig. 4A. We used a dual luciferase reporter gene assay to verify this relationship. When co-transfected with the *IGFBP3* WT reporter plasmid, miR-197 significantly reduced luciferase activity compared with the NC group,

and the mutated reporter plasmid eliminated miR-197-mediated inhibitory effect on the luciferase activity (both $p < 0.05$) (Fig. 4B). These results demonstrated that miR-197 and *IGFBP3* mRNA closely interact.

In order to show whether miR-197 can affect the expression of *IGFBP3* in GBC, the SGC-996 cell line was transfected with miR-197, in-miR-197 and their NCs; then, the expression of *IGFBP3* at the mRNA and protein levels was examined. After transfection with miR-197, the mRNA level of *IGFBP3* in SGC-996 cells was significantly reduced, while transfection with in-miR-197 caused a significant increase in the mRNA level of *IGFBP3* (all $p < 0.05$; Fig. 4C). Upregulation of miR-197 caused a decrease in *IGFBP3* protein expression, while downregulation of miR-197 exerted the reverse effect (all $p < 0.05$; Fig. 4D). Compared with

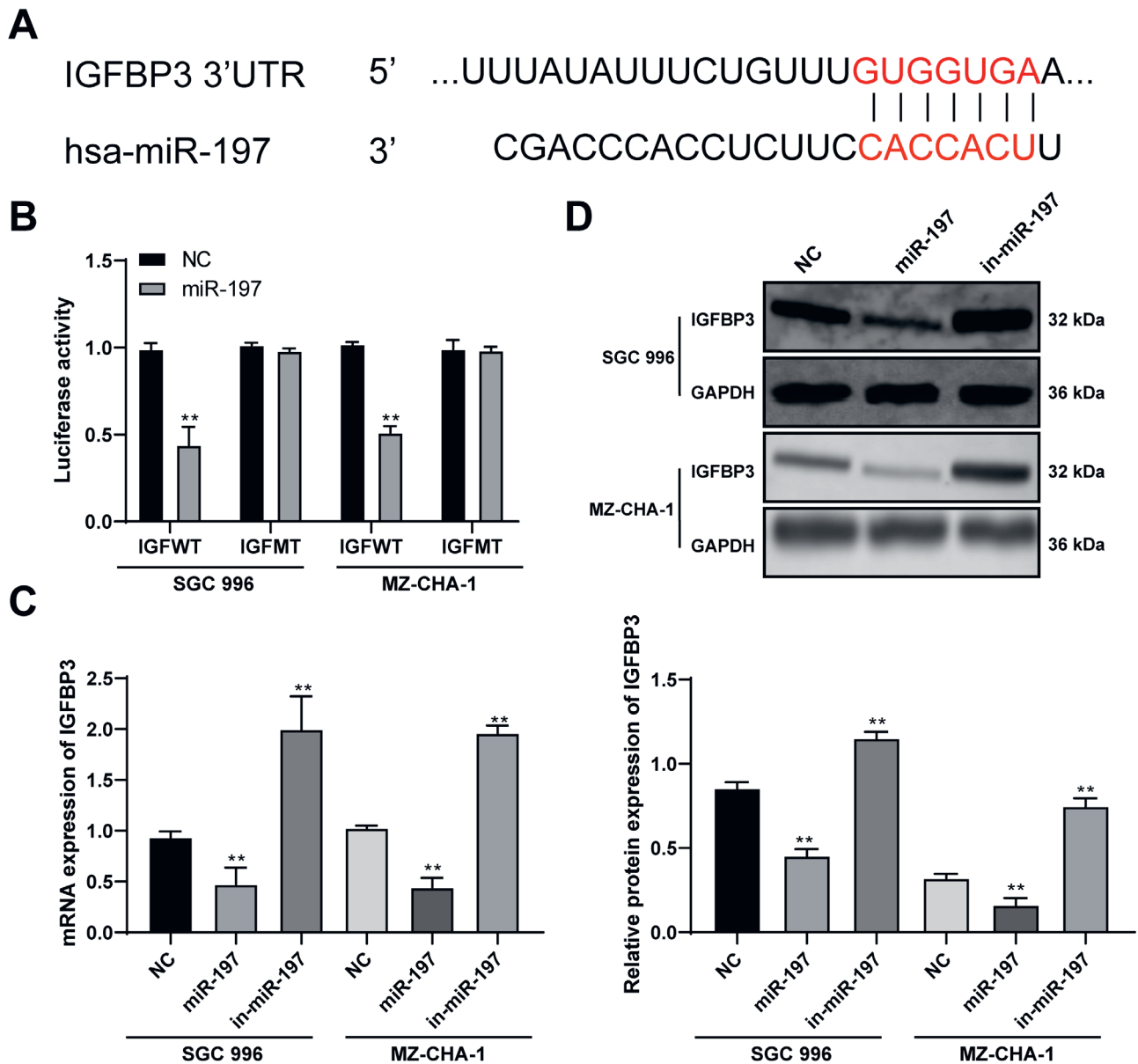


Fig. 4. MiR-197 inhibits the expression of *IGFBP3*. A. The miR-197 target sequence predicted in the 3'UTR of *IGFBP3*; B. SGC-996 and MZ-CHA-1 cells were co-transfected with miR-197 and *IGFBP3* WT or MT, and the luciferase activity was determined; C and D. SGC-996 and MZ-CHA-1 cells were transfected with miR-197/in-miR-197, and the expression of *IGFBP3* (32KD) was detected using qRT-PCR and western blotting analysis. Data represent the mean \pm SD (n = 3)

*compared with NC, $p < 0.05$; **compared with NC, $p < 0.01$.

the adjacent tissues, the *IGFBP3* expression in tumor tissues was significantly reduced (Supplementary Fig. 6B). These results indicated that *IGFBP3* was one of the target genes of miR-197 in GBC cells.

The siIGFBP3 could partially reverse the effect caused by miR-197 downregulation

The above results indicated that *IGFBP3* may participate in the miR-197-regulated proliferation and apoptosis of GBC cells, which prompted us to further explore its role. Firstly, we were able to effectively silence siIGFBP3 in MZ-CHA-1 cells (Fig. 5A,B). Then, transfection of the cells

with miR-197 inhibitor combined with siIGFBP3 (in-miR-197+siIGFBP3) increased the number of cell clones (Fig. 5C) when analyzed by the OD value (570 nm) (Fig. 5D). This group (in-miR-197+siIGFBP3) also had a lower apoptosis rate compared with the in-miR-197 group (Fig. 5E), suggesting that siIGFBP3 can partially inhibit the elevated apoptosis induced by miR-197 downregulation.

Discussion

Investigation on the pathophysiology of GBC is critical due to its high recurrence rate and poor prognosis. To date, there is no report on the role of miR-197 during the disease

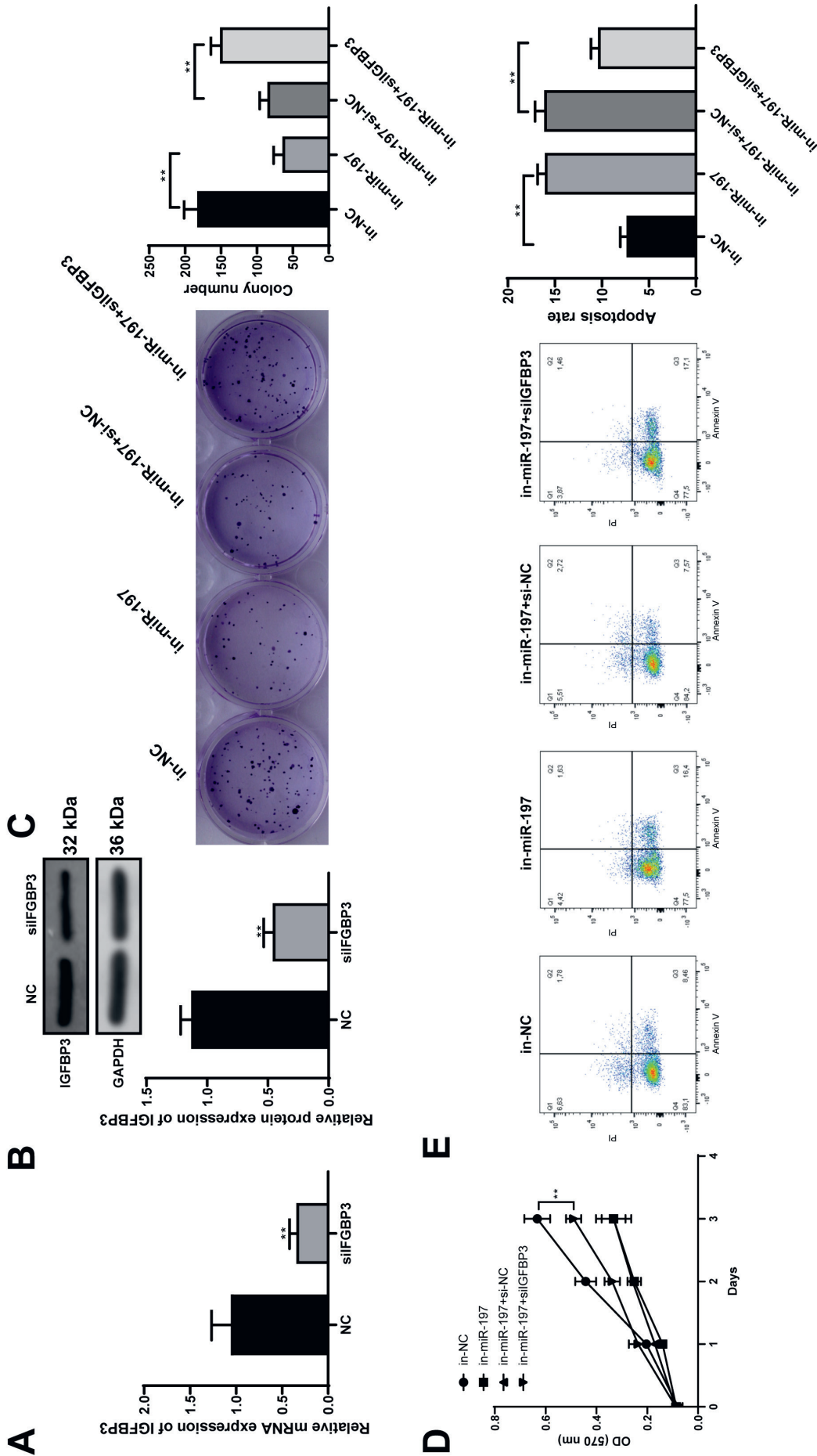


Fig. 5. siIGFBP3 partially inhibits the decrease in proliferation and the increase in apoptosis induced by miR197 downregulation. MZ-CHA-1 cells were transfected with in-miR-197 and/or siIGFBP3. A and B. The qRT-PCR and western blotting analysis were used to detect the expression of IGFBP3 (32KD); C and D. Colony formation assay and CCK-8 assay were conducted; E. Flow cytometry was used to detect the apoptosis rate. Data represent the mean \pm SD (n = 3)

*compared with NC; p < 0.05; **compared with NC; p < 0.01.

process. In this study, we found that miR-197 was highly expressed in GBC tissues, and the expression of miR-197 was closely related to the poor prognosis of GBC. MiR-197 was highly expressed in GBC cells, and downregulation of miR-197 inhibited GBC cell proliferation and promoted apoptosis. It acts through decreasing the expression of proliferation-related proteins p-ERK1/2 and p-AKT, while increasing expression of apoptosis pathway-related proteins Bax/Bcl-2 and c-caspase-3. Upregulation of miR-197, on the other hand, induced an opposite trend. MiR-197 directly regulated *IGFBP3*, as shown by silencing the gene using siIGFBP3, which partially inhibited the decrease of proliferation and the increase of apoptosis induced by downregulation of miR-197.

The function of miR-197 in oncogenesis and development is very complicated. Fiori et al. reported that miR-197 promotes tumor progression by inhibiting the apoptosis of p53 WT cells in non-small cell lung cancer (NSCLC).¹⁰ However, it also exerts a tumor suppressor function in multiple myeloma.¹¹ Moreover, miR-197 inhibits the proliferation of glioma cells,¹² but promotes the progression of stomach,¹³ pancreas,¹⁴ colorectal tumors,¹⁵ and hepatocellular carcinoma.¹⁶ Clinical studies have shown that miR-197 is of great clinical significance, and it might serve as a promising prognostic biomarker to be used to monitor several types of malignant tumors. For example, miR-197 relates to the poor outcome and distant metastases in patients with NSCLC while its expression is also relevant to the size of the tumor and histopathological classification.¹⁷ A meta-analysis confirmed that compared with a single miRNA, a group of multiple miRNAs may bear greater predictive ability.¹⁸ Recent studies demonstrated that compared with the normal population, serum miR-197 expression in NSCLC patients is significantly higher, and the expression of miR-145 is remarkably reduced. These changes are related to the clinical stages and pathological classifications of NSCLC patients, and the combination of miR-197 and miR-145 has a high sensitivity for diagnosing NSCLC.¹⁹ To date, there is no prior research of the function of miR-197 in GBC. In this study, the expression of miR-197 in the tumor tissues of GBC patients was found to be significantly higher in GBC tissues, which was consistent with the results of bioinformatics analysis.⁸ Subsequently, in 2 different GBC cell lines, downregulation of miR-197 inhibited the proliferation of GBC cells and promoted apoptosis, while upregulation induced the opposite effect. Therefore, it is possible to elucidate the biological activity of miR-197 in GBC and its regulatory mechanism for the first time.

In the present study, a target of miR-197 was shown to be *IGFBP3*, which plays an important role in tumor progression through different molecular pathways. On the one hand, *IGFBP3* attenuates the signal transduction downstream of IGF1R1 induced by IGF1 by interfering with the binding between IGF1 and IGF1R.²⁰ The IGF1/IGF1R

axis can stimulate epithelial to mesenchymal transition and promote the metastasis of various tumors.^{21,22} On the other hand, *IGFBP3* can also inhibit tumor progression in an independent manner. For example, *IGFBP3* inhibits head and neck squamous cell carcinoma by blocking the c-jun and c-fos pathways.²³ It also inhibits the progression of prostate cancer by degrading the NF- κ B signaling.²⁴ However, the function of *IGFBP3* is still controversial. Chan et al. indicated that high expression of *IGFBP3* is associated with an increased incidence of colorectal cancer in elderly males, which is independent of IGF1.²⁵ It is suggested that *IGFBP3* may have differential actions in different tumors. To date, however, no studies have reported whether *IGFBP3* is involved in the progression of GBC. Our results indicated that upregulation of miR-197 caused *IGFBP3* inhibition, that miR-197 downregulation led to *IGFBP3* overexpression, and finally silencing *IGFBP3* could partly reverse the effect induced by miR-197 suppression. Hence, it can be concluded that *IGFBP3* plays a role in inhibiting GBC progression. In the current study, miR-197 upregulation caused a decrease in the expression of *IGFBP3*, which promoted the upregulation of p-ERK1/2, p-AKT and Bcl-2 in GBC cells, and downregulation of Bax and caspase-3, all of which could be reversed after downregulation of miR-197.

Previous studies have found that *IGFBP3* plays an important role in regulating tumor cell proliferation and apoptosis. Chen et al. found that *IGFBP3* is an indicator of poor prognosis in patients with glioma, and reducing its expression can inhibit tumor growth by inducing apoptosis of glioma cells.²⁶ Day et al. found that using *IGFBP3* siRNA to treat NSCLC cells with TNFAIP8 knockdown can upregulate pAKT levels and promote cell proliferation.²⁷ By blocking the IGF1 signal cascade, it was possible to confirm to a certain degree that overexpression of *IGFBP3* can induce apoptosis in NSCLC cells in vitro and enhance cellular response to cisplatin.²⁸ In lung adenocarcinoma and hepatocellular carcinoma, testis-specific protein Y-linked 1 (TSPY1) can directly bind to the promoter of *IGFBP3* to inhibit its expression. Downregulation of *IGFBP3* activates the PI3K/AKT and RAS/RAF/MEK/ERK signaling pathway, thereby promoting tumor cell proliferation.²⁹ Overall, the mechanisms of *IGFBP3* on tumor cell regulation varies significantly, and that this difference is likely tumor-specific.

Clinical implications

The results of the five-year survival analysis of patients recruited to the present study suggest that miR-197 expression is associated with poor prognosis in GBC. This implies that increased expression of miR-197 can be used clinically as a prognostic marker. Since the downregulation of miR-197 inhibited proliferation and promoted apoptosis of GBC cells, it is tempting to speculate that the miR-197-IGFBP3 axis might serve as a therapeutic target in patients with GBC.



Limitations

In this study, patients with miR-197 overexpression in tumor tissues had short OS, but OS was not consistent with clinicopathological characteristics. The reason could be attributed to the past surgical history of the patients. Therefore, there was a lack of diversity of clinical stages amongst that recruited patients in the 2 groups of high or low miR-197 expression. In addition, the sample size of this study is relatively small, which also diminishes the quality of this study. The best way to determine the impact of miR-197 on GBC cell lines would be to determine the *IGFBP3* function in cell proliferation. Therefore, further research could focus on identifying the effect of *IGFBP3* on cell proliferation. Moreover, detection of miR-197 levels in patients' peripheral blood can also be performed, which would further support miR-197 as a promising clinical marker.

Conclusions

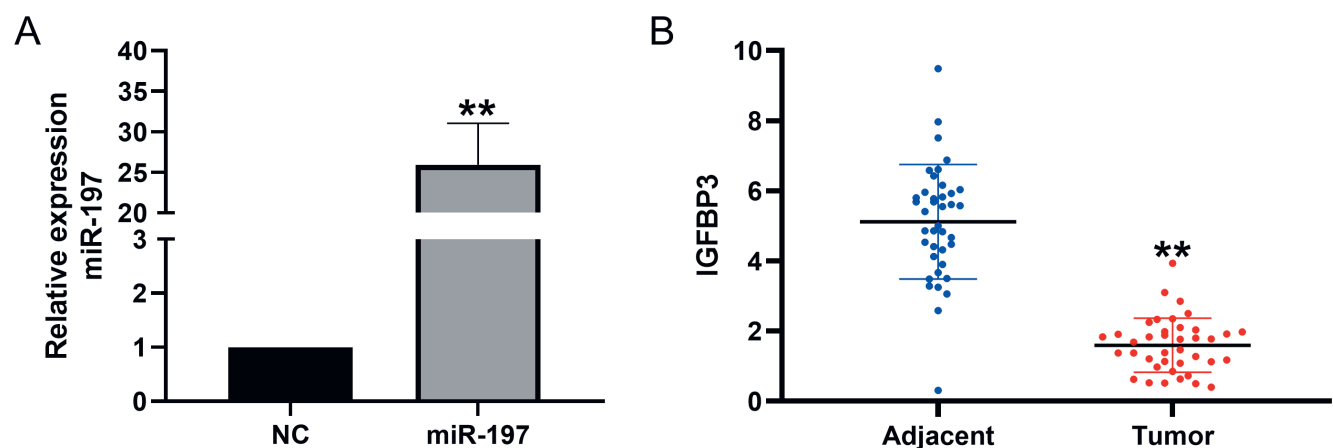
Our study demonstrated that the miR-197/*IGFBP3* axis regulates the proliferation and apoptosis of GBC cells. Downregulation of miR-197 inhibits the proliferation and promotes the apoptosis of GBC cells, indicating its potential use as a molecular target in the treatment of GBC.

ORCID iDs

Jinglin Cheng  <https://orcid.org/0000-0001-7651-4188>
 Li Tong  <https://orcid.org/0000-0002-9060-9076>
 Heping Zuo  <https://orcid.org/0000-0001-6354-0555>
 Jingrong Li  <https://orcid.org/0000-0002-3945-6713>

References

- Gamboa AC, Maithe SK. The Landmark Series: Gallbladder cancer. *Ann Surg Oncol*. 2020;27(8):2846–2858. doi:10.1245/s10434-020-08654-9
- Mao W, Deng F, Wang D, Gao L, Shi X. Treatment of advanced gallbladder cancer: A SEER-based study. *Cancer Med*. 2020;9(1):141–150. doi:10.1002/cam4.2679
- Baiu I, Visser B. Gallbladder cancer. *JAMA*. 2018;320(12):1294. doi:10.1001/jama.2018.11815
- Sharma A, Sharma KL, Gupta A, Yadav A, Kumar A. Gallbladder cancer epidemiology, pathogenesis and molecular genetics: Recent update. *World J Gastroenterol*. 2017;23(22):3978–3998. doi:10.3748/wjg.v23.i22.3978
- Shroff RT, Kennedy EB, Bachini M, et al. Adjuvant therapy for resected biliary tract cancer: ASCO Clinical Practice Guideline. *J Clin Oncol*. 2019;37(12):1015–1027. doi:10.1200/JCO.18.02178
- Chandra V, Kim JJ, Mittal B, Rai R. MicroRNA aberrations: An emerging field for gallbladder cancer management. *World J Gastroenterol*. 2016;22(5):1787–1799. doi:10.3748/wjg.v22.i5.1787
- Wang DD, Chen X, Yu DD, et al. miR-197: A novel biomarker for cancers. *Gene*. 2016;591(2):313–319. doi:10.1016/j.gene.2016.06.035
- Goepfert B, Truckenmueller F, Ori A, et al. Profiling of gallbladder carcinoma reveals distinct miRNA profiles and activation of STAT1 by the tumor suppressive miRNA-145-5p. *Sci Rep*. 2019;9(1):4796. doi:10.1038/s41598-019-40857-3
- Zhou N, Sun Z, Li N, et al. miR197 promotes the invasion and migration of colorectal cancer by targeting insulin-like growth factor binding protein 3. *Oncol Rep*. 2018;40(5):2710–2721. doi:10.3892/or.2018.6640
- Fiori ME, Barbini C, Haas TM, et al. Antitumor effect of miR-197 targeting in p53 wild-type lung cancer. *Cell Death Differ*. 2014;21(5):774–782. doi:10.1038/cdd.2014.6
- Yang Y, Li F, Saha MN, Abdi J, Qiu L, Chang H. miR-137 and miR-197 induce apoptosis and suppress tumorigenicity by targeting MCL-1 in multiple myeloma. *Clin Cancer Res*. 2015;21(10):2399–2411. doi:10.1158/1078-0432.CCR-14-1437
- Tian LQ, Liu EQ, Zhu XD, Wang XG, Li J, Xu GM. MicroRNA-197 inhibits cell proliferation by targeting GAB2 in glioblastoma. *Mol Med Rep*. 2016;13(5):4279–4288. doi:10.3892/mmr.2016.5076
- Xu L, Hou Y, Tu G, et al. Nuclear Drosha enhances cell invasion via an EGFR-ERK1/2-MMP7 signaling pathway induced by dysregulated miRNA-622/197 and their targets LAMC2 and CD82 in gastric cancer. *Cell Death Dis*. 2017;8(3):e2642. doi:10.1038/cddis.2017.5
- Hamada S, Satoh K, Miura S, et al. miR-197 induces epithelial-mesenchymal transition in pancreatic cancer cells by targeting p120 catenin. *J Cell Physiol*. 2013;228(6):1255–1263. doi:10.1002/jcp.24280
- Huang Q, Ma B, Su Y, et al. miR-197-3p represses the proliferation of prostate cancer by regulating the VDAC1/AKT/beta-catenin signaling axis. *Int J Biol Sci*. 2020;16(8):14171426. doi:10.7150/ijbs.42019
- Dai W, Wang C, Wang F, et al. Anti-miR-197 inhibits migration in HCC cells by targeting KAI1/CD82. *Biochem Biophys Res Commun*. 2014;446(2):541–548. doi:10.1016/j.bbrc.2014.03.006
- Mavridis K, Gueugnon F, Petit-Courty A, et al. The oncomiR miR-197 is a novel prognostic indicator for non-small cell lung cancer patients. *Br J Cancer*. 2015;112(9):1527–1535. doi:10.1038/bjc.2015.119
- Wang R, Wen H, Xu Y, et al. Circulating microRNAs as a novel class of diagnostic biomarkers in gastrointestinal tumors detection: A meta-analysis based on 42 articles. *PLoS One*. 2014;9(11):e113401. doi:10.1371/journal.pone.0113401
- Sui A, Zhang X, Zhu Q. Diagnostic value of serum miR197 and miR145 in non-small cell lung cancer. *Oncol Lett*. 2019;17(3):3247–3252. doi:10.3892/ol.2019.9958



Supplementary Fig. 6. A. After miR-197 transfection, the expression of miR-197 in MZ-CHA-1 cells increased significantly (**compared with NC, $p < 0.01$). B. The expression of *IGFBP3* in GBC tissues and adjacent normal tissues was detected using qRT-PCR (**compared with the adjacent group, $p < 0.01$)

20. Valadez-Bustos N, Escamilla-Silva EM, García-Vázquez FJ, Gallegos-Corona MA, Amaya-Llano SL, Ramos-Gómez M. Oral administration of microencapsulated *B. Longum* BAA-999 and lycopene modulates IGF-1/IGF-1R/IGFBP3 protein expressions in a colorectal murine model. *Int J Mol Sci.* 2019;20(17):4725. doi:10.3390/ijms20174275
21. Wang XH, Wu HY, Gao J, Wang XH, Gao TH, Zhang SF. IGF1R facilitates epithelial–mesenchymal transition and cancer stem cell properties in neuroblastoma via the STAT3/AKT axis. *Cancer Manag Res.* 2019;11:5459–5472. doi:10.2147/CMAR.S196862
22. Neuzillet Y, Chapeaublanc E, Krucker C, et al. IGF1R activation and the in vitro antiproliferative efficacy of IGF1R inhibitor are inversely correlated with IGFBP5 expression in bladder cancer. *BMC Cancer.* 2017;17(1):636. doi:10.1186/s12885-017-3618-5
23. Lee HJ, Lee JS, Hwang SJ, Lee HY. Insulin-like growth factor binding protein-3 inhibits cell adhesion via suppression of integrin beta4 expression. *Oncotarget.* 2015;6(17):15150–15163. doi:10.18632/oncotarget.3825
24. Kim H, Datta A, Talwar S, Saleem SN, Mondal D, Abdel-Mageed AB. Estradiol–ERbeta2 signaling axis confers growth and migration of CRPC cells through TMPRSS2-ETV5 gene fusion. *Oncotarget.* 2017;8(38):62820–62833. doi:10.18632/oncotarget.11355
25. Chan YX, Alsonso H, Chubb SAP, et al. Higher *IGFBP3* is associated with increased incidence of colorectal cancer in older men independently of IGF1. *Clin Endocrinol (Oxf).* 2018;88(2):333–340. doi:10.1111/cen.13499
26. Chen CH, Chen PY, Lin YY, et al. Suppression of tumor growth via *IGFBP3* depletion as a potential treatment in glioma. *J Neurosurg.* 2019;132(1):168–179. doi:10.3171/2018.8.JNS181217
27. Day TF, Kallekury BVS, Ross JS, et al. Dual targeting of EGFR and IGF1R in the TNFAIP8 knockdown non-small cell lung cancer cells. *Mol Cancer Res.* 2019;17(5):1207–1219. doi:10.1158/1541-7786.MCR-18-0731
28. Wang YA, Sun Y, Palmer J, et al. *IGFBP3* modulates lung tumorigenesis and cell growth through IGF1 signaling. *Mol Cancer Res.* 2017;15(7):896–904. doi:10.1158/1541-7786.MCR-16-0390
29. Tu W, Yang B, Leng X, et al. Testis-specific protein, Y-linked 1 activates PI3K/AKT and RAS signaling pathways through suppressing *IGFBP3* expression during tumor progression. *Cancer Sci.* 2019;110(5):1573–1586. doi:10.1111/cas.13984

Investigating the inflammatory cascade effect of basophil activation in children with allergic rhinitis or asthma, via the IgE-FcεRI-NF-κB signaling pathway

Yi Qiao^{A-F}, Jie Chen^{A-C,E,F}

Department of Otorhinolaryngology, National Children's Medical Center, Shanghai Children's Medical Center, Shanghai Jiao Tong University School of Medicine, China

A – research concept and design; B – collection and/or assembly of data; C – data analysis and interpretation; D – writing the article; E – critical revision of the article; F – final approval of the article

Advances in Clinical and Experimental Medicine, ISSN 1899–5276 (print), ISSN 2451–2680 (online)

Adv Clin Exp Med. 2021;30(7):673–679

Address for correspondence

Jie Chen
E-mail: hwen9308588@sina.com

Funding sources

None declared

Conflict of interest

None declared

Received on June 9, 2020

Reviewed on June 11, 2020

Accepted on April 13, 2021

Published online on June 11, 2021

Abstract

Background. Allergic rhinitis (AR) is a type I allergic reaction mediated by serum immunoglobulin E (IgE).

Objectives. This study aimed to investigate the basophil activation rate and serum expression of inflammatory factors in AR patients and rats. The involvement of the IgE–FcεRI–nuclear factor kappa B (NF-κB) signaling pathway in the pathogenesis of AR was also explored.

Materials and methods. Thirty patients with pediatric AR (or asthma; untreated) were enrolled in our hospital as the observation group. Fifteen healthy children were selected as the control group. The basophil activation and serum levels of interleukin (IL)-4, IL-5, IL-13, IgE, and prostaglandin D2 (PGD2) in 2 groups of children were detected. Forty-eight male Sprague Dawley rats were randomly divided into group A (AR model group), group B (AR model + IgE inhibitor), group C (AR model + omalizumab), and group D (control). The animal model was established by intraperitoneal injection of ovalbumin and nasal mucosa stimulation. The basophil activation rate, serum levels of IL-4, IL-5, IL-13, IgE, and PGD2 were analyzed.

Results. In children with AR, the blood samples contained mainly activated basophils, whereas the healthy group showed mainly non-activated basophils. The levels of IL-4, IL-5, IL-13, IgE and PGD2 in the serum of the AR group were higher than those in healthy subjects ($p < 0.05$). In animal studies, the blood samples collected from group A were mainly activated basophils, while the samples of the other groups were mainly non-activated basophils. The serum contents of IL-4, IL-5, IL-13, IgE, and PGD2 in group A were significantly higher than those in groups B and C ($p < 0.05$).

Conclusions. Patients with AR showed increased activation of basophils and elevated expression of IL-4, IL-5, IL-13, IgE, and PGD2. The upregulation of *FcεRI* and *NF-κB* was involved in the pathogenesis of AR.

Key words: allergic rhinitis, basophil, IgE-FcεRI-NF-κB

Cite as

Qiao Y, Chen J. Investigating the inflammatory cascade effect of basophil activation in children with allergic rhinitis or asthma, via the IgE-FcεRI-NF-κB signaling pathway. *Adv Clin Exp Med.* 2021;30(7):673–679. doi:10.17219/acem/135756

DOI

10.17219/acem/135756

Copyright

© 2021 by Wrocław Medical University
This is an article distributed under the terms of the Creative Commons Attribution 3.0 Unported (CC BY 3.0) (<https://creativecommons.org/licenses/by/3.0/>)

Background

Allergic rhinitis (AR) is caused by the release of histamine, mediated by serum immunoglobulin E (IgE), after exposure to allergens. A variety of immune cells and cytokines participate in the reaction.¹ The main clinical manifestations are sneezing, nasal itching and nasal mucosal swelling.² The pathogenesis of AR is complex, and is mainly associated with T lymphocyte and B lymphocyte disorders, such as Th2, which plays an important role in the occurrence and development of AR.³ In recent years, the incidence of AR has increased year by year. Compared with adults, children have a higher prevalence, and AR accounts for the majority of outpatient visits in children globally.⁴ According to statistics, the prevalence of AR in China is as high as 11.25%, and that of children under 3 years of age is as high as 20%. The clinical strategy of AR mainly involves anti-allergic treatment, but the clinical efficacy is not good.⁵

Toll-like receptors (TLRs) are widely involved in the occurrence and development of AR. Among them, activating the MyD88 dependent or independent pathways of TLRs to induce an inflammatory response is the main mechanism for the pathogenesis of AR. Both pathways activate nuclear factor kappa B (NF- κ B).^{6–8} It is a transcription factor located in the downstream signaling pathway hub of TLR. It plays a pivotal role in inflammation and the immune response by regulating a cascade amplification cascade effect between immune and inflammatory related factors and inflammatory transmitters. The main form of NF- κ B is the heterodimer, composed of p50 and p65. Normally, NF- κ B binds with its inhibitor protein (I- κ B) to form an inactive trimer, which is mainly confined to the cytoplasm to prevent nuclear uptake of NF- κ B.⁹ However, in stress and inflammatory reaction, cytokines and other factors can phosphorylate, ubiquitinate and degrade I- κ B through one or more signaling pathways, release NF- κ B, then transfer free NF- κ B to the nucleus, and activate a series of transcriptional procedures of immune-related genes to increase their expression, thus promoting large-scale inflammatory cell infiltration and degradation. They aggregate in inflammatory sites, causing or further aggravating inflammatory reactions.^{10–12} Fc ϵ RI is a high-affinity receptor of IgE and plays an important role in IgE-mediated allergic reaction. It is composed of gamma chains of a homologous dimer structure connected by alpha chains, beta chains and disulfide bonds. It exists in the form of a trimer ($\alpha\gamma_2$) and tetramer ($\alpha\beta\gamma_2$) in the human body. It has been found that many kinds of cells in vivo, such as eosinophils, mast cells, basophils, and dendritic cells, all express Fc ϵ RI. It has been confirmed that Fc ϵ RI, expressed by mast cells and basophils, plays an important role in regulating rapid and delayed allergic reactions in AR patients.¹³ This study explored the expression of IgE, Fc ϵ RI and NF- κ B in AR, and provides new ideas and an experimental basis for the prevention and treatment of AR.

Objectives

This study aimed to investigate the basophil activation rate and serum expression of inflammatory factors in AR patients and rats. The involvement of the IgE-Fc ϵ RI-NF- κ B signaling pathway in the pathogenesis of AR was also explored.

Materials and methods

Patients

This observational study included 30 children with AR or asthma (untreated) in Shanghai Children's Medical Center who were collected as observation group, and 15 healthy children who were selected as control group. The diagnosis of AR and asthma followed the "Guidelines for diagnosis, prevention and treatment of bronchial asthma in children"¹⁴ and the "Guidelines for the diagnosis and treatment of AR"¹⁵ by the Chinese Medical Association, respectively. Patients with other types of rhinitis, immune system diseases, infection within 3 months prior to the start of the study, or with long-term use of hormones and drugs were excluded; all the children from the study group met the diagnostic criteria of rhinitis. There was no significant difference in age and sex between the 2 groups ($p > 0.05$). The present study was approved by the ethics committee of the National Children's Medical Center, Shanghai Children's Medical Center, Shanghai Jiao Tong University School of Medicine, China.

Animal study

Forty-eight SPF male Sprague Dawley D rats (age: 3 months, weight: 180–220 g) were purchased from the SJA Laboratory Animal Company (Hunan, China). The animals were randomly divided into 4 groups with 12 rats in each group. In group A, a rat model of AR was established by intraperitoneal injection of ovalbumin and sensitization by nasal mucosal stimulation. No treatment was given after the model was successfully established. In group B, the IgE inhibitor E2_79 (Sigma-Aldrich, St. Louis, USA), which prevents binding of free IgE to Fc ϵ RI was given on the basis of model group. In group C, Omalizumab (Sigma-Aldrich), a recombinant DNA-derived humanized IgG1k monoclonal antibody that specifically binds to free human IgE, was injected into the tail vein on the basis of model group. In group D, a nasal drip was applied with an equivalent amount of saline as the treatment. The animal study was approved by the laboratory animal approval center of the National Children's Medical Center, Shanghai Children's Medical Center, Shanghai Jiao Tong University School of Medicine.

Whole body sensitization

In addition to group D, which received saline only, the other 3 groups were treated with 0.3 mg of ovalbumin as an antigen, 30 mg of as an adjuvant and 1 mL of saline as a suspension, and then given intraperitoneal injection, once every other day, 7 injections in total (the whole treatment lasted 14 days).

Local stimulation and intensified sensitization

After the immune phase of intraperitoneal injection was complete, from the 15th day, the bilateral nasal cavity was stimulated locally with a 10 UL nasal drip of normal saline solution containing 5% ovalbumin, once a day for 7 days. In the control group (D), this replaced by the same dose of normal saline.

Blood samples

Venous blood (2 mL) was extracted from the fasting children with a serum separating tube in the morning. The blood of each group of rats was collected from the eyeball and tail vein 14 days after treatment. The serum samples were separated using centrifugation. Basophils were separated with Percoll gradient centrifugation to reflect the activation rate of basophils. The contents of interleukin (IL)-4, IL-5, IL-13, IgE, and prostaglandin D2 (PGD2) in the serum of the children were detected with enzyme-linked immunosorbent assay (ELISA) using commercial kits (IL-4 cat. No. ab100770, IL-5 cat. No. ab267811, IL-13 cat. No. ab269547, IgE cat. No. ab157736; all from Abcam, Cambridge, USA; and PGD2 from Abbexa cat. No. abx150372; Abbexa, Cologne, Germany). Pearson correlation analysis was performed

to determine the correlation between basophil activation and the serum level of IgE. Basophils in mouse blood samples and the serum expressions of FcεRI and nuclear protein NF-κB were analyzed using western blot.

Western blotting

For western blotting, the extracted proteins were loaded on SDS-PAGE and transferred to polyvinylidene fluoride (PVDF) membranes. The membranes were then incubated with the primary antibodies of anti-NF-κB (ab209795; Abcam) and anti-FcεRI (ab229889; Abcam) followed by a conjugated secondary antibody. The films were scanned following with the EasySee Western Blot Kit (Beijing TransGen Biotech, Beijing, China).

Statistical analyses

The SPSS v. 18.0 statistical software (SPSS Inc., Chicago, USA) was used to process and analyze the data, and the measurement data were described as mean ± standard deviation (SD). Univariate analysis of variance (ANOVA) was used for multi-group comparison; we also conducted correlation analysis. Comparison between 2 groups was performed using Student's t-test and χ^2 tests were conducted for rates. A value of $p < 0.05$ was considered statistically significant.

Results

Activation rate of basophils in different groups

Figure 1A shows the activation rate of basophils in patients with AR, and Fig. 1B shows the activation rate

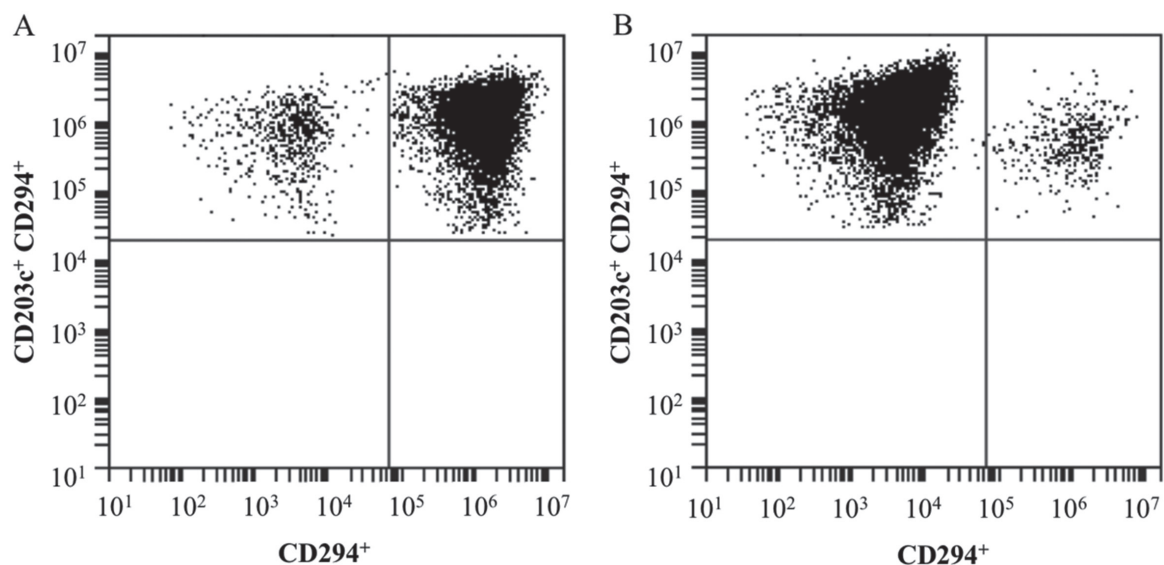


Fig. 1. Activation rate of basophils in different groups. A. Activated and inactivated basophils in AR patients; B. Activated and inactivated basophils in the control group

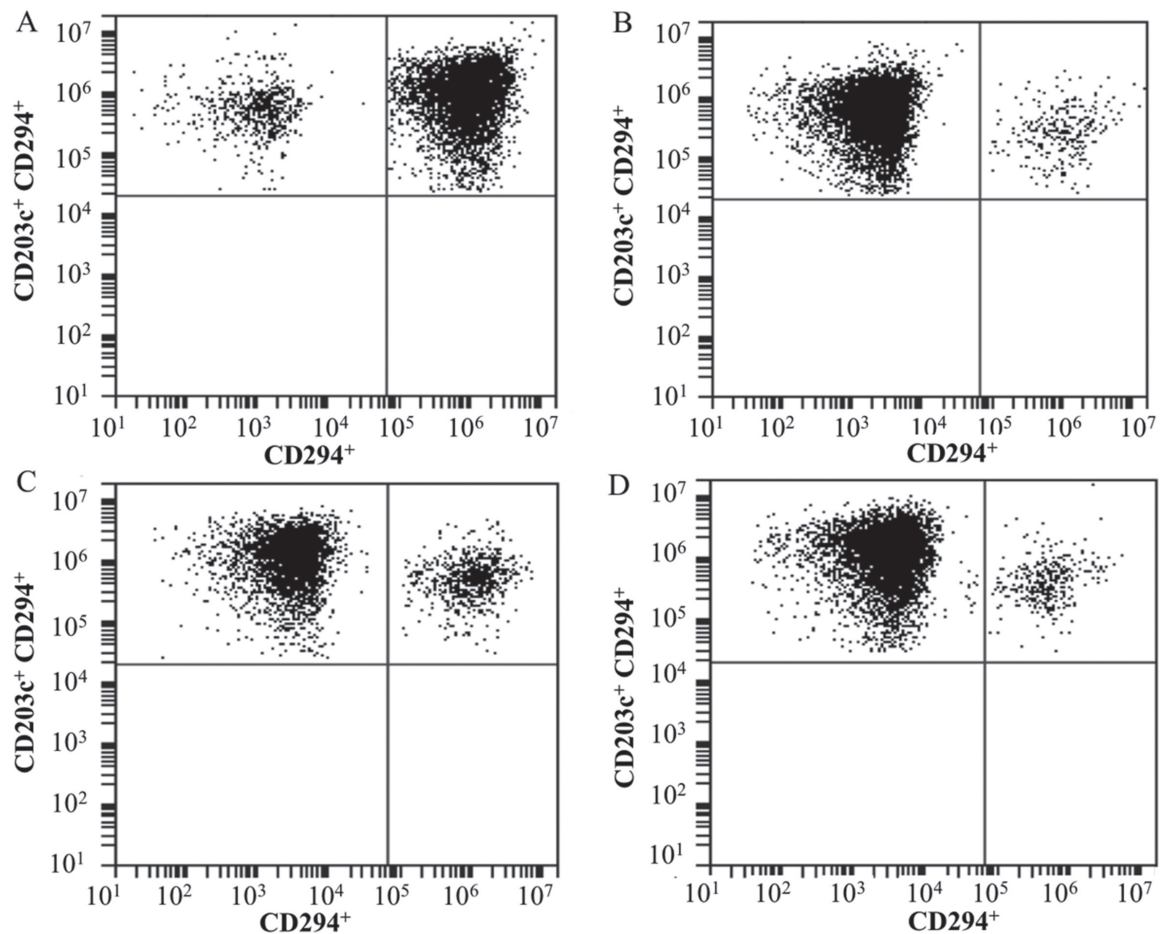


Fig. 2. Activation rate of basophils in blood samples of rats in each group. Activated and inactivated basophils in animals of the AR model group (A), the IgE inhibitor E2_79 group (B), the Omalizumab group (C), and the control group (D)

of basophils in normal subjects. The cells in the upper left corner represent the inactivated basophils, while those in the upper right corner represent the activated basophils. In AR patients, the rate of cell activation (91.10%) was significantly higher than that in the control group (6.10%) ($p < 0.05$; Table 1). No significant difference was found for age and sex. In the animal study, the rate of activated basophils in group A (91.10%) was also significantly higher than in treatment groups B (3.60%) and C (8.40%) and in the control group D (7.10%) ($p < 0.05$; Fig. 2A and Table 2).

Comparison of the contents of IL-4, IL-5, IL-13, IgE, and PGD2 in different groups

Compared with the control group, the levels of serum inflammatory factors IL-4, IL-5 and IL-13 in the observation group were significantly higher ($p < 0.05$; Table 3). Compared with the control group, the levels of serum inflammatory factors IgE and PGD2 in the observation group were also significantly higher ($p < 0.05$; Table 4).

The contents of IL-4, IL-5 and IL-13 in the serum of rats in each group were compared as shown in Table 5. The results of a one-way ANOVA showed that the contents

Table 1. Comparison of activated basophils between the observation and control groups ($X \pm S$)

Variables	Control group (n = 15)	Observation group (n = 30)
Age [years]	10.00 \pm 2.59	9.76 \pm 3.34
Sex (male:female)	9:6	17:13
CD294+ [%]	93.20	8.70*
CD203c+CD294+ [%]	6.10	91.10*

Compared with the control group; * $p < 0.05$. Rates are compared using χ^2 test between the 2 groups.

Table 2. Comparison of activated basophils in rats ($X \pm S$)

Groups	n	CD294+ [%]	CD203c+CD294+ [%]
A	12	8.90	91.10
B	12	95.70*	3.60*
C	12	91.10*	8.40*
D	12	93.20*	7.10*

* $p < 0.05$, compared with group A. Rates are compared using χ^2 test between the 2 groups.

of IL-4, IL-5 and IL-13 were significantly different among different groups ($p < 0.01$). Levels of IL-4, IL-5 and IL-13 were significantly higher in the AR model group A than

Table 3. Comparison of blood inflammatory factors between 2 groups (X ±S)

Groups	n	IL-4 [pg/mL]	IL-5 [ng/L]	IL-13 [ng/L]
Control group	15	79.81 ±23.66	6.69 ±1.37	19.85 ±4.84
Observation group	30	167.27 ±37.10*	14.05 ±4.31*	32.02 ±5.60*

Compared with the control group; * p < 0.05. Comparison between 2 groups was performed using Student's t-test; IL – interleukin.

Table 4. Comparison of IgE and PGD2 in blood between 2 groups (X ±S)

Groups	n	IgE [ug/mL]	PGD2 [ng/L]
Control group	15	185.37 ±36.07	87.07 ±10.62
Observation group	30	337.60 ±73.91*	137.95 ±31.81*

Compared with the control group; * p < 0.05. Comparison between 2 groups was performed using Student's t-test; IgE – immunoglobulin E; PGD2 – prostaglandin D2.

Table 5. Comparison of rat blood inflammatory factors IL-4, IL-5 and IL-13 (X ±S)

Group	n	IL-4 [pg/mL]	IL-5 [ng/L]	IL-13 [ng/L]
Group A	12	147.30 ±20.77	14.02 ±2.21	20.37 ±2.27
Group B	12	52.78 ±23.87	6.49 ±2.02	6.69 ±2.71
Group C	12	44.28 ±24.85	4.98 ±2.36	8.87 ±3.49
Group D	12	6.12 ±3.71	7.73 ±2.45	3.12 ±1.15
F-value	–	105.80	36.88	102.70
p-value	–	<0.001	<0.001	<0.001

The p-values and F-values were obtained by comparison among 3 or more groups using one-way analysis of variance (ANOVA); IL – interleukin.

in treatment groups B and C and the control group D (p < 0.01, Table 5). No significant difference was found between groups B and C (p > 0.05).

Comparison of the levels of inflammatory factors IgE and PGD2 in blood samples of rats in each group

The comparative results of serum IgE and PGD2 levels among groups are shown in Table 6. The results of a one-way ANOVA of IgE and PGD2 showed that there were significant differences in the contents of IgE and PGD2 among different groups (p < 0.01). The results of LSD showed that the levels of IgE and PGD2 in group A were significantly higher than those in group B, C and D (p < 0.01), and there was no significant difference between group B and group C (p > 0.05).

Expression of basophil surface receptor FcεRI and nuclear protein NF-κB in blood samples of rats in each group

As shown in Fig. 3, the basophil surface receptor FcεRI and nucleoprotein NF-κB in group A were remarkably higher than in the control group D, and both treatments (group B and C) markedly decreased protein levels (p < 0.05).

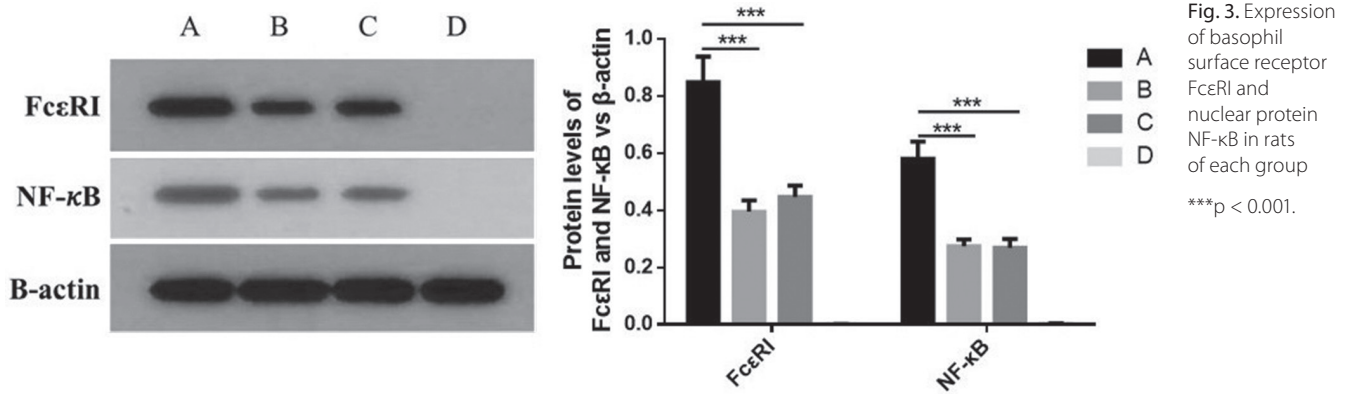
Discussion

The AR is a type I allergic reaction mediated by IgE antibody and infiltrated by eosinophils. An imbalance of T helper type 1 or type 2 (Th1/Th2) cytokines is involved in the pathogenesis of AR, which leads

Table 6. Comparison of inflammatory factors IgE and PGD2 in blood samples of rats in each group (X ±S)

Group	n	IgE [μg/mL]	PGD2 [ng/L]
Group A	12	177.80 ±24.69	223.72 ±16.56
Group B	12	68.40 ±35.66	69.24 ±15.04
Group C	12	65.98 ±32.43	75.36 ±16.32
Group D	12	13.21 ±3.44	18.56 ±2.17
F	–	77.97	486.3
p-value	–	<0.001	<0.001

IgE – immunoglobulin E; PGD2 – prostaglandin D2.



to the overproduction and release of histamine. A large number of inflammatory factors and immunoreactive cytokines participate in the regulation of chronic inflammatory responses in nasal mucosa.¹⁶ The Th1 cells mainly secrete interferon gamma (IFN- γ) and IL-2. Interferon gamma is a multifunctional protein that can effectively antagonize the synthesis and secretion of IgE, mediated by IL-4, and serves as a protective factor of AR. Interleukin 4 is the main cytokine secreted by Th2 cells, which can stimulate B cells to secrete and release IgE into the blood, thus promoting the combination of allergens and the corresponding receptors on mast cells, resulting in degranulation and the increase of inflammatory transmission. Some studies have shown that the immune activity of Th2 cells is excessively increased during the course of AR. The Th2 cells infiltrated nasal mucosa, and the serum levels of IL-4, IL-5 and IL-13 were significantly increased. In this study, we showed that the expression levels of IL-4, IL-5, IL-13, IgE, and PGD2 inflammatory factors in the serum of the observation group were significantly higher than those in the control group ($p < 0.05$).

Studies have shown that NF- κ B plays an important role in the pathogenesis of AR by stimulating the cAMP-PKA signaling pathway, promoting ICAM-1 transcription¹⁷ and inducing the release of inflammatory factors such as mast cells.¹⁸ Activation of NF- κ B can regulate the release of Th cytokines, interfere with the balance of Th1/Th2 cytokines and participate in the physiological and pathological processes of immunity, inflammation and development. The increase of serum IgE level in AR patients was related to the increased number of eosinophils.¹⁹ As a high affinity receptor of IgE, the expression level of FcεRI may be closely related to the development of AR disease. It has been reported that the expression of FcεRI in eosinophils is associated with allergic eosinophilic gastroenteritis.²⁰ These results suggest that eosinophils expressing FcεRI may be involved in the pathogenesis of allergic diseases. However, follow-up studies also found that FcεRI was highly expressed in the eosinophils of patients with allergic esophagitis and reflux esophagitis²¹ compared with healthy people. A high expression of FcεRI in dendritic cells was also observed in both chronic obstructive pulmonary

disease (COPD) and asthma patients.²² These data suggest that the increase of FcεRI in some cells may be related to a variety of inflammatory diseases.

Our results show that AR patients had increased amount of activated basophils, elevated expressions of IL-4, IL-5, IL-13, IgE, and PGD2, and upregulated levels of FcεRI and nuclear protein NF- κ B. Also, the levels of IL-4, IL-5, IL-13, IgE, and PGD2 in AR rats were significantly higher than those in the IgE inhibitors and omalizumab groups. There was no significant difference in the levels of IL-4, IL-5, IL-13, IgE, and PGD2 between the IgE inhibitors and omalizumab groups. In addition, the IgE inhibitors and omalizumab groups showed decreased expression of FcεRI and nucleoprotein NF- κ B on the basophilic granulocyte surface, reduced levels of serum IgE, and downregulated serum levels of IL-4, IL-5, IL-13 and PGD2. It is suggested that IgE, FcεRI and NF- κ B play an important role in the pathogenesis of AR.

Limitations

The present study has some limitations. The blood sample size of AR patients is limited, and we have yet to establish the underlying molecular mechanisms, such as the downstream and upstream genes and proteins for IgE-FcεRI-NF- κ B signaling during the AR process. All of these elements need more research to confirm.

Conclusions

This study found that activated basophils were predominant in the blood samples of AR patients and animal models when compared to controls. Moreover, the serum levels of IL-4, IL-5, IL-13, IgE, and PGD2 in children with AR and AR rat model were significantly higher than those in the healthy group. The upregulation of FcεRI and NF- κ B might be involved in the pathogenesis of AR.

ORCID iDs

Yi Qiao  <https://orcid.org/0000-0001-7032-1385>

Jie Chen  <https://orcid.org/0000-0002-9888-9930>

References

- Ross SM. Allergic rhinitis: A proprietary extract of *Pines pinaster* Aiton (pynogenol) is found to improve the symptoms associated with allergic rhinitis. *Holist Nurs Pract*. 2016;30(5):301–304. doi:10.1097/HNP.0000000000000170
- Wheatley LM, Togias A. Allergic rhinitis. *N Engl J Med*. 2015;372(5):456–463. doi:10.1056/NEJMcp1412282
- De Shazo RD, Kemp SF. Pathogenesis of allergic rhinitis (rhinosinusitis). <https://www.uptodate.com/contents/pathogenesis-of-allergic-rhinitis-rhinosinusitis>. Updated April 9, 2021.
- Kim HK, Kook JH, Kang KR, Oh DJ, Kim TH, Lee SH. Increased expression of the aryl hydrocarbon receptor in allergic nasal mucosa, contributing to chemokine secretion in nasal epithelium. *Am J Rhinol Allergy*. 2016;30(4):e107–e112. doi:10.2500/ajra.2016.30.4311
- Thanaviratnanich S, Cho SH, Ghoshal AG, et al. Burden of respiratory disease in Thailand: Results from the APBORD observational study. *Medicine (Baltimore)*. 2016;95(28):e4090. doi:10.1097/MD.00000000000004090
- Kawasaki T, Kawai T. Toll-like receptor signaling pathways. *Front Immunol*. 2014;5:461. doi:10.3389/fimmu.2014.00461
- Nardo DD. Toll-like receptors: Activation, signalling and transcriptional modulation. *Cytokine*. 2015;74(2):181–189. doi:10.1016/j.cyto.2015.02.025
- Deguine J, Barton GM. MyD88: A central player in innate immune signaling. *F1000Prime Rep*. 2014;6:97. doi:10.12703/P6-97
- Coimbra R, Melbostad H, Loomis W, et al. LPS-induced acute lung injury is attenuated by phosphodiesterase inhibition: Effects on pro-inflammatory mediators, metalloproteinases, NF- κ B, and ICAM-1 expression. *J Trauma*. 2006;60(1):115–125. doi:10.1097/01.ta.0000200075.12489.74
- Ma J, Liang H, Jin HR, et al. Yangonin blocks tumor necrosis factor- α -induced nuclear factor- κ B-dependent transcription by inhibiting the transactivation potential of the RelA/p65 subunit. *J Pharmacol Sci*. 2012;118(4):447–454. doi:10.1254/jphs.11215fp
- Liu S, Misquitta YR, Olland A, et al. Crystal structure of a human I kappa B kinase beta asymmetric dimer. *J Biol Chem*. 2013;288(31):22758–22767. doi:10.1074/jbc.M113.482596
- Hochrainer K, Racchumi G, Anrather J. Site-specific phosphorylation of the p65 protein subunit mediates selective gene expression by differential NF- κ B and RNA polymerase II promoter recruitment. *J Biol Chem*. 2013;288(1):285–293. doi:10.1074/jbc.M112.385625
- Kraft S, Kinet JP. New developments in FcepsilonRI regulation, function and inhibition. *Nat Rev Immunol*. 2007;7(5):365–378. doi:10.1038/nri2072
- Hong J, Bao Y, Chen A, et al. Chinese guidelines for childhood asthma 2016: Major updates, recommendations and key regional data. *J Asthma*. 2018;55(10):1138–1146. doi:10.1080/02770903.2017.1396474
- Cheng L, Chen J, Fu Q, et al. Chinese society of allergy guidelines for diagnosis and treatment of allergic rhinitis. *Allergy Asthma Immunol Res*. 2018;10(4):300–353. doi:10.4168/air.2018.10.4.300
- Kim EH, Yang L, Ye P, et al. Long-term sublingual immunotherapy for peanut allergy in children: Clinical and immunologic evidence of desensitization. *J Allergy Clin Immunol*. 2019;144(5):1320–1326.e1. doi:10.1016/j.jaci.2019.07.030
- Wang SZ, Ma FM, Zhao JD. Expressions of nuclear factor-kappa B p50 and p65 and their significance in the up-regulation of intercellular cell adhesion molecule-1 mRNA in the nasal mucosa of allergic rhinitis patients. *Eur Arch Otorhinolaryngol*. 2013;270(4):1329–1334. doi:10.1007/s00405-012-2136-y
- Kim HI, Hong SH, Ku JM, et al. Tonggyu-tang, a traditional Korean medicine, suppresses pro-inflammatory cytokine production through inhibition of MAPK and NF- κ B activation in human mast cells and keratinocytes. *BMC Complement Altern Med*. 2017;17(1):186. doi:10.1186/s12906-017-1704-5
- Demirjian M, Rumblyrt JS, Gowda VC, Klaustermeyer WB. Serum IgE and eosinophil count in allergic rhinitis: Analysis using a modified Bayes' theorem. *Allergol Immunopathol (Madr)*. 2012;40(5):281–287. doi:10.1016/j.aller.2011.05.016
- Dehlink E, Fiebiger E. The role of the high-affinity IgE receptor, FcepsilonRI, in eosinophilic gastrointestinal diseases. *Immunol Allergy Clin North Am*. 2009;29(1):159–170. doi:10.1016/j.iac.2008.09.004
- Yen EH, Hornick JL, Dokter M, et al. Comparative analysis of FcεRI expression patterns in patients with eosinophilic and reflux esophagitis. *Gastroenterology*. 2010;136(5):A-278. doi:10.1097/MPG.0b013e3181de7685
- Stoll P, Bähker A, Ulrich M, et al. The dendritic cell high-affinity IgE receptor is overexpressed in both asthma and severe COPD. *Clin Exp Allergy*. 2016;46(4):575–583. doi:10.1111/cea.12664

Periodontal condition of mandibular incisors treated with modified Kazanjian vestibuloplasty compared to untreated sites: A prospective study

Beata Wyrębek^{1,A–E}, Renata Górska^{1,A,E,F}, Katarzyna Gawron^{2,F}, Małgorzata Nędzi-Góra^{1,A,E}, Bartłomiej Górski^{1,A,D,E}, Paweł Plakwicz^{1,3,A,D–F}

¹ Department of Periodontology, Medical University of Warsaw, Poland

² Department of Molecular Biology and Genetics, Medical University of Silesia, Katowice, Poland

³ Chair and Department of Periodontology, Medical University of Lublin, Poland

A – research concept and design; B – collection and/or assembly of data; C – data analysis and interpretation;

D – writing the article; E – critical revision of the article; F – final approval of the article

Advances in Clinical and Experimental Medicine, ISSN 1899–5276 (print), ISSN 2451–2680 (online)

Adv Clin Exp Med. 2021;30(7):681–690

Address for correspondence

Beata Wyrębek

Email: beatawyrębek@gmail.com

Funding sources

None declared

Conflict of interest

None declared

Received on August 10, 2020

Reviewed on November 28, 2020

Accepted on February 19, 2021

Published online on June 11, 2021

Cite as

Wyrębek B, Górska R, Gawron K, Nędzi-Góra M, Górski B, Plakwicz P. Periodontal condition of mandibular incisors treated with modified Kazanjian vestibuloplasty compared to untreated sites: A prospective study. *Adv Clin Exp Med.* 2021;30(7):681–690. doi:10.17219/acem/133492

DOI

10.17219/acem/133492

Copyright

© 2021 by Wrocław Medical University

This is an article distributed under the terms of the Creative Commons Attribution 3.0 Unported (CC BY 3.0) (<https://creativecommons.org/licenses/by/3.0/>)

Abstract

Background. A shallow vestibule, insufficient keratinized tissue width and pulling of marginal gingiva may be associated with gingival recession, plaque accumulation and gingivitis. Conventional techniques for treatment of gingival recession use autogenous or allogenic grafts. However, these methods result in soreness at the donor site and pose an economic burden, which may cause patients to withdraw from treatment. Alternative therapy is currently not available to treat such patients.

Objectives. The aim of this study was to evaluate changes in periodontal tissue at the mandibular incisors after vestibuloplasty, focusing on functional improvement of the existing soft tissue with no grafting.

Materials and methods. Thirty patients with a shallow vestibule, minimal keratinized tissue width (KTW; ≤ 1 mm), gingival recession (REC) and pulling of gingiva underwent modified Kazanjian vestibuloplasty were included into the test group, whereas 27 patients did not undergo any surgery (control group). The probing pocket depth (PPD), clinical attachment level (CAL), gingival recession depth (GRD), and KTW were assessed at baseline and 12 months post-surgery.

Results. The mean KTW, GRD and CAL values improved in the test group. A significant increase in mean KTW value (1.17 ± 1.22 mm, $p = 0.0406$) was detected in the test group, while the control group showed a further reduction in mean KTW value (0.13 ± 0.45 mm). The mean GRD value decreased from 2.09 ± 1.78 mm to 1.22 ± 1.46 mm ($p = 0.0087$) in the test group, whereas in controls the mean GRD value increased from 1.95 ± 1.29 mm to 2.34 ± 1.44 mm ($p = 0.0164$). The mean KTW value at 3, 6 and 12 months compared to baseline showed an increase in the test group, and the mean GRD and CAL values exhibited the potential to improve.

Conclusions. Sites treated with vestibuloplasty showed increased KTW, improvement in the gingival margin and CAL gain, whereas untreated sites showed continuous deterioration of the evaluated parameters. Vestibuloplasty may be recommended for patients avoiding major surgery for which functional improvement in tissue alone would provide a sufficient therapeutic outcome.

Key words: gingival recession, keratinized tissue, vestibuloplasty

Background

A shallow vestibule in the anterior region of the lower dental arch may impede proper oral hygiene due to insufficient space for the toothbrush, leading to plaque accumulation and traumatizing brushing technique. It can result in marginal gingivitis and the potential for the occurrence or exacerbation of gingival recessions. Moreover, a shallow vestibule often coexists with a narrow zone of keratinized gingiva and attached gingiva or frena attachment with pulling of the gingival margin. Measurement of vestibule depth is not commonly performed in a standard periodontal examination. There are no established methods to measure the depth of the vestibule or reference values to classify its type, which is commonly categorized as shallow or deep.^{1–3} According to Ward, the depth of the vestibular fornix in the lower anterior region, measured from the gingiva to the mucobuccal fold, varies from 2.5 mm to 11.5 mm.⁴ In patients with excellent dental plaque control, periodontal health can be preserved in spite of lack of keratinized tissue. Conversely, in cases with suboptimal plaque removal, a thin periodontal phenotype requiring restorative, orthodontic or prosthetic treatment and deficiency of keratinized tissue may be associated with gingival recession and inflammation. As a result, coexisting esthetic impairment, dentin hypersensitivity, discomfort during tooth brushing, root caries, and non-carious cervical lesions may be a cause for concern in both patients and clinicians. Especially in the mandibular incisor region, other factors such as the presence of frena attachment, muscle pull and a shallow fornix may predispose a patient to future soft tissue loss in case of inadequate plaque control and lack of keratinized tissue.⁵ A long-standing debate in the scientific community relates to the optimal amount of keratinized tissue. It is agreed that ≥ 2 mm of keratinized tissue and ≥ 1 mm of attached gingiva is beneficial around teeth to maintain periodontal health.⁶

Various techniques for deepening the vestibule have been described; however, most of them are not used due to post-surgical complications that result from exposing a varying area of the crestal bone.^{1,7–10} Surgical methods of deepening the oral vestibule, besides vestibuloplasty procedures, include autogenic soft tissue grafting.^{5,6,11} Deepening the oral vestibule can enable maintenance of proper oral hygiene, remove improper attachment of the lower lip frenulum and eliminate pulling of the gingival margin. If soft tissue grafting is used to deepen the vestibule, an additional effect is obtained, namely widening the keratinized gingival zone and covering or decreasing the existing recessions. However, insufficient thickness of palatal tissue at the donor site, or patient refusal of grafting, effectively prevents palatal tissue graft surgery in a considerable number of patients.

Kazanjian described a less invasive technique in which a split-thickness flap is prepared.¹² Kazanjian vestibuloplasty was originally performed before prosthetic treatment to reposition the mucosa and muscle insertions and to increase

the denture area for stability of the prosthesis. Individual studies have described the positive effects of vestibular deepening performed without grafts on periodontal tissue parameters and oral hygiene in dentate segments.^{13,14} To overcome some postoperative complications associated with the Kazanjian technique, several modifications have been suggested by other authors^{15–17} as well as in our work.^{14,18}

Nevertheless, autogenous tissue grafts are still considered the gold standard for soft tissue augmentation and provide unparalleled outcomes in terms of clinical improvement.^{5,6,19} However, free gingival grafts (FGG) may be associated with patient morbidity at the donor site and poor color blending with neighboring tissues. Presently, alternative commercially available materials may partially compensate for the drawbacks of FGG, since they provide significant improvements in matching the color and texture of keratinized tissue. Moreover, graft substitutes do not require graft harvesting from a second surgical site. Autogenous soft tissue grafts can be harvested from the palate or maxillary tuberosity using different approaches, such as the trap-door technique, single incision technique, parallel incision technique, and de-epithelialization technique.^{20–22} A second surgical site and prolonged surgical time are correlated with greater postoperative pain and swelling.⁶ Moreover, in some cases, the thickness of the palatal mucosa can constitute an additional limiting factor.

There is unprecedented interest in graft substitutes, which can be divided into allogenic, xenogenic, alloplastic, and living constructs. Unrestricted availability, avoidance of a secondary surgical site, reduced surgical time, and decreased patient morbidity are some of the major benefits of these materials. Acellular dermal matrix (ADM),²³ Mucograft (Geistlich Pharma, Wolhusen, Switzerland)^{24,25} and DynaMatrix (Keystone Dental, Burlington, USA)²⁶ are examples of commercially available materials. Overall, there is evidence in the literature that graft substitutes are effective in augmenting keratinized tissue in an esthetically pleasing way. However, at present, there is not enough evidence to support or refute the superiority of any particular product. It is also important to highlight that FGG and bilaminar approaches lead to superior outcomes in terms of mean keratinized tissue width (KTW) gain.

The labial surfaces of mandibular incisors are commonly affected by inadequate KTW volume, the presence of frena attachment, muscle pull, and gingival recessions. Since the tooth germs of lateral incisors are situated more lingually with respect to the central incisors, the former teeth are more often associated with periodontal problems.²⁷ Less traumatic procedures that involve only 1 surgical site, require less chair time and provide an optimal cost-to-benefit ratio for improving periodontal condition are still needed. Kazanjian vestibuloplasty seems to represent an alternative and functional approach to more advanced grafting techniques, especially for patients who do not want or cannot have (due to palate soft tissue condition) conventional treatment.

Objectives

The aim of this study was to evaluate changes in periodontal tissue at lower incisors with a lack of keratinized tissue, muscle pull and gingival recessions 12 months after modified Kazanjian vestibuloplasty, compared to untreated sites.

Materials and methods

Study design and patient population

This study was planned as a prospective, non-randomized, parallel trial (Fig. 1). The investigator who evaluated the clinical outcomes was not aware of the treatment protocol. Patients in the test group underwent vestibuloplasty in the anterior region of the mandible, whereas patients in the control group did not undergo any surgical treatment. The study design and all clinical procedures were performed in accordance with the Helsinki Declaration of 1975, as revised in Tokyo in 2004, after approval of the study protocol by the Bioethics Committee of the Medical University of Warsaw, Poland (approval

No. AKBE/106/15). Participants were recruited among patients referred to the Department of Periodontology and Oral Mucosa Diseases at the Medical University of Warsaw by their general dentists between January 2013 and December 2015 due to decreased vestibular depth, pulling of the gingival margin, narrow keratinized gingiva, single or multiple gingival recessions, or an aberrant frenum position in the area of the lower anterior teeth. One examiner (M.N-G.) qualified patients into the study. All patients were informed about all plausible treatment options, including soft tissue augmentation with either autogenous soft tissue graft or collagen matrix, as well as modified vestibuloplasty according to the Kazanjian method. Patients who declined soft tissue augmentation but allowed vestibuloplasty, together with patients who decided not to receive any surgery at all, were enrolled in the study. Patients were thoroughly informed of the nature of the study and the potential risks and benefits of their participation. All patients signed an informed consent form. Subsequently, patients were meticulously instructed on how to use the roll technique with a soft toothbrush and provided with a professional full-mouth cleaning and polishing.

Fifty-seven patients (45 women and 12 men, aged 21–56; mean age 37.58 ±6.11 years) participated in this

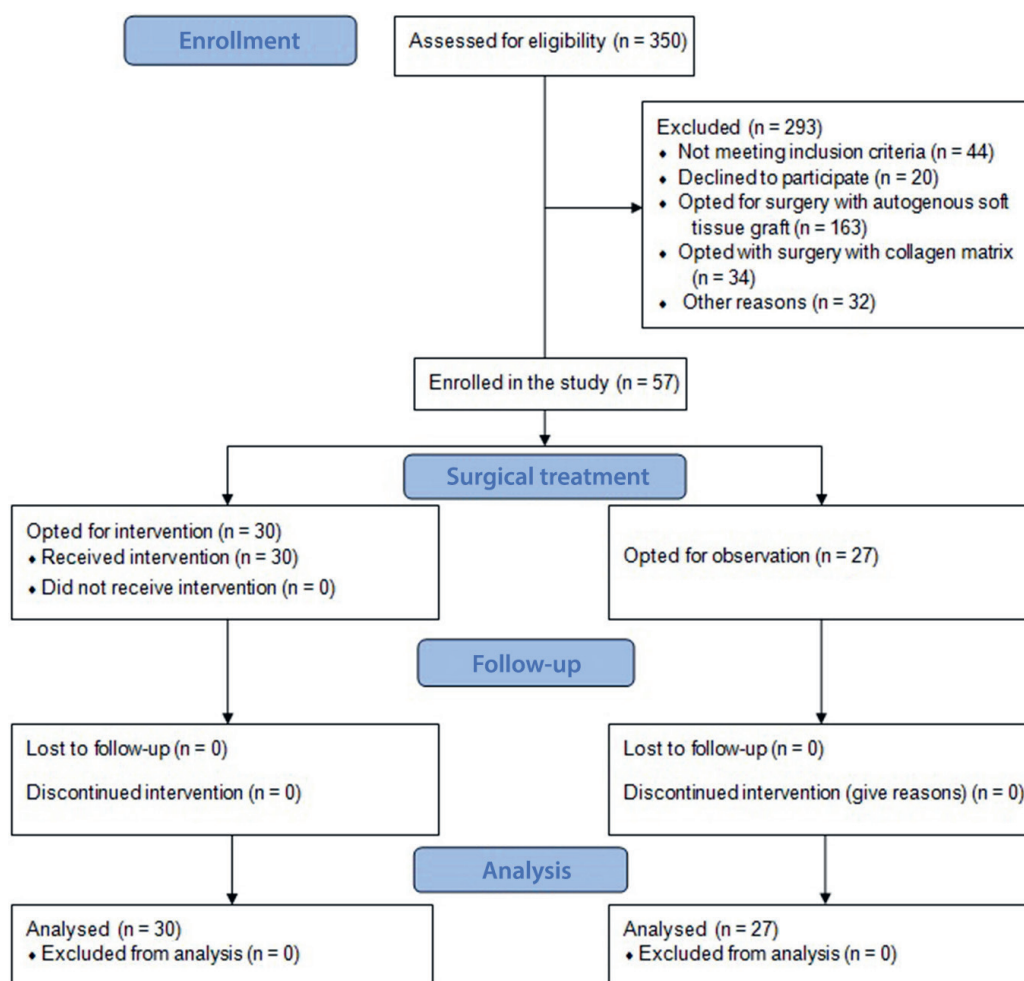


Fig. 1. Diagram showing the study design

study, of which 30 patients underwent modified Kazanjian vestibuloplasty (test group). The control group consisted of 27 patients (20 women and 7 men, aged 24–54, mean age 39.13 ± 5.62 years) who declined any surgical treatment but agreed to a 12-month observation.

Inclusion and exclusion criteria

The following inclusion criteria were applied: 1) a shallow vestibule, muscle pull, frena attachment with pull syndrome, and at least q lower incisor with KTW ≤ 1 mm in the apico-coronal dimension; 2) full mouth plaque score (FMPS) $\leq 20\%$; 3) full mouth bleeding on probing score (FMBOP) $\leq 20\%$; 4) no active gingivitis or periodontitis; 5) over 18 years of age; 6) no systemic disease with compromised healing potential; 7) no intake of medications affecting periodontal status; 8) no smoking; 9) no pregnant or lactating women; and 10) no previous periodontal plastic surgery in the anterior mandible.

Clinical measurements

Clinical parameters were evaluated by 1 experienced examiner (BW). A total of 5 patients with gingival recessions on the buccal surfaces of the lower incisors were recruited for the calibration exercise. The examiner recorded the periodontal parameters in the mandible with an interval of 24 h between measurements. Calibration was accepted when $\geq 90\%$ of the recorded values were reproduced within a difference of 1.0 mm and exact data were reported in 75% of measurements. The following parameters were assessed using a graded periodontal probe (UNC probe 15 mm; Hu-Friedy, Chicago, USA): 1) probing pocket depth (PPD), distance from the gingival margin to the bottom of the gingival sulcus at 6 points per tooth (mesio-buccal (MB), mid-buccal (B), disto-buccal (DB), mesio-lingual (MD), mid-lingual (ML), and disto-lingual (DL)); 2) clinical attachment level (CAL), distance from the cemento-enamel junction (CEJ) to the bottom of the gingival sulcus at 6 points per tooth (MB, B, DB, ML, L, and DL); 3) gingival recession depth (GRD), distance from CEJ to the most apical extension of the gingival margin at the mid-buccal point of the tooth; 4) KTW, the distance between the most apical point of the gingival margin and the mucogingival junction (MGJ), with the MGJ demarcated by staining the mucogingival complex with iodine solution; 5) FMPS, the percentage of total surfaces (4 aspects per tooth) that revealed the presence of plaque²⁸; and 6) FMBOP, assessed dichotomously at 6 points per tooth (MB, B, DB, ML, L, and DL) as the percentage of bleeding points.²⁹ The GRD was classified according to the Miller classification (Class I – GRD does not extend to MGJ and there is no loss of interdental bone and soft tissue; Class II – GRD extends to or beyond MGJ and there is no loss of interdental bone and soft tissue; Class III – GRD extends to or beyond MGJ with alveolar bone and soft tissue

loss in the interdental area; and Class IV – GRD extends to or beyond MGJ with severe alveolar bone and soft tissue loss in the interdental area) and in line with the Cairo classification (RT1 – GRD with no loss of interproximal attachment; RT2 – the amount of interproximal attachment loss is equal to or lower than the buccal attachment loss; and RT3 – the amount of interproximal attachment is greater than the buccal attachment loss).^{30,31} In the test group, clinical parameters were recorded at baseline and at 3, 6 and 12 months postoperatively. In the control group, clinical parameters were assessed at baseline and 12 months after baseline examination.

Surgical treatment

For the test group, the surgical procedures were performed by 1 experienced surgeon (P.P.) in accordance with modified Kazanjian vestibuloplasty under local anesthesia with 4% articaine hydrochloride with adrenaline (1:100,000) (Ubistesin Forte 1.7 mL; 3M ESPE, Saint Paul, USA). A single horizontal incision was made with a scalpel blade from the lower right canine to the lower left canine within the mucosa of the inner part of the lip, 9–12 mm from the mucogingival junction. A split-thickness pedicle flap was prepared with its base on the alveolar part of the mandible to the level of the keratinized gingiva. The muscle attachments beneath the free margin of the flap were separated and moved apically. The remnants of muscle tissue were removed from the periosteum on the vestibular part of the anterior mandible. Limited flap preparation and only small correction of submucosal tissue constituted modifications of the original technique. The mobilized flap was then stabilized apically with resorbable single sutures (PGA Resorba 6/0 11 mm, 3/8; RESORBA Medical GmbH, Nuremberg, Germany) to the underlying periosteum at the level of the newly established vestibular depth (Fig. 2). The area on the inner surface of the lower lip was left to heal by secondary intention.

Postoperative period

After surgery, patients received 800 mg of ibuprofen and were asked to take a 2nd dose 8 h later as well as additional tablets later on if required to control postoperative pain. Patients were instructed to take azithromycin (500 mg once daily) for 3 days. Meticulous written postoperative instructions to avoid brushing, flossing and chewing in the treated area for a period of 2 weeks were handed to all subjects after surgery. Patients were asked to apply 1% chlorhexidine gel topically to the operative site and to rinse their mouth twice daily for 1 min using 0.2% chlorhexidine solution. At week 2, the sutures were removed and patients resumed careful brushing with a soft toothbrush. Follow-up appointments were scheduled for 1, 2, and 4 weeks after surgery, as well as 3, 6 and 12 months after the baseline

examination. Each session included reinforcement of oral hygiene instructions (teeth brushing with the roll technique and dental flossing twice a day) and supragingival plaque removal. Two clinical cases are shown in Fig. 2 and Fig. 3.



Fig. 2. A. Pre-operative view of test site; B. immediate post-operative view; C. 12 months post-operative view



Fig. 3. A. Baseline view of control site; B. 12 months post-operative view

Statistical analyses

Statistical analyses were performed using R v. 3.2.3 software (R Core Team 2019; R Foundation for Statistical Computing, Vienna, Austria). Clinical parameters were compared between the 2 groups. The primary outcome variable was an increase in the keratinized tissue width at 12 months, and the secondary variables were gingival recession height reduction and gain in clinical attachment level at 12 months. Descriptive statistics were carried out using mean values, 95% confidence intervals (95% CI), standard deviations (SD), frequencies, and percentages. The Shapiro–Wilk test was used to assess data distribution normality. As all quantitative variables in this study were normally distributed, Student's t-test was applied for intragroup and intergroup comparisons. To evaluate the effectiveness of treatment, the following calculations were done: 1) $KTW_{gain} = KTW_{12} - KTW_0$; 2) $gingival\ recession\ reduction = GRD_0 - GRD_{12}$. To compare measurements at the 4 time points (baseline, 3, 16, and 12 months) in the test group, two-way analysis of variance (ANOVA) was used. Statistical significance was set at $p < 0.05$.

Results

The test group included 30 patients (25 women and 5 men, aged 21–56, mean age 36.03 ± 6.61 years) who underwent modified Kazanjian vestibuloplasty on the vestibular surfaces of the lower incisors. Post-surgical healing was uneventful in all patients, all of whom completed the 12-month follow-up. Hypertrophic scar formation was observed in 3 patients, while scar lines were visible in the apical regions in 5 patients. The control group consisted of 27 patients (20 women and 7 men, aged 24–54, mean age 39.13 ± 5.62 years) who declined any surgical treatment but agreed to 12-month observation. The majority of observed labial gingival recessions at baseline in both groups were class I according to Miller and recession type 1 (RT1) according to Cairo (Table 1).

The clinical characteristics of the groups at baseline and 12-month follow-up are depicted in Table 2. With the exception of KTW, both groups had similar clinical parameters at baseline. The FMPS and FMBOP values remained low throughout the observation period. However, in the test group, we observed statistically significant improvement in local bleeding on probing score (BOP) for the treated areas as compared to controls. At the end of the study, the mean PPD value assessed at 6 points per incisor, as well as only in buccal aspects of the tooth, increased significantly in controls from 1.70 ± 0.59 to 1.77 ± 0.63 mm and from 1.79 ± 0.59 mm to 1.88 ± 0.65 mm, respectively. Twelve months after surgical treatment, the mean CAL, GRD and KTW values improved in the test group. At test sites the mean CAL value decreased from 2.28 ± 1.91 mm to 1.63 ± 1.66 mm ($p = 0.3802$), whereas at control sites the mean CAL value increased from 1.86 ± 1.63 mm to 2.07 ± 1.79 mm ($p = 0.2292$). The statistical significance of the changes in CAL measured at the mid-buccal point of the teeth is presented in Table 3. At test sites the mean GRD value decreased from 2.09 ± 1.78 mm to 1.22 ± 1.46 mm ($p = 0.0087$), whereas at control sites the mean GRD value increased from 1.95 ± 1.29 mm to 2.34 ± 1.44 mm ($p = 0.0164$). Surgical treatment resulted in a significant increase in the mean KTW value

(1.17 ± 1.22 mm, $p = 0.0406$) in the test group. By contrast, in the control group, further reduction in the mean KTW value to 0.13 ± 0.45 mm was observed. The mean KTW value at 3, 6 and 12 months compared to baseline showed a tendency to increase in the test group (Table 3). The relative mean GRD values exhibited the potential to decrease over time. From baseline to 12 months, there were statistically significant increases in mean CAL and KTW, as well as significant GRD reduction, for the mid-buccal aspects of the lower incisors in the test group. No changes were observed in terms of the mean PPD value.

Discussion

A poor mucogingival condition is common in the lower incisor area. In case of inadequate KTW, decreased vestibular depth and muscle pull, mucogingival surgery may be performed to ease plaque control, improve patient comfort during tooth brushing, and reduce, halt or avoid gingival recession formation. Different procedures provide varying degrees of success. The present study evaluated periodontal condition at the lower incisors in patients who underwent simple vestibuloplasty versus untreated patients who served as controls. Each patient had at least 1 incisor with $KTW \leq 1$ mm, gingival recession, and the presence of muscle pull or high frenula attachment. To the best of our knowledge, this is the first study to compare these 2 approaches in natural teeth. At the end of the follow-up period, the test group showed significant gains in KTW and CAL (at the mid-buccal point) and reduction in GRD, which improved continuously during the observation period. The KTW increased by 1.17 mm. In the control group, the abovementioned parameters worsened over time, together with significant increases in PPD, as a result of impaired plaque control at the affected sites. Our study suggests that modified Kazanjian vestibuloplasty is associated with more stable periodontal tissue compared to untreated sites. This procedure has the benefits of simplicity, less time required, no need for a second surgical site (which lowers morbidity), and an esthetically pleasing tissue match. It may be an alternative approach in case of patients who want to avoid major surgery and for whom functional improvement of periodontal soft tissues alone will bring a sufficient treatment outcome.

Our findings also indicate that, apart from the expected vestibular deepening, it is possible to obtain the additional effect of reducing existing recessions where the vestibule is shallow. One has to bear in mind, however, that the main objective of vestibuloplasty is not coverage of recessions but elimination of recession-inducing factors. It has been argued that FGG should be considered the first and the most effective choice for increasing developmentally missing or lost keratinized tissue and may eliminate muscle pull. Agudio et al. evaluated changes in the amount of keratinized tissue in 103 patients treated

Table 1. Baseline characteristics of the test and control groups with respect to gingival recession

Variables	Test group (N = 30)	Control group (N = 27)
Class of GRD according to Miller (n)		
Class I	57	63
Class II	24	22
Class III	10	7
Class IV	0	0
Type of GRD according to Cairo (n)		
RT1	76	78
RT2	13	11
RT3	2	3

N – number of patients; n – number of defects; GRD – gingival recession depth; RT – recession type.

Table 2. Clinical parameters (mean, 95% CI, SD) at the lower incisors at baseline and after 12 months

Variables	Baseline	12 months	p-value
PPD tests [mm]	1.69 [1.64;1.74] ±0.69	1.70 [1.65;1.75] ±0.69	0.5032
PPD controls [mm]	1.70 [1.65;1.74] ±0.59	1.77 [1.72;1.82] ±0.63	0.0332*
#p-value	0.4324	0.0398*	
PPDb tests [mm]	1.79 [1.71;1.87] ±0.74	1.76 [1.69;1.83] ±0.68	0.3503
PPDb controls [mm]	1.79 [1.73;1.86] ±0.59	1.88 [1.81;1.95] ±0.65	0.0229*
#p-value	0.7803	0.0065*	
CAL tests [mm]	1.79 [1.66;1.92] ±1.77	1.38 [1.26;1.50] ±1.58	0.6764
CAL controls [mm]	1.37 [1.26;1.48] ±1.46	1.49 [1.37;1.61] ±1.57	0.7018
#p-value	0.8932	0.903	
CALb tests [mm]	20.28 [1.69;1.83] ±1.91	1.63 [1.45;1.80] ±1.66	0.3802
CALb controls [mm]	10.86 [1.68;2.04] ±1.63	2.07 [1.87;2.27] ±1.79	0.2292
#p-value	0.2765	0.3007	
GRD tests [mm]	2.09 [1.76;2.41] ±1.78	1.22 [0.95;1.48] ±1.46	0.0087*
GRD controls [mm]	1.95 [1.70;2.20] ±1.29	2.34 [2.06;2.61] ±1.44	0.0164*
#p-value	0.6320	0.0421*	
GRD red tests [mm]	–	0.85 [0.67;1.04] ±1.04	–
GRD red controls [mm]	–	–0.38 [–0.51;–0.24] ±0.69	–
#p-value		0.2139	
KTW tests [mm]	2.24 [2.05;2.43] ±1.06	3.42 [3.18;3.66] ±1.29	0.0406*
KTW controls [mm]	1.77 [1.62;1.92] ±0.78	1.64 [1.48;1.79] ±0.80	0.7002
#p-value	0.0339*	0.0299*	
KTWgain tests [mm]	–	1.17 [–1.40;–0.95] ±1.22	–
KTWgain controls [mm]	–	–0.13 [0.04;0.22] ±0.45	–
#p-value		0.04489*	
FMPS tests [mm]	0.14 [0.11;0.16] ±0.23	0.13 [0.10;0.15] ±0.21	0.8721
FMPS controls [mm]	0.20 [0.16;0.23] ±0.28	0.18 [0.15;0.21] ±0.25	0.7088
#p-value	0.3412	0.2081	
PS tests [mm]	0.19 [0.14;0.23] ±0.26	0.20 [0.15;0.25] ±0.26	0.9301
PS controls [mm]	0.25 [0.20;0.31] ±0.30	0.29 [0.24;0.35] ±0.26	0.9118
#p-value	0.2291	0.3010	
FMBOP tests [mm]	0.16 [0.14;0.18] ±0.21	0.06 [0.04;0.07] ±0.11	0.7356
FMBOP controls [mm]	0.19 [0.16;0.22] ±0.23	0.16 [0.14;0.19] ±0.20	0.8021
#p-value	0.4328	0.2281	
BOP tests [mm]	0.24 [0.20;0.29] ±0.24	0.07 [0.05;0.09] ±0.12	0.0108*
BOP controls [mm]	0.29 [0.25;0.33] ±0.22	0.27 [0.23;0.31] ±0.19	0.3294
#p-value	0.8743	0.0381*	

PPD – mean value of probing pocket depth at 6 measurement points (MB, B, DB, ML, L, DL); PPDb – mean value of probing pocket depth on buccal surfaces at 3 measurement points (MB, B, DB); CAL – mean value of clinical attachment level at 6 measurement points (MB, B, DB, ML, L, DL); CALb – mean value of clinical attachment level on buccal surfaces at 3 measurement points (MB, B, DB); GRD – mean value of gingival recession depth; GRDred – mean value of gingival recession depth reduction; KTW – mean value of keratinized tissue width; KTWgain – mean value of gain in keratinized tissue; FMPI – full mouth plaque index; PS – plaque score at lower incisors; FMBOP – full mouth bleeding on probing score; BOP – bleeding on probing score at lower incisors; p for intragroup comparison; #p for intergroup comparison; * statistically significant at p ≤ 0.05.

Table 3. Changes in clinical parameters (mean, 95% CI, SD) at the lower incisors at the mid-buccal point over time in the study groups

Variables	Baseline	3 months	6 months	12 months	p1	p2 baseline – 12 months
PPD mid-buccal [mm]	1.25 [1.17;1.33] ±0.45	1.19 [1.12;1.26] ±0.39	1.17 [1.10;1.24] ±0.38	1.17 [1.10;1.24] ±0.38	0.4235	0.1662
CAL mid-buccal [mm]	3.20 [2.84;3.55] ±1.94	2.65 [2.27;3.03] ±2.09	2.23 [1.87;2.59] ±1.98	2.00 [1.67;2.34] ±1.81	0.3241	<0.0001*
GR mid-buccal [mm]	2.09 [1.76;2.41] ±1.78	1.78 [1.45;2.10] ±1.79	1.41 [1.11;1.71] ±1.65	1.22 [0.95;1.48] ±1.46	0.0147*	0.0005*
KTW mid-buccal [mm]	2.24 [2.05;2.43] ±1.06	2.49 [2.29;2.68] ±1.06	3.04 [2.82;3.26] ±1.19	3.42 [3.18;3.66] ±1.29	0.0078*	0.0002*

Mean value of probing pocket depth (PPD) at the mid-buccal point (B), mean value of clinical attachment level (CAL) at the mid-buccal point (B), mean value of gingival recession depth (GRD), mean value of keratinized tissue width (KTW); p1 for comparison of changes at 4 time points (baseline, 3 months, 6 months, 12 months); p2 for comparison of differences between baseline and 12 months; * statistically significant at p ≤ 0.05.

with gingival augmentation procedures with FGG, and observed a 4.2 mm increase in KTW and a 0.8 mm gingival margin shift 10 years after surgery.³² Furthermore, 18–35 years after treatment, 83% of augmented sites showed

gingival recession reduction, whereas 48% of untreated sites showed increased recession.³³ The reported keratinized tissue augmentation with FGG varied from 3.1 mm to 5.6 mm. Limitations associated with FGG include

mucogingival junction misalignment as well as poor color and texture match with neighboring tissues.^{5,6} For these reasons, FGG utilization should be thoroughly evaluated, especially in cases involving the anterior region of the maxilla or mandible. Several disadvantages of FGG have been overcome by the use of subepithelial connective tissue grafts (SCTG).³⁴ They are considered the gold standard in mucogingival surgery, but also have some disadvantages. The surgery requires a 2nd operation to obtain the donor tissue from the palate, the amount of donor tissue is limited, and the procedure significantly increases complications and pain due to the need to surgically open a 2nd site to obtain the donor tissue.^{5,11,19,20} Vestibuloplasty does not aim to increase the width of the gingival keratinized structure either, as it is the case with FGG, since it is determined by cells at the genetic level and the grafted palatal tissue is keratinized.³⁶ It is noteworthy, however, that in the 12-month observation period the keratinized gingival zone increased in the test group at the incisors; by contrast, in the control group, KG remained at a similar level or decreased slightly. The results in the test group, which were based on clinical probing, should be treated with caution due to the absence of histological examination of the relevant tissue. It is difficult to conclusively determine if the procedure itself reduced recession or if it occurred due to changes in the patients' oral hygiene practices (all patients switched to the roll tooth brushing technique). Reduction of gingival recession and increase of the attached gingiva zone may have been caused by the resolution of gingival inflammation following elimination of pulling of marginal gingiva and proper oral hygiene. It is likely that elimination of pulling restores proper function of keratinizing cells within the free gingiva and enables reconstruction of the keratinized gingiva zone previously reduced by the inflammatory process.^{1,36} It may support the already postulated observation that elimination of gingival margin pulling restores the conditions for proper functioning of keratinizing cells within the free gingiva. The results also indicate that the elimination of pulling and resolution of marginal gingivitis enabled reconstruction of clinical attachment.

According to Ward, however, it appears that satisfactory periodontal and gingival health can be maintained even where the vestibule is shallow.⁴ Moreover, the findings demonstrate that it is possible to maintain periodontal health and attachment through control of gingival inflammation despite the absence of attached gingiva.³⁷ On the other hand, more recent studies have shown that narrow gingiva in combination with a shallow vestibular fornix might promote the accumulation of food debris during mastication and impede proper oral hygiene. Hence, vestibular deepening should be considered when patients experience discomfort while brushing and chewing. Changes in tooth brushing habits may be of greater importance than increased gingival thickness

for long-term maintenance of the surgically established position of the soft tissue margin.³⁸

The results of this study revealed changes in the presence of plaque and bleeding in the test group. Decreased plaque and bleeding may be due to the creation of better conditions for maintaining oral hygiene as well as frequent follow-up visits (every 3 months in the 12-month observation period), creating an opportunity to reinforce oral hygiene instructions. In the control group, in which patients only received follow-up after 12 months, relevant oral hygiene parameters did not improve. Wade also reported a correlation between plaque scores and vestibule depth when carrying out the deepening of the vestibule according to the Edlan and Mejchar technique.³⁹ He concluded that it is a reliable technique and maintains gingival health in the case of a limited amount of gingival tissue on the labial aspect of the mandibular anterior teeth.

The apically positioned flap (APF) technique seems to be a simple and cost-effective procedure that does not involve a secondary donor site and supplemental biomaterials. Lim et al. reported a KTW of 3.24 ± 1.12 mm 6 months after surgery which decreased to 2.11 ± 0.69 mm after 12 months, as well as higher scores for contour and texture compared to FGG-treated sites.²⁵ Carnio et al. described a modified apically repositioned flap (MARF) technique without donor areas or the use of commercial products.⁴⁰ This approach involved a single horizontal incision within keratinized tissue, preparation of a split-thickness flap, and its suturing to the periosteum in the apical position. The exposed periosteum healed by secondary intention, resulting in a significant increase in KTW from 2.14 mm to 4.24 mm. The reported values are greater than those in our study, but they might be explained by different surgical protocols.

Commercially available ADM yielded inferior outcomes to FGG in terms of obtained KTW and tissue thickness, but that the esthetic results and color match were superior. Wei et al. reported statistically smaller keratinized tissue increases for ADM-treated sites than FGG-treated sites (2.59 ± 0.92 mm compared to 5.57 ± 0.44 mm).²³ Mucograft is a non-cross-linked porcine bilayer collagen matrix (CM) composed of pure type I and III collagen, which was also shown to increase KTW.^{24,25} The CTG attained a mean KTW of 2.6 ± 0.9 mm, while CM attained 2.5 ± 0.9 mm, 6 months after surgery. DynaMatrix is obtained from the submucosa of the small intestine of pigs and is a cell-free matrix where the natural matrix molecules are preserved. Thirteen months after surgical intervention, sites treated with DynaMatrix showed an increased KTW of 2.6 ± 1.1 mm compared to 5.3 ± 1.3 mm of KTW gain as a result of augmentation with autogenous gingival graft.²⁶

In our study, apart from the gain in keratinized tissue, we also observed GRD reduction and CAL gain that were beneficial from a clinical point of view. We speculate that, due to optimizing plaque control and eliminating pulling

syndrome, the proper function of keratinized cells within free gingiva was restored, which enabled reconstruction of keratinized tissues previously reduced by the inflammatory process. Even if the observed changes were small compared to those achieved by previously described techniques, some patients may still benefit from the modified Kazanjian procedure to facilitate plaque control and optimize periodontal health. Such surgery might be more critical for elderly patients, as well as for patients who, for whatever reason – financial or psychological – do not agree to more advanced surgery. In the surgical protocol of this study, patients were prescribed antibiotic prophylaxis for 3 days after the procedure. It can be assumed that taking antibiotics is not necessary after this type of surgery. However, we presented a consecutive group of first operated patients and did not change the protocol until the end of the study.

Limitations

Our research has some limitations. First and foremost, the study is not randomized. Thus, accidental bias, including selection bias, is present. The study groups were formed according to patients' preferences. It would be ethically questionable to purposefully prevent individual patients from receiving treatment. Moreover, the baseline condition of the patients in the present study was not statistically comparable, as controls had a lower amount of KTW. Thus, this is another shortcoming of a non-randomized study. However, the mean KTW value accounted for the labial surfaces of all mandibular incisors and the inclusion criterion was at least 1 tooth with $KTW \leq 1$ mm. The difference may stem from a greater number of teeth with more severely reduced KTW in the controls. Nevertheless, the observed increase in KTW 12 months after treatment in the test group was statistically significant. Even though these issues are important and deserve recognition, we believe that the outcomes of our study might be helpful for practitioners, since there is a gap between protocols being widely investigated and those carried out in clinical practice.

Secondly, although we observed improvement in CAL measurements, it should be stressed that the wound-healing process presumably resulted in the development of long junctional epithelium and not real regeneration. To evaluate the true nature of healing, histological analysis needs to be carried out. Furthermore, the CAL results suggest that the creeping attachment phenomenon may have occurred in the test group on teeth with gingival recession. As mentioned above, the reason for this may be better condition (more space) for the roll tooth brushing technique to be performed.

Thirdly, patient-reported outcomes were not collected. Such data should be included in future studies. The post-surgical course of events, patients' discomfort and pain, esthetic outcomes, and patients' general satisfaction with

the treatment modality should be taken into account. In light of these facts, there is an obvious need for further long-term, well-designed clinical trials with a larger sample size to verify the present findings. Future research should focus on alternative approaches that improve treatment outcomes while also being less invasive and time-consuming and more cost-effective.

Conclusions

Within the limitations of our study, it can be concluded that modified Kazanjian vestibuloplasty is a simple method that increases KTW and improves periodontal health at buccal aspects of the lower incisors. This procedure may be recommended for patients for whom an increase in KTW, reduction in muscle pull and frena elimination are desired, but surgical palatal trauma must be avoided, as well as for patients who do not want to be submitted to a secondary surgical procedure at the palate.

ORCID iDs

Beata Wyrębek  <https://orcid.org/0000-0001-9977-0125>
 Renata Górska  <https://orcid.org/0000-0002-2769-7587>
 Katarzyna Gawron  <https://orcid.org/0000-0003-0937-4749>
 Małgorzata Nędzi-Góra  <https://orcid.org/0000-0003-4041-2678>
 Bartłomiej Górski  <https://orcid.org/0000-0002-3918-4332>
 Paweł Plakwicz  <https://orcid.org/0000-0003-4713-2142>

References

- Schmid M, Mormann W, Bachman A. Mucogingival surgery: The sub-periosteal vestibule extension. Clinical results 2 years after surgery. *J Clin Periodontol.* 1979;6(1):22–32. doi:10.1111/j.1600-051x.1979.tb02287.x
- Mehta P, Peng L. The width of the attached gingiva: Much ado about nothing? *J Dent.* 2010;38(7):517–525. doi:10.1016/j.jdent.2010.04.007
- Cortellini P, Bissada NF. Mucogingival conditions in the natural dentition: Narrative review, case definitions, and diagnostic considerations. *J Clin Periodontol.* 2018;89(Suppl 1):S204–S213. doi:10.1002/JPER.16-0671
- Ward VJ. The depth of the vestibular fornix in the mandibular anterior region in health. *J Periodontol.* 1976;47(11):651–655. doi:10.1902/jop.1976.47.11.651
- Zucchelli G, Marzadori M, Mounssif I, Mazzotti C, Stefanini M. Coronally advanced flap + connective tissue graft techniques for the treatment of deep gingival recession in the lower incisors: A controlled randomized clinical trial. *J Clin Periodontol.* 2014;41(8):806–813. doi:10.1111/jcpe.12269
- Kim DM, Neiva R. Periodontal soft tissue non-root coverage procedures: A systematic review from the AAP regeneration workshop. *J Periodontol.* 2015;86(Suppl 2):S56–S72. doi:10.1902/jop.2015.130684
- Clark HB. Deepening the labial sulcus by mucosal flap advancement: Report of a case. *J Oral Surg.* 1953;11(2):165–168. PMID:13035574
- Friedman N. Mucogingival surgery: The apically repositioned flap. *J Periodontol.* 1962;33(4):328–340. doi:10.1902/jop.1962.33.4.328
- Edlan A, Mejchar B. Plastic surgery of vestibulum in periodontal therapy. *Int Dent J.* 1963;13:593. doi:10.1111/j.1600-0765.1969.tb01984
- Tortorelli AF. A technique for vestibular sulcus extension. *J Prosthet Dent.* 1968;20(1):14–20. doi:10.1016/0022-3913(68)90208-4
- Thoma DS, Benić GI, Zwahlen M, Hämmerle CHF, Jung RE. A systematic review assessing soft tissue augmentation techniques. *Clin Oral Implants Res.* 2009;20(Suppl 4):146–165. doi:10.1111/j.1600-0501.2009.01784.x
- Kazanjian VH. Surgery as an aid to more efficient service with prosthetic dentures. *J Am Dent Assoc.* 1935;22(4):566–581. doi:10.7860/JCDR/2016/16606.7192

13. Kiernicka M, Owczarek B, Gałkowska E, Wysokińska-Miszczuk J. Reduction of gingival recessions as unplanned additional effect of surgical procedures of the oral vestibule. *Annales Universitatis Mariae Curie-Skłodowska*, Lublin. 2007; LXII, N 1, 23, D.
14. Wyrębek B, Górka R, Nędzi-Góra M, Plakwicz P. Effect of vestibular deepening on the periodontal status of teeth: Preliminary study. *J Stoma*. 2016;69(5):531–537. doi:10.5604/00114553.1230107
15. Al-Mahdy ABF. Mandibular anterior ridge extension: A modification of the Kazanjian vestibuloplasty technique. *J Oral Maxillofac Surg*. 1997;55(10):1057–1059, discussion 1060. doi:10.1016/s0278-2391(97)90278-0
16. Ponzoni D, Jardim EC, de Carvalho PS. Vestibuloplasty by modified Kazanjian technique in treatment with dental implants. *J Craniofac Surg*. 2013;24(4):1373–1375. doi:10.1097/SCS.0b013e3182860524
17. Liposky RB. Elimination of the “V” in vestibuloplasty. *J Oral Maxillofac Surg*. 1983;41(5):339–340. doi:10.1016/0278-2391(83)90304-x
18. Wyrębek B, Orzechowska A, Plakwicz P. Vestibular deepening using the modified Kazanjian technique. A case report. *TPS*. 2016;1–2:42–47.
19. Chambrone L, Tatakis DN. Periodontal soft tissue root coverage procedures: A systematic review from the AAP Regeneration Workshop. *J Periodontol*. 2015;86(Suppl 2):S8–S51. doi:10.1902/jop.2015.130674
20. Zucchelli G, Mele M, Stefanini M, et al. Patient morbidity and root coverage outcome after subepithelial connective tissue and deepithelialized gingival grafts: A comparative randomized-controlled clinical trial. *J Clin Periodontol*. 2010;37(8):728–738. doi:10.1111/j.1600-051X.2010.01550.x
21. Wessel JR, Tatkis DN. Patient outcomes following subepithelial connective tissue graft and free gingival graft procedures. *J Periodontol*. 2008;79(3):425–430. doi:10.1902/jop.2008.070325
22. Grzech-Leśniak K, Matys J, Jurczyszyn K, et al. Histological and thermometric examination of soft tissue de-epithelialization using digitally controlled Er:YAG laser handpiece: An ex vivo study. *Photomed Laser Surg*. 2018;36(6):313–319. doi:10.1089/pho.2017.4413
23. Wei PC, Laurell L, Geivelis M, Lingen MW, Maddalozzo D. Acellular dermal matrix allografts to achieve increased attached gingiva. Part 1. A clinical study. *J Periodontol*. 2000;71(8):1297–1305. doi:10.1902/jop.2000.71.8.1297
24. Sanz M, Lorenzo R, Aranda JJ, Martin C, Orsini M. Clinical evaluation of a new collagen matrix (mucograft prototype) to enhance the width of keratinized tissue in patients with fixed prosthetic restorations: A randomized prospective clinical trial. *J Clin Periodontol*. 2009;36(10):868–876. doi:10.1111/j.1600-051X.2009.01460.x
25. Lim HC, An SC, Lee DW. A retrospective comparison of three modalities for vestibuloplasty in the posterior mandible: Apically positioned flap only vs. free gingival graft vs. collagen matrix. *Clin Oral Investig*. 2018;22(5):2121–2128. doi:10.1007/s00784-017-2320-y
26. Nevins M, Nevins ML, Camelo M, Camelo JM, Schupbach P, Kim DM. The clinical efficacy of DynaMatrix extracellular membrane in augmenting keratinized tissue. *Int J Periodontics Restorative Dent*. 2010;30(2):151–161. PMID:20228974
27. Kaya Y, Alkan O, Keskin S. An evaluation of the gingival biotype and the width of keratinized gingiva in the mandibular anterior region of individuals with different dental malocclusion groups and levels of crowding. *Korean J Orthod*. 2017;47(3):176–185. doi:10.4041/kjod.2017.47.3.176
28. O’Leary TJ, Drake RB, Naylor JE. The plaque control record. *J Periodontol*. 1972;43(1):38. doi:10.1902/jop.1972.43.1.38
29. Ainamo J, Bay I. Problems and proposal for recording gingivitis and plaque. *Int Dent J*. 1975;25(4):229–235. PMID:1058834
30. Miller PD. A classification of marginal tissue recession. *Int J Periodontics Restorative Dent*. 1985;5(2):8–13. PMID:3858267
31. Cairo F, Nieri M, Cincinelli S, Mervelt J, Pagliaro U. The interproximal clinical attachment level to classify gingival recessions and predict root coverage outcomes: An explorative and reliability study. *J Clin Periodontol*. 2011;38(7):661–666. doi:10.1111/j.1600-051X.2011.01732.x
32. Agudio G, Nieri M, Rotundo R, Cortellini P, Pini Prato G. Free gingival grafts to increase keratinized tissue: A retrospective long-term evaluation (10 to 25 years) of outcomes. *J Periodontol*. 2008;79(4):587–594. doi:10.1902/jop.2008.070414
33. Agudio G, Cortellini P, Buti J, Pini Prato G. Periodontal conditions of sites treated with gingival augmentation surgery compared with untreated contralateral homologous sites: An 18- to 35-year long-term study. *J Periodontol*. 2016;87(12):1371–1378. doi:10.1902/jop.2016.160284
34. Langer B, Langer L. Subepithelial connective tissue graft technique for root coverage. *J Periodontol*. 1985;56(12):715–720. doi:10.1902/jop.1985.56.12.715
35. Zucchelli G, Mounssif G. Periodontal plastic surgery. *Periodontol 2000*. 2015;68(1):333–368. doi:10.1111/prd.12059
36. Karring T, Lang NP, Loe H. The role of gingival connective tissue in determining epithelial differentiation. *J Periodontol Res*. 1975;10(1):1–11. doi:10.1111/j.1600-0765.1975.tb00001.x
37. Kennedy JE, Bird WC, Palcanis KG, Dorfman HS. A longitudinal evaluation of varying widths of attached gingiva. *J Clin Periodontol*. 1985;12(8):667–675. doi:10.1111/j.1600-051x.1985.tb00938.x
38. Wennström JL, Zucchelli G. Increased gingival dimensions: A significant factor for successful outcome of root coverage procedures? A 2-year prospective clinical study. *J Clin Periodontol*. 1996;23(8):770–777. doi:10.1111/j.1600-051x.1996.tb00608.x
39. Wade AB. Vestibular deepening by the technique of Edlan and Mejchar. *J Periodontol Res*. 1969;4(4):300–313. doi:10.1111/j.1600-0765.1969.tb01984.x
40. Carnio J, Miller PD Jr. Increasing the amount of attached gingiva using a modified apically repositioned flap. *J Periodontol*. 1999;70(9):1110–1117. doi:10.1902/jop.1999.70.9.1110

Upregulation of centromere protein K is crucial for lung adenocarcinoma cell viability and invasion

Yongbo Wang^{1,A,C,D,F}, Yue Wang^{1,A–C}, Chunna Ren^{2,B,C,F}, Haicun Wang^{3,B,C,F}, Yang Zhang^{2,B,C,F}, Yunxia Xiu^{2,A,E,F}

¹ Department of Respiratory Medicine, Second Affiliated Hospital of Mudanjiang Medical University, China

² Medical Laboratory, Second Affiliated Hospital of Mudanjiang Medical University, China

³ Internal Medicine–Cardiovascular Department, Second Affiliated Hospital of Mudanjiang Medical University, China

A – research concept and design; B – collection and/or assembly of data; C – data analysis and interpretation;

D – writing the article; E – critical revision of the article; F – final approval of the article

Advances in Clinical and Experimental Medicine, ISSN 1899–5276 (print), ISSN 2451–2680 (online)

Adv Clin Exp Med. 2021;30(7):691–699

Address for correspondence

Yunxia Xiu

E-mail: xiuyunxia83067@163.com

Funding sources

None declared

Conflict of interest

None declared

Received on September 10, 2020

Reviewed on January 13, 2021

Accepted on March 2, 2021

Published online on June 11, 2021

Abstract

Background. Identification of functional genes or biomarkers may be helpful for developing new treatment strategies in lung adenocarcinoma (LUAD). The centromere protein K (*CENPK*) gene has been discovered to be overexpressed and could influence tumor progression in several tumor types. However, its role in LUAD has never been revealed.

Objectives. The purpose of the current study was to detect the effects of *CENPK* and its mechanisms in the progression of LUAD.

Materials and methods. Data from The Cancer Genome Atlas (TCGA) and Oncomine databases was used to analyze the expression of *CENPK*. The relationship between *CENPK* expression and the prognosis of LUAD was investigated using Kaplan–Meier and Cox regression analyses. The cell viability was monitored with Cell Counting Kit-8 (CCK-8) and colony forming assays, while migration and invasion were analyzed with a transwell assay. The effect of *CENPK* on the expression of epithelial–mesenchymal transition (EMT) markers were estimated using western blotting.

Results. *CENPK* was significantly overexpressed in LUAD tissues and cells ($p < 0.01$). The overall survival rate in the low *CENPK* expression group was significantly higher than in the high *CENPK* expression group ($p = 0.003$). Furthermore, the overexpression of *CENPK* facilitated cell viability, migration and invasion of tumor cells, while knockdown of *CENPK* prevented these behaviors ($p < 0.01$). Moreover, upregulation of *CENPK* decreased the expression of E-cadherin and enhanced the expression of N-cadherin, vimentin and Snail in LUAD cells ($p < 0.01$). Conversely, knockdown of *CENPK* resulted in the opposite trend ($p < 0.01$).

Conclusions. *CENPK* was upregulated in LUAD tissues and cells, and the enhancement of *CENPK* promoted the viability, migration, invasion, and EMT of LUAD cells.

Key words: *CENPK*, viability, migration, epithelial–mesenchymal transition, lung adenocarcinoma

Cite as

Wang Y, Wang Y, Ren C, Wang H, Zhang Y, Xiu Y.

Upregulation of centromere protein K is crucial for lung adenocarcinoma cell viability and invasion.

Adv Clin Exp Med. 2021;30(7):691–699.

doi:10.17219/acem/133820

DOI

10.17219/acem/133820

Copyright

© 2021 by Wrocław Medical University

This is an article distributed under the terms of the Creative Commons Attribution 3.0 Unported (CC BY 3.0)

(<https://creativecommons.org/licenses/by/3.0/>)

Background

Lung cancer is one of the most common cancers and the leading cause of cancer-related death worldwide,^{1–3} with the five-year overall survival (OS) of less than 20%.⁴ Lung adenocarcinoma (LUAD) accounts for approx. 40% of all lung cancers, and is frequently diagnosed at an advanced stage.^{5–7} Currently, the most effective methods for the treatment of LUAD are surgical, radiation and targeted, and immunotherapies directed at the molecular or immunological traits of tumors. Nevertheless, the survival rate of patients with LUAD that have received curative resection is only about 50%.⁸ Therefore, further research into the mechanisms of LUAD and identification of effective biomarkers will contribute to early diagnosis, precise prognosis and development of effective treatments for LUAD.

The kinetochore is a protein structure on chromatids and plays a crucial role in the segregation of chromosomes, the dysfunction or dysregulation of which may lead to aneuploidy and promote carcinogenesis.⁹ Centromere protein K (*CENPK*), also named AF5 α , FKSG14, P33, or Solt5,¹⁰ is a subunit of CENPH-CENPI-associated centromeric complex, which targets centromere protein A (CENPA) to centromeres and is critical for proper kinetochore function and mitotic progression.¹¹ In many malignant tumors, *CENPK* has been reported to be dysregulated and related to tumor progression.^{12–14} For example, *CENPK* is specifically up-regulated in ovarian and hepatocellular cancer tissues, and its overexpression is associated with worse overall survival.¹² More importantly, Wang et al. has previously demonstrated that depletion of *CENPK* could repress the proliferation, migration, invasion, and epithelial–mesenchymal transition (EMT) of hepatocellular carcinoma cells.¹³ Furthermore, through genome-wide gene expression profiling analysis, *CENPK* was screened out as one of the novel therapeutic targets for triple negative breast cancer and knockdown of *CENPK* attenuated cell viability.¹⁴ However, it remains unclear as to whether *CENPK* plays a role in LUAD.

Objectives

In the current study, we analyzed the expression of *CENPK* in LUAD cells and evaluated its prognostic value in patients with LUAD through Kaplan–Meier and Cox regression analyses. Then, the effects on viability, invasion and migration of LUAD cells were explored. Finally, we investigated the influence of *CENPK* on the expression of the key markers of EMT, including E-cadherin, N-cadherin, vimentin, and Snail, in LUAD cells.

Materials and methods

Bioinformatics analysis

The gene expression profile and clinical data of 535 LUAD tumor samples and 59 normal samples were downloaded from The Cancer Genome Atlas (TCGA) (<https://cancergenome.nih.gov/>). Patients diagnosed as LUAD were divided into high and low *CENPK* expression groups based on the median expression of *CENPK*. Then, Kaplan–Meier analysis and univariate and multivariate Cox regression analyses were performed to assess the prognostic value of *CENPK*. In addition, the expression profiles of 45 LUAD samples and 65 normal samples in the OncoPrint database (www.oncoPrint.org) were downloaded to analyze the mRNA expression of *CENPK*.

Cell culture

The LUAD cell lines, including HA109, A549 and Calu-3, were purchased from the Cell Bank of the Shanghai Institute of Cell Biology, Chinese Academy of Medical Sciences (Shanghai, China). The normal human lung epithelial cell line BEAS2B was purchased from American Type Culture Collection (ATCC, Manassas, USA). All the cell lines were serially cultured in Roswell Park Memorial Institute (RPMI)-1640 medium mixed with 10% fetal bovine serum (FBS; Gibco, Rockville, USA), 100 U/mL of penicillin and 100 μ g/mL of streptomycin (Life Technologies, Gaithersburg, USA) at 37°C with 5% CO₂. Tumor cells between passages 4 and 6 were utilized in the experiments.

Cell transfection

Cell transfection was conducted when the cell confluence reached 80% in a six-well plate. Calu-3 cells were transfected with small interfering RNA (siRNA) to downregulate the expression of *CENPK*. The siRNAs used include si-CENPK#1 (5'-TGAGTACCTTGGGCGAGTTTC-3') and si-CENPK#2 (5'-ATATCTGAGGTGGCATAATTT-3'), together with Si-con (5'-CGAACUCACUGGUCUGACC-3') that was transfected as the negative control. Meanwhile, pcDNA3.1-CENPK vector was constructed and transfected into HA109 cells. An empty vector (pcDNA3.1; Genpharma, Shanghai, China) was used as the negative control. Cell transfection was conducted using the Lipofectamine 2000 reagent kit (Invitrogen, Carlsbad, USA). The expression of *CENPK* in LUAD cell lines was detected using quantitative real-time polymerase chain reaction (qRT-PCR) and western blotting 48 h following transfection.

RNA extraction and quantitative real-time PCR

RNA trizol reagent (Invitrogen) was used to extract the total RNA from conventionally cultured cells or cells transfected

Table 1. The sequences of *CENPK* and *GAPDH* primers in qRT-PCR

Genes	Sequences
<i>CENPK</i>	F:5'-ACCGCTGAACTCAGTCAATGGC-3' R:5'-TTGACTCCTTAGTGAGCAGTACC-3'
<i>GAPDH</i>	F:5'-TGTGTCCGTCGTGGATCTGA-3' R:5'-CCTGCTTACCACCTTCTTGA-3'

48 h prior. Subsequently, the extracted RNA was converted to cDNA using a MiRcute miRNA First-strand cDNA synthesis kit (Tiangen Biotech, Beijing, China). Then, the mRNA expression of *CENPK* was measured using quantitative real-time polymerase chain reaction (qRT-PCR) analysis. The relative *CENPK* level was calculated using the $2^{-\Delta\Delta C_t}$ method and normalized to *GAPDH*. The sequences of the primers for *CENPK* and *GAPDH* are shown in Table 1.

Western blotting

Protein was isolated from the cells 48 h following transfection with ice-cold IPA lysis buffer and the concentration was measured using a BCA protein assay kit (Beyotime, Shanghai, China). Then, 20 μ g of protein was put into each well of a vertical electrophoresis tank and separated using sodium dodecyl sulfate polyacrylamide gel electrophoresis (SDS-PAGE). The protein was transferred onto polyvinylidene fluoride (PVDF) membranes, blocked with 5% skim milk powder diluted in TBST buffer (Tris-buffered saline, 0.1% Tween 20) for 1 h then incubated with primary antibodies at 4°C overnight. The rabbit-anti-human primary antibodies against *CENPK* (ab236739, 1:1000; Abcam, Cambridge, UK), E-cadherin (#3195, 1:1000; Cell Signaling Technology, Danvers, USA), N-cadherin (#4061, 1:1000; Cell Signaling Technology), Vimentin (#5741, 1:1000; Cell Signaling Technology), Snail (#3879, 1:1000; Cell Signaling Technology), and *GAPDH* (#5174, 1:1000; Cell Signaling Technology) were used. Next, samples were washed 3 times (5 mins each) with TBST, before the goat-anti-rabbit secondary antibody (#7074, 1:3000; Cell Signaling Technology) was added and incubated at room temperature for 1 h. The blots were visualized using the ECL-Plus western blotting detection system (Thermo Fisher Scientific, Waltham, USA) after washing. The relative protein expression levels of *CENPK*, E-cadherin, N-cadherin, vimentin, and Snail were separately measured through scanning the gray value with QUANTITY ONE software (Bio-Rad, Hercules, USA) and *GAPDH* was used as the internal reference.

Cell Counting Kit-8 assay

The cells were removed from culture and counted 48 h after transfection. A cell suspension was prepared and plated into 96-well plates at a concentration of 1×10^3 cells/well. Then the plate was kept in an incubator at 37°C with 5% CO₂. The cell viability was tested every 24 h using Cell Counting Kit-8 (CCK-8; Dojindo Laboratories, Kumamoto,

Japan) reagent according to manufacturer's instruction. After being incubated for 1.5 h at 37°C, the optical density (OD) value of each well was measured at 450 nm using a microplate reader to reflect cell viability.

Colony formation assay

Following transfection, cells were suspended and seeded into a 60 mm plate (400 cells/plate) with 5 mL of pre-warmed medium at 37°C. Then the cells were cultured at 37°C with 5% CO₂ for 1–2 weeks until colonies were visible. After that, 4% paraformaldehyde and 0.1% crystal violet were used to fix and stain the colonies, respectively, and the number of colonies with a diameter greater than 0.8 mm was counted.

Cell invasion and migration

To analyze cell invasion, 100 μ L of Matrigel was prepared in advance by incubating in serum-free medium overnight and then added into the upper transwell chamber. After being shaken well, the chamber was maintained at 37°C and maintained for 4–6 h. Then, 500 μ L of serum-free medium was put into the lower chamber and incubated for ½ h. Next, 100 μ L of cell suspension (1×10^5 cells) was prepared using serum-free medium after 48 h of transfection and inoculated into the upper chamber, while 500 μ L of complete culture solution was put into the lower chamber. Twenty four hours later, the chamber was removed and washed with phosphate-buffered saline (PBS). It was then fixed with 4% paraformaldehyde for 30 min and stained using 0.1% crystal violet for 20 min. The number of invading cells were quantified. For the cell migration assay, chamber was not coated with Matrigel and the remaining procedures were the same as the invasion assay.

Statistical analyses

Data analyses were performed using SPSS v. 22.0 software (IBM Corp., Armonk, USA) and the figures were plotted in GraphPad Prism software v. 5.0 (GraphPad Software, San Diego, USA). The difference between ranked data as well as the association between *CENPK* expression and clinical factors were analyzed with a χ^2 test. In addition, Kaplan–Meier analysis was performed to estimate the relationship between *CENPK* expression and the overall survival of patients with LUAD. The difference between these groups was evaluated with log-rank test. The prognostic significance of numerous variables was analyzed with univariate and multivariate Cox regression analyses. For the experimental data, the statistical evaluation between 2 groups was performed with Student's t-test, while the statistical evaluation among 3 groups was conducted using one-way analysis of variance (ANOVA) followed by Dunnett's post hoc test. A value of $p < 0.05$ was used to determine statistical significance.

Results

The prognostic value of *CENPK* mRNA expression in LUAD

We analyzed genes that were differentially expressed between LUAD and normal tissue samples using TCGA. As a result, 3430 differentially expressed genes were found, including 2094 upregulated genes and 1336 downregulated genes. Among them, *CENPK* was upregulated in tumor tissues when compared to normal tissues (Fig. 1A, $p < 0.001$). To confirm this result, we analyzed the expression of *CENPK* in LUAD and normal lung tissues with the data from the Oncomine database, finding higher expression of *CENPK* in LUAD tumor tissues than in normal lung tissues (Fig. 1B, $p < 0.001$). To further investigate the expression of *CENPK* in LUAD, we detected its expression

in the LUAD cell lines HA109, A549 and Calu-3, and in normal lung cell line BEAS2B. These results showed that *CENPK* was significantly overexpressed in LUAD cells compared with normal BEAS2B cells (Fig. 1C, $p < 0.001$).

As *CENPK* was upregulated in LUAD, we decided to test whether *CENPK* was related to patient prognosis. After analyzing the relationship between clinical factors and *CENPK* expression in LUAD samples, we found that the expression of *CENPK* was statistically associated with gender ($p = 0.048$), tumor stage ($p = 0.028$) and pathologic-N (lymph node) stage ($p = 0.007$) of patients with LUAD (Table 2). Subsequently, we evaluated the influence of *CENPK* on the overall survival of patients with LUAD using Kaplan–Meier analysis, observing the overall survival time of patients with higher *CENPK* expression was shorter than those with lower expression (Fig. 1D, log-rank test, $p = 0.003$). Finally, univariate and multivariate Cox

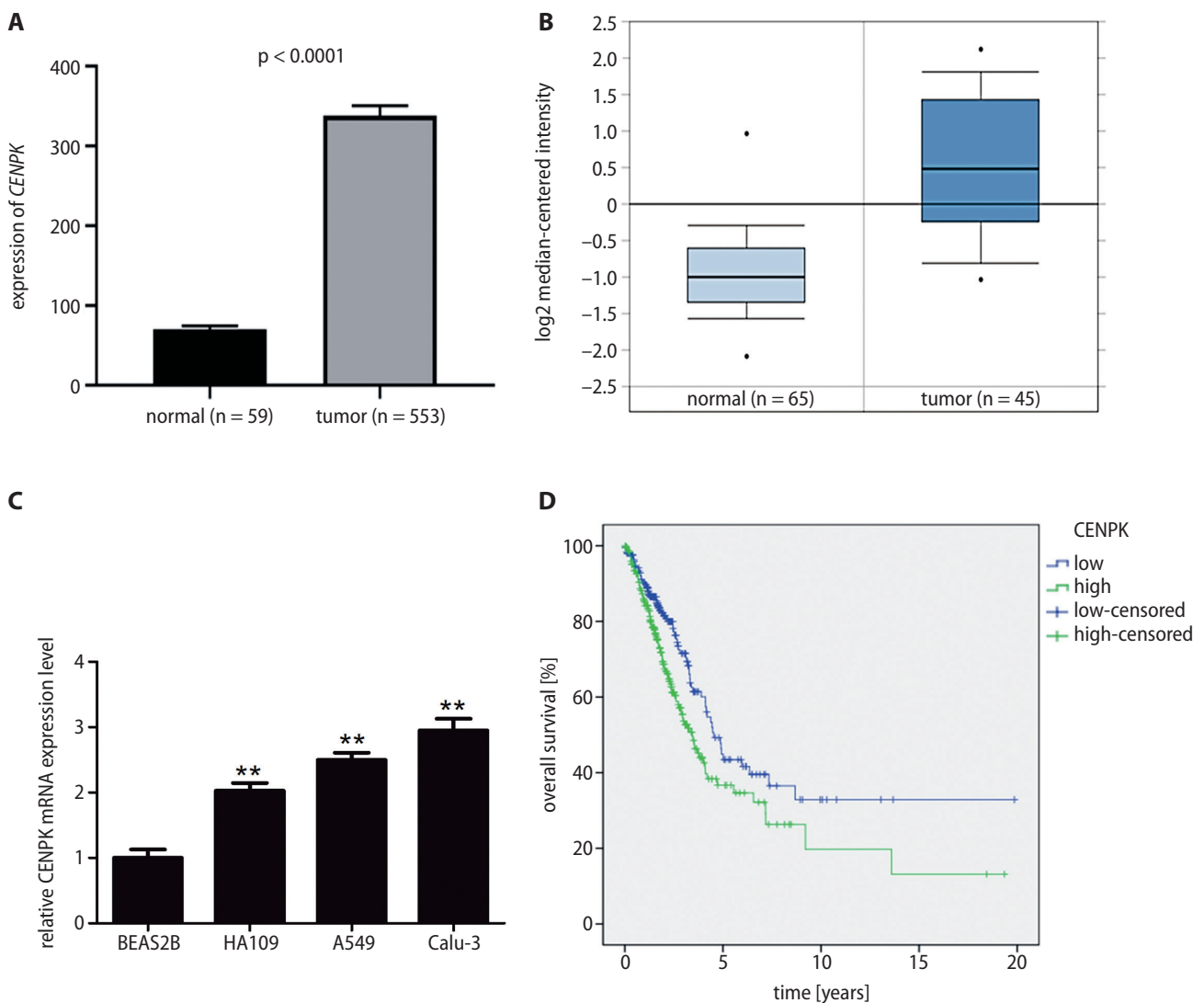


Fig. 1. The overexpression of *CENPK* and its association with cancer prognosis in LUAD. A and B. The mRNA expression of *CENPK* in tumor tissues was higher than in normal tissues according to TCGA (A) and Oncomine (B) databases; C. *CENPK* was upregulated in LUAD cell lines in comparison to normal lung cell lines. The data were analyzed using the $2^{-\Delta\Delta ct}$ method and presented as the mean \pm SD; D. Kaplan–Meier analysis of *CENPK* expression in samples from TCGA showed that patients with higher *CENPK* level had a much shorter survival time

* $p < 0.05$; ** $p < 0.01$.

Table 2. The relationship between clinical characteristics and the expression of *CENPK*

Characteristics	Expression of <i>CENPK</i>		p-value
	low	high	
Age			
<60	62	74	0.205
≥60	184	170	
Gender			
female	146	124	0.048*
male	104	126	
Clinical stage			
I-II	201	184	0.028*
III-IV	43	64	
Pathologic-T			
T1+T2	215	218	0.776
T3+T4	33	31	
Pathologic-N			
N0	174	149	0.007*
N1	68	98	
Pathologic-M			
M0	162	170	0.143
M1	8	16	

p < 0.05 indicated statistical significance.

regression analyses were used to determine the prognostic significance of *CENPK* in LUAD. This data revealed that *CENPK* expression (p = 0.004), clinical stage (p < 0.001), pathologic-T (tumor) (p < 0.001), pathologic-M (metastasis) (p = 0.006), and pathologic-N (p = 0.000) were all unfavorable LUAD prognostic factors. Furthermore, multivariate Cox regression analysis suggested that pathologic-T (hazard ratio (HR) = 1.687, 96% confidence interval (95% CI) = 1.049–2.713, p = 0.031) and pathologic-N (HR = 2.031, 95% CI = 1.363–3.026, p < 0.001) can serve as independent prognostic markers, but *CENPK* (HR = 1.399, 95% CI = 0.898–1.979, p = 0.058) cannot be a significant predictor of disease progression in patients with LUAD (Table 3).

CENPK promotes the viability of LUAD cells

Calu-3 and HA109 cells were used to conduct the loss and gain of function of *CENPK* assays, respectively. Calu-3 cells with downregulated *CENPK* (p < 0.001) and HA109 cells with overexpressed *CENPK* (p = 0.001) were successfully constructed (Fig. 2A–D).

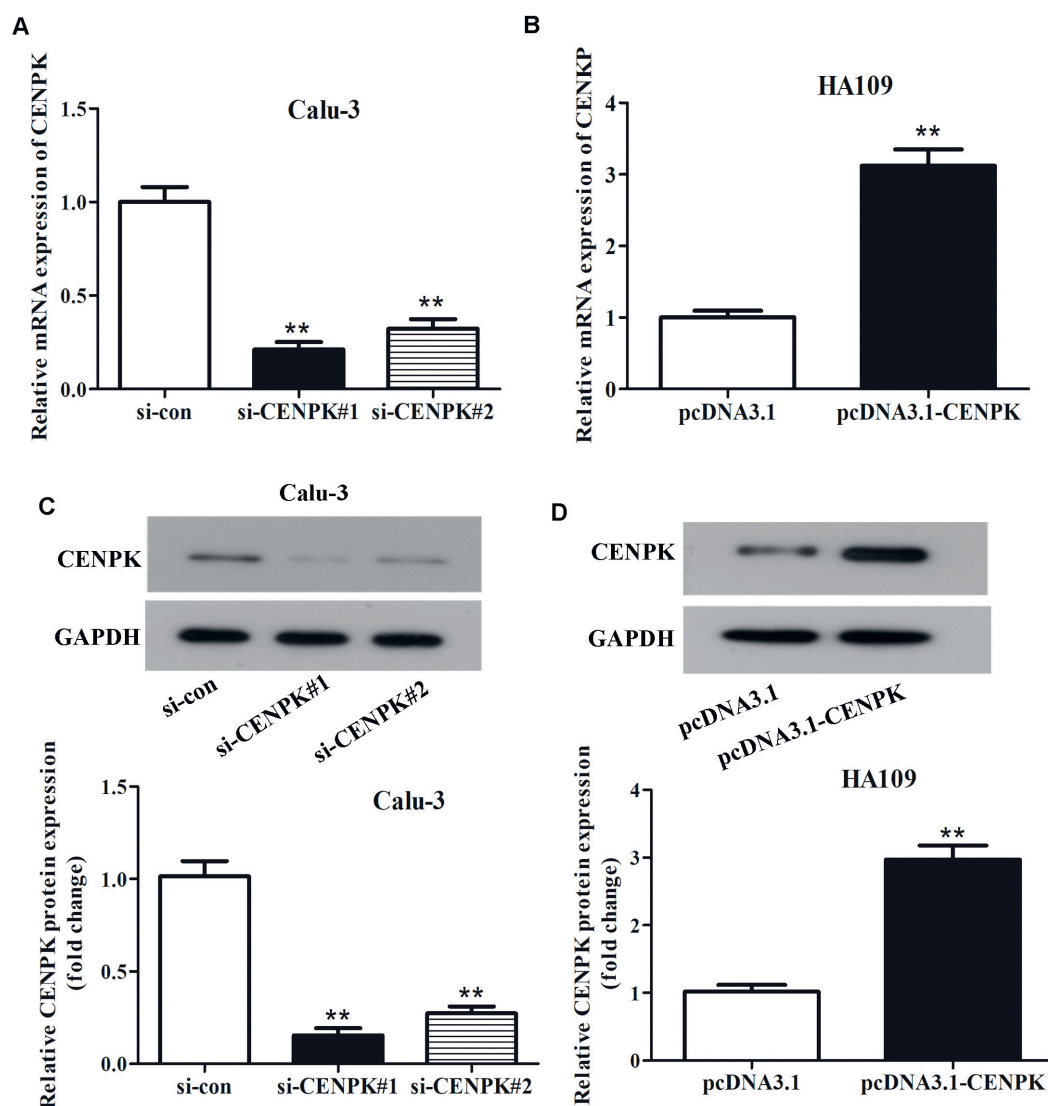


Fig. 2. The expression of *CENPK* in LUAD cells was examined with qRT-PCR and western blotting. A and C. *CENPK* was knocked down in Calu-3 cells by si-CENPK; B and D. *CENPK* was overexpressed in HA109 cells after transfection with pcDNA3.1-CENPK. The data are shown as mean ± SE
*p < 0.05; **p < 0.01.

Table 3. Univariate and multivariate Cox regression analysis

Variables	Univariate analysis			Multivariate analysis		
	p-value	HR	95% CI	p-value	HR	95% CI
<i>CENPK</i> expression (high/low)	0.004*	1.551	1.154–2.084	0.058	1.399	0.898–1.979
Clinical stage (I+II/III+IV)	<0.001*	2.466	1.810–3.360	0.276	1.317	0.803–2.160
Pathologic-T (T1+T2/T3+T4)	<0.001*	2.147	1.467–3.140	0.031*	1.687	1.049–2.713
Pathologic-M (M0/M1)	0.006*	2.132	1.244–3.653	0.354	1.356	0.712–2.582
Pathologic-N (N0/N1+N2+N3)	<0.001*	2.507	1.864–3.370	<0.001*	2.031	1.363–3.026
Age (<60/≥60)	0.746	1.056	0.760–1.468	–	–	–
Gender (female/male)	0.616	1.077	0.805–1.442	–	–	–

HR – hazard ratio; 95% CI – 95% confidence interval; p < 0.05 indicated statistical significance.

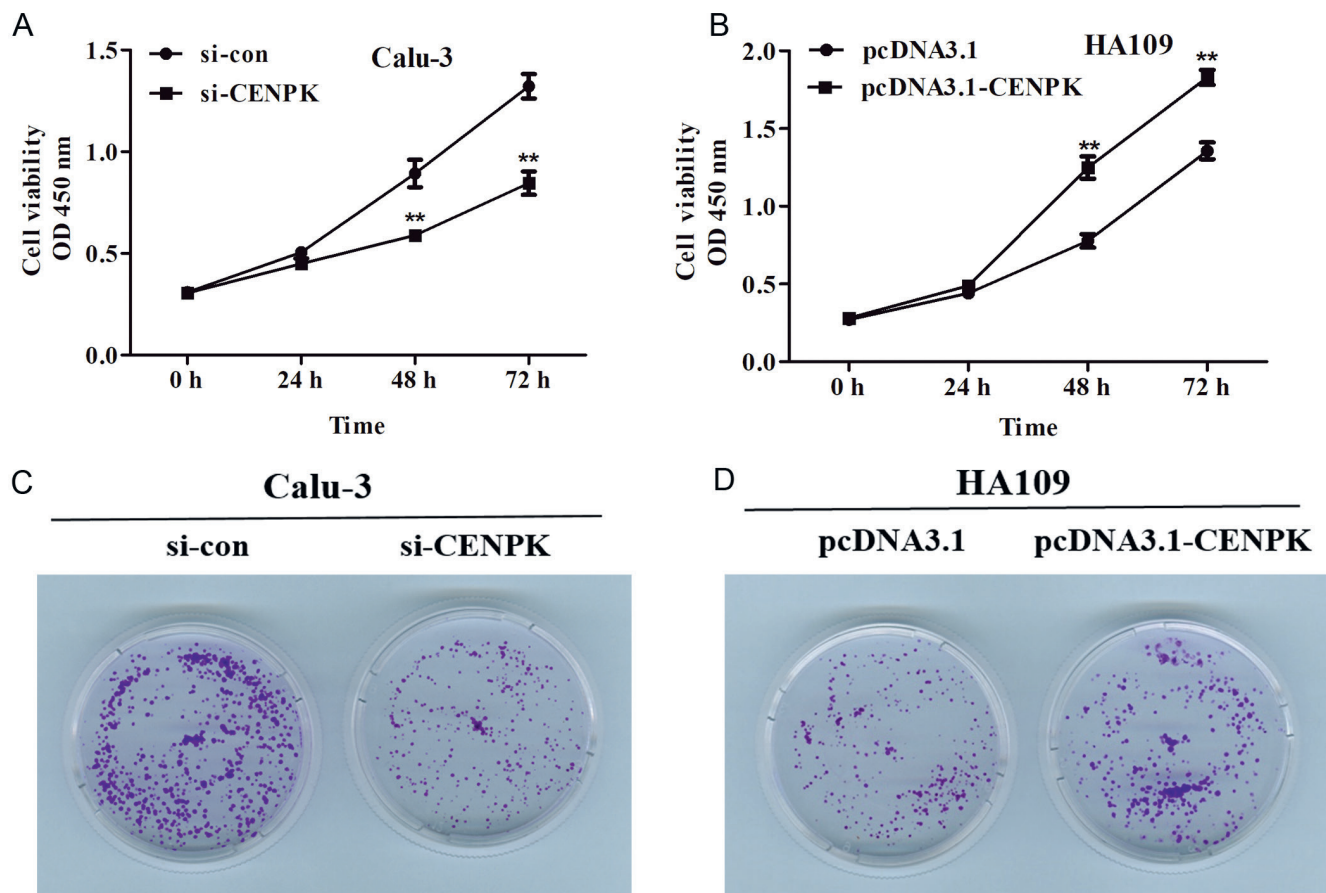


Fig. 3. The role of *CENPK* in the viability of LUAD cells. A and B. The cell viability of LUAD cells was detected using a CCK-8 assay after *CENPK* was knocked down in Calu-3 cell line (A) and overexpressed in HA109 cell line (B). The data was shown as mean \pm SD; C and D. The colonies formed by Calu-3 cell line with depleted *CENPK* (C) and HA109 cell line with overexpressed *CENPK* (D)

*p < 0.05; **p < 0.01.

To study the role of *CENPK* in the viability of LUAD cells, the CCK-8 assay and colony forming assay were performed. The CCK-8 results demonstrated that knock-down of *CENPK* could inhibit the viability of Calu-3 cells (p = 0.002; p = 0.001), while the overexpression of *CENPK* accelerated the growth of HA109 cells (p = 0.001; p < 0.001) at 48 h and 72 h (Fig. 3A,B; p < 0.001). To verify this conclusion, we implemented colony forming assays. The data indicated that the number of the colonies of Calu-3 cells

was decreased (p = 0.002), while the number of the colonies of HA109 cells was increased (p = 0.014) compared with their corresponding control groups (Fig. 3C,D).

***CENPK* enhances cell migration and invasion, and promotes EMT of LUAD cells**

We next investigated the function of *CENPK* on the migration and invasion of LUAD cells by employing a transwell

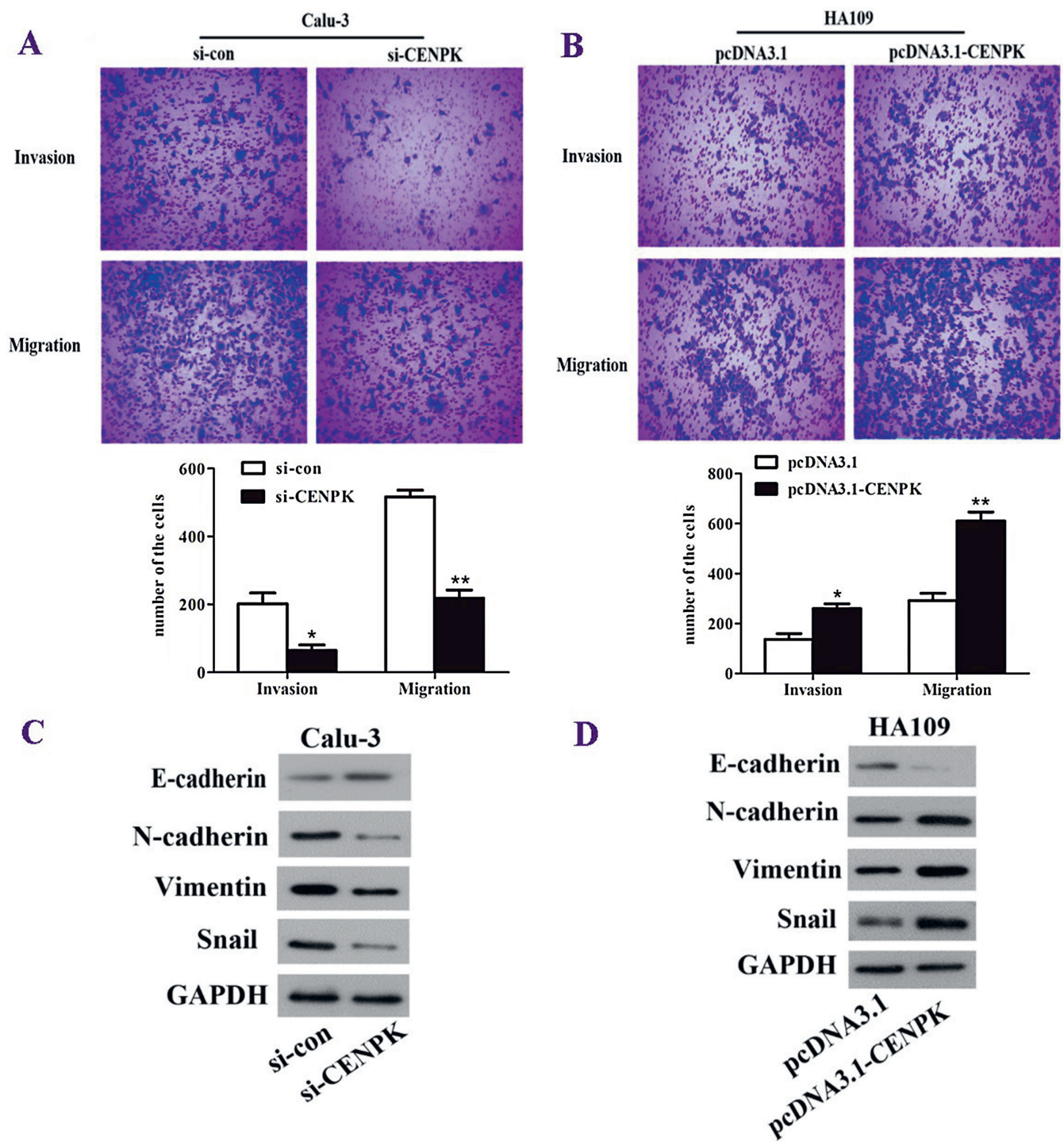


Fig. 4. The function of *CENPK* on cell migration and invasion. **A.** Knockdown of *CENPK* inhibited the migration and invasion of Calu-3 cells. The data are shown as mean ±SE; **B.** Overexpressed *CENPK* promoted cell migration and invasion of HA109 cells. The data is shown as mean ±SE; **C.** Knockdown of *CENPK* increased the expression of E-cadherin and decreased the expression of N-cadherin, vimentin and Snail in Calu-3 cells; **D.** Overexpression of *CENPK* decreased the expression of E-cadherin and increased the expression of N-cadherin, vimentin and Snail in HA109 cells

*p < 0.05; **p < 0.01.

assay system. Knockdown of *CENPK* alleviated the migration ($p < 0.001$) and invasion ($p = 0.018$) of Calu-3 cell (Fig. 4A), while in contrast, both the migratory ($p = 0.002$) and invasive ($p = 0.014$) abilities of HA109 cells were strengthened when *CENPK* was overexpressed (Fig. 4B).

The EMT participates in the progression of many tumor types and it is thought to regulate the function of some

genes in LUAD.^{15,16} The main characteristic of EMT is the loss of cell–cell adhesion markers, such as E-cadherin, along with an increased rate of cell migration and invasiveness.¹⁷ Therefore, we hypothesized that the function of *CENPK* might be connected with EMT. To explore this hypothesis, we detected the expression of the EMT markers E-cadherin, N-cadherin, vimentin, and Snail. As expected,

CENPK could mediate the expression of E-cadherin, N-cadherin, vimentin, and Snail. Knockdown of *CENPK* increased the expression of E-cadherin but reduced the levels of N-cadherin, vimentin and Snail in Calu-3 cells (Fig. 4C). Conversely, the overexpression of *CENPK* was found to increase the levels of N-cadherin, vimentin and Snail and decrease the expression of E-cadherin in HA109 cells (Fig. 4D). These results suggested that *CENPK* facilitates the EMT process of LUAD cells.

Discussion

In the present study, we demonstrated that *CENPK* was upregulated in LUAD tissues and cells, and higher expression of *CENPK* was correlated with shorter survival time of patients. Biological experiments then revealed that enhancement of *CENPK* expression promoted the viability, migration, invasion, and the EMT process of LUAD cells, suggesting the participation of *CENPK* in LUAD progression.

CENPK is located on chromosome 5q12.3 and has previously been verified to play a crucial role in several types of cancers.¹⁸ In the study by Lee et al., *CENPK* was shown to be upregulated and could serve as a novel tumor marker for ovarian cancer.¹² Furthermore, Wang et al. discovered that the expression of *CENPK* was increased in hepatocellular carcinoma and it promoted its aggressive progression by regulating YAP1.¹³ Finally, Komatsu et al. confirmed that *CENPK* was upregulated in triple-negative breast cancer and could act as a novel molecular therapeutic target.¹⁴ All these published reports hint at the critical role of *CENPK* in tumor progression. In the current study, we also found for the first time that *CENPK* was overexpressed in both LUAD tissue samples and cell lines which suggested the oncogenic role of *CENPK* in LUAD.

As the prognosis of LUAD is poor,¹⁹ it is meaningful to seek some functional genes or biomarkers to predict the prognosis of LUAD. For that reason, we estimated the prognostic value of *CENPK* in LUAD. Firstly, we assessed the connection between *CENPK* expression and clinical features which showed that *CENPK* expression was related to gender, pathologic tumor stage and pathologic-N (lymph node involvement). Then, we performed the Kaplan–Meier analysis, and demonstrated that patients with high expression of *CENPK* often had much shorter survival times than those with low expression of *CENPK*, indicating that *CENPK* expression was connected with the prognosis of LUAD. However, *CENPK* was not found to be an independent prognostic predictor, and should be utilized with other markers.

As mentioned above, *CENPK* can promote the malignant progression of some tumors such as hepatocellular carcinoma, ovarian cancer and triple-negative breast cancer. However, the role of *CENPK* in LUAD has never been evaluated. Of note, CENPA, CENPE and CENPH, which

are also members of CENP family of proteins, have been discovered to be abnormally expressed in cancer and are correlated with tumor growth in lung cancer.^{20–24} Wu et al. reported that enhanced CENPA expression is correlated with shorter overall survival of LUAD patients and could be an independent marker for LUAD.²³ Centromere protein A was also screened as a member of potential diagnostic biomarkers in LUAD by an integrated microarray analysis.²² Through bioinformatics, Qi et al. uncovered that CENPA was a pivotal gene that was closely related to the overall survival of patients with lung squamous cell carcinoma.²⁰ CENPE, which highly expressed in the G2/M phase of the cell cycle, was also found to be upregulated in LUAD tissues, and could facilitate the proliferation of LUAD cells by directly mediating by FOXM1.²¹ Similarly, CENPH presented at higher levels in non-small cell lung cancer cells and tissues than the surrounding normal tissue as well, and this high expression was associated with poor outcome in patients.²⁴ This data suggested the vital role of CENP family proteins in the progression of lung cancer. Hence, we analyzed the effects of *CENPK* on cell viability, cell migration and invasion of LUAD cells in our study. We discovered that overexpressed *CENPK* could enhance the cell viability, cell migration and invasion of LUAD cells, hinting the involvement of *CENPK* in the aggressive progression of LUAD tumors.

The EMT is a reversible progression during which polarized epithelial cells can transform into a mesenchymal phenotype according to the interaction with the surrounding mesenchyme and the basement membrane.²⁵ It has been reported that EMT is related to embryonic development and organ formation, wound healing and fibrosis, and cancer progression.²⁶ Previous studies have shown that the initiation of EMT in tumor cells may regulate cancer metastasis, recurrence and therapeutic resistance, and has been shown to play an important role in the tumorigenesis of lung cancer.²⁷ Meng et al. found that the overexpression of Williams syndrome transcription factor (WSTF) promoted the proliferation and invasiveness of lung cancer cells by upregulating the expression of EMT-related genes.²⁸ The EMT is also considered to be associated with the prognosis of lung cancers.²⁹ With respect to LUAD, there is a large volume of literature regarding the function of EMT in its development and progression. In the study by Yuanhua et al., the overexpression of KRT16 was induced by TFAP2A and it promoted tumorigenicity via regulating EMT in LUAD.¹⁹ Pang et al. revealed that RCC2 promoted intrapulmonary metastases, and cell migration, invasion and proliferation via inducing EMT and stimulating the expression of matrix metalloproteinase (MMP)-2 and MMP-9.³⁰ In addition, the activation of EMT was also shown to influence the malignant behavior or prognosis of LUAD via regulating different genes.^{31–33} Finally, *CENPK* could accelerate cell proliferation, migration and invasion, as well as EMT progression in hepatocellular carcinoma

cells.¹³ Herein, we speculated that the expression of *CENPK* may have effects on EMT-related genes in LUAD cells, so we detected the expression of EMT markers including E-cadherin, N-cadherin, vimentin, and Snail. It was shown that N-cadherin, vimentin and Snail were all decreased while E-cadherin was raised in LUAD cells when *CENPK* was knocked down, and that this was reversed when *CENPK* was overexpressed. This might indicate that *CENPK* affects tumor progression of LUAD by activating EMT. However, we have only detected the relative expression of genes connecting with EMT, and the detailed mechanism of how *CENPK* communicates with these EMT markers deserves further investigation.


Conclusions


The enhanced expression of *CENPK* functioned as a promoter of the viability, migration, invasion, and EMT of LUAD cells in vitro, which suggests the oncogenic role of *CENPK* in LUAD. However, larger case-control studies containing clinical data and the corresponding experiments in vivo are lacking herein. Furthermore, the detailed and accurate mechanisms still need further research.

ORCID iDs

Yongbo Wang  <https://orcid.org/0000-0002-3344-9360>

Yue Wang  <https://orcid.org/0000-0003-4573-8554>

Chunna Ren  <https://orcid.org/0000-0003-3117-7004>

Haicun Wang  <https://orcid.org/0000-0001-6636-3822>

Yang Zhang  <https://orcid.org/0000-0002-4520-2293>

Yunxia Xiu  <https://orcid.org/0000-0002-4187-5191>

References

- Siegel RL, Miller KD, Jemal A. Cancer statistics, 2019. *CA Cancer J Clin*. 2019;69(1):7–34. doi:10.3322/caac.21551
- Jemal A, Bray F, Center MM, Ferlay J, Ward E, Forman D. Global cancer statistics. *CA Cancer J Clin*. 2011;61(2):69–90. doi:10.3322/caac.20107
- Didkowska J, Wojciechowska U, Mańczuk M, Łobaszewski J. Lung cancer epidemiology: Contemporary and future challenges worldwide. *Ann Transl Med*. 2016;4(8):150. doi:10.21037/atm.2016.03.11
- Bi R, Bai Q, Zhu X, et al. ALK rearrangement: A high-frequency alteration in ovarian metastasis from lung adenocarcinoma. *Diagn Pathol*. 2019;14(1):96. doi:10.1186/s13000-019-0864-7
- Ryan BM. Lung cancer health disparities. *Carcinogenesis*. 2018;39(6):741–751. doi:10.1093/carcin/bgy047
- Patel MI, Cheng I, Gomez SL. US lung cancer trends by histologic type. *Cancer*. 2015;121(7):1150–1152. doi:10.1002/cncr.29180
- Zappa C, Mousa SA. Non-small cell lung cancer: Current treatment and future advances. *Transl Lung Cancer Res*. 2016;5(3):288–300. doi:10.21037/tlcr.2016.06.07
- Xia W, Yu X, Mao Q, et al. Improvement of survival for non-small cell lung cancer over time. *Onco Targets Ther*. 2017;10:4295–4303. doi:10.2147/OTT.S145036
- Scully R. The spindle assembly checkpoint, aneuploidy, and gastrointestinal cancer. *N Engl J Med*. 2010;363(27):2665–2666. doi:10.1056/NEJMe1008017
- Taki T, Hayashi Y, Taniwaki M, et al. Fusion of the MLL gene with two different genes, AF-6 and AF-5alpha, by a complex translocation involving chromosomes 5, 6, 8 and 11 in infant leukemia. *Oncogene*. 1996;13(10):2121–2130. PMID:8950979
- Okada M, Cheeseman IM, Hori T, et al. The CENP-H-I complex is required for the efficient incorporation of newly synthesized CENP-A into centromeres. *Nat Cell Biol*. 2006;8(5):446–457. doi:10.1038/ncb1396
- Lee YC, Huang CC, Lin DY, Chang WC, Lee KH. Overexpression of centromere protein K (*CENPK*) in ovarian cancer is correlated with poor patient survival and associated with predictive and prognostic relevance. *PeerJ*. 2015;3:e1386. doi:10.7717/peerj.1386
- Wang J, Li H, Xia C, et al. Downregulation of *CENPK* suppresses hepatocellular carcinoma malignant progression through regulating YAP1. *Onco Targets Ther*. 2019;12:869–882. doi:10.2147/OTT.S190061
- Komatsu M, Yoshimaru T, Matsuo T, et al. Molecular features of triple negative breast cancer cells by genome-wide gene expression profiling analysis. *Int J Oncol*. 2013;42(2):478–506. doi:10.3892/ijo.2012.1744
- Song J, Wang W, Wang Y, et al. Epithelial–mesenchymal transition markers screened in a cell-based model and validated in lung adenocarcinoma. *BMC Cancer*. 2019;19:680. doi:10.1186/s12885-019-5885-9
- Huang Q, Han J, Fan J, et al. IL-17 induces EMT via Stat3 in lung adenocarcinoma. *Am J Cancer Res*. 2016;6(2):440–451. PMID:27186414
- Nath D, Li X, Mondragon C, et al. Abi1 loss drives prostate tumorigenesis through activation of EMT and non-canonical WNT signaling. *Cell Commun Signal*. 2019;17(1):120. doi:10.1186/s12964-019-0410-y
- Gerhard DS, Wagner L, Feingold EA, et al; MGC Project Team. The status, quality, and expansion of the NIH full-length cDNA project: the Mammalian Gene Collection (MGC). *Genome Res*. 2004;14(10B):2121–2127. doi:10.1101/gr.2596504
- Yuanhua L, Pudong Q, Wei Z, et al. TFAP2A induced KRT16 as an oncogene in lung adenocarcinoma via EMT. *Int J Biol Sci*. 2019;15(7):1419–1428. doi:10.7150/ijbs.34076
- Qi L, Gao C, Feng F, et al. MicroRNAs associated with lung squamous cell carcinoma: New prognostic biomarkers and therapeutic targets. *J Cell Biochem*. 2019;120(11):18956–18966. doi:10.1002/jcb.29216
- Shan L, Zhao M, Lu Y, et al. CENPE promotes lung adenocarcinoma proliferation and is directly regulated by FOXM1. *Int J Oncol*. 2019;55(1):257–266. doi:10.3892/ijo.2019.4805
- Liu WT, Wang Y, Zhang J, et al. A novel strategy of integrated microarray analysis identifies CENPA, CDK1 and CDC20 as a cluster of diagnostic biomarkers in lung adenocarcinoma. *Cancer Lett*. 2018;425:43–53. doi:10.1016/j.canlet.2018.03.043
- Wu Q, Qian YM, Zhao XL, et al. Expression and prognostic significance of centromere protein A in human lung adenocarcinoma. *Lung Cancer*. 2012;77(2):407–414. doi:10.1016/j.lungcan.2012.04.007
- Liao WT, Wang X, Xu LH, et al. Centromere protein H is a novel prognostic marker for human nonsmall cell lung cancer progression and overall patient survival. *Cancer*. 2009;115(7):1507–1517. doi:10.1002/cncr.24128
- Otsuki Y, Saya H, Arima Y. Prospects for new lung cancer treatments that target EMT signaling. *Dev Dyn*. 2018;247(3):462–472. doi:10.1002/dvdy.24596
- Kalluri R, Weinberg RA. The basics of epithelial–mesenchymal transition. *J Clin Invest*. 2009;119(6):14–20–1428. doi:10.1172/JCI39104
- Huber MA, Kraut N, Beug H. Molecular requirements for epithelial–mesenchymal transition during tumor progression. *Curr Opin Cell Biol*. 2005;17(5):548–558. doi:10.1016/j.ceb.2005.08.001
- Meng J, Zhang XT, Liu XL, et al. WSTF promotes proliferation and invasion of lung cancer cells by inducing EMT via PI3K/Akt and IL-6/STAT3 signaling pathways. *Cell Signal*. 2016;28(11):1673–1682. doi:10.1016/j.cellsig.2016.07.008
- Feng J, Zhang X, Zhu H, Wang X, Ni S, Huang J. FoxQ1 overexpression influences poor prognosis in non-small cell lung cancer, associates with the phenomenon of EMT. *PLoS One*. 2012;7(6):e39937. doi:10.1371/journal.pone.0039937
- Pang B, Wu N, Guan R, et al. Overexpression of RCC2 enhances cell motility and promotes tumor metastasis in lung adenocarcinoma by inducing epithelial–mesenchymal transition. *Clin Cancer Res*. 2017;23(18):5598–5610. doi:10.1158/1078-0432.CCR-16-2909
- Bian T, Zheng L, Jiang D, et al. Overexpression of fibronectin type III domain containing 3B is correlated with epithelial–mesenchymal transition and predicts poor prognosis in lung adenocarcinoma. *Exp Ther Med*. 2019;17(5):3317–3326. doi:10.3892/etm.2019.7370
- Hou XM, Yuan SQ, Zhao D, Liu XJ, Wu XA. LDH-A promotes malignant behavior via activation of epithelial-to-mesenchymal transition in lung adenocarcinoma. *Biosci Rep*. 2019;39(1):BSR20181476. doi:10.1042/BSR20181476
- Lin H, Cheng W, Yan H, Zhang X. Overexpression of the long noncoding RNA CCAT1 promotes metastasis via epithelial-to-mesenchymal transition in lung adenocarcinoma. *Oncol Lett*. 2018;16(2):1809–1814. doi:10.3892/ol.2018.8813

MiR-124 protects against cognitive dysfunction induced by sevoflurane anesthesia in vivo and in vitro through targeting calpain small subunit 1 via NF- κ B signaling pathway

*Zijun Zhao^{1,2,A,B,D,F}, *Li Ma^{3,B,C}, Yishuai Li^{4,B,C}, Qi Zhang^{5,B,D}, Ying Wang^{6,B,C,F}, Yanlei Tai^{1,B-D,F}, QiuJun Wang^{1,E,F}

¹ Department of Anesthesiology, The Third Hospital of Hebei Medical University, Shijiazhuang, China

² Department of Anesthesiology, Hebei Provincial Chest Hospital, Shijiazhuang, China

³ Department of Surgery, Faculty of Clinical Medicine, Shijiazhuang People's Medical College, China

⁴ Department of Thoracic Surgery, Hebei Provincial Chest Hospital, Shijiazhuang, China

⁵ Department of Anesthesiology, Hebei Children's Hospital, Shijiazhuang, China

⁶ Department of Anesthesiology, Tangshan Gongren Hospital, China

A – research concept and design; B – collection and/or assembly of data; C – data analysis and interpretation;

D – writing the article; E – critical revision of the article; F – final approval of the article

Advances in Clinical and Experimental Medicine, ISSN 1899–5276 (print), ISSN 2451–2680 (online)

Adv Clin Exp Med. 2021;30(7):701–709

Address for correspondence

QiuJun Wang

E-mail: wangqiuJun@163.com

Funding sources

National Natural Science Foundation of China (grant No. 81771134);

Natural Science Foundation of Hebei Province (grant No.

H2018206305); Hebei Province Technology Innovation Guide Project Science and Technology Winter Olympics special project (grant No. 19977790D); Hebei Provincial government funded the specialty capacity building and specialty leader training program.

Conflict of interest

None declared

* Zijun Zhao and Li Ma contributed equally to this study.

Received on August 29, 2020

Reviewed on September 8, 2020

Accepted on March 22, 2021

Published online on June 11, 2021

Cite as

Zhao Z, Ma L, Li Y, et al. MiR-124 protects against cognitive dysfunction induced by sevoflurane anesthesia in vivo and in vitro through targeting Calpain small subunit 1 via NF- κ B signaling pathway. *Adv Clin Exp Med.* 2021;30(7):701–709. doi:10.17219/acem/134740

DOI

10.17219/acem/134740

Copyright

© 2021 by Wrocław Medical University

This is an article distributed under the terms of the Creative Commons Attribution 3.0 Unported (CC BY 3.0)

(<https://creativecommons.org/licenses/by/3.0/>)

Abstract

Background. Postoperative cognitive dysfunction (POCD) is an impairment of cognition that affects post-surgery patients. Sevoflurane anesthesia is linked to cognitive dysfunction correlated to the expression of miRNA levels.

Objectives. In the current study, we investigated if miR-124 can offer protection against cognitive deficits induced by sevoflurane in a spatial learning paradigm, and examined the molecular mechanisms through cell cultures.

Materials and methods. Escape latency, platform crossings in probe trials and swimming speed in the Morris water maze in sevoflurane-treated mice were utilized as a measure of cognitive function. The relative miR-124 expression, and mRNA expressions of Bax, caspase-3 and Bcl-2 in sevoflurane-treated hippocampal cultures were measured using real-time quantitative polymerase chain reaction (RT-qPCR). Moreover, the changes in interleukin (IL)-1 β , tumor necrosis factor alpha (TNF- α) and IL-6 were determined using enzyme-linked immunosorbent assay (ELISA). The binding between miR-124 and calpain small subunit 1 (Capn4) was verified with site-directed mutagenesis. The involvement of the nuclear factor kappa B (NF- κ B) signaling pathway was examined using western blot analysis.

Results. Our findings indicated that the miR-124 expression was inhibited by sevoflurane treatment in live rats and mouse hippocampal neurons to prevent apoptosis and inflammatory responses. We confirmed Capn4 as a target of miR-124. Treatment with sevoflurane enhanced the expression of Capn4, while overexpression of miR124 suppressed the enhanced expression of Capn4. Also, miR-124 inhibited apoptosis in murine hippocampal neurons induced by sevoflurane via the NF- κ B signaling pathway.

Conclusions. Our findings demonstrated that miR-124 exerted its neuroprotective role against sevoflurane via targeting Capn4 and NF- κ B signaling pathways. Our work may provide a novel and efficacious treatment for sevoflurane anesthesia-related cognitive dysfunction.

Key words: sevoflurane, NF- κ B signaling pathway, miR-124, postoperative cognitive dysfunction, Capn4

Background

Postoperative cognitive dysfunction (POCD) is a syndrome characterized by a reduction in cognitive abilities tested before and after surgery, and is associated with high mortality and morbidity.^{1,2} The morbidity caused by POCD is more severe in people above 60 years of age.^{3,4} Evidence showed that neuroinflammation exerts a vital role in the prognosis of POCD via facilitating the infiltration of macrophages into the brain, compromising the blood–brain barrier, and damaging neurons and synapses.⁵ Another study revealed that sevoflurane anesthesia reduces neurogenesis and neuronal survival in the hippocampus related to cognitive dysfunction.⁶ A recent study showed that sevoflurane treatment leads to the reduction of cell survival and apoptosis as well as inflammation in cultured hippocampal neurons.⁷ Therefore, sevoflurane anesthesia may serve as a good model for the development of POCD by elevating the apoptosis and inflammatory responses.⁸ Given the impact of POCD on patients' quality of life and its demonstrated neurotoxic effects in vitro, there is an unmet need for an efficient neuroprotective agent for the prevention of POCD. MicroRNAs (miRNAs) are a group of small RNAs consisting of 18–22 nucleotides, involved in regulating gene transcription through binding to 3'-UTR of their targets.⁹ Previous research suggests that miRNA regulates cognition, plasticity and synaptic transmission. For example, miR-134 overexpression decreases the size of dendritic spines in the hippocampus.^{10–12} Similarly, miR-124 plays a vital role in the regulation of synaptic facilitation induced by serotonin at the sensory-motor synapse, and the overexpression of miR-124 reduced the expression of *CREB*, which is a gene related to synaptic plasticity.¹³ Emerging evidence suggests that miR-9, miR-124 and miR-29a/b-1 are dysregulated and enhanced the production of A β in the brains of patients with Alzheimer's disease (AD).^{14,15} MiR-124 is also preferentially expressed in the central nervous system (CNS), up to 100-fold in neurons compared to other organs in the rat.¹⁶ It was also found to regulate cholinergic anti-inflammatory action via decreasing the release of inflammatory mediators such as tumor necrosis factor alpha (TNF- α) and interleukin (IL)-6.¹⁷ It acted as an anti-apoptotic regulator and exerted its neuroprotective effect towards ischemic injury by suppressing the apoptosis of neurons in the cerebral ischemic stroke.¹⁸ However, the role of miR-124 on sevoflurane anesthesia-induced cognitive dysfunction has not been elucidated.

Nuclear factor kappa B (NF- κ B) is a nuclear transcription factor that contributes to various cellular processes, and its activation is closely related to the stimulation of cytokines.¹⁹ It can be activated by several neurotrophic factors and induces the activation of genes associated with differentiation, growth, activation of immune cells, and survival involving apoptotic factor Bax and inhibition of apoptosis factor Bcl-2.²⁰ Another study showed that

NF- κ B activation is responsible for modulating inflammatory mediators, including IL-6, TNF- α and IL-1 β , in inflammatory lung injury.²¹ Recent research revealed that inflammation is the key factor in the regulation of brain injury pathology. Therefore, NF- κ B expressions might be critical during the regulation of cognitive dysfunction.²² However, the exact mechanism by which NF- κ B exerts its effect in the progression of cognitive dysfunction induced by sevoflurane anesthesia is unknown.

Objectives

In this study, in vitro and in vivo models of POCD was implemented with sevoflurane treatment. The impact of miR-124 was investigated in its role as a neuroprotectant to POCD.

Materials and methods

Animals

Sixteen male Sprague Dawley rats (18-month-old) were obtained from the Experimental Animal Center of Hebei Medical University (Shijiazhuang, China) and separated into 2 groups (8 rats in control group and 8 in sevoflurane group). The control group rats were exposed to air inhalation for 6 h. In comparison, the rats in the sevoflurane groups were exposed to 2.5% sevoflurane (600 μ g/kg/min) for 6 h in 100% oxygen. The oxygen and sevoflurane levels were monitored using a gas monitor. The rats were intracerebroventricularly injected with lentivirus-miR-124 agomiR (10 μ L, n = 4) or agomiR-negative control (n = 4) in the left lateral cerebral ventricles after sodium pentobarbital anesthesia (35 mg/kg). These rats were given a five-day recovery period before start of the sevoflurane inhalation.

All experiments were approved by the Animal Care and Use Committee of Hebei Medical University and were done in line with the instructions provided by the Institutional Animal Care and Use Committee of Hebei Medical University. We took all possible actions to reduce the number of rats used and their suffering.

Morris water maze

The hidden platform was positioned and concealed 1 cm below the surface of the water in the Morris water maze. Starting positions for each trial was pseudo-randomized. Each trial lasted for 60 s, or until the rats were able to locate the hidden platform. If rats were not able to find the hidden platform in 60 s, they were gently guided to the location of the platform. Rats were left on the platform for 15 s before their removal from the pool. We recorded escape latency and platform crossing manually with a stopwatch.

Cell culture

Primary mouse hippocampal neurons were obtained from Thermo Fisher Scientific (Waltham, USA), and cultured in RPMI 1640 (VWR International, Mississauga, Canada) medium with 10% fetal bovine serum (FBS), streptomycin (100 µg/mL) and penicillin (100 U/mL) at 5% CO₂ and 37°C. These neurons were treated with sevoflurane (20 µM) for 48 h and transfected with vectors described below.

Cell transfection

MiR-124 agomiR, pcDNA-Capn4, and their negative controls were obtained from Genomeditech (Shanghai, China). These vectors were transfected into hippocampal neuronal culture using Lipofectamine 2000 (Bioz, Inc., Los Altos, USA) using protocol supplied by the manufacturer.

RT-qPCR

M-MLV Reverse Transcriptase (BioChain, Newark, USA) was used to extract total RNA, and 1 µg of total RNA was used to synthesize cDNA using Prime Script RT reagent kit (TaKaRa Bio Inc., Gothenburg, Sweden) using protocol supplied by the manufacturer. SYBR Premix Ex Taq II (Bioz, Inc.) was used to measure the expression level of miR-124, calpain small subunit 1 (Capn4), Bax, caspase-3, and Bcl-2. A 2^{-ΔΔCt} method was used to determine the fold changes. β-actin was used as an internal control for Capn4, Bax, caspase-3, and Bcl-2, while U6 served as an internal control for miR-124. The primers used are given in Table 1.

Western blot analysis

Total protein content was assessed using a bicinchoninic acid (BCA) kit (Bosterbio, Pleasanton, USA). An equal amount of protein was used in SDS-PAGE. Proteins were transferred onto the polyvinylidene fluoride (PVDF) membranes (Biocompare, San Francisco, USA) after electrophoresis, followed by the blocking with 5% skim milk powder in Tween and Tris-buffered saline (BioLegend, San Diego, USA) for 50 min. These membranes were incubated with primary antibodies including anti-Capn4 (ab92333; 1:2000; Abcam, Cambridge, USA), anti-NF-κB (#8242; 1:1000; Cell Signaling, Beijing, China), anti-phospho-NF-κB (ab183559; 1:1000; Abcam), anti-IKK-β (ab124957; 1:1000; Abcam), anti-p-IKK-β (ab194519; 1:1000; Abcam), and β-actin (ab8227; 1:2000; Abcam) at 4°C overnight followed by the incubation with Goat anti-Rabbit horseradish peroxidase (HRP) (ab7090; 1:2000; Abcam) at 37°C for 1 h. β-actin was the internal control. The chemiluminescence reagent (Thermo Fisher Scientific) was used to visualize the bands and detected under a Las-3000 imaging system (Biocompare).

Table 1. Primer sequences

Primer	Sequence
Capn4 ACCCAATCCGTAACCTC	Forward
Capn4 GGGTAGCAACCGTGAA	Reverse
miR-124 TCGTTAAGGCACGCGGTG	Forward
miR-124 GTGCAGGGTCCGAGGT	Reverse
U6 CTCGCTTCGCAGCACA	Forward
U6 AACGCTTCACGAATTGCGT	Reverse
Bax TCCAAGAAGCCCTAACGTGT	Forward
Bax ATGATCGTCTGGCTGCTGTA	Reverse
Bcl-2 GTGGTGGCAGATGTGCTTAG	Forward
Bcl-2 TTCAGAGCCACAAACAAGGC	Reverse
Caspase-3 TCGGTCTGGTACAGATGTCG	Forward
Caspase-3 CTTCACCATGGCTCAGAAGC	Reverse
β-actin ACCCAGAAGACTGTGGATGG	Forward
β-actin TCAGCTCAGGGATGACCTTG	Reverse

Luciferase assay

Online bioinformatic prediction tools including the starBase website (<http://starbase.sysu.edu.cn/starbase2/index.php>) and the TargetScan website (<http://www.targetscan.org>) were employed to predict the binding sites between Capn4 and miR-124. The primers were designed to target the 3'-UTR of the *Capn4* gene. The target and the mutated *Capn4* sequence were cloned into luciferase reporters to create mutant type (Capn4-MUT) or wild-type (Capn4-WT) plasmids. Neurons were co-transfected with miR-124 mimics or its negative control vector and the Capn4 luciferase reporter plasmids. After 48 h, a dual-luciferase reporter assay (BioVision, Milpitas, USA) was used to determine miR-124 and Capn4 binding.

ELISA assay

Enzyme-linked immunosorbent assay (ELISA; Abcam) was employed to determine the protein levels of IL-1β, IL-6 and TNF-α following the manufacturer's protocol. Supernatants from cell cultures were collected, and a microplate reader (BMG LabTech, Ortenberg, Germany) was used to detect absorbance at 450 nm. The protein levels of cytokines were referenced against a standard curve.

Statistical analyses

IBM SPSS v. 19.0 (IBM Corp., Armonk, USA) and GraphPad Prism v. 7.0 (GraphPad Software, San Diego, USA) software was used to analyze the data. Student's *t*-test and one-way analysis of variance (ANOVA) were used for the comparison between groups. Post hoc analysis was done using Tukey's correction method. All the experiments were performed in triplicate, and a *p*-value less than 0.05 was considered statistically significant. Data are presented as the mean \pm standard deviation (SD).

Results

The expression of miR-124 was reduced in rats treated with sevoflurane anesthesia

We show that sevoflurane treatment increased escape latency and reduced hidden platform crossings in the Morris

water maze, indicating deficits in spatial cognition (Fig. 1A,B). Real-time quantitative polymerase chain reaction (RT-qPCR) showed that miR-124 expression was significantly reduced in sevoflurane treated rats compared to the control group (Fig. 1C). Our findings demonstrated that the reduction in miR-124 expression was associated with cognitive deficits in sevoflurane-treated rats.

MiR-124 suppressed apoptosis induced by sevoflurane treatment in hippocampal neuron culture

The influence of miR-124 on sevoflurane-induced apoptosis in cultured hippocampal neurons was examined. Our results indicate that the expression of miR-124 was markedly reduced in sevoflurane-treated hippocampal neurons compared to that of the control group (***p* < 0.001 compared to the control group) (Fig. 2A). Figure 2B shows that miR-124 overexpression in hippocampal neurons in the miR-124 agomiR group (***p* < 0.001

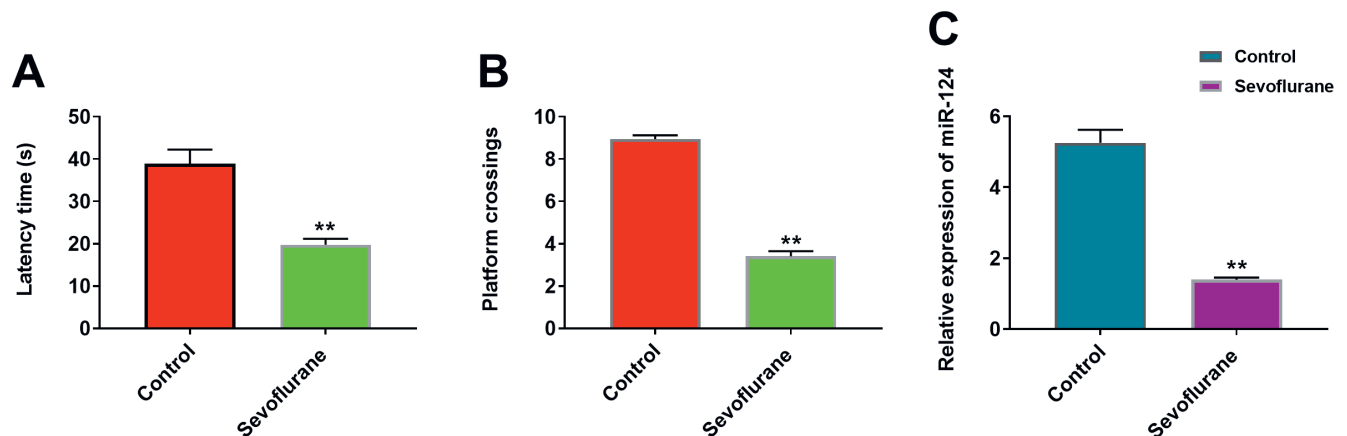


Fig. 1. MiR-124 was inhibited in rats treated with sevoflurane

A and B. The escape latency and platform crossing were assessed in the Morris water maze; C. MiR-124 expression was determined in the left lateral cerebral ventricle of the rats using RT-qPCR (***p* < 0.001).

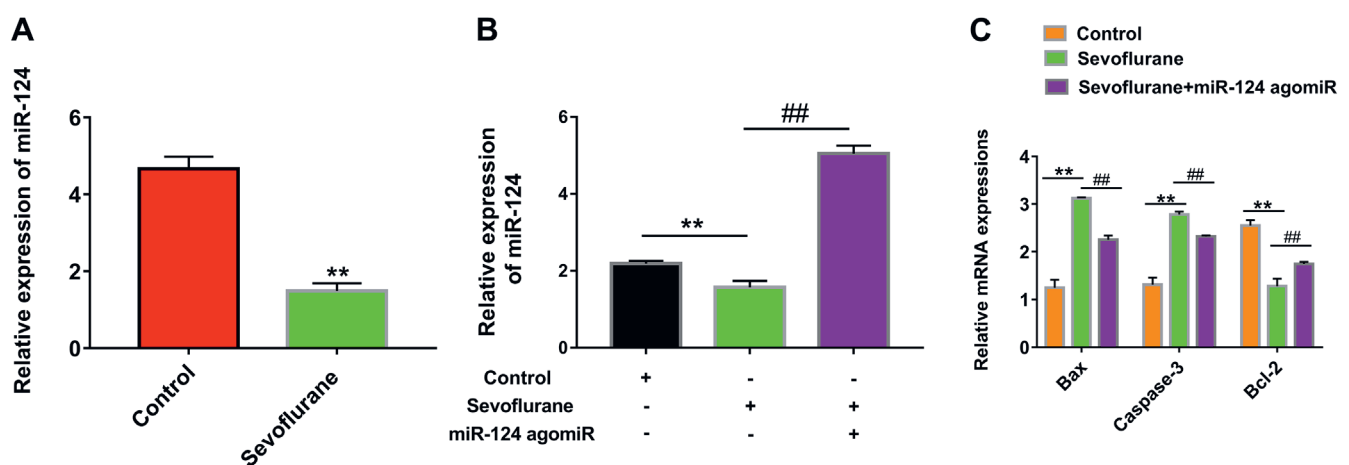


Fig. 2. MiR-124 decreased sevoflurane-induced apoptosis in hippocampal neurons

A and B. RT-qPCR was performed to determine the relative expression of miR-124 in hippocampal neurons; C. Bax, caspase-3 and Bcl-2 mRNA expression levels were determined in sevoflurane-treated hippocampal neurons using RT-qPCR (***p* < 0.001 compared to the control group, ##*p* < 0.001 compared to the sevoflurane group).

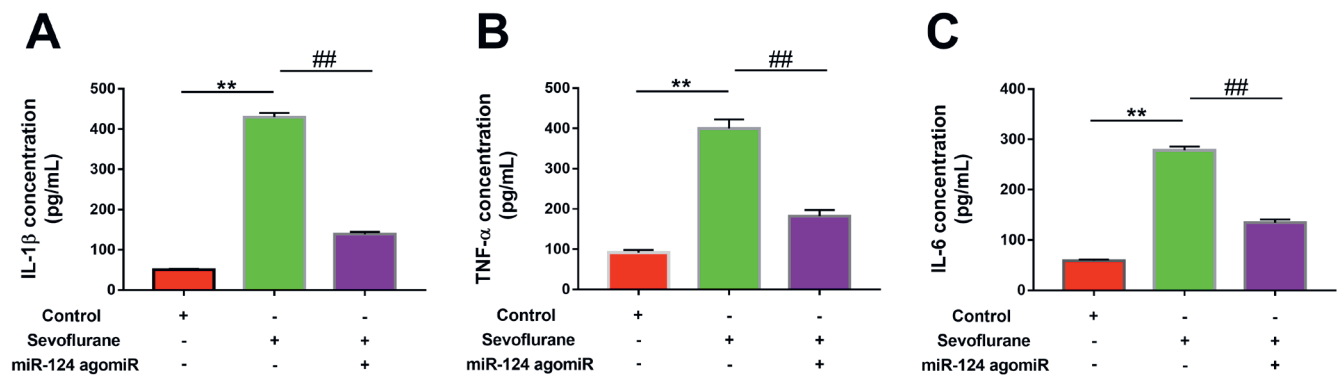


Fig. 3. MiR-124 suppressed the inflammation induced by sevoflurane in hippocampal neurons

A–C. The protein concentrations of IL-1β, IL-6 and TNF-α in sevoflurane-treated hippocampal neurons were detected using ELISA (**p < 0.001 compared to the control group, ##p < 0.001 compared to the sevoflurane group).

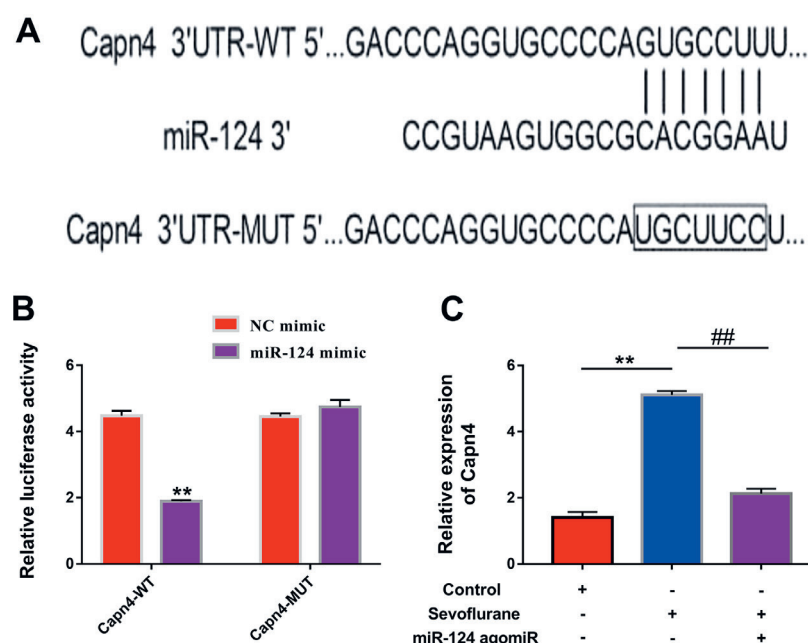


Fig. 4. Capn4 is a direct target of miR-124

A and B. The starBase software and luciferase assay were employed to predict and verify the relationship between miR-124 and Capn4; C. RT-qPCR was performed to measure the mRNA expression of Capn4 in sevoflurane-treated hippocampal neurons (**p < 0.001 compared to the control group, ##p < 0.001 compared to the sevoflurane group).

compared to the sevoflurane group). Also, Bax, caspase-3 and Bcl-2 RNA levels from RT-qPCR revealed that sevoflurane treatment increased the mRNA level of Bax and caspase-3 and decreased the level of Bcl-2. On the other hand, miR-124 agomiR reversed the impact of sevoflurane on the mRNA expression of these pro-apoptotic mediators (Fig. 2C). These data showed that miR-124 suppressed apoptosis induced by sevoflurane in hippocampal neurons.

Impact of miR-124 on sevoflurane-induced neuroinflammation in hippocampal neurons

Our ELISA data show that the level of IL-1β, IL-6 and TNF-α was increased by sevoflurane treatment compared to control. At the same time, miR-124 agomiR inhibited the level of these inflammatory mediators (**p < 0.001 compared to the control group, ##p < 0.001 compared

to the sevoflurane group) (Fig. 3A–C). These data support that miR-124 inhibits sevoflurane-induced neuroinflammation in hippocampal neurons.

Capn4 was target of miR-124

Bioinformatic prediction tools – the starBase website and the TargetScan website – indicated that miR-124 may bind to Capn4. Our luciferase assay confirmed the binding between miR-124 and Capn4. Our results show that miR-124 mimics significantly reduced the luciferase activity in the Capn4-WT group compared to the Capn4-MUT group (Fig. 4A,B). Moreover, the expression of Capn4 was measured by using RT-qPCR, and our findings revealed an increased expression of Capn4 in response to sevoflurane treatment in hippocampal neurons compared to the controls. At the same time, miR-124 inhibited the mRNA level of Capn4 in hippocampal neurons (Fig. 4C). These results demonstrated that Capn4 is a direct target of miR-124.

MiR-124 inhibited sevoflurane-induced apoptosis in hippocampal neurons via the NF- κ B signaling pathway

To investigate the downstream effectors of miR-124, we applied LY294002 to hippocampal neurons to test the involvement of the NF- κ B pathway. The RT-qPCR results show that the miR-124 mimics reduced caspase-3 and Bax mRNA levels and enhanced the level of Bcl-2. On the other hand, treatment with NF- κ B inhibitor and Capn4 overexpression reversed the effects of miR-124 mimics on sevoflurane-induced apoptosis in hippocampal neurons ($^{\#}p < 0.001$ compared to the sevoflurane group, $^{\$}p < 0.001$ compared to the miR-124 mimic group, nonsignificant compared to pcDNA-Capn4; Fig. 5A). Our western blot data indicate that miR-124 mimics suppressed the Capn4 protein level and increased the phosphorylation of NF- κ B and IKK- β in sevoflurane-treated hippocampal neurons. However, the overexpression of Capn4 and treatment with NF- κ B inhibitor showed the opposite effect on Capn4, p-NF- κ B and p-IKK- β protein levels ($^{\#}p < 0.001$ compared to the sevoflurane group, $^{\$}p < 0.001$ compared to the miR-124 mimic group, nonsignificant compared to pcDNA-Capn4; Fig. 5B). These data demonstrated that miR-124 attenuated the apoptosis induced by sevoflurane treatment in hippocampal neurons via the NF- κ B signaling pathway.

MiR-124 rescued cognitive function in rats treated with sevoflurane anesthesia

Next, we explored the impact of miR-124 on cognitive deficits induced by sevoflurane exposure in rats. Our results indicate that miR-124 decreased the escape latency and increased platform crossing in rats treated with

sevoflurane compared to controls ($^{**}p < 0.001$ compared to the control group, $^{\#\#}p < 0.001$ compared to the sevoflurane group, Fig. 6A–C). Moreover, western blot analysis results revealed that miR-124 agomiR reversed sevoflurane-induced increases in protein levels of Capn4, p-NF- κ B and p-IKK- β ($^{**}p < 0.001$ compared to the control group, $^{\#\#}p < 0.001$ compared to the sevoflurane group; Fig. 6D). These findings revealed that miR-124 improved cognitive function in rats treated with sevoflurane.

Discussion

In the current study, we showed that miR-124 expression was decreased in the freely moving rats and cultured mouse hippocampal neurons by sevoflurane. This decrease was associated with a general increase in the expression of apoptotic factors and neuroinflammatory markers in cultured hippocampal neurons. We were also able to show that Capn4 binds to miR-124 and triggers downstream effects through the NF- κ B signaling pathway. All these molecular changes may be related to the amelioration of spatial cognition in sevoflurane-treated rats by miR-124.

The miRNAs play a critical role in sevoflurane-induced apoptosis. For instance, miR-96 enhanced the apoptosis in hippocampal neurons after treatment with sevoflurane, exacerbating the impact of sevoflurane on hippocampal neurons and cognitive function.²³ Another study revealed that miR-34a was involved in the modulation of hippocampal apoptosis induced by sevoflurane which was inhibited by the knockdown of miR-34a in hippocampal neurons.²⁴ Furthermore, miR-665 has been shown to play a neuroprotective role by reducing sevoflurane-induced apoptosis in hippocampal neurons.²⁵ Previous studies showed that

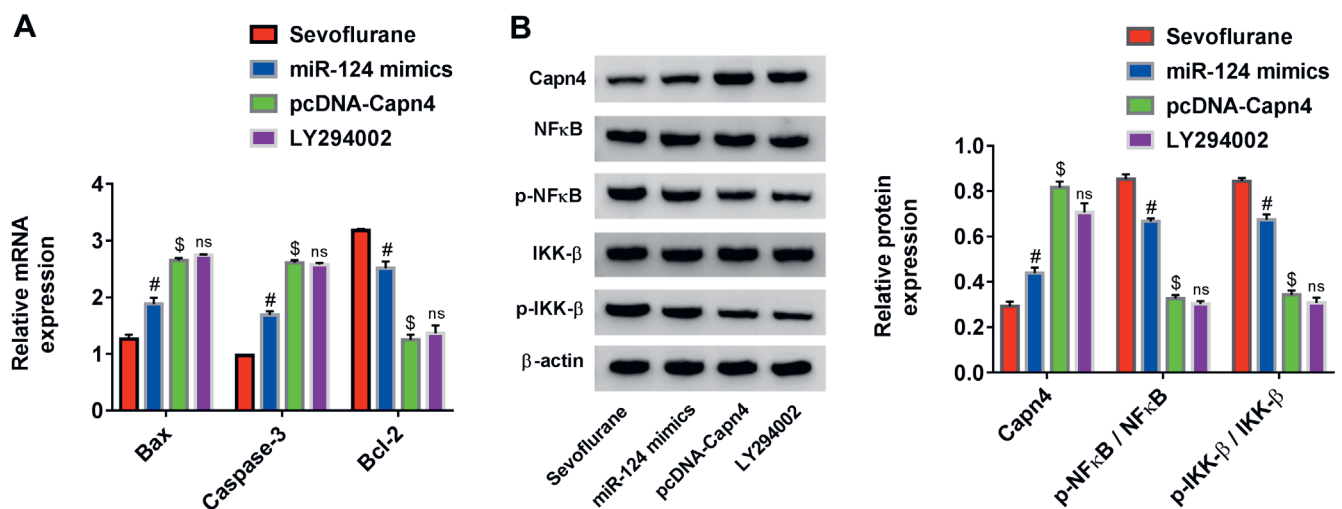


Fig. 5. MiR-124 attenuated sevoflurane-induced apoptosis in hippocampal neurons via the NF- κ B signaling pathway

A. The mRNA levels of Bax, caspase-3 and Bcl-2 were determined using RT-qPCR; B. Protein expression levels of Capn4 and NF- κ B signaling pathways were assessed using western blot ($^{\#}p < 0.001$ compared to the sevoflurane group, $^{\$}p < 0.001$ compared to the miR-124 mimic group, nonsignificant (ns) compared to pcDNA-Capn4).

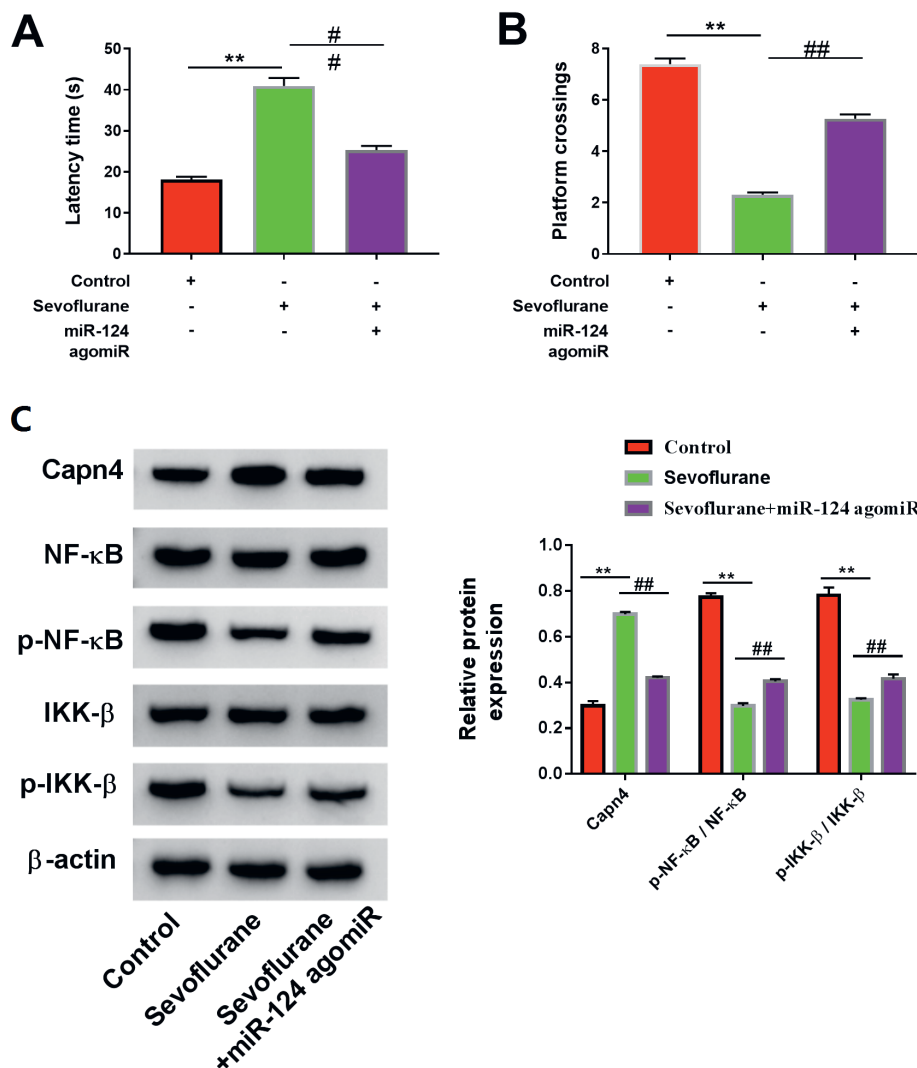


Fig. 6. MiR-124 improved spatial cognition in rats treated with sevoflurane

A and B. The escape latency and hidden platform crossings in the Morris water maze; C. Western blot analysis was used to examine the protein expressions of Capn4, and NF-κB signaling pathways (**p < 0.001 compared to the control group, ##p < 0.001 compared to the sevoflurane group; ns – nonsignificant).

miR-124 was upregulated in the neural precursor cells and during CNS development related to synaptic plasticity.^{26,27} There is also evidence that miR-124 exerts its function in modulating inflammatory process by suppressing the release of inflammatory modulators.^{17,28} Recent research revealed that miR-124 enhanced the spatial learning and memory in rats, offering resistance to apoptosis, and improved viability in hippocampal neurons.²⁹ Despite converging evidence showing that miRNAs play a major role in neuroprotection and neural plasticity relating to normal cognition, the impact of miR-124 in the context of sevoflurane exposure has not been described previously. In our research, we elucidated that miR-124 suppressed sevoflurane-induced apoptosis in cultured hippocampal neurons by decreasing the mRNA expressions of caspase-3 and Bax, while enhancing the expressions of Bcl-2. Previous research suggested that the expressions of inflammatory mediators such as IL-1β and TNF-α are elevated in sevoflurane-treated hippocampal neurons, while miR-410-3p suppressed the expressions of IL-1β, IL-6 and TNF-α.³⁰ Expressions of IL-1β, IL-6 and TNF-α can also be inhibited by the overexpression of miR-640 in sevoflurane-treated

hippocampal neurons.³¹ Our findings show that also miR-124 inhibited the expression of IL-1β, IL-6 and TNF-α in hippocampal neurons. These data support the role of miR-124 in suppressing inflammation and apoptosis induced by sevoflurane in vitro, subserving the rescue of sevoflurane-induced cognitive deficits.

The calpains belong to a calcium-dependent neutral cysteine proteases family and are involved in various biological activities, including cell cycle progression and cell mobility.³² Calpain small subunit 1 (Capn4) exerts an important function in maintaining the activity and stability of calpain.³³ It plays a critical role in the modulation of cell differentiation and proliferation in osteoblasts,³⁴ and also mediates apoptosis in cardiomyocytes.³⁵ A recent study showed that miR-124 suppressed the invasion and proliferation of neural progenitor cells (NPC) cells by regulating its target gene *Capn4*.³⁶ Calpain can induce apoptosis, inflammatory response and NF-κB signaling following myocardial infarction, and the targeted deletion of *Capn4* leads to improvement of cardiac function and decrease in mortality.³⁷ A previous study showed that andrographolide ameliorated POCD in aged rats via downregulating

NF- κ B/MAPK pathways.³⁸ Upon the activation of resident microglia and macrophage in the hippocampus, NF- κ B signaling is stimulated to promote neuroinflammation and increase transcription, subsequently contributing to cognitive impairment.^{39,40} It has been reported that during surgical treatment, sevoflurane suppresses the NF- κ B-mediated production of epithelial cell-derived inflammatory mediators, such as IL-8 and IL-6, which are the leading cause of ischemia/reperfusion injury.⁴¹ Furthermore, suppression of NF- κ B signaling pathways may inhibit cognitive dysfunction after sevoflurane anesthesia via inhibiting IL-6, I κ B α , TNF- α , and IL-1 β .⁴² Similarly, our results revealed that miR-124 could inhibit the apoptosis induced by sevoflurane in hippocampal neurons by NF- κ B signaling. The overexpression of miR-124 rescued apoptosis induced by sevoflurane in hippocampal neurons in the presence of an NF- κ B inhibitor. Lastly, our research revealed that miR-124 significantly reduced the escape latency and increased hidden platform crossing, suggesting that miR-124 can improve or mitigate cognitive dysfunction induced by sevoflurane via the NF- κ B signaling pathway.

Our data are consistent with the idea that miR-124 exerts its neuroprotective role against sevoflurane-induced cognitive dysfunction through Capn4 binding to modulate the NF- κ B signaling pathway. These findings support for the further exploration of miR-124 related manipulations for POCD.

Limitations

This study only related the NF- κ B signaling pathway, which is a limitation.

Conclusions

Our findings demonstrated that miR-124 exerted its neuroprotective role against sevoflurane via targeting Capn4 and NF- κ B signaling pathways. Our work may provide a direction for sevoflurane anesthesia-related cognitive dysfunction.

ORCID iDs

Zijun Zhao  <https://orcid.org/0000-0002-0472-6808>
 Li Ma  <https://orcid.org/0000-0002-6190-8579>
 Yishuai Li  <https://orcid.org/0000-0002-4762-9231>
 Qi Zhang  <https://orcid.org/0000-0003-0634-152X>
 Ying Wang  <https://orcid.org/0000-0003-4456-5532>
 Yanlei Tai  <https://orcid.org/0000-0003-2124-4824>
 Qiujun Wang  <https://orcid.org/0000-0001-9090-6276>

References

- Shoair OA, Grassoli MP, Lahaye LA, Daniel R, Biddle CJ, Slattum PW. Incidence and risk factors for postoperative cognitive dysfunction in older adults undergoing major noncardiac surgery: A prospective study. *J Anaesthesiol Clin Pharmacol*. 2015;31(1):30–36. doi:10.4103/0970-9185.150530
- Berger M, Nadler JW, Brownhyde J, et al. Postoperative cognitive dysfunction: Minding the gaps in our knowledge of a common postoperative complication in the elderly. *Anesthesiol Clin*. 2015;33(3):517–550. doi:10.1016/j.anclin.2015.05.008
- Krenk L, Rasmussen LS, Kehlet H. New insights into the pathophysiology of postoperative cognitive dysfunction. *Acta Anaesthesiol Scand*. 2010;54(8):951–956. doi:10.1111/j.1399-6576.2010.02268.x
- Morimoto Y, Yoshimura M, Utada K, Setoyama K, Matsumoto M, Sakabe T. Prediction of postoperative delirium after abdominal surgery in the elderly. *J Anesth*. 2009;23(1):51–56. doi:10.1007/s00540-008-0688-1
- Yildizeli B, Ozyurtkan MO, Batirel HF, Kuşcu K, Bekiroğlu N, Yüksel M. Factors associated with postoperative delirium after thoracic surgery. *Ann Thorac Surg*. 2005;79(3):1004–1009. doi:10.1016/j.athoracsur.2004.06.022
- Riedel B, Browne K, Silbert B. Cerebral protection: Inflammation, endothelial dysfunction, and postoperative cognitive dysfunction. *Curr Opin Anaesthesiol*. 2014;27(1):89–97. doi:10.1097/ACO.0000000000000032
- Zhang X, Zhou Y, Xu M, Chen G. Autophagy is involved in the sevoflurane anesthesia-induced cognitive dysfunction of aged rats. *PLoS One*. 2016;11(4):e0153505. doi:10.1371/journal.pone.0153505
- Zhao Y, Ai Y. Overexpression of lncRNA Gm15621 alleviates apoptosis and inflammation response resulting from sevoflurane treatment through inhibiting miR-133a/Sox4. *J Cell Physiol*. 2020;235(2):957–965. doi:10.1002/jcp.29011
- Lv G, Li C, Wang W, Li N, Wang K. Silencing SP1 alleviated sevoflurane-induced POCD development via cholinergic anti-inflammatory pathway. *Neurochem Res*. 2020;45(9):2082–2090. doi:10.1007/s11064-020-03070-7
- Bartel DP. MicroRNAs: Target recognition and regulatory functions. *Cell*. 2009;136(2):215–233. doi:10.1016/j.cell.2009.01.002
- Siegel G, Saba R, Schrott G. microRNAs in neurons: Manifold regulatory roles at the synapse. *Curr Opin Genet Dev*. 2011;21(4):491–497. doi:10.1016/j.gde.2011.04.008
- Schrott G. microRNAs at the synapse. *Nat Rev Neurosci*. 2009;10(12):842–849. doi:10.1038/nrn2763
- Schrott GM, Tuebing F, Nigh EA, et al. A brain-specific microRNA regulates dendritic spine development. *Nature*. 2006;439(7074):283–289. doi:10.1038/nature04367
- Rajasethupathy P, Fiumara F, Sheridan R, et al. Characterization of small RNAs in Aplysia reveals a role for miR-124 in constraining synaptic plasticity through CREB. *Neuron*. 2009;63(6):803–817. doi:10.1016/j.neuron.2009.05.029
- Femminella GD, Ferrara N, Rengo G. The emerging role of microRNAs in Alzheimer's disease. *Front Physiol*. 2015;6:40. doi:10.3389/fphys.2015.00040
- Delay C, Mandemakers W, Hébert SS. MicroRNAs in Alzheimer's disease. *Neurobiol Dis*. 2012;46(2):285–290. doi:10.1016/j.nbd.2012.01.003
- Mishima T, Mizuguchi Y, Kawahigashi Y, Takizawa T, Takizawa T. RT-PCR-based analysis of microRNA (miR-1 and -124) expression in mouse CNS. *Brain Res*. 2007;1131(1):37–43. doi:10.1016/j.brainres.2006.11.035
- Sun Y, Li Q, Gui H, et al. MicroRNA-124 mediates the cholinergic anti-inflammatory action through inhibiting the production of pro-inflammatory cytokines. *Cell Res*. 2013;23(11):1270–1283. doi:10.1038/cr.2013.116
- Sun Y, Gui H, Li Q, et al. MicroRNA-124 protects neurons against apoptosis in cerebral ischemic stroke. *CNS Neurosci Ther*. 2013;19(10):813–819. doi:10.1111/cns.12142
- Lysiak JJ, Bang HJ, Nguyen QA, Turner TT. Activation of the nuclear factor kappa B pathway following ischemia-reperfusion of the murine testis. *J Androl*. 2005;26(1):129–135. PMID:15611577
- Li L, Wu W, Huang W, Hu G, Yuan W, Li W. NF- κ B RNAi decreases the Bax/Bcl-2 ratio and inhibits TNF- α -induced apoptosis in human alveolar epithelial cells. *Inflamm Res*. 2013;62(4):387–397. doi:10.1007/s00011-013-0590-7
- Peng S, Hang N, Liu W, et al. Andrographolide sulfonate ameliorates lipopolysaccharide-induced acute lung injury in mice by down-regulating MAPK and NF- κ B pathways. *Acta Pharm Sin B*. 2016;6(3):205–211. doi:10.1016/j.apsb.2016.02.002
- Dinel AL, Joffre C, Trifillieff P, et al. Inflammation early in life is a vulnerability factor for emotional behavior at adolescence and for lipopolysaccharide-induced spatial memory and neurogenesis alteration at adulthood. *J Neuroinflammation*. 2014;11:155. doi:10.1186/s12974-014-0155-x
- Xu C, Niu JJ, Zhou JF, Wei YS. MicroRNA-96 is responsible for sevoflurane-induced cognitive dysfunction in neonatal rats via inhibiting IGF1R. *Brain Res Bull*. 2019;144:140–148. doi:10.1016/j.brainresbull.2018.09.001

25. Zhao X, Sun Y, Ding Y, Zhang J, Li K. miR-34a inhibitor may effectively protect against sevoflurane-induced hippocampal apoptosis through the Wnt/ β -catenin pathway by targeting Wnt1. *Yonsei Med J*. 2018;59(10):1205–1213. doi:10.3349/ymj.2018.59.10.1205
26. Lu X, Lv S, Mi Y, Wang L, Wang G. Neuroprotective effect of miR-665 against sevoflurane anesthesia-induced cognitive dysfunction in rats through PI3K/Akt signaling pathway by targeting insulin-like growth factor 2. *American J Transl Res*. 2017;9(3):1344–1356. PMID:28386360
27. Tapocik JD, Luu TV, Mayo CL, et al. Neuroplasticity, axonal guidance and micro-RNA genes are associated with morphine self-administration behavior. *Addict Biol*. 2013;18(3):480–495. doi:10.1111/j.1369-1600.2012.00470.x
28. Maiorano NA, Mallamaci A. The pro-differentiating role of miR-124: Indicating the road to become a neuron. *RNA Biol*. 2010;7(5):528–533. doi:10.4161/rna.7.5.12262
29. Willemsen HL, Huo XJ, Mao-Ying QL, Zijlstra J, Heijnen CJ, Kavelaars A. MicroRNA-124 as a novel treatment for persistent hyperalgesia. *J Neuroinflammation*. 2012;9:143. doi:10.1186/1742-2094-9-143
30. Yang W, Guo Q, Li J, et al. microRNA-124 attenuates isoflurane-induced neurological deficits in neonatal rats via binding to EGR1. *J Cell Physiol*. 2019;234(12):23017–23032. doi:10.1002/jcp.28862
31. Su R, Sun P, Zhang D, Xiao W, Feng C, Zhong L. Neuroprotective effect of miR-410-3p against sevoflurane anesthesia-induced cognitive dysfunction in rats through PI3K/Akt signaling pathway via targeting C-X-C motif chemokine receptor 5. *Genes Genomics*. 2019;41(10):1223–1231. doi:10.1007/s13258-019-00851-5
32. Xu W, Zhao Y, Ai Y. Overexpression of lncRNA Gm43050 alleviates apoptosis and inflammation response induced by sevoflurane treatment by regulating miR-640/ZFP91. *Am J Transl Res*. 2020;12(8):4337–4346. PMID:32913509
33. Storr SJ, Carragher NO, Frame MC, Parr T, Martin SG. The calpain system and cancer. *Nat Rev Cancer*. 2011;11(5):364–374. doi:10.1038/nrc3050
34. Cai JJ, Qi ZX, Chen LC, Yao Y, Gong Y, Mao Y. miR-124 suppresses the migration and invasion of glioma cells in vitro via Capn4. *Oncol Rep*. 2016;35(1):284–290. doi:10.3892/or.2015.4355
35. Shimada M, Greer PA, McMahon AP, Bouxsein ML, Schipani E. In vivo targeted deletion of calpain small subunit, Capn4, in cells of the osteoblast lineage impairs cell proliferation, differentiation, and bone formation. *J Biol Chem*. 2008;283(30):21002–21010. doi:10.1074/jbc.M710354200
36. Li Y, Li Y, Feng Q, Arnold M, Peng T. Calpain activation contributes to hyperglycaemia-induced apoptosis in cardiomyocytes. *Cardiovasc Res*. 2009;84(1):100–110. doi:10.1093/cvr/cvp189
37. Shi B, Wang Y, Yin F. MALAT1/miR-124/Capn4 axis regulates proliferation, invasion and EMT in nasopharyngeal carcinoma cells. *Cancer Biol Ther*. 2017;18(10):792–800. doi:10.1080/15384047.2017.1373214
38. Ma J, Wei M, Wang Q, et al. Deficiency of Capn4 gene inhibits nuclear factor- κ B (NF- κ B) protein signaling/inflammation and reduces remodeling after myocardial infarction. *J Biol Chem*. 2012;287(33):27480–27489. doi:10.1074/jbc.M112.358929
39. Ding Y, Shi C, Chen L, et al. Effects of andrographolide on postoperative cognitive dysfunction and the association with NF- κ B/MAPK pathway. *Oncol Lett*. 2017;14(6):7367–7373. doi:10.3892/ol.2017.7088
40. Wang HL, Liu H, Xue ZG, Liao QW, Fang H. Minocycline attenuates post-operative cognitive impairment in aged mice by inhibiting microglia activation. *J Cell Mol Med*. 2016;20(9):1632–1639. doi:10.1111/jcmm.12854
41. Terrando N, Eriksson LI, Ryu JK, et al. Resolving postoperative neuroinflammation and cognitive decline. *Ann Neurol*. 2011;70(6):986–995. doi:10.1002/ana.22664
42. Watanabe K, Iwahara C, Nakayama H, et al. Sevoflurane suppresses tumour necrosis factor- α -induced inflammatory responses in small airway epithelial cells after anoxia/reoxygenation. *Br J Anaesth*. 2013;110(4):637–645. doi:10.1093/bja/aes469
43. Zheng JW, Meng B, Li XY, Lu B, Wu GR, Chen JP. NF- κ B/P65 signaling pathway: A potential therapeutic target in postoperative cognitive dysfunction after sevoflurane anesthesia. *Eur Rev Med Pharmacol Sci*. 2017;21(2):394–407. PMID:28165545

FGF21 promotes wound healing of rat brain microvascular endothelial cells through facilitating TNF- α -mediated VEGFA and ERK1/2 signaling pathway

Weiting Chen^{1,A,D,F}, Zhongen Shen^{2,A,B,E}, Shuiqi Cai^{1,B,C}, Long Chen^{1,C}, Dabin Wang^{1,E}

¹ No. 1 Department of Orthopedics, The Third People's Hospital, Cixi, China

² Department of Anesthesiology, Cixi People Hospital, China

A – research concept and design; B – collection and/or assembly of data; C – data analysis and interpretation;

D – writing the article; E – critical revision of the article; F – final approval of the article

Advances in Clinical and Experimental Medicine, ISSN 1899–5276 (print), ISSN 2451–2680 (online)

Adv Clin Exp Med. 2021;30(7):711–720

Address for correspondence

Dabin Wang

E-mail: juf56689@126.com

Funding sources

None declared

Conflict of interest

None declared

Received on October 17, 2020

Reviewed on November 4, 2020

Accepted on February 19, 2021

Published online on June 11, 2021

Cite as

Chen W, Shen Z, Cai S, Chen L, Wang D. FGF21 promotes wound healing of rat brain microvascular endothelial cells through facilitating TNF- α -mediated VEGFA and ERK1/2 signaling pathway. *Adv Clin Exp Med.* 2021;30(7):711–720. doi:10.17219/acem/133494

DOI

10.17219/acem/133494

Copyright

© 2021 by Wrocław Medical University

This is an article distributed under the terms of the

Creative Commons Attribution 3.0 Unported (CC BY 3.0)

(<https://creativecommons.org/licenses/by/3.0/>)

Abstract

Background. Wound healing is an essential physiological process in recovery after microsurgery.

Objectives. To further understand the functions of fibroblast growth factor 21 (FGF21), the roles of this factor were examined and its correlations with inflammation, vascular endothelial growth factor A (VEGFA) and ERK1/2 signaling pathway activation were analyzed.

Materials and methods. Rat brain microvascular endothelial cells (RBMECs) were treated with interleukin (IL)-1 β and used for the experiments. Cell Counting Kit-8 (CCK-8) was used to detect the cell viability of RBMECs after treatment with IL-1 β (1 ng/mL) and FGF21 or VEGFA overexpression, while changes in apoptosis were measured through flow cytometry. Migration was checked through the scratch test. FGF21 and VEGFA RNA expression was assessed using reverse-transcription quantitative polymerase chain reaction (RT-qPCR), which was also used to examine RNA expression of Bcl-2, Bax and caspase-3. After IL-1 β treatment and FGF21 overexpression, tumor necrosis factor alpha (TNF- α) and tumor growth factor β 1 (TGF- β 1) proteins level were observed with enzyme-linked immunosorbent assay (ELISA), which was also applied to check the expression of ERK1/2 after overexpression of FGF21 and VEGFA. PD98059 (50 μ M), an ERK1/2 inhibitor, was used to examine the roles of ERK1/2 in regulating cell viability and apoptosis.

Results. The IL-1 β treatment significantly decreased the viability of RBMECs and TGF- β 1, but promoted cell apoptosis and TNF- α expression. FGF21 was downregulated by IL-1 β treatment but its overexpression enhanced the viability of RBMECs and TGF- β 1 and ERK1/2 protein levels, and attenuated cell apoptosis and TNF- α . Upregulated TNF- α restrained cell viability and apoptosis of RBMECs after FGF21 overexpression, and its upregulation not only suppressed FGF21, but also VEGFA. Moreover, VEGFA suppression by TNF- α increased cell viability and ERK1/2 protein levels, and suppressed the apoptosis of RBMECs through its upregulation. However, PD98059 obstructed the functions of FGF21 and VEGFA.

Conclusions. FGF21 promoted the cell viability of RBMECs through upregulating TNF- α -mediated VEGFA and ERK1/2 signaling.

Key words: VEGFA, FGF21, ERK1/2 signaling pathway, RBMEC

Background

Acute stroke remains the leading cause of morbidity and mortality worldwide,¹ and is the main cause of disability.² Stroke results from transient or permanent cerebral ischemia caused by arterial stenosis or occlusion, and common manifestations of this disease are focal neurological deficits.^{3,4} Intravenous thrombolysis and endovascular thrombectomy (EVT) are the 2 main treatments for revascularization.¹ Recent randomized clinical trials have shown that EVT has a strong therapeutic effect on acute ischemic stroke caused by large vessel occlusions.⁵ However, damage to pig extracranial arteries, particularly endothelial cells, has been reported following EVT.⁶ A key step during wound healing after surgery is the transition from an inflammatory stage to a proliferative stage, where inflammation can recruit the innate immune system and help to remove dead tissues.⁷ However, prolonged inflammation can lead to uncontrolled activation, resulting in the inhibition of wound healing.⁸ Therefore, cytokines that can attenuate the influence of EVT on cerebral vessels and control the inflammatory response attract attention.

Fibroblast growth factor 21 (FGF21) belongs to the FGF19 subfamily of FGF growth factors, which have a low affinity for heparin and the ability to circulate throughout the body as endocrine factors binding at FGF receptors.^{9,10} It functions as a potent regulator of lipid or energy metabolism, and can lengthen the lifespan of mice with overexpression.¹¹ Moreover, FGF21 is highly expressed in a mouse model of steatohepatitis, and injection of FGF21 attenuates the development of steatohepatitis in methionine- and choline-deficient mice.¹² A study examining the effects of FGF21 on the progression of atherosclerosis has also reported that this growth factor can significantly downregulate the expression of inflammatory factors, including interleukin (IL)-1 α , IL-6, and tumor necrosis factor alpha (TNF- α), and can suppress the NF- κ B signaling pathway in macrophages.¹³ In addition to repressing the inflammatory response, FGF21 has also been shown to facilitate wound healing in diabetic mice by promoting granulation, collagen deposition and re-epithelialization.¹⁴ Unlike other members in FGF family, FGF21 is the only one that has no mitogen activity and does not accelerate cancer occurrence.¹⁵ Thus, FGF21 has a great potential for clinical usage.

Following brain injury in rats, FGF21 can exert a protective effect by promoting neuronal survival, inhibiting the apoptosis of neurons through the PI3K/AKT signaling pathway, and decreasing cerebral infarct volume.¹⁶ As for angiogenesis in the brain, FGF21 has been shown to improve this process and to promote the healing of human brain microvascular endothelial cells through the formation of a FGF21/FGFR1/b-klotho complex and peroxisome proliferator-activated receptor gamma (PPAR γ) activation. However, whether FGF21 can mediate wound healing of the brain microvasculature in other ways is unknown.

Thus, we explored additional mechanisms whereby FGF21 could regulate angiogenesis and the healing of rat brain microvascular endothelial cells (RBMECs).

Angiogenesis is an important part of wound healing and vascular endothelial growth factor A (VEGFA) is one of the most efficient factors that promotes this process.¹⁷ In diabetic mice, the upregulation of TNF- α reduces angiogenesis through inhibiting VEGFA expression.¹⁸ In addition, the downregulation of VEGFA expression reduces the proliferation of endothelial cells, angiogenesis and re-epithelialization in mice.¹⁹ In human dermal fibroblasts, VEGFA can be induced by visfatin to promote cell proliferation and metastasis, and VEGFA upregulation in wound healing is associated with activation of the ERK pathway.^{20,21} Moreover, FGF21 has been reported to suppress melanogenesis in alpaca melanocytes by upregulating the expression of p-ERK1/2.²² Based on these findings, we hypothesized that FGF21 regulates VEGFA during wound healing and angiogenesis through activation of the ERK1/2 signaling pathway and regulation of the inflammatory response.

Objectives

Thus, to further understand the functions of FGF21, the roles of this factor were examined and its correlations with inflammation, VEGFA and ERK1/2 signaling pathway activation were analyzed.

Materials and methods

Cell culture

The RBMECs were purchased from Procell (Wuhan, China). These cells, which were isolated from brain tissues, are the main component of the blood–brain barrier. After the RBMECs were thawed in warm water at 37°C, they were cultured in high-glucose Dulbecco's modified Eagle's medium (DMEM; Gibco, Waltham, USA) containing 10% fetal bovine serum (FBS), 100 U/mL of penicillin and 100 mg/mL of streptomycin (Gibco) at 37°C in 5% CO₂. The medium was replaced every 2 days and the cells selected for the experiments were all in the 3rd to 6th generation. To simulate an inflammatory environment, RBMECs were treated with rat IL-1 β (1 ng/mL; Sigma-Aldrich, St. Louis, USA) for 3 h. After IL-1 β treatment, the RBMECs were treated with the ERK1/2 specific upstream inhibitor PD98059 (50 μ M; MedChemExpress, Monmouth Junction, USA) for 1 h. PD98059 is an effective inhibitor of the MEK signaling pathway through its blockade of MEK1 and MEK2 with an IC₅₀ of 5 μ M. It also inhibits the ERK1/2 signaling pathway by blocking phosphorylation. In preparation for the experiments, the cells were grouped and named the negative control (NC) group, the IL-1 β group and the PD98059 group.

Cell transfection

To analyze the functions of FGF21, VEGFA and TNF- α , overexpression of these 3 genes was carried out. To create overexpressed FGF21, VEGFA and TNF- α in RBMECs, the pcDNA 3.1 vector (Invitrogen, Carlsbad, USA) was selected for transfection. Briefly, a compounded fragment of FGF21 was inserted into the pcDNA3.1 to create overexpressed FGF21. Overexpressed VEGFA and TNF- α were created in the same way. For cell transfection, RBMECs were seeded into 24-well plates and cultured at 37°C with 5% CO₂. Transfection was performed until 50% confluence and Lipofectamine 3000 (Invitrogen) was used to mediate transfection. Then, 2 μ L of Lipofectamine 3000 and 0.5 μ g of RNA were added into serum-free Opti-MEM medium to incubate cells at 37°C for 2 h. Later, the medium used for cell incubation was added for cell culturing at 37°C for 24 h. The RNA expression of FGF21 and VEGFA was measured using reverse-transcription quantitative polymerase chain reaction (RT-qPCR), and TNF- α protein expression was measured using enzyme-linked immunosorbent assay (ELISA). After transfection, the cells were divided into the following groups: oeNC, oeFGF21, TNF- α , oeVEGFA, oeFGF21 with TNF- α , oeFGF21 with PD98059, and oeVEGFA with PD98059.

RT-qPCR

To measure the RNA levels of FGF21, TNF- α and VEGFA, total RNA was extracted using the TRIzol reagent (Invitrogen) from untreated and IL-1 β -treated RBMECs, according to manufacturer's instructions. Thereafter, reverse transcription was performed using a High-Capacity cDNA Reverse Transcription kit (Applied Biosystems, Foster City, USA). Based on the manufacturer's instructions, the PCR reactions were conducted using the 7500 Fast Real-Time PCR system (Applied Biosystems), and data were quantified using the 2^{- $\Delta\Delta$ Ct} method. The primers used are listed in Table 1.

The conditions of the PCR were predenaturation at 95°C for 1 min followed by 40 cycles of denaturation at 95°C for 30 s, annealing at 60°C for 30 s, and extension at 72°C for 30 s. The results were obtained from three independent trials.

CCK-8 assay

Untreated and IL-1 β -treated RBMECs were seeded into 96-well plates at a density of 5 \times 10³ cells/well and incubated for 24 h at 37°C with 5% CO₂. Thereafter, 10 μ L of Cell Counting Kit-8 (CCK-8; Beyotime, Shanghai, China) was added to cells at 24 h, 48 h and 72 h. Following this, the cells were cultured for 1 h and optical density (OD) values were detected at the 450 nm wavelength using a Varioskan™ LUX Multimode Microplate Reader (Thermo Fisher Scientific, Waltham, USA). All samples were run in a triplicate.

Flow cytometry

The RBMECs with and without IL-1 β treatment were digested using 0.25% trypsin (Gibco) and rinsed twice in phosphate-buffered saline (PBS). Next, an Annexin V-FITC Apoptosis Detection kit (Beyotime) was used for apoptosis detection. Cells were resuspended at a density of 1 \times 10⁵ in 195 μ L of Annexin V-FITC binding buffer. Later, 5 μ L of Annexin V-FITC and 10 μ L of propidium iodide (PI) were added and the cells were cultured in darkness at 25°C for 20 min. Thereafter, an Attune NxT Flow Cytometer (Invitrogen) was used to analyze the apoptosis rate of RBMECs. All measurements were repeated 3 times.

Scratch test

The scratch test was used to evaluate the migration ability of RBMECs. Briefly, untreated and IL-1 β -treated RBMECs were seeded into six-well plates and incubated until cells covered the plate. Thereafter, 20- μ L tips were used to create vertical scratches on the RBMECs. Later, the cells were rinsed with PBS 3 times to remove the scraped cells. The RBMECs were then cultured in serum-free medium at 37°C with 5% CO₂. Images were taken 24 h after incubation. All measurements were repeated 3 times.

ELISA

To examine the protein expression of TNF- α , TGF- β 1 and ERK1/2, Rat TNF alpha ELISA (ab46070; Abcam, Cambridge, UK), Rat TGF- β 1 ELISA (ab119558; Abcam)

Table 1. Primer sequences

RNA names	Forward	Reverse	Reference
FGF21	5'-GGGTCAAGTCCGACAGAGGTAT-3'	5'-ATCAAAGTGAGCGATCCATAGA-3'	23
VEGFA	5'-CCAGGAGTACCCCG ATGAGATAG-3'	5'-CTGGCTTTGGTGAGGTTTGATC-3'	24
Bcl-2	5'-GAGTACCTGAACCGGCATCT-3	5'-GAAATCAAACAGAGGTCCGA-3'	25
Bax	5'-TTGCTACAGGGTTTCATCCA-3'	5'-GAGTACCTGAACCGGCATCT-3'	25
Caspase-3	5'-GGACCTGTGGACCTGAAAAA -3'	5'-GCATGCCATAT CATCGTCAG-3'	26
TNF- α	5'-TACTGAACTTCGGGGTGATTGGTCC-3'	5'-CAGCCTTGCCCTTGAAGAGAACC-3'	27
GAPDH	5'-TGCCACTCAGAAG ACTGTGG-3'	5'-GGATGCAGGGATGATGTCT -3'	25

and ERK1 (pT202/pY204; Abcam) + ERK2 (pT185/pY187; Abcam) + total ERK1/2 ELISA (ab126445; Abcam) kits were used. According to the manufacturer's instructions, antibodies were first settled into 96-well plates and proteins from the RBMECs were then added. Next, biotinylated anti-TNF- α , biotin-conjugated anti-rat TGF- β 1 monoclonal antibody, detection antibody Erk1 (T202/Y204)/Erk2 (T185/Y187) and detection antibody Erk1/2 were mixed and incubated at room temperature. Thereafter, streptavidin-horseradish peroxidase (HRP) was pipetted into wells followed by washing with wash buffer. Next, TMB Substrate Reagent (BD Biosciences, Shanghai, China) was added and Stop Solution (BD Biosciences) was used for reaction termination. Color intensity was measured at 450 nm using a Varioskan™ LUX Multimode Microplate Reader (Thermo Fisher Scientific). The results for this experiment were from 3 independent trials.

Statistical analyses

Data are shown as mean \pm standard deviation (SD) and the results were analyzed using GraphPad Prism v. 7.0

(GraphPad Software, San Diego, USA) and SPSS v. 19.0 software (IBM Corp., Armonk, USA). Comparisons between the 2 groups were analyzed using the Student's *t*-test and multiple comparisons between the groups were performed using the S-N-K method. An alpha level of $p < 0.05$ was considered statistically significant.

Results

IL-1 β treatment induces cell apoptosis and inflammation of RBMECs, and decreases cell viability

To confirm the effects of IL-1 β treatment, the cell viability of RBMECs was first examined. The CCK-8 assay showed that the viability of RBMECs was significantly decreased by IL-1 β treatment as compared to untreated RBMECs ($p < 0.05$, Fig. 1A). In addition, IL-1 β -treated RBMECs showed a significantly higher level of apoptosis rate compared to untreated RBMECs ($p < 0.05$, Fig. 1B). The RT-qPCR also indicated that RBMECs treated with

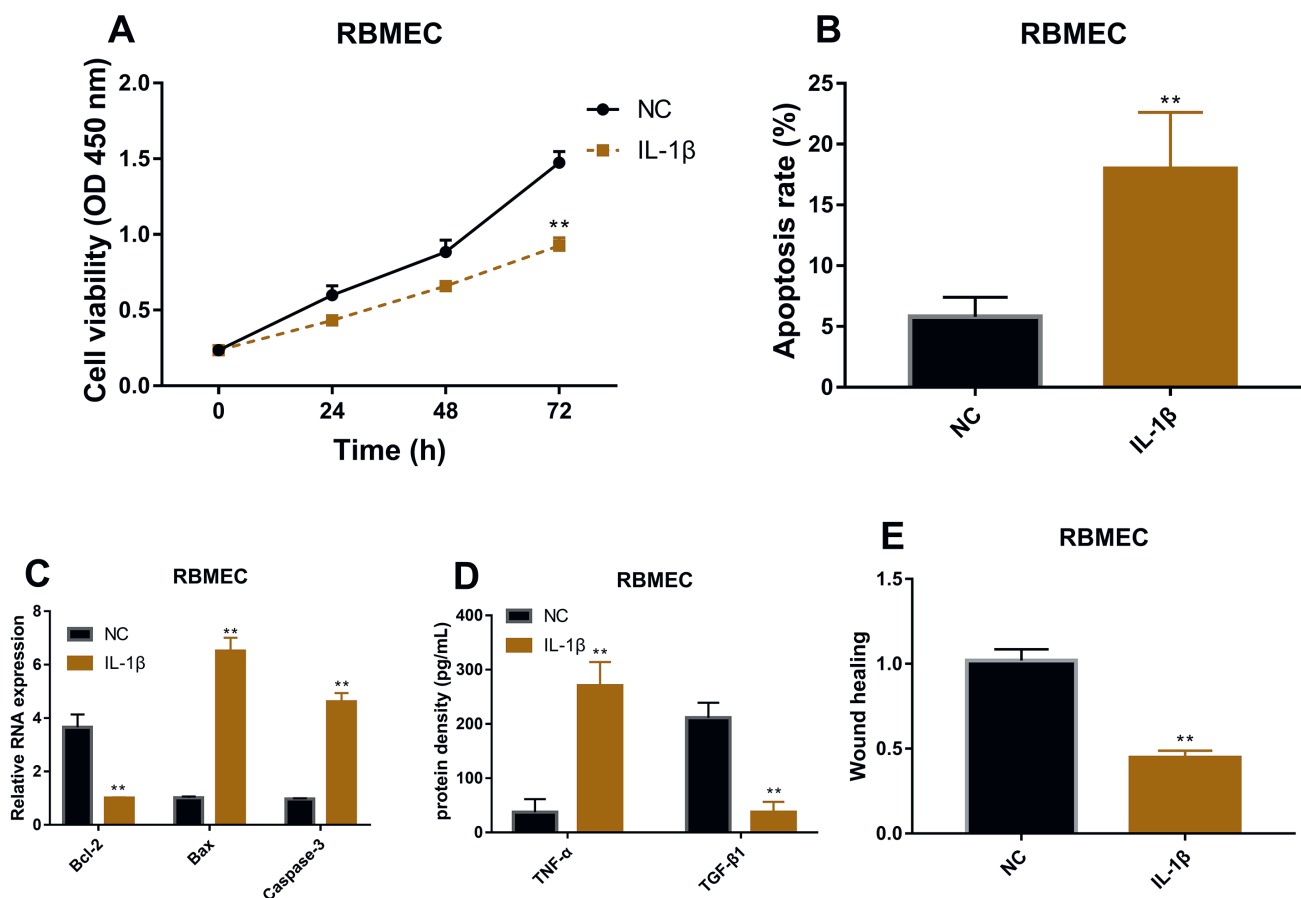


Fig. 1. IL-1 β treatment induces cell apoptosis and inflammation of RBMECs, and decreases cell viability

A. Cell viability of untreated and IL-1 β -treated (1 ng/mL) RBMECs as detected using CCK-8 (** $p < 0.05$ compared to the NC group); B. Flow cytometry was used to examine apoptosis of untreated and IL-1 β -treated (1 ng/mL) RBMECs (** $p < 0.05$ compared to the NC group); C. RNA expression of Bcl-2, Bax and caspase-3 were evaluated with RT-qPCR in untreated and IL-1 β -treated (1 ng/mL) RBMECs (** $p < 0.05$ compared with the NC group); D. TNF- α and TGF- β 1 protein levels in untreated and IL-1 β -treated (1 ng/mL) RBMECs were measured with ELISA (** $p < 0.05$ compared to the NC group); E. Wound healing of untreated and IL-1 β -treated (1 ng/mL) RBMECs was analyzed with the scratch test (** $p < 0.05$ compared to the NC group).

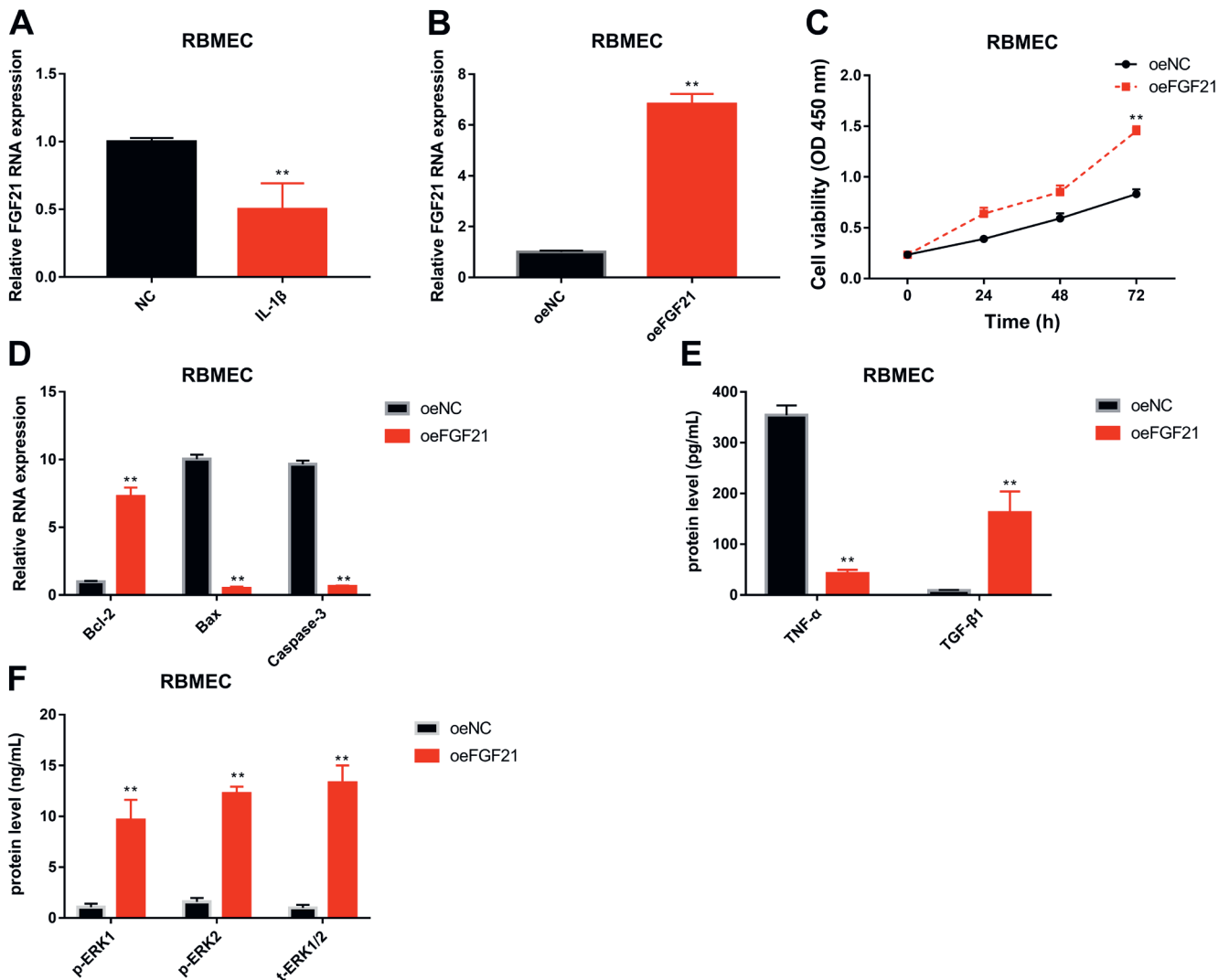


Fig. 2. Overexpression of FGF21 promotes cell viability, and inhibits cell apoptosis and inflammation of RBMECs via the ERK1/2 signaling pathway

A. FGF21 RNA expression in untreated and IL-1 β -treated (1 ng/mL) RBMECs were measured using RT-qPCR (**p < 0.05 compared to the NC group); B. RT-qPCR was used to analyze FGF21 RNA expression in RBMECs after overexpression (**p < 0.05 compared with the oeNC group); C. Cell viability of RBMECs transfected with oeNC and oeFGF21 (**p < 0.05 compared to the oeNC group); D. Bcl-2, Bax and caspase-3 RNA expression in RBMECs transfected with oeNC and oeFGF21 were assessed using RT-qPCR (**p < 0.05 compared to the oeNC group); E. ELISA was used to detect TNF- α and TGF- β 1 protein levels in RBMECs after oeNC and oeFGF21 transfection (**p < 0.05 compared to the oeNC group); F. Phosphorylated ERK1/2 and total ERK1/2 were measured with ELISA in RBMECs after oeNC and oeFGF21 transfection (**p < 0.05 compared to the oeNC group).

IL-1 β exhibited a significantly lower level of Bcl-2, and a higher expression of Bax and caspase-3, compared to RBMECs without treatment (p < 0.05, Fig. 1C). Inflammatory cytokines were also examined and it was shown that TNF- α was significantly increased, and TGF- β 1 significantly decreased by treatment with IL-1 β (p < 0.05, Fig. 1D). Moreover, the wound healing of RBMECs after IL-1 β treatment was examined, and the results indicated that RBMECs after IL-1 β treatment had a significantly larger migration area than untreated RBMECs (p < 0.05, Fig. 1E). To better understand the functions of inflammation in wound healing, RBMECs treated with IL-1 β were further examined.

Overexpression of FGF21 promotes cell viability, and inhibits cell apoptosis and inflammation of RBMECs via the ERK1/2 signaling pathway

The RT-qPCR showed that FGF21 RNA expression was significantly upregulated after IL-1 β treatment (p < 0.05, Fig. 2A). Based on this finding, we overexpressed FGF21 in RBMECs to examine the potential functions of this factor in cell growth. FGF21 RNA expression in RBMECs transfected with a compounded fragment of FGF21 was significantly upregulated compared to RBMECs transfected with a NC (p < 0.05, Fig. 2B). The CCK-8 assays showed that overexpressed FGF21 greatly increased the cell viability of RBMECs (p < 0.05, Fig. 2C). In addition, Bcl-2

was significantly upregulated, and Bax and caspase-3 were markedly downregulated by FGF21 upregulation ($p < 0.05$, Fig. 2D). Moreover, overexpressed FGF21 suppressed the inflammatory response, which was manifested by a low expression of TNF- α and upregulated TGF- β 1 ($p < 0.05$, Fig. 2E). The FGF21 mediated progression of wound healing was also examined, showing that the ERK1/2 signaling pathway was activated through phosphorylated ERK1/2 proteins ($p < 0.05$, Fig. 2F).

Upregulated TNF- α inhibits cell viability and promotes the apoptosis of RBMECs through suppressing FGF21

As TNF- α was downregulated by FGF21 overexpression, the role of this factor in the wound healing of RBMECs was further analyzed. Overexpression of TNF- α significantly increased the protein level of TNF- α compared to the NC group ($p < 0.05$, Fig. 3A). Thereafter, FGF21 RNA expression was measured, indicating that the increased expression of FGF21 caused by the overexpression of FGF21 was reversed to a lower level by TNF- α ($p < 0.05$, Fig. 3B). Furthermore, the increased cell viability of RBMECs after FGF21

upregulation was significantly inhibited by TNF- α promotion, while overexpressed TNF- α increased the apoptosis rate of RBMECs whose apoptosis rate was declined by overexpressed FGF21 ($p < 0.05$, Fig. 3C,D). Moreover, Bcl-2 expression was decreased, while Bax and caspase-3 were both promoted after TNF- α overexpression ($p < 0.05$, Fig. 3E). The scratch test also indicated that overexpressed FGF21 significantly decreased the healing area of RBMECs, while TNF- α upregulation reversed the impact of FGF21 and reduced the migration of RBMECs ($p < 0.05$, Fig. 3F).

Overexpression of VEGFA promotes cell viability and represses apoptosis of RBMECs through the ERK1/2 signaling pathway

Because of TNF- α upregulation, FGF21 was significantly downregulated. This treatment also decreased the RNA levels of VEGFA ($p < 0.05$, Fig. 4A). Thus, to examine the functions of VEGFA in RBMEC wound healing, an overexpression of VEGFA was carried out. After upregulation, VEGFA RNA expression was largely increased compared to the NC transfection group ($p < 0.05$, Fig. 4B). The cell viability

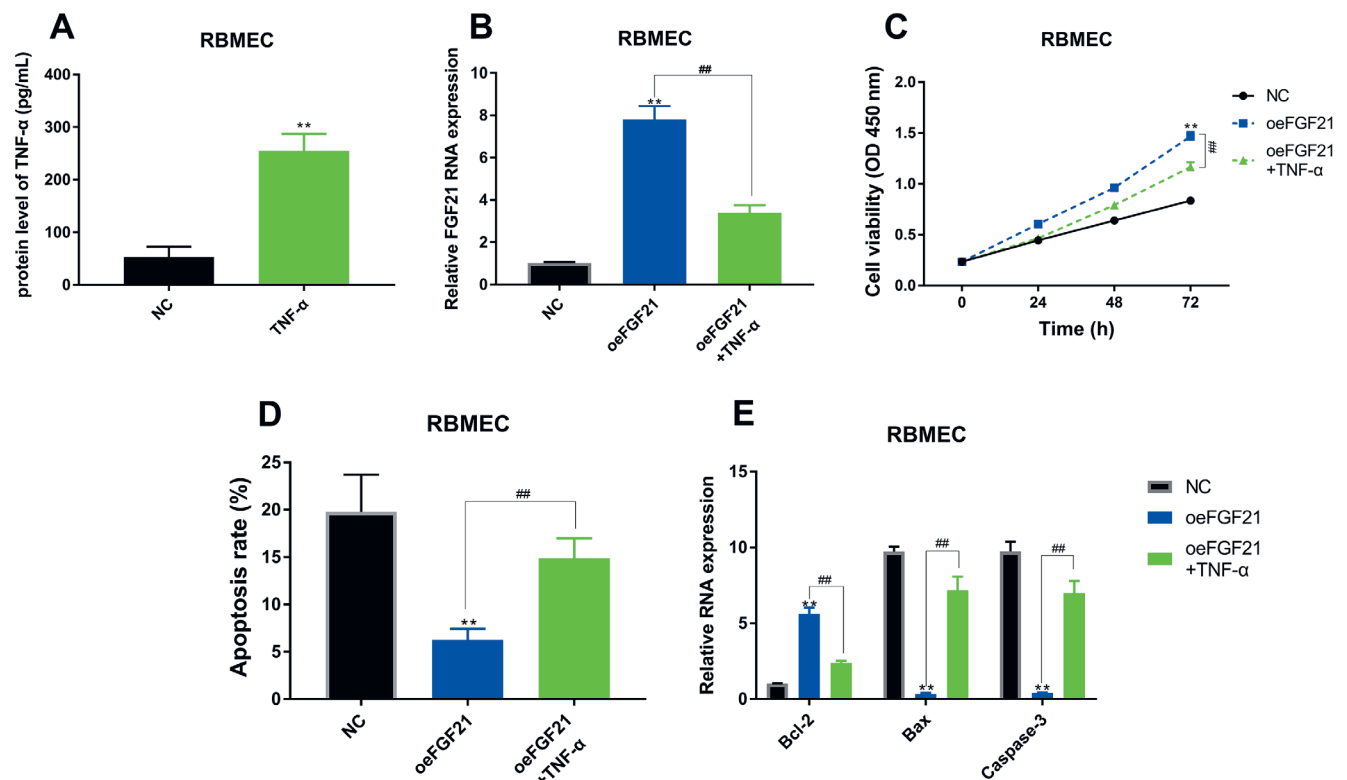


Fig. 3. Upregulated TNF- α inhibits cell viability and promotes cell apoptosis of RBMECs through the suppression of FGF21

A. Protein expression of TNF- α in RBMECs after TNF- α upregulation was evaluated with ELISA (** $p < 0.05$ compared to the NC group); B. FGF21 RNA expression after FGF21 overexpression and TNF- α upregulation were detected with RT-qPCR (** $p < 0.05$ in comparison with the oeNC group and ## $p < 0.05$ compared to the oeFGF21 group); C. Cell viability of RBMECs after FGF21 and TNF- α overexpression (** $p < 0.05$ compared to the oeNC group and ## $p < 0.05$ compared to the oeFGF21 group); D. Flow cytometry was used to measure apoptosis rate of RBMECs after transfection with oeFGF21 and oeTNF- α (** $p < 0.05$ compared to the oeNC group and ## $p < 0.05$ compared to the oeFGF21 group); E. RT-qPCR was used to analyze Bcl-2, Bax and caspase-3 RNA expression in RBMECs transfected with FGF21 and TNF- α overexpression (** $p < 0.05$ compared to the oeNC group and ## $p < 0.05$ compared to the oeFGF21 group); F. Scratch test was used to detect wound healing of RBMECs transfected with oeFGF21 and oeTNF- α (** $p < 0.05$ compared to the oeNC group and ## $p < 0.05$ compared to the oeFGF21 group).

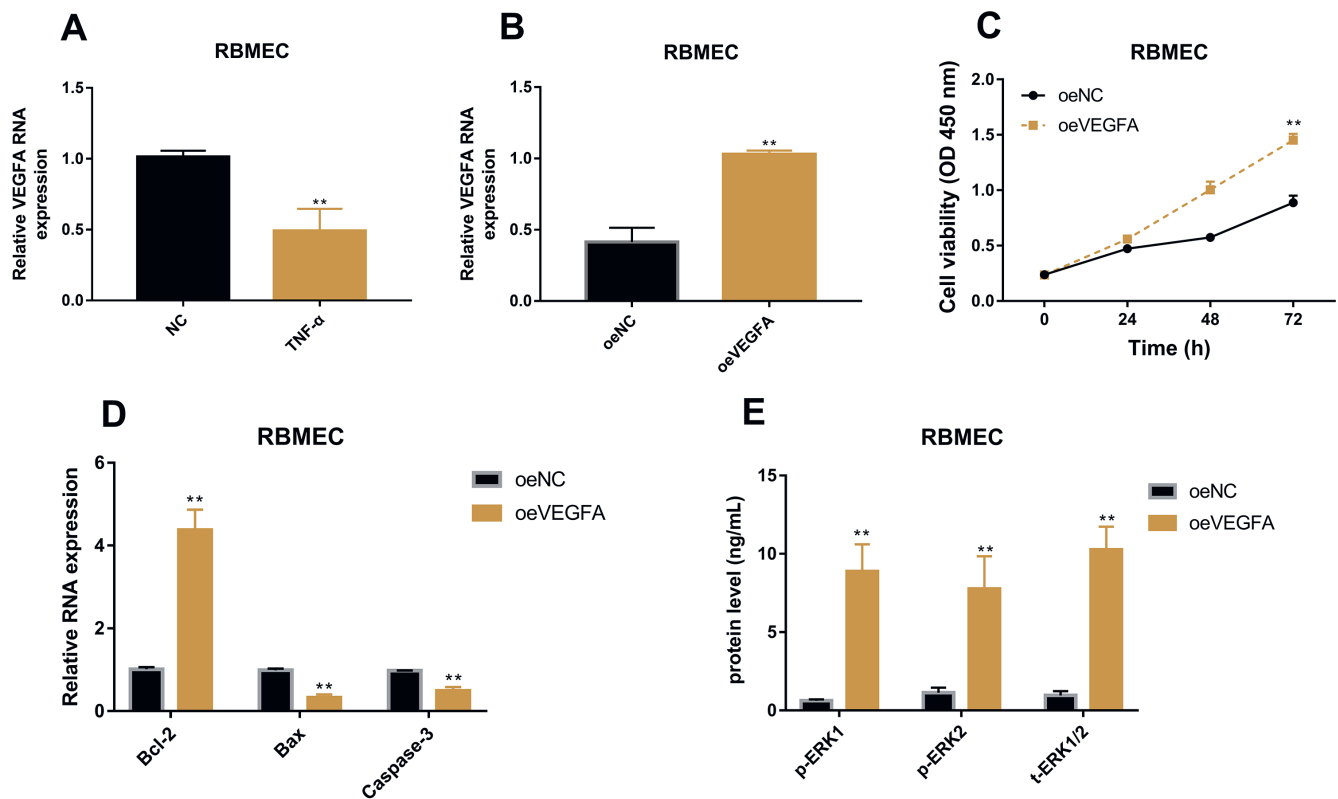


Fig. 4. Overexpression of VEGFA promotes cell viability and represses apoptosis of RBMECs through the ERK1/2 signaling pathway

A. VEGFA RNA expression in normal RBMECs and RBMECs after TNF- α overexpression were assessed with RT-qPCR (** $p < 0.05$ compared to the NC group); B. VEGFA RNA expression in RBMECs transfected with oeNC and oeVEGFA were measured with RT-qPCR (** $p < 0.05$ compared to the oeNC group); C. CCK-8 was applied to detect cell viability of RBMECs after oeNC and oeVEGFA transfection (** $p < 0.05$ compared to the oeNC group); D. Bcl-2, Bax and caspase-3 RNA expression were detected with RT-qPCR in RBMECs after oeNC or oeVEGFA transfection (** $p < 0.05$ compared to the oeNC group); E. ERK1/2 phosphorylation and total ERK1/2 were measured with ELISA in RBMECs transfected using oeNC and oeVEGFA (** $p < 0.05$ compared to the oeNC group).

of RBMECs was significantly improved by VEGFA overexpression ($p < 0.05$, Fig. 4C). In addition, RT-qPCR indicated that the Bcl-2 RNA level was significantly upregulated after VEGFA overexpression, while Bax and caspase-3 RNA expression were both significantly lower compared to the NC group ($p < 0.05$, Fig. 4D). To investigate the mechanism by which VEGFA mediates cell viability and apoptosis, the effects of this factor on ERK phosphorylation were also examined. The results showed that the protein expression of phosphorylated ERK1/2 was significantly upregulated by VEGFA upregulation ($p < 0.05$, Fig. 4E).

Suppression of the ERK1/2 signaling pathway inhibits the effects of FGF21 and VEGFA on cell viability and apoptosis of RBMECs

As the ERK1/2 signaling pathway was activated by FGF21 and VEGFA in RBMECs, we examined the potential functions of this pathway in the wound healing progression of these cells. To this end, PD98059, an ERK1/2 signaling pathway suppressor, was used to block activation of ERK1/2. PD98059 treatment significantly inhibited not only the protein levels of phosphorylated ERK1/2, but total ERK1/2 protein expression ($p < 0.05$, Fig. 5A).

Thereafter, the roles of the ERK1/2 signaling pathway were examined after FGF21 and VEGFA were upregulated. PD98059 treatment significantly inhibited the increased cell viability caused by overexpressed FGF21 and VEGFA ($p < 0.05$, Fig. 5B), and enhanced the apoptosis rate of RBMEC after suppression by FGF21 and VEGFA upregulation ($p < 0.05$, Fig. 5C). Moreover, the high levels of Bcl-2 caused by upregulated FGF21 and VEGFA were reversed after PD98059 treatment, while the lower levels of Bax and caspase-3 were both upregulated ($p < 0.05$, Fig. 5D). The scratch test showed that the decreased migration areas induced by overexpressed FGF21 and VEGFA were inhibited by PD98059 treatment in RBMECs ($p < 0.05$, Fig. 5E).

Discussion

Endovascular surgery has been shown to treat stroke successfully.²⁸ However, the vessel damage that can result from mechanical thrombectomy²⁹ is an urgent clinical problem that needs to be addressed.^{30–32} Accelerating the efficiency of wound healing following this procedure might bring a better future for endovascular surgeries. In the progression of wound healing, inflammation is an important step

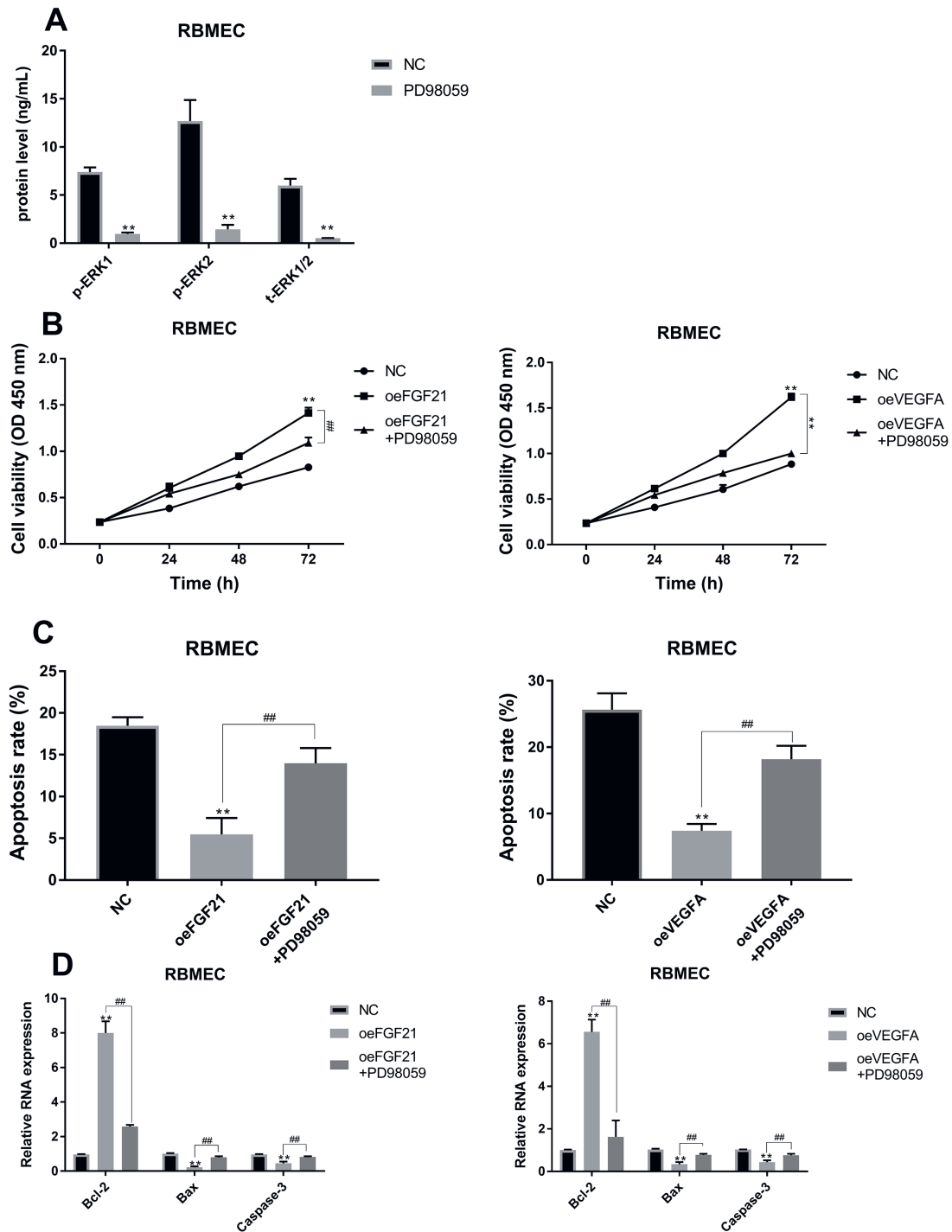


Fig. 5. Suppression of the ERK1/2 signaling pathway inhibits FGF21 and VEGFA regulation of RBMEC viability and apoptosis

A. Phosphorylated ERK1/2 and total ERK1/2 were measured in normal and PD98059 (50 μ M)-treated RBMECs (** p < 0.05 compared to the NC group); B. Cell viability of RBMECs after overexpression of FGF21 or VEGFA and overexpression of FGF21 or VEGFA with PD98059 were examined through CCK-8 (** p < 0.05 compared to the oeNC group and ## p < 0.05 compared to the oeFGF21 or oeVEGFA group); C. Apoptosis rate of RBMECs transfected with oeFGF21 or oeVEGFA, and RBMECs treated with PD98059 after transfection were evaluated using flow cytometry (** p < 0.05 compared to the oeNC group and ## p < 0.05 compared to the oeFGF21 or oeVEGFA group); D. Bcl-2, Bax and caspase-3 RNA expression were measured using RT-qPCR in RBMECs transfected with oeFGF21 and oeVEGFA and PD98059 treatment (** p < 0.05 compared to the oeNC group and ## p < 0.05 compared to the oeFGF21 or oeVEGFA group); E. Wound healing of RBMECs after oeFGF21 and oeVEGFA transfection and PD98059 treatment were checked using the scratch test (** p < 0.05 compared to the oeNC group and ## p < 0.05 compared to the oeFGF21 or oeVEGFA group).

that can induce immune system activation, restore homeostasis and repair tissue damage.³³ However, persistent and overactivated inflammation can result in further damage.³⁴ In examinations of inflammatory cytokines, TNF- α has

been identified as a factor that can inhibit the metastasis of keratinocytes through upregulation of TIMP-1 expression, but a TNF- α antagonist has been shown to improve the progression of wound healing in diabetic rats models.³⁵

By contrast, TGF- β 1 has also been reported to attenuate the inflammatory response via the ERK1/2 signaling pathway and can facilitate the progression of wound healing.^{36,37} Based on these studies, we examined the effects of inflammation on the wound healing of RBMECs. Using CCK-8 assays and flow cytometry, we determined that RBMECs treated with IL-1 β showed lower cell viability and a higher cell apoptosis rate. Moreover, downregulated Bcl-2 RNA expression, and upregulated Bax and caspase-3 expression, also indicated that IL-1 β facilitated cell apoptosis. As for the effects of IL-1 β on inflammatory cytokines, TNF- α protein expression was upregulated, while TGF- β 1 was significantly decreased. Hence, in the current study, prolonged inflammation in RBMECs has been shown to decrease cell viability and migration, and to promote cell apoptosis, through the stimulation of TNF- α and the suppression of TGF- β 1.

Studies examining the functions of FGF21 have commonly focused on homeostasis, especially its role in energy metabolism.³⁸ However, FGF21 can also act as an anti-inflammatory cytokine, which has been shown in experimental pancreatitis and myocardial ischemia.³⁸ In addition, FGF21 has been reported to promote wound healing through increasing the activation of c-Jun N-terminal kinase (JNK).³⁹ In rat myocardial ischemia reperfusion and H9c2 hypoxia re-oxygenation models, FGF21 significantly reduced cell apoptosis and inhibited TNF- α through binding miR-145.⁴⁰ However, whether FGF21 can also influence TNF- α during the progression of wound healing has seldom been mentioned. Thus, we have investigated the role of FGF21 in the wound healing of RBMECs, which revealed that FGF21 promoted cell viability and inhibited cell apoptosis. Moreover, FGF21 suppressed the protein levels of TNF- α and increased TGF- β 1. Therefore, we hypothesized that FGF21 might promote wound healing through a suppression of TNF- α . Apart from inflammation, the ERK1/2 signaling pathway has also been shown to play an important role in FGF signaling transmission.³⁸ Activation of the ERK1/2 signaling pathway helps FGF21 facilitate glucose uptake by inducing expression of glucose transporter-1 in adipocytes.⁴¹ Moreover, p-ERK1/2 was activated and promoted during the wound healing of diabetic rats after propranolol treatment.⁴² Based on these studies, we analyzed the expression of ERK1 and ERK2 and showed that these proteins were significantly upregulated. Therefore, FGF21 might accelerate the wound healing of RBMECs through activation of the ERK1/2 signaling pathway.

As outlined above, FGF21 inhibited TNF- α in the RBMEC model. Others have reported that TNF- α can suppress β -Klotho expression and attenuate the roles of FGF21 in adipocytes.⁴³ In the current study, TNF- α also increased cell apoptosis, and reduced the viability and wound healing of RBMECs by inhibiting the functions of FGF21. Therefore, inflammation might retard the progression of wound healing by inhibiting FGF21. Moreover, TNF- α was found to inhibit VEGFA in RBMEC cells, which is an important factor in the progression of wound healing.⁴⁴ The VEGFA

has been reported to accelerate angiogenesis in human umbilical vein endothelial cells (HUVECs) via ERK1/2 phosphorylation and ACE2 inhibition.⁴⁵ Therefore, we examined the functions of VEGFA in RBMECs, showing that it could improve cell viability and depress cell apoptosis. Moreover, VEGFA enhanced phosphorylation of ERK1/2 in RBMECs. Therefore, we hypothesized that TNF- α might also inhibit wound healing through downregulating VEGFA.

In the current study, the ERK1/2 signaling pathway was activated by FGF21 and VEGFA. Based on this finding, we speculated if activation of the ERK1/2 signaling pathway was a necessary step in wound healing. To test this idea, we used PD98059 to inhibit ERK1/2. Treatment with this agent significantly repressed the promotion of cell viability and migration caused by FGF21 and VEGFA, while inhibition of the apoptosis rate was also reversed to a higher level. PD98059 has been shown to inhibit the wound healing progression of human keratinocytes by suppressing p-ERK1 and p-ERK2, which was also shown in a rat wound model.⁴⁶ In our study, FGF21 mediated cell viability and cell apoptosis of RBMECs via the inhibition of TNF- α and activation of the ERK1/2 signaling pathway. Furthermore, TNF- α suppressed FGF21 functions and VEGFA, while VEGFA also regulated the viability and apoptosis of RBMECs via the ERK1/2 signaling pathway. Thus, FGF21 may accelerate wound healing through upregulating VEGFA and activating the ERK1/2 signaling pathway by suppressing TNF- α . However, this finding will need to be confirmed in future work.

Conclusions

The FGF21 facilitated the viability and inhibited the apoptosis of RBMECs through the activation of ERK1/2 and VEGFA, caused by inhibition of TNF- α . These findings suggest that FGF21 might be a useful factor to improve wound healing. However, in vivo and clinical studies will be needed to demonstrate the effectiveness of this approach.

ORCID iDs

Weiting Chen  <https://orcid.org/0000-0001-7624-0754>
 Zhongen Shen  <https://orcid.org/0000-0003-4146-1113>
 Shuiqi Cai  <https://orcid.org/0000-0002-1983-1029>
 Long Chen  <https://orcid.org/0000-0001-9430-6817>
 Dabin Wang  <https://orcid.org/0000-0001-9377-5830>

References

- Morotti A, Poli P, Costa P. Acute stroke. *Semin Neurol*. 2019;39(1):61–72. doi:10.1055/s-0038-1676992
- O'Donnell MJ, Lim Chin S, Rangarajan S, et al; INTERSTROKE investigators. Global and regional effects of potentially modifiable risk factors associated with acute stroke in 32 countries (INTERSTROKE): A case-control study. *Lancet*. 2016;388(10046):761–775. doi:10.1016/S0140-6736(16)30506-2
- Khandelwal P, Yavagal DR, Sacco RL. Acute ischemic stroke intervention. *J Am Coll Cardiol*. 2016;67(22):2631–2644. doi:10.1016/j.jacc.2016.03.555
- Saver JL. Time is brain-quantified. *Stroke*. 2006;37(1):263–266. doi:10.1161/01.STR.0000196957.55928.ab

5. Wang A, Abramowicz AE. Endovascular thrombectomy in acute ischemic stroke: New treatment guide. *Curr Opin Anaesthesiol*. 2018;31(4):473–480. doi:10.1097/ACO.0000000000000621
6. Peschillo S, Diana F, Berge J, Missori P. A comparison of acute vascular damage caused by ADAPT versus a stent retriever device after thrombectomy in acute ischemic stroke: A histological and ultrastructural study in an animal model. *J Neurointerv Surg*. 2017;9(8):743–749. doi:10.1136/neurintsurg-2016-012533
7. Reinke JM, Sorg H. Wound repair and regeneration. *Eur Surg Res*. 2012;49(1):35–43. doi:10.1159/000339613
8. Mustoe TA, O'Shaughnessy K, Kloeters O. Chronic wound pathogenesis and current treatment strategies: A unifying hypothesis. *Plast Reconstr Surg*. 2006;117(7 Suppl):355–415. doi:10.1097/01.prs.0000225431.63010.1b
9. Ornitz DM, Itoh N. The fibroblast growth factor signaling pathway. *Wiley Interdiscip Rev Dev Biol*. 2015;4(3):215–266. doi:10.1002/wdev.176
10. Potthoff MJ, Klier SA, Mangelsdorf DJ. Endocrine fibroblast growth factors 15/19 and 21: From feast to famine. *Genes Dev*. 2012;26(4):312–324. doi:10.1101/gad.184788.111
11. Salminen A, Kaarniranta K, Kauppinen A. Regulation of longevity by FGF21: Interaction between energy metabolism and stress responses. *Ageing Res Rev*. 2017;37:79–93. doi:10.1016/j.arr.2017.05.004
12. Fisher FM, Chui PC, Nasser IA, et al. Fibroblast growth factor 21 limits lipotoxicity by promoting hepatic fatty acid activation in mice on methionine and choline-deficient diets. *Gastroenterology*. 2014;147(5):1073–1083.e6. doi:10.1053/j.gastro.2014.07.044
13. Wang N, Li JY, Li S, et al. Fibroblast growth factor 21 regulates foam cells formation and inflammatory response in Ox-LDL-induced THP-1 macrophages. *Biomed Pharmacother*. 2018;108:1825–1834. doi:10.1016/j.biopha.2018.09.143
14. Liu H, Zhao Y, Zou Y, et al. Heparin-polyoxamer hydrogel-encapsulated rhFGF21 enhances wound healing in diabetic mice. *FASEB J*. 2019;33(9):9858–9870. doi:10.1096/fj.201802600RR
15. Coskun T, Bina HA, Schneider MA, et al. Fibroblast growth factor 21 corrects obesity in mice. *Endocrinology*. 2008;149(12):6018–6027. doi:10.1210/en.2008-0816
16. Ye L, Wang X, Cai C, et al. FGF21 promotes functional recovery after hypoxic-ischemic brain injury in neonatal rats by activating the PI3K/Akt signaling pathway via FGFR1/ β -Klotho. *Exp Neurol*. 2019;317:34–50. doi:10.1016/j.expneurol.2019.02.013
17. Nissen NN, Polverini PJ, Koch AE, Volin MV, Gamelli RL, DiPietro LA. Vascular endothelial growth factor mediates angiogenic activity during the proliferative phase of wound healing. *Am J Pathol*. 1998;152(6):1445–1452. PMID:9626049
18. Lim JC, Mattos M, Fang M, et al. TNF α contributes to diabetes impaired angiogenesis in fracture healing. *Bone*. 2017;99:26–38. doi:10.1016/j.bone.2017.02.014
19. Jeon HH, Yu Q, Lu Y, et al. FOXO1 regulates VEGFA expression and promotes angiogenesis in healing wounds. *J Pathol*. 2018;245(3):258–264. doi:10.1002/path.5075
20. Chamorro-Jorganes A, Lee MY, Araldi E, et al. VEGF-induced expression of miR-17-92 cluster in endothelial cells is mediated by ERK/ELK1 activation and regulates angiogenesis. *Circ Res*. 2016;118(1):38–47. doi:10.1161/CIRCRESAHA.115.307408
21. Lee BC, Song J, Lee A, Cho D, Kim TS. Visfatin promotes wound healing through the activation of ERK1/2 and JNK1/2 pathway. *Int J Mol Sci*. 2018;19(11):3642. doi:10.3390/ijms19113642
22. Wang R, et al. FGF21 regulates melanogenesis in alpaca melanocytes via ERK1/2-mediated MITF downregulation. *Biochem Biophys Res Commun*. 2017;490(2):466–471. doi:10.1016/j.bbrc.2017.06.064
23. Liu Q, Wang S, Wei M, et al. Improved FGF21 sensitivity and restored FGF21 signaling pathway in high-fat diet/streptozotocin-induced diabetic rats after duodenal-jejunal bypass and sleeve gastrectomy. *Front Endocrinol (Lausanne)*. 2019;10:566. doi:10.3389/fendo.2019.00566
24. Cui J, Gong C, Cao B, Li L. MicroRNA-27a participates in the pathological process of depression in rats by regulating VEGFA. *Exp Ther Med*. 2018;15(5):4349–4355. doi:10.3892/etm.2018.5942
25. Mahdavi S, Khodarahmi P, Roodbari NH. Effects of cadmium on Bcl-2/Bax expression ratio in rat cortex brain and hippocampus. *Hum Exp Toxicol*. 2018;37(3):321–328. doi:10.1177/0960327117703687
26. Yin HY, Wei JR, Zhang R, Ye XL, Zhu YF, Li WJ. Effect of glutamine on caspase-3 mRNA and protein expression in the myocardium of rats with sepsis. *Am J Med Sci*. 2014;348(4):315–318. doi:10.1097/MAJ.0000000000000237
27. Martuscello RT, Spengler RM, Boniu AC, et al. Increasing TNF levels solely in the rat hippocampus produces persistent pain-like symptoms. *Pain*. 2012;153(9):1871–1882. doi:10.1016/j.pain.2012.05.028
28. Goyal M, Menon BK, van Zwam WH, et al; HERMES collaborators. Endovascular thrombectomy after large-vessel ischaemic stroke: A meta-analysis of individual patient data from five randomised trials. *Lancet*. 2016;387(10029):1723–1731. doi:10.1016/S0140-6736(16)00163-X
29. Koge J, Kato S, Hashimoto T, Nakamura Y, Kawajiri M, Yamada T. Vessel wall injury after stent retriever thrombectomy for internal carotid artery occlusion with duplicated middle cerebral artery. *World Neurosurg*. 2019;123:54–58. doi:10.1016/j.wneu.2018.11.223
30. Leishangthem L, Satti SR. Vessel perforation during withdrawal of Trevo ProVue stent retriever during mechanical thrombectomy for acute ischemic stroke. *J Neurosurg*. 2014;121(4):995–998. doi:10.3171/2014.4.JNS132187
31. Arai D, Ishii A, Chihara H, Ikeda H, Miyamoto S. Histological examination of vascular damage caused by stent retriever thrombectomy devices. *J Neurointerv Surg*. 2016;8(10):992–995. doi:10.1136/neurintsurg-2015-011968
32. Truong M, Bloch KM, Andersen M, Andsberg G, Töger J, Wassélius J. Subacute vessel wall imaging at 7-T MRI in post-thrombectomy stroke patients. *Neuroradiology*. 2019;61(10):1145–1153. doi:10.1007/s00234-019-02242-9
33. Landén NX, Li D, Stähle M. Transition from inflammation to proliferation: A critical step during wound healing. *Cell Mol Life Sci*. 2016;73(20):3861–3885. doi:10.1007/s00018-016-2268-0
34. Smigiel KS, Parks WC. Macrophages, wound healing, and fibrosis: Recent insights. *Curr Rheumatol Rep*. 2018;20(4):17. doi:10.1007/s11926-018-0725-5
35. Huang SM, Wu CS, Chiu MH, et al. High glucose environment induces M1 macrophage polarization that impairs keratinocyte migration via TNF- α : An important mechanism to delay the diabetic wound healing. *J Dermatol Sci*. 2019;96(3):159–167. doi:10.1016/j.jdermsci.2019.11.004
36. Lichtman MK, Otero-Vinas M, Falanga V. Transforming growth factor beta (TGF- β) isoforms in wound healing and fibrosis. *Wound Repair Regen*. 2016;24(2):215–222. doi:10.1111/wrr.12398
37. Zhang J, Li Z, Chen F, et al. TGF- β 1 suppresses CCL3/4 expression through the ERK signaling pathway and inhibits intervertebral disc degeneration and inflammation-related pain in a rat model. *Exp Mol Med*. 2017;49(9):e379. doi:10.1038/emmm.2017.136
38. Fisher FM, Maratos-Flier E. Understanding the physiology of FGF21. *Annu Rev Physiol*. 2016;78:223–241. doi:10.1146/annurev-physiol-021115-105339
39. Song YH, Zhu YT, Ding J, et al. Distribution of fibroblast growth factors and their roles in skin fibroblast cell migration. *Mol Med Rep*. 2016;14(4):3336–3342. doi:10.3892/mmr.2016.5646
40. Hu S, Cao S, Tong Z, Liu J. FGF21 protects myocardial ischemia-reperfusion injury through reduction of miR-145-mediated autophagy. *Am J Transl Res*. 2018;10(11):3677–3688. PMID:30662618
41. Ge X, Chen C, Hui X, Wang Y, Lam KS, Xu A. Fibroblast growth factor 21 induces glucose transporter-1 expression through activation of the serum response factor/Ets-like protein-1 in adipocytes. *J Biol Chem*. 2011;286(40):34533–34541. doi:10.1074/jbc.M111.248591
42. Chang X, Li S, Xue XD, Chang F. Propranolol regulates ERK1/2 signaling pathway and promotes chronic wound healing in diabetic rats. *Eur Rev Med Pharmacol Sci*. 2019;23(10):4498–4506. doi:10.26355/eurev_201905_17962
43. Diaz-Delfín J, Hondares E, Iglesias R, Giral M, Caelles C, Villarroya F. TNF- α represses β -Klotho expression and impairs FGF21 action in adipose cells: Involvement of JNK1 in the FGF21 pathway. *Endocrinology*. 2012;153(9):4238–4245. doi:10.1210/en.2012-1193
44. Ren S, Chen J, Duscher D, et al. Microvesicles from human adipose stem cells promote wound healing by optimizing cellular functions via AKT and ERK signaling pathways. *Stem Cell Res Ther*. 2019;10(1):47. doi:10.1186/s13287-019-1152-x
45. Zhang Q, Lu S, Li T, et al. ACE2 inhibits breast cancer angiogenesis via suppressing the VEGFA/VEGFR2/ERK pathway. *J Exp Clin Cancer Res*. 2019;38(1):173. doi:10.1186/s13046-019-1156-5
46. Wang Y, Zheng J, Han Y, et al. JAM-A knockdown accelerates the proliferation and migration of human keratinocytes, and improves wound healing in rats via FAK/Erk signaling. *Cell Death Dis*. 2018;9(9):848. doi:10.1038/s41419-018-0941-y

Notch pathway activation promotes the differentiation of beagle dog periodontal ligament stem cells to Schwann cells

Xiaojie Li^{1,A–F}, Dapeng Liao^{2,A–F}, Gang Sun^{2,B,C,E,F}, HanWen Chu^{2,B,C,E,F}

¹ Department of Dentistry, Sir Run Run Shaw Hospital, Zhejiang University School of Medicine, China

² Department of Dentistry, The Second Affiliated Hospital, Zhejiang University School of Medicine, China

A – research concept and design; B – collection and/or assembly of data; C – data analysis and interpretation; D – writing the article; E – critical revision of the article; F – final approval of the article

Advances in Clinical and Experimental Medicine, ISSN 1899–5276 (print), ISSN 2451–2680 (online)

Adv Clin Exp Med. 2021;30(7):721–726

Address for correspondence

Xiaojie Li
E-mail: 3312026@zju.edu.cn

Funding sources

The Project was supported by National Natural Science Foundation of China under grant No. 81702222 and Zhejiang Provincial Natural Science Foundation of China under grant No. LQ17H170001.

Conflict of interest

None declared

Received on July 8, 2020

Reviewed on July 15, 2020

Accepted on December 6, 2020

Published online on June 11, 2021

Abstract

Background. Periodontal ligament stem cells (PDLSCs) have demonstrated the potential for differentiation into many cell types, though the molecular mechanism of their neural differentiation in particular remains largely unknown.

Objectives. The Notch signaling pathway plays a key role in regulating cell differentiation and development. In this article, we explore its potential role in the differentiation of PDLSCs to Schwann cells (SCs).

Materials and methods. The PDLSCs were either transfected with viral vectors carrying genetic material for Notch Delta ligands, thereby induced their overexpression, or treated with DAPT (a Notch-pathway-specific inhibitor) to inhibit γ -secretase. The potential effects of Notch signaling on myelination and SCs differentiation were then investigated using western blotting, immunostaining and reverse transcriptase polymerase chain reaction (RT-PCR) to detect the expression of SC-specific marker genes.

Results. Specifically inhibiting Notch signaling with DAPT decreased the expression of SC-specific marker genes *GFAP*, *S100* and *P75*, as well as of SC-myelin-related genes *PMP22*, *MBP*, connexin, and *PO* in cells undergoing induced differentiation from PDLSCs. Conversely, activating Notch signaling through overexpression of Delta ligands enhanced the expression of SC-specific marker genes as well as myelin-related genes in cells undergoing induced differentiation from PDLSCs. This promotion was reversed by DAPT.

Conclusions. The Notch signaling pathway positively regulated the process of PDLSC differentiation into SCs, and the activation of this signaling was important in maintaining the differentiation of PDLSCs to SCs, and then SC myelination. These results may improve the method of obtaining pure SCs from PDLSCs for transplantation application.

Key words: differentiation, Schwann cells, periodontal ligament stem cells, Notch signaling pathway

Cite as

Li X, Liao D, Sun G, Chu HW. Notch pathway activation promotes the differentiation of beagle dog periodontal ligament stem cells to Schwann cells. *Adv Clin Exp Med.* 2021;30(7):721–726. doi:10.17219/acem/131219

DOI

10.17219/acem/131219

Copyright

© 2021 by Wrocław Medical University
This is an article distributed under the terms of the Creative Commons Attribution 3.0 Unported (CC BY 3.0) (<https://creativecommons.org/licenses/by/3.0/>)

Background

The Schwann cells (SCs) are a glial nerve cell type that form an important part of the Ruffini body of periodontal nerve endings, and play an important role in growth, development and regeneration of peripheral nerves.^{1,2} Schwann cells are essential in increasing the density of peripheral nerve endings, and in the improvement of osseoperception. They respond rapidly to nerve injury, and promote axon re-growth and nerve regeneration. Schwann cells also produce various growth factors that are involved in phagocytosis and the clearance of myelin fragments. All these characteristics have made SCs the first and the most widely used support cells to be used for peripheral nerve regeneration.^{3–5}

In our previous study, we found that periodontal ligament stem cells (PDLSCs) isolated from beagle dogs effectively differentiated into SCs with exposure to a combination of dimethyl sulfoxide (DMSO), basic fibroblast growth factor (bFGF), brain-derived neurotrophic factor (BDNF), nerve growth factor (NGF) and forskolin.^{6,7} Multiple signaling pathways, transcription factors, and neurotrophic factors had been implicated in their differentiation.^{3,8} However, the mechanisms underlying the process of PDLSC differentiation to SCs are poorly characterized.

We have previously demonstrated that the Erk1/2 signaling pathway is involved in the differentiation of PDLSCs to SCs.⁹ Although inhibition of the Erk1/2 pathway is shown to prevent the differentiation of PDLSCs to SCs, we still find evidence of a number of SCs in culture. This suggests that other signaling pathways are also involved in the process.

In this study, we investigate whether the Notch signaling pathway is involved in the differentiation of PDLSCs to SCs. The Notch signaling pathway is a highly conserved system that regulates cell differentiation and development in many multicellular organisms.^{10,11} Moreover, many reports indicate that Notch signaling is involved in different stages of SCs development, including acting on neural crest stem cells and mediating the generation of immature SCs.^{12,13} The structure of Notch family members is highly conserved, and the regulatory mechanism is very complex. Notch signaling in vertebrates consists of Notch, Notch ligands (Delta and Jagged proteins) and CSL DNA binding proteins. Following Notch receptor binding to Delta or Jagged ligands, Notch is cleaved by the γ -secretase activity of presenilin-1 (PS1) to release the cytoplasmic domain of the Notch receptor – the Notch intracellular domain (NIC) – which translocates to the nucleus and binds to the transcription factor CSL, leading to the transcriptional activation of downstream target genes.¹⁴

Objectives

In this study, we provide evidence that Notch signaling represents a key regulatory pathway in regulating PDLSC

differentiation. We used the γ -secretase inhibitor DAPT to specifically inhibit the Notch signaling pathway, and overexpressed the Delta ligand to activate it. The effect of the Notch signaling pathway on the differentiation of PDLSCs to SCs was examined.

Materials and methods

All animals were purchased from Sichuan University and the experimental protocol was approved by the Ethical Guideline Committee of Animal Care, West China College of Medical Sciences, Sichuan University, Chengdu, China.

Isolation and culture of PDLSCs

The PDLSCs were isolated from the periodontal ligaments of beagle dogs using the single-colony selection method as described previously.¹⁵ Two healthy beagle dogs, 12-month-old, weighing about 10 kg, were selected. The premolars were extracted, and the periodontal ligaments were carefully scraped off. The PDLSCs were dissociated by digesting the periodontal ligaments with Trypsin-EDTA (0.25%) (Catalog No. 25200056; Gibco, Waltham, USA) and cultured following gradient centrifugation. Next, PDLSCs were identified by a combination of optical microscopy and flow cytometry, as described previously.¹⁶

Differentiation of PDLSCs to SCs

We induced the differentiation of PDLSCs to SCs as described previously.⁶ The PDLSCs were then treated with 2% DMSO for 5 h, before culturing in differentiation medium, which contained 10 ng/mL bFGF, 10 ng/mL NGF, 10 ng/mL BDNF, 14 mM forskolin, and 20% (v/v) fetal bovine serum (FBS) in minimal essential medium (MEM) alpha modification, with L-glutamine, with ribo- and deoxyribonucleosides (Sigma-Aldrich, St. Louis, USA).

Co-culture of PDLSCs and DRG cells

For co-culture assays, cells were grown in six-cell culture inserts following the manufacturer's instructions (BD Biosciences, Franklin Lakes, USA). A population of 1×10^4 dorsal root ganglion (DRG) cells was diluted in 1 mL medium and loaded into the upper chamber of a transwell cell insert (Lot 3450; Corning Inc., Corning, USA), while a population of 2×10^4 PDLSCs in 2 mL medium was added to the lower chambers. The transwell cell inserts allowed PDLSCs and DRG cells to share the same medium without direct contact.

Western blotting

S100, GFAP, P75, MYT1L, SNW1, ASPN, and GAPDH antibodies were purchased from Cell Signaling Technology

(Danvers, USA) and diluted at 1:100 in Tris-buffered saline with Tween (TBST). Total protein was extracted using RIPA lysis buffer, and protein concentration was determined using a bicinchoninic acid (BCA) assay kit (M&E Gene Technology, Beijing, China). Western blotting was performed as described previously.⁹

Immunofluorescence

Protein zero (P0) and myelin basic protein (MBP) antibodies were purchased from Abcam (Cambridge, UK). DAPT and fluorescein isothiocyanate-conjugated secondary antibody were purchased from BD Biosciences. After 2 weeks of induction, cells were immunoassayed as described previously.⁹ Immunofluorescence was visualized under an Olympus IX 71 microscope (Olympus Corp., Tokyo, Japan).

Quantitative real-time PCR

Total RNA was extracted using Trizol reagent according to the manufacturer's guidelines. Reverse transcription of mRNA was performed using the PrimeScript RT kit (TaKaRa, Kyoto, Japan). The quantitative real-time polymerase chain reaction (qRT-PCR) was performed on an ABI 7500 (Applied Biosystems, Foster City, USA) using a SYBR Premix Ex Taq Kit (TaKaRa) according to the manufacturer's guidelines. GAPDH was used as an internal control.

Statistical analyses

Each experiment was performed 3 times. One-way analysis of variance (ANOVA) and the Student's t-test were used to determine statistical differences between groups. All data are expressed as mean \pm standard deviation (SD). A value of $p < 0.05$ was considered significant.

Results

Characterization of PDLSCs

The PDLSCs appeared mainly polygonal with a typical spindle-shaped, fibroblast-like morphology (Fig. 1A). Flow cytometry was performed to detect stem cell surface markers. These cells showed relatively high expression levels of the surface markers STRO-1 and CD146 (Fig. 1B), indicating that they indeed had the characteristics of stem cells. The concentration of PDLSCs in the sample was very high.

Activation of the Notch signaling pathway promotes the differentiation of PDLSCs into SCs

Firstly, we characterized Notch signaling in the differentiation of PDLSCs into SCs. The PDLSCs were cultured

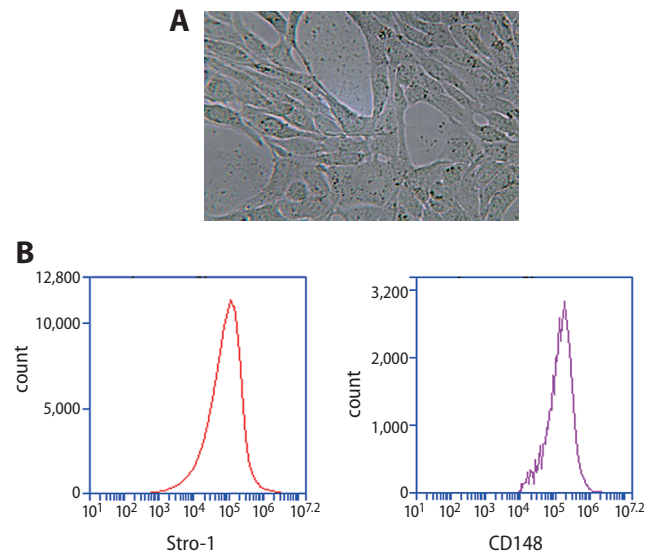


Fig. 1. Identification of PDLSCs. A. Inverted microscopy revealing the cell morphology of PDLSCs; B. Detection of PDLSC markers using flow cytometry

in differentiation medium containing DMSO, bFGF, BDNF, NGF, and forskolin to induce SC phenotypes. Differentiation into SCs was confirmed by the high expression of SC protein markers, including S100, GFAP and P75, as detected using western blot. We also found that differentiated PDLSCs exhibited upregulation of key proteins in the Notch 1 signaling pathway compared with undifferentiated PDLSCs (Fig. 2), such as the myelin transcription factor 1-like protein (MYT1L), a coactivator for Notch transcriptional activation, SNW domain-containing protein 1 (SNW1) and ASPN. These results suggested that the Notch pathway was activated during the differentiation of PDLSCs to SCs.

To further evaluate whether the Notch pathway was involved in the differentiation of PDLSCs into SCs, we investigated the effect of activation or inhibition of Notch signaling, using viruses overexpressing the Delta Notch ligand or an inhibitor of the Notch pathway, respectively. We found that activation of Notch signaling through the overexpression of the Delta ligand (which was confirmed by the upregulation of the MYT1L protein) increased the expression of SC-specific markers, including S100, GFAP and P75, compared to the control group. Further, the addition of DAPT to the differentiation medium decreased the expression of SC-specific markers compared with the control group (Fig. 3). These data suggest that activation of Notch signaling promotes the differentiation of PDLSCs into SCs, while inhibition of Notch signaling hinders this process. Taking all of these evidences into account, it appears that the Notch signaling pathway is involved in the differentiation of PDLSCs into SCs.

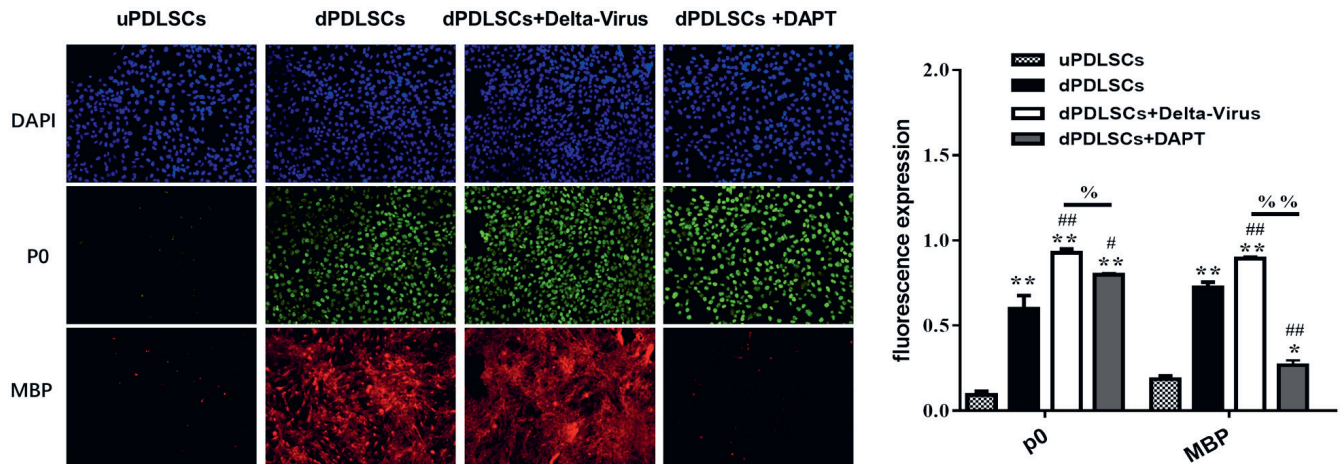


Fig. 2. Notch signaling pathway is involved in myelin formation during the differentiation of PDLSCs to SCs. Co-culture of PDLSCs and DRGs was conducted as described in the legend of Fig. 3. The expression of SC myelin-formation-related proteins P0 and MBP was analyzed with immunofluorescent staining. Blue spots represent nuclei stained with DAPI

* $p < 0.05$, ** $p < 0.01$ compared to uPDLSC group; # $p < 0.05$, ## $p < 0.01$ compared to corresponding dPDLSC group; % $p < 0.05$, %% $p < 0.01$ compared to dPDLSC+Delta-Virus group.

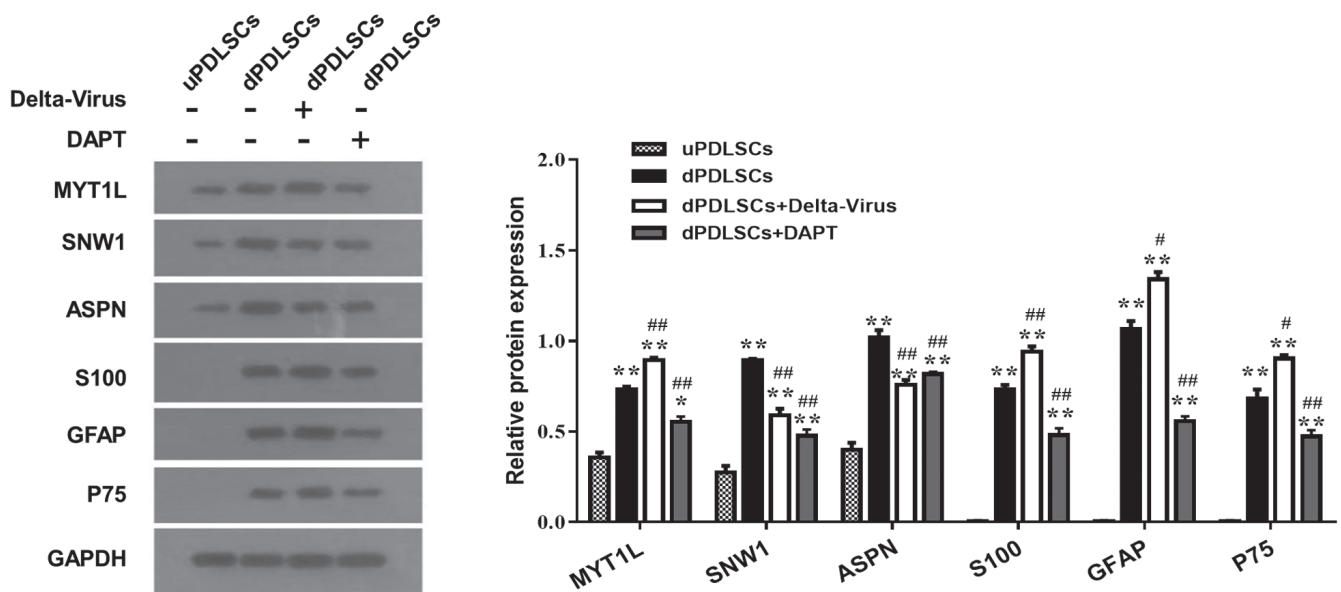


Fig. 3. Notch signaling pathway is involved in differentiation of PDLSCs to SCs. PDLSCs were induced to differentiate into SCs. In one group, PDLSCs were transfected by viral vector expressing the Delta ligand. In the other group, DAPT was added to the medium to specifically inhibit the Notch signaling pathway. Protein was extracted from: undifferentiated PDLSCs (uPDLSCs); differentiated PDLSCs (dPDLSCs); differentiated PDLSCs transfected with the Delta viral vector; or differentiated PDLSCs treated with DAPT. The expression of Notch-pathway-related proteins MYT1L, SNW1 and ASPN, as well as SC-specific proteins S100, GFAP and P75, was analyzed with western blotting. Relative protein expressions were normalized to levels of GAPDH

* $p < 0.05$, ** $p < 0.01$ compared to uPDLSC group; # $p < 0.05$, ## $p < 0.01$ compared to corresponding dPDLSC group.

Activation of Notch signaling promotes myelin formation during differentiation of PDLSCs into SCs

We co-cultured PDLSCs with dorsal DRG cells to evaluate the effect of Notch signaling on myelin formation during the differentiation of PDLSCs into SCs. Immunostaining was performed in order to assess myelin formation. We found that co-culture with DRG under induced differentiation conditions significantly promoted the expression

of P0 and MBP in the cytoplasm of differentiated PDLSCs, confirming that PDLSCs were induced to differentiate into SCs (Fig. 3). We further evaluated whether changes in Notch signaling would affect the expression of these genes in differentiated PDLSCs that had been co-cultured with DRG. We found that the overexpression of Delta in PDLSCs promoted the expression of P0 and MBP, and that differentiated cells treated with DAPT showed decreased P0 and MBP expression (Fig. 3). The RT-PCR results showed that the expression of myelin-related genes

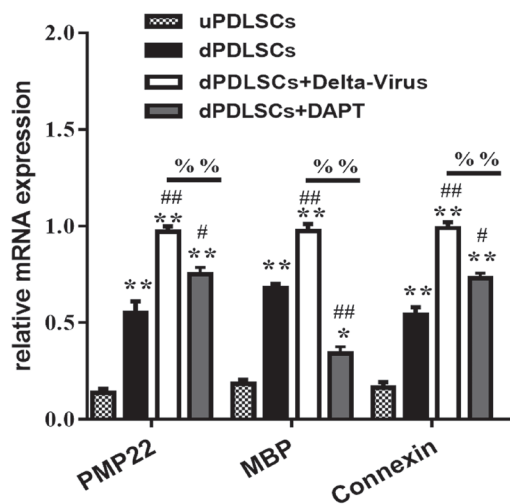


Fig. 4. Myelin-related genes in SCS were changed during the differentiation of PDLSCs to SCs. The expression of SC myelin-formation-related-genes *PMP22*, *MBP* and connexin was analyzed using RT-PCR

* $p < 0.05$, ** $p < 0.01$ compared to uPDLSC group; # $p < 0.05$; ## $p < 0.01$ compared to the corresponding dPDLSC group; % $p < 0.05$, %% $p < 0.01$ compared to dPDLSC+Delta-Virus group.

(including *PMP22*, *MBP* and connexin) were upregulated in the Delta overexpression group compared with control group, but downregulated in DAPT-treated cells (Fig. 4). These results suggest that activation of Notch signaling promotes myelin formation during the differentiation of PDLSCs into SCs, while the inhibition of this signaling impairs myelin formation under the differentiation condition.

Discussion

In recent years, it has been confirmed that the Notch signaling pathway plays an important role in regulating the differentiation of adult stem cells into SCs.¹¹ We previously demonstrated that PDLSCs isolated from beagle dogs could differentiate into SCs, and that this differentiation, as well as SC myelination, was interrupted by specific inhibition of the Erk1/2 signaling pathway.^{6,9}

In this study, we demonstrated that Notch signaling was important in promoting the differentiation of PDLSCs into SCs. First, we found that protein levels of MYT1L, SNW1 and ASPN were upregulated when PDLSCs were cultured in induction media. MYT1L, SNW1 and ASPN act as coactivators for Notch transcriptional activation,¹⁶ indicating that the Notch pathway was activated in the differentiation process of PDLSCs into SCs. Next, we found that inhibition of the Notch pathway in differentiated cells by treating with a γ -secretase inhibitor decreased the expression of SC-specific markers S100, GFAP and P75. Meanwhile, the activation of the Notch pathway through the overexpression of Delta increased the expression of these markers.

Notch has complex and extensive regulatory functions in SCs. In primary SCs isolated from neonatal rats, Notch activation promotes the generation of SCs, and negatively regulates SC myelination.^{12,13} Moreover, in contrast to primary SCs, Notch signaling has no effect on the neurotrophic activity and myelination capability of adipose-derived stem cells (ASCs) undergoing differentiation into SCs,¹⁷ indicating that the effect of Notch on gliogenesis is not universal. On the contrary, we showed that specific inhibition of the Notch pathway downregulated the expression of SC myelination-related genes (including *P0*, *MBP*, *PMP22*, and connexin), whereas activation of the Notch pathway increased the expression of these genes in DRG neurons. Our findings raise the possibility that the activation of Notch signaling in PDLSCs may initiate myelination by upregulating SC myelination-related genes.

Limitations

There are some limitations of this study. First, differentiation into SCs was only investigated in PDLSCs isolated from the periodontal ligaments of beagle dogs. The current findings need to be validated in primary human cells and animal models. Second, the Notch signaling pathway is comprised of a complex network. Many other signaling molecules related to PDLSC differentiation and Notch signaling remain to be investigated in future researches.

Conclusions

The genes associated with the Notch pathway were upregulated in differentiated PDLSCs, and the activation of the Notch pathway through the overexpression of Delta ligands promoted the differentiation of PDLSCs into SCs, as well as SC myelination. In contrast, the inhibition of the Notch pathway by DAPT treatment prevented the differentiation of PDLSCs into SCs, and also SC myelination. Therefore, the Notch signaling pathway appears to positively regulate the process of PDLSC differentiation into SCs, and the activation of this signaling is important in maintaining that differentiation, as well as SC myelination. These results may improve methods of obtaining pure SCs from PDLSCs for transplantation use.

ORCID iDs

Xiaojie Li <https://orcid.org/0000-0002-6363-6255>
 Dapeng Liao <https://orcid.org/0000-0001-6751-7838>
 Gang Sun <https://orcid.org/0000-0002-5353-3463>
 HanWen Chu <https://orcid.org/0000-0001-8289-0593>

References

- Mirsky R, Jessen KR. Schwann cell development, differentiation and myelination. *Curr Opin Neurobiol.* 1996;6(1):89–96. doi:10.1016/s0959-4388(96)80013-4
- Frostick SP, Yin Q, Kemp GJ. Schwann cells, neurotrophic factors, and peripheral nerve regeneration. *Microsurgery.* 1998;18(7):397–405. doi:10.1002/(sici)1098-2752(1998)18:7<397::aid-micr2>3.0.co;2-f

3. Jessen KR, Mirsky R. The origin and development of glial cells in peripheral nerves. *Nat Rev Neurosci.* 2005;6(9):671–682. doi:10.1038/nrn1746
4. Hammarberg H, Risling M, Hokfelt T, Cullheim S, Piehl F. Expression of insulin-like growth factors and corresponding binding proteins (IGFBP 1-6) in rat spinal cord and peripheral nerve after axonal injuries. *J Comp Neurol.* 1998;400(1):57–72. PMID:9762866
5. Mosahebi A, Woodward B, Wiberg M, Martin R, Terenghi G. Retroviral labeling of Schwann cells: In vitro characterization and in vivo transplantation to improve peripheral nerve regeneration. *Glia.* 2001;34(1):8–17. doi:10.1002/glia.1035
6. Li X, Gong P, Liao D. In vitro neural/glia differentiation potential of periodontal ligament stem cells. *Arch Med Sci.* 2010;6(5):678–685. doi:10.5114/aoms.2010.17080
7. Li X, Liao D, Gong P, Dong Y, Sun G. Biological behavior of neurally differentiated periodontal ligament stem cells on different titanium implant surfaces. *J Biomed Mater Res A.* 2014;102(8):2805–2812. doi:10.1002/jbm.a.34953
8. Ijuin K, Nakanishi K, Ito K. Different downstream pathways for Notch signaling are required for gliogenic and chondrogenic specification of mouse mesencephalic neural crest cells. *Mech Dev.* 2008;125(5–6):462–474. doi:10.1016/j.mod.2008.01.008
9. Dapeng L, Xiaojie L, Ping G, Yan D, Gang S. Erk1/2 signalling is involved in the differentiation of periodontal ligament stem cells to Schwann cells in dog. *Arch Oral Biol.* 2014;59(5):487–491. doi:10.1016/j.archoralbio.2014.02.010
10. Joseph NM, Mukoyama YS, Mosher JT, et al. Neural crest stem cells undergo multilineage differentiation in developing peripheral nerves to generate endoneurial fibroblasts in addition to Schwann cells. *Development.* 2004;131(22):5599–5612. doi:10.1242/dev.01429
11. Shi Y, Shao Q, Li Z, et al. Myt1L promotes differentiation of oligodendrocyte precursor cells and is necessary for remyelination after lysolécithin-induced demyelination. *Neurosci Bull.* 2018;34(2):247–260. doi:10.1007/s12264-018-0207-9
12. Woodhoo A, Alonso MB, Droggiti A, et al. Notch controls embryonic Schwann cell differentiation, postnatal myelination and adult plasticity. *Nat Neurosci.* 2009;12(7):839–847. doi:10.1038/nn.2323
13. Wu LM, Wang J, Conidi A, et al. Zeb2 recruits HDAC-NuRD to inhibit Notch and controls Schwann cell differentiation and remyelination. *Nat Neurosci.* 2016;19(8):1060–1072. doi:10.1038/nn.4322
14. Fiuza UM, Arias AM. Cell and molecular biology of Notch. *J Endocrinol.* 2007;194(3):459–474. doi:10.1677/JOE-07-0242
15. Seo BM, Miura M, Gronthos S, et al. Investigation of multipotent postnatal stem cells from human periodontal ligament. *Lancet.* 2004;364(9429):149–155. doi:10.1016/S0140-6736(04)16627-0
16. Vasquez-Del Carpio R, Kaplan FM, Weaver KL, et al. Assembly of a Notch transcriptional activation complex requires multimerization. *Mol Cell Biol.* 2011;31(7):1396–1408. doi:10.1128/MCB.00360-10
17. Kingham PJ, Mantovani C, Terenghi G. Notch independent signaling mediates Schwann cell-like differentiation of adipose derived stem cells. *Neurosci Lett.* 2009;467(2):164–168. doi:10.1016/j.neulet.2009.10.030

Baicalein modulates the radiosensitivity of cervical cancer cells in vitro via *miR-183* and the JAK2/STAT3 signaling pathway

Hongwei Lei^{1,A,D,F}, Jingbin Shi^{1,B,D}, Yun Teng^{1,B,E}, Chenghui Song^{2,C,E}, Lijuan Zou^{1,E}, Fuxiu Ye^{1,E}, Haichen Zhang^{1,E}

¹ Department of Radiation Oncology, The Second Hospital of Dalian Medical University, China

² Maternal and Child Health Hospital of Shahekou District, Dalian, China

A – research concept and design; B – collection and/or assembly of data; C – data analysis and interpretation; D – writing the article; E – critical revision of the article; F – final approval of the article

Advances in Clinical and Experimental Medicine, ISSN 1899–5276 (print), ISSN 2451–2680 (online)

Adv Clin Exp Med. 2021;30(7):727–736

Address for correspondence

Haichen Zhang

E-mail: qvvgllhnczk@163.com

Funding sources

Dalian Science and Technology Projects 2015 (grant No. 2015E12SF150).

Conflict of interest

None declared

Received on October 30, 2020

Reviewed on November 17, 2020

Accepted on April 6, 2021

Published online on June 11, 2021

Cite as

Lei H, Shi J, Teng Y, et al. Baicalein modulates the radiosensitivity of cervical cancer cells in vitro via *miR-183* and the JAK2/STAT3 signaling pathway. *Adv Clin Exp Med.* 2021;30(7):727–736. doi:10.17219/acem/135478

DOI

10.17219/acem/135478

Copyright

© 2021 by Wrocław Medical University

This is an article distributed under the terms of the Creative Commons Attribution 3.0 Unported (CC BY 3.0) (<https://creativecommons.org/licenses/by/3.0/>)

Abstract

Background. Increasing radiosensitivity of cancer cells can enhance the efficacy of cervical cancer treatment.

Objectives. This study evaluated the potential roles and mechanism of baicalein in regulating the radiosensitivity of cervical cancer cells in vitro.

Materials and methods. Real-time quantitative polymerase chain reaction (RT-qPCR) was used to assess *miR-183* expression in End1/E6E7 cells, HeLa cells and HeLa cells irradiated with X-ray (0 Gy, 1 Gy, 3 Gy, 5 Gy, and 10 Gy). Cell Counting Kit-8 (CCK-8) method measured cell viability of HeLa cells after *miR-183* regulation, baicalein or R08191 treatment. Apoptosis rates were detected using flow cytometry. Thereafter, expression of Bcl-2, Bax and caspase-3 RNA was also detected through RT-qPCR. Protein concentrations of E-cadherin, N-cadherin, Vimentin in epithelial–mesenchymal transition (EMT), phospho-JAK2/STAT3, and total Janus kinase 2/signal transducer and activator of transcription 3 (JAK2/STAT3) were examined using enzyme-linked immunosorbent assay (ELISA) methods. R08191, a JAK2/STAT3 activator, was used to activate the JAK2/STAT3 signaling pathway.

Results. The *miR-183* expression was significantly lower in HeLa cells compared to End1/E6E7 cells. Following upregulation of *miR-183* in HeLa cells, cell viability was inhibited while apoptosis was promoted. Moreover, EMT was inhibited after *miR-183* over-expression. X-ray treatment markedly reduced the cell survival rate and increased *miR-183* RNA expression. Baicalein treatment severely reduced the cell viability of 10-Gy X-ray-irradiated HeLa cells, partially reversing the effect of *miR-183*, and also increased apoptosis and prevented EMT in irradiated cells. Y1007/8 in JAK2 and tyrosine (Tyr) residue 705 of STAT3 were phosphorylated, resulting in high expression of JAK2/STAT3, which was decreased by irradiation and baicalein treatment. R08191 activated JAK2/STAT3 signaling, promoted cell viability and EMT, and inhibited cell apoptosis, while baicalein partly reversed the functions of R08191.

Conclusions. Baicalein inhibited cell viability and EMT, and induced cell apoptosis of HeLa cells, through upregulating *miR-183* via inactivation of the JAK2/STAT3 signaling pathway.

Key words: irradiation, JAK2/STAT3, baicalein, *miR-183*

Background

Cervical cancer is the 2nd most common female malignant cancer worldwide. It has the 2nd highest fatality rate in gynecologic oncology in developing countries,¹ where it represents one of the most challenging public health problems.² Recently, studies in cervical cancer have indicated a close correlation with human papillomavirus (HPV) infection, although there are still subgroups of cervical cancer patients reporting no HPV infections, suggesting that genetic factors also participate in cervical cancer progression.³ To date, the main therapeutic methods of cervical cancer are surgery, radiotherapy and chemotherapy. For patients with advanced-stage cervical cancer, radiotherapy remains the standard treatment method.⁴ Radiotherapy can affect the stability of DNA structure and repair through ionizing radiation (IR).^{5,6} If DNA damage caused by IR cannot be repaired by the DNA repair system, genomic instability, apoptosis and even death can arise in tumor cells.^{7,8} Based on previous studies, high doses of irradiation to the pelvic lymph nodes can increase the risk of toxicity in genitourinary (GU) and gastrointestinal (GI) cells, suggesting a need to increase the radiosensitivity of cervical cancer cells.^{9,10} New biomarkers and targets related to radiosensitivity regulation are therefore required to obtain further information relating to cervical cancer cells.

MicroRNAs (miRNAs) are small endogenous noncoding RNAs about 22 nucleotides in length, which interact with mRNAs to negatively modulate expression, resulting in inhibition of mRNA transcription and degradation.¹¹ In recent research, miRNAs appear to play essential roles in tumor formation and progression,¹² with miRNA levels correlating with patient survival and cancer treatment. Abnormal expression of miRNAs contributes to the biological progression of cancers.¹³ The miR-183 is a newly detected miRNA in cervical cancer, which has already been linked to many other cancers.

The *miR-183* is a member of a miRNA family including *miR-183*, *miR-182* and *miR-96*, which is a 2-4 kb cluster at locus 7q32. The miRNAs in this cluster are abnormally expressed in hepatocellular tumors,¹⁴ colorectal cancer¹⁵ and breast cancer,¹⁶ amongst other conditions. In osteosarcoma, ectopic expression of *miR-183* can inhibit the migration and invasion abilities of F5M2 cells by suppressing the expression of ezrin.¹⁷ In cervical cancer, miR-183 is sequestered by *CRNDE*, acting as a sponge, resulting in upregulated expression of *CCNBI*, leading to increased cell proliferation, migration and invasion, and reduced cell apoptosis.¹⁸ It acts as a cervical tumor suppressor, inhibiting cervical cancer cell metastasis and invasion by targeting matrix metalloproteinase-9 (MMP-9).¹⁹ However, whether *miR-183* could mediate radiosensitivity in cervical cancer cells is unknown. Hence, in our study, we chose an in vitro cervical cancer cell model to determine the role of *miR-183* in regulating radiosensitivity.

Baicalein is an active compound of the root of *Scutellaria baicalensis*, a traditional Chinese herbal medicine, which has activity considered to be anti-tumor, anti-viral and anti-bacterial.²⁰ According to a previous study, baicalein can induce cell apoptosis by upregulating death receptor 5 (DR5) in colon cancer.²¹ Moreover, baicalein inhibits cell proliferation in MCF-7 cells and reduces HIF stability, which could also cause radiosensitization in MCF-7 cells, resulting in a high level of cell apoptosis.²² In a prior study of cervical cancer, baicalein induced cell apoptosis and repressed cell proliferation in an in vitro model by downregulating the Notch1/Hes1 signaling pathway.²³ Baicalein has also been reported to suppress proliferation and promote apoptosis of osteosarcoma cells through upregulation of *miR-183*.²⁴ However, we were not aware of any studies demonstrating baicalein mediating radiosensitivity in cervical cancer.

Objectives

This study evaluated the potential roles and mechanism of baicalein in regulating the radiosensitivity of cervical cancer cells in vitro. We decided to analyze the effects of baicalein on regulating the radiosensitivity of cervical cancer cells and any correlation with miR-183.

Materials and methods

Cell culture

End1/E6E7 is an epithelial HPV-16 E6/E7 transformed cell line extracted from a 43-year-old Caucasian female endometriosis patient, while the HeLa cell line was the first epithelial cell line, extracted from a 31-year-old Black cervical cancer patient. Both are adherent. We used Dulbecco's modified Eagle's medium (DMEM; Gibco, Waltham, USA) supplemented with 10% fetal bovine serum (FBS), 100 U/mL of penicillin and 100 mg/mL of streptomycin, incubating the cells at 37°C and 5% CO₂. After incubation, HeLa cells were treated with baicalein (Sigma-Aldrich, St. Louis, USA; 0 μM, 10 μM and 100 μM). Irradiated HeLa cells treated with baicalein (100 μM) were incubated with RO8191 (10 μM; MedChemExpress (MCE), Monmouth Junction, USA), a Janus kinase 2/signal transducer and activator of transcription 3 (JAK2/STAT3) inhibitor, for 24 h. According to studies by Eriksson et al., 10 Gy X-ray provides a significant effect compared to doses lower than 10 Gy, and this dose has been reported to cause retarded growth of tumors.²⁵ Normal HeLa cells were irradiated with X-ray (0 Gy, 1 Gy, 5 Gy, and 10 Gy) for 3 h. HeLa cells treated by baicalein and RO8191 were irradiated with 10 Gy X-ray. After the cells received treatment and irradiation, they were used in preparations for the following experiments.

Cell transfection

To confirm the activity of miR-183 in the HeLa cell line, an inhibitor and mimics of miR-183 were compounded by GenePharma (Shanghai, China). The sequence of the miR-183 inhibitor was UAUGGCACUGGUAGAAU-UCACU. Before transfection, cells were first assigned to the negative control (NC) inhibitor group, miR-183 inhibitor group, NC mimics group, or miR-183 mimics group. HeLa cells were seeded on a six-well plate at a density of 1×10^5 cells per well. For inhibition, transfection was conducted after the confluence reached 50%, while the confluence was 85% in overexpression. Thereafter, we followed the manufacturer's instructions. The NC inhibitor, miR-183 inhibitor, NC mimics, and miR-183 mimics were transfected into HeLa cells using Lipofectamine 3000 (Invitrogen, Carlsbad, USA). Cells were then incubated for 24 h. The miR-183 transfection efficiency was assessed using real-time quantitative polymerase chain reaction (RT-qPCR). After transfection, cells were collected and used for further assays.

RT-qPCR

RNA expression of miR-183 and factors related to apoptosis in the HeLa and End1/E6E7 cell lines were measured using RT-qPCR. In accordance with the manufacturer's instructions for Trizol reagent (Invitrogen), total RNA was extracted from cells and reverse transcription of 10 µg of total RNA was processed using a BeyoRT™II First Strand cDNA Synthesis Kit (Beyotime, Shanghai, China). The PCR was performed using the QuantStudio™ 7 Pro Real-Time PCR System (Applied Biosystems, Foster City, USA), using the following cycle conditions: pre-denaturation at 95°C for 5 min, followed by 40 cycles of denaturation at 95°C for 30s, annealing at 60°C for 30 s, and extension at 72°C for 30 s. RNA expression levels were calculated using $2^{-\Delta\Delta C_t}$ methods and GAPDH and U6 were employed to be the internal controls. The experiment was run in triplicate. The sequences of primers used are listed in Table 1.

Table 1. Sequences of primers used in RT-qPCR

RNA	Sequences of primers	Reference
miR-183	Forward, 5'- CGCGGTATGGCACTGGTAGA-3'; Reverse, 5'- AGTGCAGGGTCCGAGGTATTC-3'	[26]
Bcl-2	Forward, 5'- TCCATGTCTTTGGACAACCA-3'; Reverse, 5'- CTCCACCAGTGTCCCATCT-3'	[27]
Bax	Forward, 5'- ATGGACGGGTCCGGGGAG-3'; Reverse, 5'- ATCCAGCCCAACAGCCGC-3'	[28]
Caspase-3	Forward, 5'- ATGGTTTGAGCCTGAGCAGA-3'; Reverse, 5'- GGCAGCATCATCCACACATAC-3'	[29]
GAPDH	Forward, 5'- CAAGATCATCAGCAATGCCTCC-3'; Reverse, 5'- GCCATCAGCCACAGTTTCC-3'	[30]
U6	Forward, 5'- CTCGCTTCGGCAGCACATATAC-3'; Reverse, 5'- GGAACGCTTCACGAATTTGC-3'	[30]

CCK-8

To analyze the effect of baicalein on the cell survival rate of HeLa cells after irradiation, a Cell Counting Kit-8 (CCK-8) assay was performed to measure cell viability and toxicity. HeLa cells were seeded onto a 96-well plate at a density of 5×10^3 cells per well. The HeLa cells were then incubated with baicalein (0 µM, 10 µM and 100 µM) for 24 h, 48 h and 72 h. Normal cells were irradiated with X-rays (0 Gy, 1 Gy, 5 Gy, and 10 Gy) for 3 h. Baicalein-treated HeLa cells were irradiated with 10 Gy X-ray. After irradiation or treatment, cells were cultured with 10 µL of CCK-8 (Beyotime) for 1 h. For cell toxicity detection, the cell survival rate was checked after irradiation using a Multiskan™ FC Microplate Reader (Thermo Fisher Scientific, Waltham, USA) at 450 nm wavelength, and cell viability was measured using the same reader at the same wavelength. This experiment was repeated 3 times.

Flow cytometry

To measure the apoptosis rate of irradiated HeLa cells after baicalein treatment, flow cytometry was performed using an Annexin V-FITC Apoptosis Detection Kit (Beyotime). Irradiated cells having received baicalein and RO8191 treatment were resuspended in phosphate-buffered saline (PBS). Following the manufacturers' instructions, 1×10^5 cells were collected and resuspended in 195 µL of Annexin V-FITC binding buffer. Next, 5 µL of Annexin V-FITC (50 µg/mL) and 10 µL of propidium iodide (PI; 20 µg/mL) were applied to cells and the solutions incubated for 15 min at room temperature without light. Following incubation, the apoptosis rate was determined using an Attune Flow Cytometer (Invitrogen). Results were collected from 3 independent experiments.

ELISA

To measure protein expression during epithelial-mesenchymal-transition (EMT) and the JAK2/STAT3 signaling pathway, the Human E-Cadherin ELISA Kit (ab233611; Abcam, Cambridge, UK), Human N-Cadherin ELISA Kit (ab254512; Abcam), Human Vimentin ELISA Kit (ab246526; Abcam), JAK2 (Phospho) [pY1007/pY1008] Human ELISA Kit, JAK2 (Total) Human ELISA Kit (Life Technologies, Carlsbad, USA), and STAT3 (Total/Phospho) Human Instant-One™ ELISA Kit (Invitrogen) were applied to measure protein densities. Enzyme-linked immunosorbent assay (ELISA) protocols strictly followed the manufacturers' instructions for each ELISA kit. The experiment was run in triplicate.

Statistical analysis

All data were presented as mean ± standard deviation (SD) and analyzed using IBM SPSS v. 19.0 (IBM Corp., Armonk, USA) and GraphPad Prism v. 7 (GraphPad Software,

San Diego, USA). Student's t-test (2 groups) and one-way analysis of variance (ANOVA) (3 or more groups, S-N-K method) were used to compare groups. The Bonferroni correction was used to correct significance values for multiple comparisons and $p < 0.05$ was considered to have statistical significance.

Results

miR-183 upregulation could inhibit cell viability and promote apoptosis

To confirm the RNA expression of miR-183 in cervical cancer cells, RT-qPCR was applied, indicating that expression of miR-183 RNA was significantly lower in HeLa cells than in End/E6E7 cells (Fig. 1A). Thereafter, we used miR-183 overexpression to measure its functions. Following upregulation of *miR-183*, miR-183 RNA expression was significantly increased in HeLa cells compared to the NC mimic group (Fig. 1B). The cell viability of HeLa cells after miR-183 overexpression was analyzed, indicating that viability of HeLa cells in the miR-183 mimic group was much lower than in the NC mimic group (Fig. 1C). The cell

apoptosis rate, as detected using flow cytometry, revealed that miR-183 mimics remarkably increased the apoptosis rate of HeLa cells compared with the result in the NC mimics group (Fig. 1D).

Factors related to apoptosis were also analyzed, indicating that Bcl-2 RNA expression was significantly reduced after *miR-183* upregulation, while Bax and caspase-3 RNA levels both greatly increased with miR-183 overexpression (Fig. 1E). We also measured the EMT of HeLa cells, revealing that E-cadherin protein density was much higher in HeLa cells transfected by miR-183 mimics, while N-cadherin and Vimentin levels had notably decreased (Fig. 1F).

Baicalein enhanced cell viability and EMT and repressed cell apoptosis of HeLa cells after irradiation

The effects of irradiation on HeLa cells were examined, indicating that the cell survival rate of HeLa cells decreased in a dose-dependent manner (Fig. 2A). The viability of HeLa cells irradiated with 10 Gy X-ray was measured after baicalein treatment, showing that cell viability gradually decreased as baicalein concentration increased (Fig. 2B). Flow cytometry was used to analyze cell apoptosis, indicating

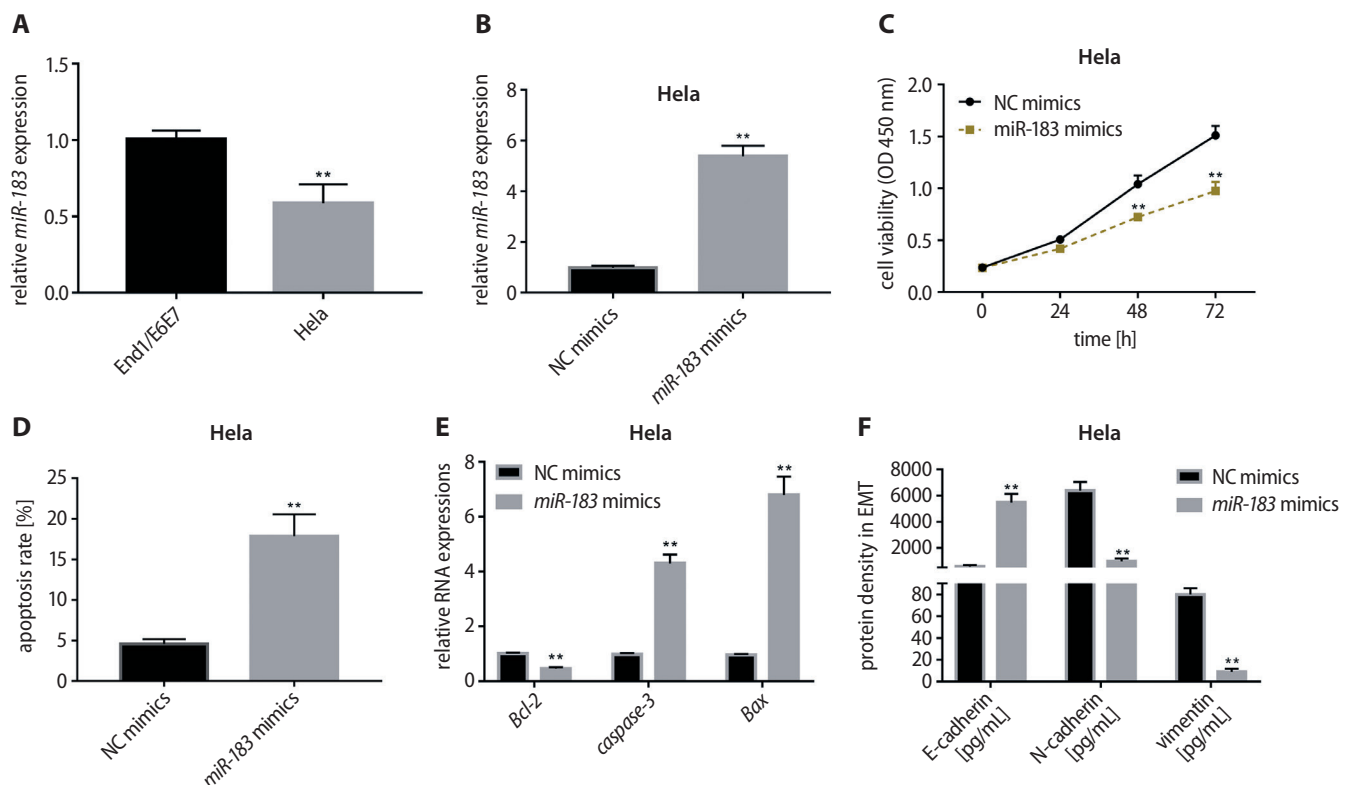


Fig. 1. Upregulation of *miR-183* in HeLa cells promoted cell apoptosis and inhibited cell viability and EMT

A. RNA expression of *miR-183* in END1/E6E7 cells and HeLa cells, as detected using RT-qPCR ($p < 0.05$); ** denotes a significant distinction from End1/E6E7 cells; B. *miR-183* RNA expression was examined with RT-qPCR in HeLa cells following overexpressed transfection ($p < 0.05$); ** denotes a significant difference in comparison with the NC mimics group; C. HeLa cell viability after miR-183 overexpression was evaluated using CCK-8 ($p < 0.05$); ** denotes significance in comparison with the NC mimics group; D. Flow cytometry was applied to measure HeLa cell apoptosis after *miR-183* overexpression ($p < 0.05$); ** denotes significant difference from the NC mimics group; E. *Bcl-2*, *Bax* and *caspase-3* RNA expression in HeLa cells with *miR-183* upregulation, assessed using RT-qPCR ($p < 0.05$); ** denotes significant difference from NC mimics group; F. E-cadherin, N-cadherin and vimentin protein densities, as measured using ELISA in HeLa cells following *miR-183* overexpression ($p < 0.05$); ** denotes a significant difference from the NC mimics group.

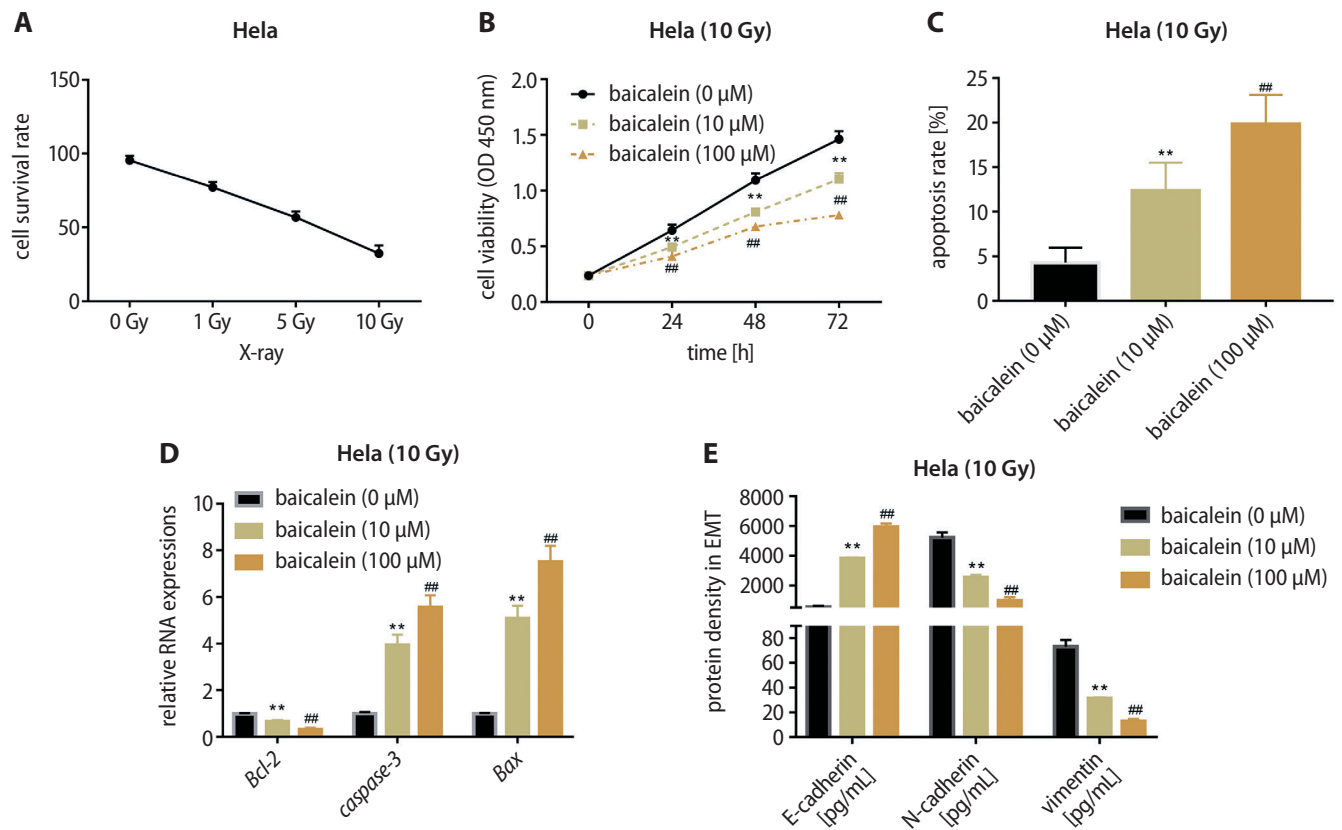


Fig. 2. Baicalein promoted cell apoptosis and inhibited cell viability and proliferation of HeLa cells after irradiation

A. Cell survival rates of HeLa cells treated with X-rays (0 Gy, 1 Gy, 5 Gy, and 10 Gy), evaluated using CCK-8; B. CCK-8 validation of cell viability of 10 Gy-irradiated HeLa cells following baicalein treatment (0 μM, 10 μM and 100 μM; $p < 0.01$); ** denotes a prominent difference from the 0 μM group; ## denotes a prominent difference between the 10 μM and 100 μM group; C. Apoptosis rates of irradiated HeLa cells analyzed using flow cytometry following treatment with baicalein (0 μM, 10 μM and 100 μM; $p < 0.01$); ** denotes a prominent difference from the 0 μM group; ## denotes a prominent difference between 10 μM and 100 μM group; D. Bcl-2, Bax and caspase-3 RNA expression was measured using RT-qPCR in HeLa cells after baicalein treatment (0 μM, 10 μM and 100 μM; $p < 0.01$); ** denotes a prominent difference from the 0 μM group; ## denotes a prominent difference between the 10 μM and 100 μM group; E. E-cadherin, N-cadherin and vimentin protein concentrations of irradiated HeLa cells were examined using ELISA after baicalein treatment (0 μM, 10 μM and 100 μM; $p < 0.01$); ** denotes a prominent difference from the 0 μM group; ## denotes a prominent difference between the 10 μM and 100 μM group.

that the apoptosis rate of irradiated HeLa cells significantly increased as the concentration of baicalein increased (Fig. 2C).

The RT-qPCR was applied to measure the RNA expression of factors after baicalein treatment, showing that Bcl-2 RNA expression notably decreased, and caspase-3 and Bax RNA expression greatly increased, in a dose-dependent manner (Fig. 2D). Meanwhile, E-cadherin protein density was markedly increased, while N-cadherin and Vimentin protein concentrations were largely reduced, again dose-dependently (Fig. 2E).

Baicalein promoted apoptosis and inhibited cell viability and EMT of irradiated HeLa cells by upregulating miR-183

Having confirmed the effects of miR-183 and baicalein treatment, we detected changes of miR-183 RNA expression after irradiation. The results of RT-qPCR showed that the level of miR-183 RNA was steeply increased

as the density of X-ray increased (Fig. 3A). Furthermore, we examined miR-183 with baicalein treatment in HeLa cells irradiated with 10 Gy X-ray, which revealed the miR-183 inhibitor largely decreased its RNA expression compared with the NC inhibitor. Baicalein treatment significantly increased miR-183 RNA level after inhibition (Fig. 3B).

We examined the cell viability of irradiated HeLa cells after knockdown of *miR-183*. In knockdown HeLa cells, the miR-183 inhibitor greatly increased cell viability in comparison with the NC inhibitor group, while baicalein treatment partly reversed the promotion of cell viability caused by miR-183 inhibition (Fig. 3C). In contrast, knockdown of *miR-183* significantly decreased cell apoptosis compared to levels in the NC inhibitor group. In the NC inhibitor group, apoptosis activity could be restored by baicalein (Fig. 3D). To further explore cell apoptosis, related factors were also examined. The miR-183 inhibitor clearly increased Bcl-2 RNA expression when compared to the NC inhibitor, while baicalein treatment decreased the Bcl-2 RNA level. The Bcl-2 RNA level was increased by miR-183 inhibition, while caspase-3 and Bax RNA expression levels

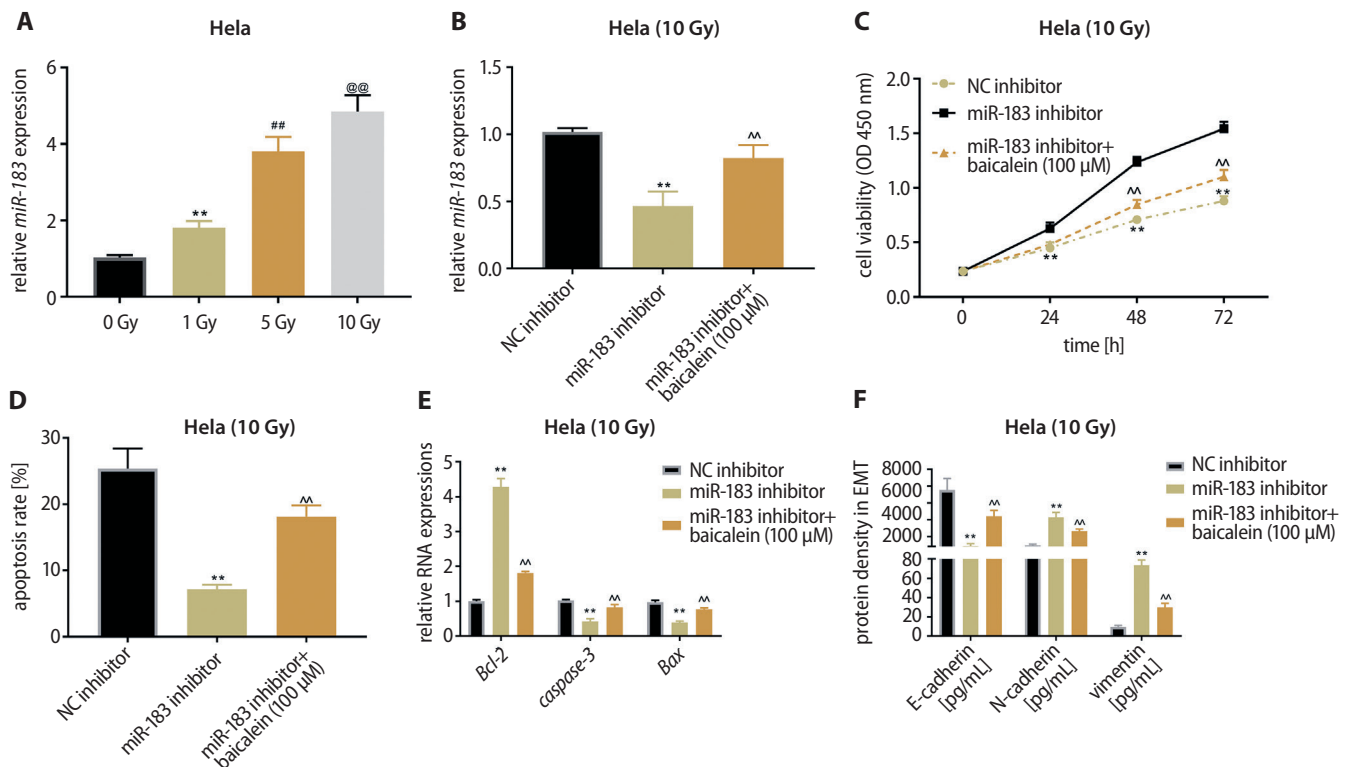


Fig. 3. Baicalein promoted apoptosis and inhibited cell viability and EMT of irradiated HeLa cells by upregulating *miR-183*

A. *miR-183* RNA expression in HeLa cells after X-ray treatment (0 Gy, 1 Gy, 5 Gy, and 10 Gy) were detected using RT-qPCR ($p < 0.001$); ** denotes a significant difference from the 0 Gy group; ## denotes prominent difference between the 5 Gy group and 1 Gy group; @@ denotes significant difference between the 10 Gy group and 5 Gy group; B. RT-qPCR was used to measure *miR-183* RNA expression in irradiated HeLa cells after *miR-183* inhibition and baicalein treatment ($p < 0.05$); ** denotes notable difference from NC inhibitor group; ^^ denotes significant difference between the *miR-183* inhibitor group and the combined *miR-183* inhibitor and baicalein (100 μ M) group; C. Cell viability of irradiated HeLa cells after *miR-183* suppression and baicalein treatment ($p < 0.05$); ** denotes notable difference from the NC inhibitor group; ^^ denotes significant difference between the *miR-183* inhibitor group and combined *miR-183* inhibitor and baicalein (100 μ M) group; D. Apoptosis rates of irradiated HeLa cells were evaluated using flow cytometry after downregulation of *miR-183* and baicalein treatment ($p < 0.05$); ** denotes a notable difference from the NC inhibitor group; ^^ denotes significant difference between the *miR-183* inhibitor group and combined *miR-183* inhibitor and baicalein (100 μ M) group; E. RT-qPCR was used to detect RNA expression of Bcl-2, Bax and caspase-3 in HeLa cells after irradiation, *miR-183* inhibition and baicalein treatment ($p < 0.05$); ** denotes a notable difference from the NC inhibitor group; ^^ denotes a significant difference between the *miR-183* inhibitor group and combined *miR-183* inhibitor and baicalein (100 μ M) group; F. ELISA was applied to measure E-cadherin, N-cadherin, and vimentin protein densities in HeLa cells after irradiation, *miR-183* inhibition and baicalein treatment ($p < 0.05$); ** denotes a notable difference from the NC inhibitor group; ^^ denotes a significant difference between the *miR-183* inhibitor group and combined *miR-183* inhibitor and baicalein (100 μ M) group.

were remarkably decreased following *miR-183* downregulation. This effect was reversed after baicalein treatment (Fig. 3E).

An analysis of the EMT indicated that the *miR-183* inhibitor significantly decreased E-cadherin, and increased N-cadherin and Vimentin protein densities compared to the NC inhibitor group. Baicalein treatment attenuated the activity of *miR-183* by promoting E-cadherin and inhibiting N-cadherin and Vimentin production (Fig. 3F).

Baicalein mediated apoptosis, EMT and cell viability of irradiated HeLa cells via the JAK2/STAT3 signaling pathway

The correlation between *miR-183* and baicalein could be linked to the related signaling pathway. Phosphorylation of JAK2/STAT3 and total JAK2/STAT3 were both

significantly higher in HeLa cells than in End/E6E7 cells (Fig. 4A). Following irradiation phosphorylated JAK2/STAT3 and total JAK2/STAT3 protein concentrations both sharply decreased with increasing doses of radiation (Fig. 4B).

We used RO8191, a JAK2/STAT3 signaling pathway activator, to examine the role of the JAK2/STAT3 pathway and to correlate this with baicalein application. The ELISA results showed that RO8191 treatment greatly increased phosphorylation of JAK2/STAT3 and total JAK2/STAT3 protein density in irradiated HeLa cells, compared to untreated HeLa cells after irradiation. Baicalein significantly reduced protein concentrations of JAK2/STAT3 (Fig. 4C). Moreover, the cell viability of irradiated HeLa cells was measured, indicating that RO8191 usage extensively promoted cell viability of irradiated HeLa cells when compared to the negative control. Conversely, baicalein usage

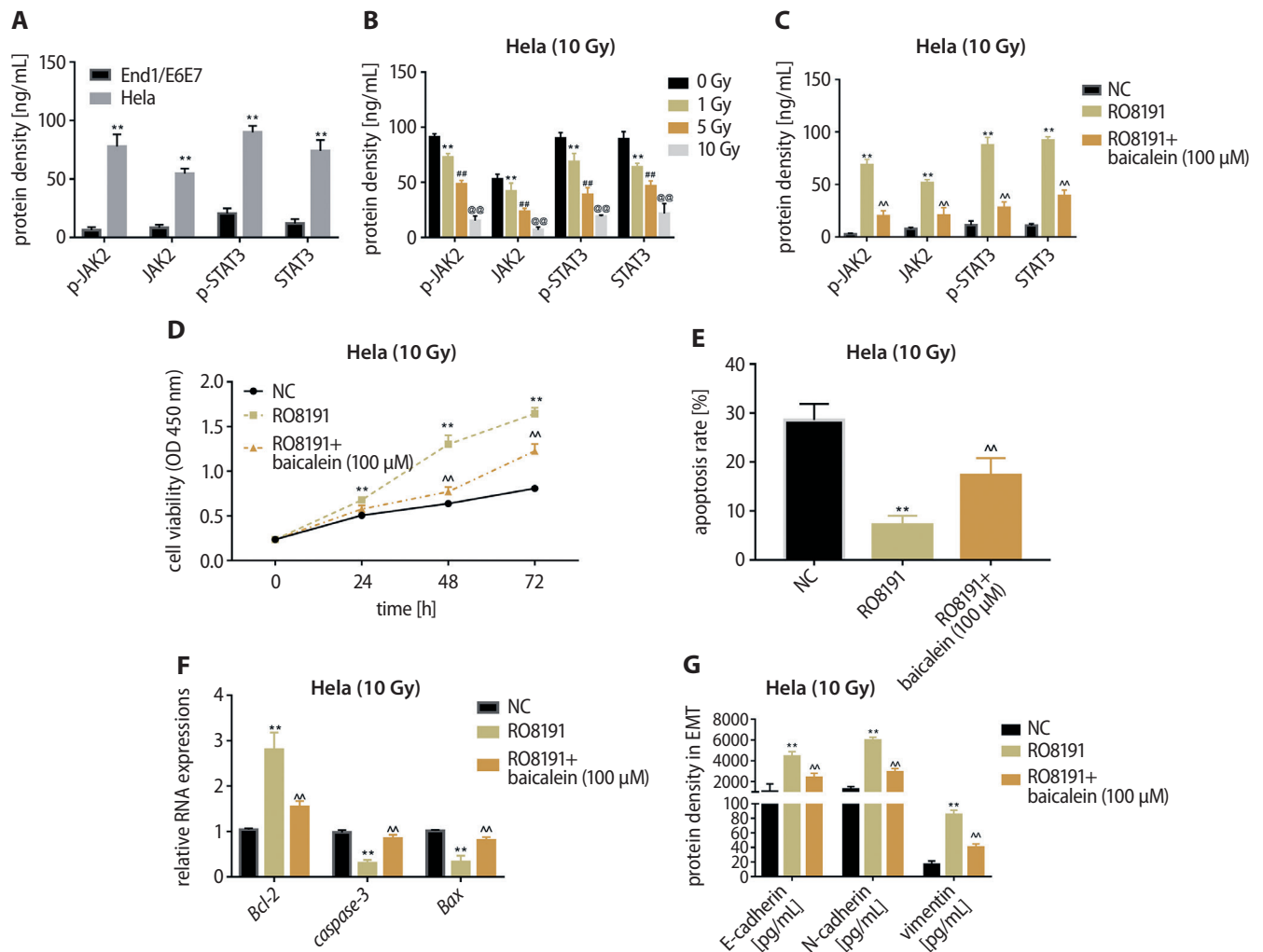


Fig. 4. Baicalein mediated irradiated HeLa cell viability, cell apoptosis and EMT via the JAK2/STAT3 signaling pathway

A. Phosphorylated JAK2/STAT3 and total JAK2/STAT3 protein concentrations in End1/E6E7 cells and HeLa cells ($p < 0.05$); *** denotes notable difference of protein densities from the End1/E6E7 group; B. Phosphorylation of JAK2/STAT3 and total JAK2/STAT3 protein densities in HeLa cells after treatment with X-rays (0 Gy, 1 Gy, 5 Gy, and 10 Gy) were detected using ELISA ($p < 0.001$); ** denotes a significant difference from the 0 Gy group; ## signifies a notable difference between the 5 Gy group and the 1 Gy group; @ denotes a significant difference between the 10 Gy group and the 5 Gy group; C. Protein densities of phosphorylated and total JAK2/STAT3, as detected using ELISA following RO8191 (a JAK2/STAT3 activator) usage and baicalein (100 μ M) treatment ($p < 0.05$); *** denotes a notable difference from the NC group; ^^ denotes a significant difference between the RO8191 group and combined RO8191 and baicalein (100 μ M) group; D. Cell viability of HeLa cells after RO8191 and baicalein treatment ($p < 0.05$); *** denotes a notable difference from the NC group; ^^ denotes a significant difference between the RO8191 group and combined RO8191 and baicalein (100 μ M) group; E. Apoptosis rates examined with flow cytometry in irradiated HeLa cells following RO8191 usage and baicalein treatment ($p < 0.05$); ** denotes a notable difference from the NC group; ^^ denotes a significant difference between the RO8191 group and combined RO8191 and baicalein (100 μ M) group; F. Bcl-2, Bax and caspase-3 RNA expression were analyzed using RT-qPCR in irradiated HeLa cells after treatment with RO8191 and baicalein ($p < 0.05$); *** denotes a notable difference from the NC group; ^^ denotes a significant difference between the RO8191 group and combined RO8191 and baicalein (100 μ M) group; G. E-cadherin, N-cadherin, and vimentin protein densities in irradiated HeLa cells after RO8191 treatment and baicalein usage were evaluated using ELISA ($p < 0.05$); ** denotes a notable difference from the NC group; ^^ denotes a significant difference between the RO8191 group and combined RO8191 and baicalein (100 μ M) group.

reversed the promotion caused by RO8191, keeping JAK2/STAT3 protein density and cell viability at lower levels (Fig. 4D), while increasing the cell apoptosis rate (Fig. 4E). Factors related to apoptosis were analyzed as well, showing that Bcl-2 RNA expression was significantly upregulated, while caspase-3 with Bax was significantly decreased after RO8191 treatment compared to the NC. Conversely, baicalein treatment reduced Bcl-2 RNA expression and increased caspase-3 and Bax RNA expressions (Fig. 4F).

Furthermore, the EMT was examined to measure migration and invasion abilities. These results showed that E-cadherin protein density was notably decreased, while N-cadherin with Vimentin protein concentrations were remarkably promoted by RO8191 usage in comparison with the NC. Baicalein treatment reversed the effect of RO8191 by increasing E-cadherin protein and decreasing the N-cadherin and Vimentin protein densities (Fig. 4G).

Discussion

In cervical cancer treatment, chemoradiotherapy is considered an alternative solution for patients who are not good candidates for surgery, and have pelvic or para-aortic lymph node metastases.³¹ Unfortunately, radio-resistance of cervical cancer cells is the primary reason for failures in treatment, suggesting that increasing the radiosensitivity of cervical cancer cells could be an important method to improve the prognoses of patients.³² In this study, we examined baicalein, a traditional Chinese herbal medicine, and a newly found miRNA, miR-183, to measure their correlation and effects on cervical cancer cells.

According to prior studies, miR-183 acts as a tumor suppressor in cervical cancer cells.^{18,19} Therefore, we analyzed the function of miR-183 in HeLa cells and its mediation of radiosensitivity in HeLa cells. We first examined RNA expression, indicating that the RNA expression of miR-183 was much lower in HeLa cells than in normal End1/E6E7 cells, which was similar to the findings of previous studies. We promoted expression of miR-183 to measure its role in cell outcomes. Our results showed that overexpression of miR-183 highly inhibited the viability of HeLa cells and increased their cell apoptosis rate. We also analyzed factors in apoptosis to prove our result, indicating that RNA expression of Bcl-2 was significantly downregulated and Bax with caspase-3 RNA expressions was remarkably promoted.

We also examined the role of miR-183 in mediating EMT. The EMT plays important roles in the progression and metastasis of cervical cancer.^{33,34} With cancer cells metastasizing to other parts of the body, the prognosis for cervical cells was significantly decreased. Considering indications from former studies, we analyzed E-cadherin, N-cadherin and Vimentin to measure miR-183 mediation of EMT in cervical cancer cells, indicating that the progression of EMT was markedly inhibited by upregulation of *miR-183*. Therefore, we have proven that miR-183 suppressed cell viability and EMT and promoted cell apoptosis in HeLa cells, suggesting that miR-183 might be a tumor suppressor of cervical cancer.

As these roles of miR-183 were confirmed, we measured the effects of irradiation and baicalein on HeLa cells. After X-ray treatment, the survival rate of HeLa cells was significantly decreased in a dose-dependent manner. We selected 10 Gy X-ray-induced HeLa cells for subsequent experiments, which showed that viability of HeLa cells was remarkably increased dose-dependently, while the apoptosis rate was markedly increased, reflected by lowered Bcl-2 levels and increased caspase-3 and Bax. The EMT was also progressively inhibited by increased baicalein concentrations, reflected in decreased concentration of E-cadherin and increased N-cadherin and Vimentin. According to a study by Peng et al., baicalein repressed the proliferation and migration of cervical cancer cells, which also induced cervical cancer cell apoptosis and cell cycle arrest.³⁵ In this study, baicalein was reported to play an anti-tumor role

by downregulating the production of BDLNR and suppressing the PI3K/AKT signaling pathway. Baicalein also induced HeLa cell apoptosis through mitochondria and death receptor pathways dose-dependently.³⁵ In prostatic cancer, baicalein treatment increased the sensitivity of prostatic cancer cells under the mediation of 12-LOX,³⁶ implying that baicalein can be used as a radiosensitizer. In our study, we have detected a primary role of baicalein in mediating radiosensitivity and showed that baicalein magnified the effects of radiation on radiosensitivity regulation.

We analyzed a correlation between miR-183 and baicalein in irradiated HeLa cells. This first confirmed that miR-183 RNA expression was significantly upregulated by radiation in HeLa cells. Thereafter, a miR-183 inhibitor was used to decrease its expression in irradiated HeLa cells, which was then promoted following baicalein treatment. As seen in Fig. 3C,D, the miR-183 inhibitor promoted cell viability, but repressed apoptosis in irradiated cells, while baicalein reversed the mediations caused by knockdown of miR-183. The upregulation of *BCL2* and repression of caspase-3 and Bax expression in irradiated HeLa cells caused by *miR-183* downregulation was affected by baicalein, resulting in *BCL2* upregulation as well as Bax and caspase-3 inhibition. Moreover, EMT was promoted by the miR-183 inhibitor, an effect which was attenuated by baicalein treatment.

We conducted a first analysis of the correlation between miR-183 and baicalein, showing that baicalein can upregulate *miR-183* RNA expression. Furthermore, we also detected their interactions with radiation, indicating that miR-183 and baicalein in combination could improve the efficiency of radiation treatment in HeLa cells. Therefore, *miR-183* may be the miRNA that contributes to the radiosensitivity promoted by baicalein.

We explored a potential mechanism for baicalein increasing the radiosensitivity of HeLa cells. Janus kinase 2, a member of the Janus kinase family, belongs to the non-receptor tyrosine kinase superfamily.³⁷ Proteins in the Janus kinase family contain 4 conserved domains: FERM, SH2, JH2 pseudo-kinase, and JH1 kinase. A key step in JAK kinase activation is the interaction between the N-terminus of FERM and SH2.³⁸ The JH1 domain contains 2 tyrosine residues (Y1007/8), which control conformation and activation through phosphorylation.^{39,40} Phosphorylation of Y637, Y868, Y972, and Y966 can also magnify JAK2 kinase activity, while phosphorylated Y317, Y570, Y913, and Y119 are involved in downregulation of JAK2 activation.^{41,42} Moreover, JAK is a potential upstream activator of STAT3, which has been shown to be activated by phosphorylation of tyrosine (Tyr) residue 705, leading to dimer formation and activation of target gene transcription.^{43–45} The STAT3 has been reported to be activated by oncoproteins, which are involved in oncogenesis by stimulating cell proliferation and repressing apoptosis.⁴⁶ In contrast, inhibition of STAT3 results in the activation of apoptotic signaling pathways, as evidenced by upregulation of *BAX* and *CASP3* and downregulation of *BCL2*.⁴⁷

In addition to proliferation regulation, the JAK2/STAT3 signaling pathway has been reported to facilitate EMT progression in oral squamous cell carcinoma, breast cancer and gastric cancer amongst other conditions.^{48–50} The JAK2/STAT3 signaling pathway has already been reported to be suppressed by ellagic acid, resulting in promoted cell apoptosis and inhibited cell proliferation of HeLa cells. Moreover, baicalein attenuated inflammation induced by lipopolysaccharides (LPS) by suppressing JAK2 and STAT3 in RAW264.7 cells, suggesting that inhibiting the activation of the JAK/STAT signaling pathway amplifies the effects of baicalein on cells.⁵¹

We detected a correlation between the JAK2/STAT3 signaling pathway and baicalein in HeLa cells. Initially, we examined the protein densities of p-JAK2, p-STAT3, t-JAK2, and t-STAT3, showing that HeLa cells had higher levels of phosphorylated JAK and STAT3 and total JAK2 and STAT3, while these protein concentrations largely decreased after dose-dependently radiation. To measure the activity of JAK2/STAT3, we chose a previously demonstrated activator, RO8191 (also called CDM-3008), to activate the JAK/STAT signaling pathway.⁵² Based on the same study, we also used RO8191 to confirm the functions of JAK2 and STAT3, showing that RO8191 significantly increased the phosphorylation of JAK2 and STAT3, and increased the density of total JAK2 and STAT3 in HeLa cells. Baicalein treatment greatly decreased the concentrations of these proteins, showing that baicalein could inhibit expression of JAK2 and STAT3 in HeLa cells. Thereafter, cell viability, apoptosis and EMT were also checked, indicating that RO8191-induced high cell viability was reduced after baicalein treatment, while the inhibition of cell apoptosis caused by RO8191 was reversed. The EMT was also increased by RO8191 usage, and baicalein treatment could reduce EMT in HeLa cells. This implies that baicalein might promote the radiosensitivity of HeLa cells via the JAK2/STAT3 signaling pathway.

Limitations

This study only examined the functions of baicalein in vitro. To further validate its potential in cervical cancer, animal model should be examined. This is a limitation of this study.

Conclusions

Baicalein promoted cell apoptosis and radiosensitivity, and inhibited cell viability and progression of EMT in HeLa cells through *miR-183* upregulation and JAK2/STAT3 inhibition, suggesting that baicalein may be a potential treatment method for increasing the radiosensitivity of HeLa cells. Further studies in vivo and clinical studies are warranted to increase the knowledge about radiotherapy for cervical cancer.

ORCID iDs

Hongwei Lei  <https://orcid.org/0000-0002-4985-9858>
 Jingbin Shi  <https://orcid.org/0000-0002-1555-4044>
 Yun Teng  <https://orcid.org/0000-0003-2365-1626>
 Chenghui Song  <https://orcid.org/0000-0002-3119-5555>
 Lijuan Zou  <https://orcid.org/0000-0002-9908-2987>
 Fuxiu Ye  <https://orcid.org/0000-0001-7504-0785>
 Haichen Zhang  <https://orcid.org/0000-0001-6829-3063>

References

- Suh SH, Kim JW, Aziz MF, et al. Asian society of gynecologic oncology workshop 2010. *J Gynecol Oncol.* 2010;21(3):137–150. doi:10.3802/jgo.2010.21.3.137
- Grellier N, Quéro L. Cervical cancer: Particularities in HIV patients [in French]. *Bull Cancer.* 2014;101(11):1040–1047. doi:10.1684/bdc.2014.2034
- Woodman CB, Collins SI, Young LS. The natural history of cervical HPV infection: Unresolved issues. *Nature Rev Cancer.* 2007;7(1):11–22. doi:10.1038/nrc2050
- Kim JY, Byun SJ, Kim YS, Nam JH. Disease courses in patients with residual tumor following concurrent chemoradiotherapy for locally advanced cervical cancer. *Gynecol Oncol.* 2017;144(1):34–39. doi:10.1016/j.ygyno.2016.10.032
- Petrelli F, De Stefani A, Raspagliesi F, Lorusso D, Barni S. Radiotherapy with concurrent cisplatin-based doublet or weekly cisplatin for cervical cancer: A systematic review and meta-analysis. *Gynecol Oncol.* 2014;134(1):166–171. doi:10.1016/j.ygyno.2014.04.049
- Alizadeh E, Orlando TM, Sanche L. Biomolecular damage induced by ionizing radiation: The direct and indirect effects of low-energy electrons on DNA. *Ann Rev Phys Chem.* 2015;66:379–398. doi:10.1146/annurev-physchem-040513-103605
- Velic D, Couturier AM, Ferreira MT, et al. DNA damage signalling and repair inhibitors: The long-sought-after Achilles' heel of cancer. *Biomolecules.* 2015;5(4):3204–3259. doi:10.3390/biom5043204
- McMahon SJ, McGarry CK, Butterworth KT, et al. Cellular signalling effects in high precision radiotherapy. *Phys Med Biol.* 2015;60(11):4551–4564. doi:10.1088/0031-9155/60/11/4551
- Choi KH, Kim JY, Dong SL, et al. Clinical impact of boost irradiation to pelvic lymph node in uterine cervical cancer treated with definitive chemoradiotherapy. *Medicine (Baltimore).* 2018;97(16):e0517. doi:10.1097/md.00000000000010517
- Wang W, Hou X, Yan J, et al. Outcome and toxicity of radical radiotherapy or concurrent chemoradiotherapy for elderly cervical cancer women. *BMC Cancer.* 2017;17(1):510. doi:10.1186/s12885-017-3503-2
- Bartel DP. MicroRNAs: Genomics, biogenesis, mechanism, and function. *Cell.* 2004;116(2):281–297. doi:10.1016/s0092-8674(04)00045-5
- Papagiannakopoulos T, Kosik KS. MicroRNAs: Regulators of oncogenesis and stemness. *BMC Medicine.* 2008;6:15. doi:10.1186/1741-7015-6-15
- Cortez MA, Valdecanas D, Zhang X, et al. Therapeutic delivery of miR-200c enhances radiosensitivity in lung cancer. *Mol Ther.* 2014;22(8):1494–1503. doi:10.1038/mt.2014.79
- Ladeiro Y, Couchy G, Balabaud C et al. MicroRNA profiling in hepatocellular tumors is associated with clinical features and oncogene/tumor suppressor gene mutations. *Hepatology.* 2008;47(6):1955–1963. doi:10.1002/hep.22256
- Motoyama K, Inoue H, Takatsuno Y, et al. Over- and under-expressed microRNAs in human colorectal cancer. *Int J Oncol.* 2009;34(4):1069–1075. doi:10.3892/ijo_00000233
- Mattie MD, Benz CC, Bowers J, et al. Optimized high-throughput microRNA expression profiling provides novel biomarker assessment of clinical prostate and breast cancer biopsies. *Mol Cancer.* 2006;5:24. doi:10.1186/1476-4598-5-24
- Zhao H, Guo M, Zhao G, et al. miR-183 inhibits the metastasis of osteosarcoma via downregulation of the expression of Ezrin in F5M2 cells. *Int J Mol Med.* 2012;30(5):1013–1020. doi:10.3892/ijmm.2012.1111
- Bai X, Wang W, Zhao P, et al. LncRNA CRNDE acts as an oncogene in cervical cancer through sponging miR-183 to regulate CCNB1 expression. *Carcinogenesis.* 2020;41(1):111–121. doi:10.1093/carcin/bgz166
- Fan D, Wang Y, Qui P, et al. MicroRNA-183 functions as the tumor suppressor via inhibiting cellular invasion and metastasis by targeting MMP-9 in cervical cancer. *Gynecol Oncol.* 2016;141(1):166–174. doi:10.1016/j.ygyno.2016.02.006

20. Zhao T, Tang H, Xie L, et al. *Scutellaria baicalensis* Georgi. (*Lamiaceae*): A review of its traditional uses, botany, phytochemistry, pharmacology and toxicology. *J Pharm Pharmacol*. 2019;71(9):1353–1369. doi:10.1111/jphp.13129
21. Taniguchi H, Yoshida T, Horinaka M, et al. Baicalein overcomes tumor necrosis factor-related apoptosis-inducing ligand resistance via two different cell-specific pathways in cancer cells but not in normal cells. *Cancer Res*. 2008;68(21):8918–8927. doi:10.1158/0008-5472.Can-08-1120
22. Gade S, Gandhi NM. Baicalein inhibits MCF-7 cell proliferation in vitro, induces radiosensitivity, and inhibits hypoxia inducible factor. *J Environ Pathol Toxicol Oncol*. 2015;34(4):299–308. doi:10.1615/jenviropatholtoxiconcol.2015013806
23. Lian H, Hui Y, Xiaoping T, Wei T, Jiye X, Xiaolan Y. Baicalein suppresses the proliferation of human cervical cancer cells via Notch 1/Hes signaling pathway. *J Cancer Res Ther*. 2019;15(6):1216–1220. doi:10.4103/0973-1482.204899
24. Zhang J, Yang W, Zhou YB, et al. Baicalein inhibits osteosarcoma cell proliferation and invasion through the miR-183/Ezrin pathway. *Mol Med Rep*. 2018;18(1):1104–1112. doi:10.3892/mmr.2018.9036
25. Eriksson D, Löfroth PO, Johansson L, Riklund KA, Stigbrand T. Cell cycle disturbances and mitotic catastrophes in HeLa Hep2 cells following 2.5 to 10 Gy of ionizing radiation. *Clin Cancer Res*. 2007;13(18 Pt 2):5501s–5508s. doi:10.1158/1078-0432.Ccr-07-0980
26. Zhang Y, Wang G. MicroRNA-183 inhibits A375 human melanoma cell migration and invasion by targeting Ezrin and MMP-9. *Oncol Lett*. 2019;17(1):548–554. doi:10.3892/ol.2018.9603
27. Zhang Y, et al. The expression of Toll-like receptor 8 and its relationship with VEGF and Bcl-2 in cervical cancer. *Int J Med Sci*. 2014;11(6):608–613. doi:10.7150/ijms.8428
28. Britton-Jones C, Lok IH, Po AL, Cheung CK, Chiu TT, Haines C. Changes in the ratio of Bax and Bcl-2 mRNA expression and their cellular localization throughout the ovulatory cycle in the human oviduct. *J Assist Reprod Genet*. 2006;23(3):149–156. doi:10.1007/s10815-005-9012-2
29. Asadi M, Shanebandi D, Asvadi Kermani T, Sanaat Z, Zafari V, Hashemzadeh S. Expression level of caspase genes in colorectal cancer. *Asian Pac J Cancer Prev*. 2018;19(5):1277–1280. doi:10.22034/apjcp.2018.19.5.1277
30. Han X, Zheng J, Wang Y, Gao Z. miRNA-29a inhibits colon cancer growth by regulation of the PTEN/Akt/GSK3 β and Wnt/ β -catenin signaling pathways. *Oncol Lett*. 2018;16(2):2638–2644. doi:10.3892/ol.2018.8905
31. Vordermark D. Radiotherapy of cervical cancer. *Oncol Res Treatment*. 2016;39(9):516–520. doi:10.1159/000448902
32. Ronco G, Dillner J, Elfström KM, et al. Efficacy of HPV-based screening for prevention of invasive cervical cancer: Follow-up of four European randomised controlled trials. *Lancet*. 2014;383(9916):524–532. doi:10.1016/s0140-6736(13)62218-7
33. Qureshi R, Arora H, Rizvi MA. EMT in cervical cancer: Its role in tumour progression and response to therapy. *Cancer Lett*. 2015;356(2 Pt B):321–331. doi:10.1016/j.canlet.2014.09.021
34. Jing L, Bo W, Yourong G, Tian W, Shixuan W, Mingfu M. Sema4C mediates EMT inducing chemotherapeutic resistance of miR-31-3p in cervical cancer cells. *Sci Rep*. 2019;9(1):17727. doi:10.1038/s41598-019-54177-z
35. Peng Y, Gou C, Yang Y, et al. Baicalein induces apoptosis of human cervical cancer HeLa cells in vitro. *Mol Med Rep*. 2015;11(3):2129–2134. doi:10.3892/mmr.2014.2885
36. Lövey J, Nie D, Tóvári J, et al. Radiosensitivity of human prostate cancer cells can be modulated by inhibition of 12-lipoxygenase. *Cancer Lett*. 2013;335(2):495–501. doi:10.1016/j.canlet.2013.03.012
37. Liu CS, Yang-Yen HF, Suen CS, Hwang MJ, Yen JJ. Cbl-mediated K63-linked ubiquitination of JAK2 enhances JAK2 phosphorylation and signal transduction. *Sci Rep*. 2017;7(1):4613. doi:10.1038/s41598-017-04078-w
38. McNally R, Toms AV, Eck MJ. Crystal structure of the FERM-SH2 module of human Jak2. *PLoS One*. 2016;11(5):e0156218. doi:10.1371/journal.pone.0156218
39. Vanderkuur J, Allevato G, Billestrup N, Norstedt G, Carter-Su C. Growth hormone-promoted tyrosyl phosphorylation of SHC proteins and SHC association with Grb2. *J Biol Chem*. 1995;270(13):7587–7593. doi:10.1074/jbc.270.13.7587
40. Zhao Y, Wagner F, Frank SJ, Kraft AS. The amino-terminal portion of the JAK2 protein kinase is necessary for binding and phosphorylation of the granulocyte-macrophage colony-stimulating factor receptor beta c chain. *J Biol Chem*. 1995;270(23):13814–13818. doi:10.1074/jbc.270.23.13814
41. Argetsinger LS, Stuckey JA, Robertson SA, et al. Tyrosines 868, 966, and 972 in the kinase domain of JAK2 are autophosphorylated and required for maximal JAK2 kinase activity. *Mol Endocrinol*. 2010;24(5):1062–1076. doi:10.1210/me.2009-0355
42. Robertson SA, Koleva RI, Argetsinger LS, et al. Regulation of Jak2 function by phosphorylation of Tyr317 and Tyr637 during cytokine signaling. *Mol Cell Biol*. 2009;29(12):3367–3378. doi:10.1128/mcb.00278-09
43. Darnell JE Jr, Kerr IM, Stark GR. Jak-STAT pathways and transcriptional activation in response to IFNs and other extracellular signaling proteins. *Science*. 1994;264(5164):1415–1421. doi:10.1126/science.8197455
44. Garcia R, Bowman TL, Niu G, et al. Constitutive activation of Stat3 by the Src and JAK tyrosine kinases participates in growth regulation of human breast carcinoma cells. *Oncogene*. 2001;20(20):2499–2513. doi:10.1038/sj.onc.1204349
45. Zhong Z, Wen Z, Darnell JE Jr. Stat3: A STAT family member activated by tyrosine phosphorylation in response to epidermal growth factor and interleukin-6. *Science*. 1994;264(5155):95–98. doi:10.1126/science.8140422
46. Bowman T, Garcia R, Turkson J, Jove R. STATs in oncogenesis. *Oncogene*. 2000;19(21):2474–2488. doi:10.1038/sj.onc.1203527
47. Guha P, Gardell J, Darpolor J, et al. STAT3 inhibition induces Bax-dependent apoptosis in liver tumor myeloid-derived suppressor cells. *Oncogene*. 2019;38(4):533–548. doi:10.1038/s41388-018-0449-z
48. Chen Y, Shao Z, Jiang E, et al. CCL21/CCR7 interaction promotes EMT and enhances the stemness of OSCC via a JAK2/STAT3 signaling pathway. *J Cell Physiol*. 2020;235(9):5995–6009. doi:10.1002/jcp.29525
49. Kim MS, Jeong J, Seo J, Kim HS, Kim SJ, Jin W. Dysregulated JAK2 expression by TrkC promotes metastasis potential, and EMT program of metastatic breast cancer. *Sci Rep*. 2016;6:33899. doi:10.1038/srep33899
50. Tao Y, Yang S, Wu Y, et al. MicroRNA-216a inhibits the metastasis of gastric cancer cells by targeting JAK2/STAT3-mediated EMT process. *Oncotarget*. 2017;8(51):88870–88881. doi:10.18632/oncotarget.21488
51. Qi Z, Yin F, Lu L, et al. Baicalein reduces lipopolysaccharide-induced inflammation via suppressing JAK/STATs activation and ROS production. *Inflamm Res*. 2013;62(9):845–855. doi:10.1007/s00011-013-0639-7
52. Furutani Y, Toguchi M, Shiozaki-Sato Y, et al. An interferon-like small chemical compound CDM-3008 suppresses hepatitis B virus through induction of interferon-stimulated genes. *PLoS One*. 2019;14(6):e0216139. doi:10.1371/journal.pone.0216139

Ultrafiltration in acute heart failure: Current knowledge and fields for further research

Szymon Urban^{1,B,D,F}, Mikołaj Błaziak^{1,D,E}, Jan Biegus^{2,3,D,E}, Robert Zymliński^{2,3,D–F}

¹ Student scientific organization, Department of Heart Diseases, Wrocław Medical University, Poland

² Department of Heart Diseases, Wrocław Medical University, Poland

³ Centre for Heart Diseases, Wrocław University Hospital, Poland

A – research concept and design; B – collection and/or assembly of data; C – data analysis and interpretation;

D – writing the article; E – critical revision of the article; F – final approval of the article

Advances in Clinical and Experimental Medicine, ISSN 1899–5276 (print), ISSN 2451–2680 (online)

Adv Clin Exp Med. 2021;30(7):737–746

Address for correspondence

Szymon Urban

E-mail: szymon.urban.wro@gmail.com

Funding sources

None declared

Conflict of interest

None declared

Received on January 23, 2021

Reviewed on March 11, 2021

Accepted on April 1, 2021

Published online on June 11, 2021

Abstract

Heart failure is one of the leading causes of death in developed countries and remains a significant burden to the healthcare system. Fluid overload is a process responsible for the majority of the heart failure symptoms. Pharmacotherapy is a first-line treatment for this condition; however, due to the phenomenon of diuretic resistance, drug therapy can frequently be insufficient. Ultrafiltration is a promising but still understudied procedure that effectively targets the underlying pathophysiological mechanisms of congestion. The increased availability of simplified ultrafiltration devices, especially in intensive care units, prompted us to perform a current literature review on this treatment. In the present paper, we provide a concise review of the published trials on ultrafiltration, with a brief commentary on their conclusions and shortcomings. We also discuss the practical aspects of this treatment that remain unclear, such as the accurate selection of patients, choosing a suitable protocol for ultrafiltration, the proper time of initiation, monitoring of the therapy, and its desirable effects on renal function with further restoration of diuretic agent responsiveness.

Key words: heart failure, renal replacement therapy, ultrafiltration, kidney injury, decongestion

Cite as

Urban S, Błaziak M, Biegus J, Zymliński R. Ultrafiltration in acute heart failure: Current knowledge and fields for further research. *Adv Clin Exp Med.* 2021;30(7):737–746. doi:10.17219/acem/135347

DOI

10.17219/acem/135347

Copyright

© 2021 by Wrocław Medical University

This is an article distributed under the terms of the Creative Commons Attribution 3.0 Unported (CC BY 3.0) (<https://creativecommons.org/licenses/by/3.0/>)

The pathophysiology of congestion

Congestion is considered one of the most important pathophysiological mechanisms in heart failure (HF). Fluid overload is responsible for approx. 90% of the 1 million hospitalizations due to HF in the USA and Europe annually.¹ The initial accumulation of fluid is usually asymptomatic. However, increased intravascular volume, manifested by elevated central venous pressure, induces congestion and impedes flow in the renal veins, causing a net decrease in glomerular filtration. When acute heart disease leads to acute kidney injury (AKI), this condition is known as cardiorenal syndrome type 1 (acute CRS).² Congestion also causes the elevation of inflammatory markers, endothelial activation, as well as hepatic and intestinal disorders.^{3,4} The adequate and complete management of congestion is vital for maintaining renal function, especially with regard to Na⁺ excretion, and improves survival among patients with acute decompensated heart failure (ADHF),^{5–7} regardless of transient increases in serum creatinine (sCr) levels. Another major concern associated with acute CRS is a decreased diuretic responsiveness due to the braking phenomenon. Moreover, hepatic dysfunction has been shown to predict worse outcomes in ADHF patients; thus, proper decongestion seems to be beneficial in this area as well.^{8–10}

Differences between diuretics and ultrafiltration

The mode of action of diuretics and ultrafiltration (UF) differs significantly (Table 1). The biochemical composition of the urine produced by diuretic agents and the fluid produced by the UF procedure is one of the main distinctions between these treatments. Loop diuretics act in the ascending loop of Henle by antagonizing the Na/K/2Cl cotransporter; therefore, the activity of these agents is inherently linked with natriuresis.¹¹ By blocking sodium

transport, diuretics create an osmotic gradient crucial for water reabsorption. The prolonged use of diuretics can lead to an impairment of natriuresis and the production of hypoosmotic urine. With reduced elimination of sodium, a reduction in intravascular water volume impairs fluid displacement from the interstitium. Proper natriuresis has been shown to be an essential factor for decongestion. Low sodium concentration in the urine or lack of a response to loop diuretics have been associated with a restricted diuretic response, increases in tubular injury markers, and a higher risk of all-cause mortality at one-year follow-up.^{12,13} Moreover, diuretics are suspected to activate the renin-angiotensin-aldosterone system (RAAS) and the sympathetic nervous system, which can eventually result in a resistance to diuretics.¹⁴ The precise management of fluid overload and forecasting fluid transfers for diuretic therapy still remains unclear.¹⁵

Conversely, UF seems to overcome the aforementioned pathophysiological issues seen with the use of diuretics. Ultrafiltration produced in an extracorporeal circuit is isoosmotic with plasma, which results in higher sodium output, a reduction of central venous pressure and an increase in the renal pressure gradient.¹⁶ The transition of fluid from the extravascular space reduces the symptoms of dyspnea and orthopnea, and improves lung mechanics and radiological signs of pulmonary edema.¹⁷ Furthermore, the improvement in respiratory parameters with UF can last up to 6 months after treatment.¹⁸ A reduction in pulmonary artery wedge pressure, as well as increase in cardiac output, diuresis and natriuresis without impacts on heart rate, systolic blood pressure (SBP), and electrolyte balance have been observed.¹⁹ The UF conducted with proper filtration rates also diminishes neurohormonal and RAAS activation, and can cause abnormalities in this area only in the case of excessive fluid elimination. Moreover, the amount of cleared fluid and electrolyte parameters can be thoroughly controlled. Some of the disadvantages of UF are related to the extracorporeal circuit (Fig. 1), which requires anticoagulation, increases the possibility of bleeding, sometimes requires central venous access, and

Table 1. Comparison of loop diuretics and ultrafiltration

Parameter	Diuretics	Ultrafiltration
Plasma norepinephrine level	increased	decreased
Cardiac output	variable	increased or unchanged
Mean arterial blood pressure	decreased	no change
Systolic blood pressure	not changed/decreased	not changed/decreased
Osmotic concentration of urine	hypoosmotic urine output	isoosmotic fluid removal
Predictability of fluid removal	unpredictable	accurate amount of fluid removal
Diuretic resistance	risk of development of diuretic resistance	reversing diuretic resistance
Risk of hypokalemia and hypomagnesemia	possible	not possible
Access	peripheral venous	peripheral or central venous
Anticoagulation	not necessary	necessary
Extracorporeal circuit	no	yes

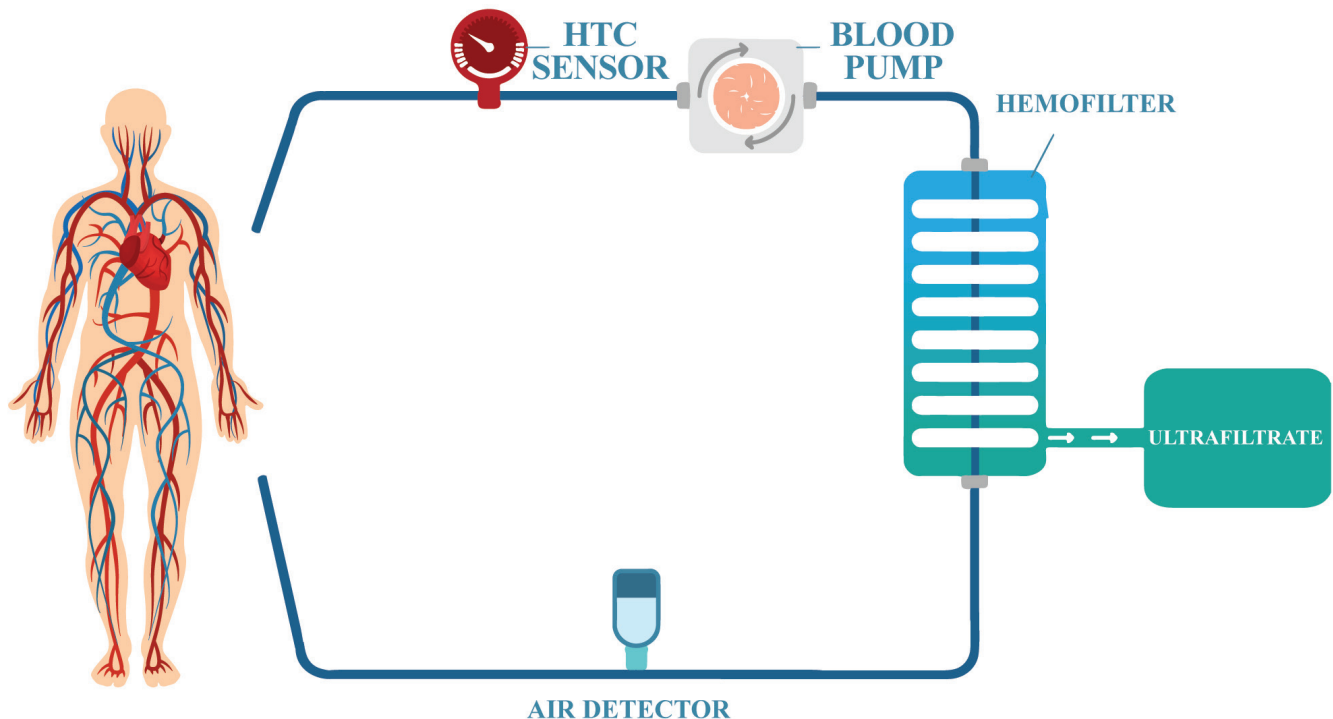


Fig. 1. Sample scheme of ultrafiltration circuit. Circuits can require single or double lumen cannulas inserted in peripheral venous access. Necessary pressure is created by the system of pumps. Ultrafiltrate is produced in hemofilter mostly due to convection process. Mass or volume of removed fluid is monitored. Circuit can be equipped with number of sensors such as hematocrit (HCT) or air detector. In modern machines, blood is usually withdrawn and returned to the same vessel

is associated with a higher incidence of catheter-related complications.²⁰ It is worth noting that there are also different modalities of renal replacement therapy (RRT), such as peritoneal UF, that can produce encouraging results and are cost-effective.²¹ Regrettably, a detailed discussion of these methods is beyond the scope of this article.

Objectives

The increasing availability of UF devices prompted us to carry out a concise literature review of this treatment. Here, we review the published studies on UF and provide brief comments on their conclusions and shortcomings. We hope that this paper can help clinical physicians to reach an up-to-date perspective on the UF procedure, especially with regard to practical issues such as patient selection, choosing the most beneficial protocol, the proper time of initiation, and its desirable effects on renal function.

Clinical trials comparing UF and diuretic treatment

Appropriate decongestion remains essential for ADHF therapy. One of the most dangerous issues associated with the process of fluid removal is volume depletion, and a number of potential methods for monitoring this procedure have arisen. The safety and efficacy of one of them

– the Reprise System – has been confirmed in TARGET-1 and TARGET-2 studies.²²

As the theoretical beneficial effects of UF became noticed, this treatment was considered as an alternative to traditional therapy. Since the early 2000s, a number of clinical trials have been conducted to examine the safety and efficacy of UF in the treatment of ADHF (Table 2).

In the first randomized controlled trial (RAPID-HF), patients with chronic heart failure (CHF) were randomized into UF ($n = 20$) and standard care (SC; $n = 20$) groups. Weight loss after 24 h was the primary endpoint. The UF patients received a single eight-hour treatment at a rate chosen by the physician (up to 500 mL/h). Diuretics were held during UF, unless the physician decided to implement them. The volume removed at the time of the primary endpoint was larger in the UF group (4650 mL compared to 2838 mL, $p = 0.001$), and weight loss was also increased, but not significantly, in this group. The symptoms of dyspnea and CHF also improved more in the UF group. No significant differences in heart rate, blood pressure or electrolytes were observed between groups, and no serious complications, including acute kidney failure, occurred.²³

Another single center, single-arm study (EUPHORIA) investigated 20 ADHF patients with $sCr \geq 1.5$ mg/dL or diuretic resistance (≥ 80 mg furosemide) and fluid overload. Patients received UF at a fixed rate of 500 mL/h or, if SBP dropped to ≤ 80 mm Hg, the UF rate was reduced to 200 mL/h. The procedure was conducted until ADHF

Table 2. Trials evaluating ultrafiltration for the treatment of acute decompensated heart failure (ADHF)

Study	RAPID-HF	EUPHORIA	UNLOAD	ULTRADISCO	CARRESS-HF	CUORE	AVOID-HF	Hanna et al.	Hu et al.
Year	2005	2005	2007	2011	2012	2014	2015	2012	2020
Rationale/endpoint	safety and efficacy of UF	hospitalization time and WRF in UF	weight loss at 48 h	hemodynamic parameters during UF and SC	UF among ADHF with WRF	rehospitalization rate for HF at 1 year	time to first HF event in UF and SC group	time to PCWP maintain ≤ 18 mm Hg for a minimum of 4 h	efficacy and safety of UF and SC
Inclusion criteria	HF, congestion, no EF cutoff	ADHF, renal insufficiency or diuretic resistance, congestion, no EF cutoff	ADHF, congestion, no EF cutoff	ADHF, congestion, no EF cutoff	ADHF, WRF, congestion, no EF cutoff	NYHA III/IV, estimated fluid overload ≥ 4 kg in 2 months, EF $\leq 40\%$	ADHF, congestion, no EF cutoff	NYHA III/IV, EF $< 40\%$, PCWP ≥ 20 mm Hg	ADHF, congestion, no EF cutoff
Valvular heart disease	severe stenosis excluded	no information	no information	severe stenotic excluded	severe stenosis excluded	no information	severe stenosis excluded	severe aortic stenosis/regurgitation, severe mitral stenosis excluded	severe mitral or aortic stenosis, tricuspid disease excluded
Follow-up	90 days	90 days	90 days	36 h	60 days	1 year	90 days	90 days	90 days
Patients	40	20	200	30	188	56	224	36	100
UF parameters	single 8 h procedure, rate determined by physician	rate determined by protocol, duration determined by physician	duration and rate of UF determined by physician	rate determined by protocol, duration determined by physician	fixed UF rate – 200 mL/h, duration determined by physician	duration and rate of UF determined by physician	protocol-based UF rate and duration	UF rate of 400 mL/h for 6 h, then 200 mL/h	rate and duration determined by physician
Diuretics during UF	no	no	no	no	no	yes	no	no	no
Results	fluid loss greater in UF group	reduction of length of stay and readmissions, positive effect for 3 months in UF	greater weight loss and reduced amount of rehospitalizations in UF	greater improvement in hemodynamic parameters, NT-proBNP, aldosterone in UF	higher increase in creatinine level, with no advantage in weight loss in UF	longer stabilization and smaller number of rehospitalizations in UF	trend toward longer time to first HF event in UF	UF is a safe method, can remove fluid faster than diuretics and can lead to shorter hospitalization	better volume control and higher urine output increase in UF

UF – ultrafiltration; WRF – worsening renal function; SC – standard care; NT-proBNP – N-terminal brain natriuretic peptide; PCWP – pulmonary capillary wedge pressure; EF – ejection fraction.

symptoms were resolved. Weight decreased significantly and remained lower until the end of the follow-up period (90 days). An improvement in global clinical status and brain natriuretic peptide (BNP) parameters were also noticed. The EUPHORIA patients' hospitalization time was about 4.3 days shorter than those in the ADHERE registry.²⁴ The study also showed that aggressive fluid removal (8500 mL using UF) did not provoke worsening renal function (WRF), electrolyte abnormalities or hypotension.²⁵ An interesting aspect of the EUPHORIA study is that in the 3 months preceding UF, 9 patients required hospitalization, and after the procedure, only 1 needed hospitalization in the same period following UF. These results are consistent with previous studies.²⁶ The aforementioned improvement can be explained by a reversal of "braking phenomenon" caused by a "diuretic holiday".

An additional multi-center randomized controlled trial that was supposed to confirm the efficacy of UF in ADHF treatment was the UNLOAD study. Two hundred patients hospitalized due to ADHF and presenting with symptoms of hypervolemia were enrolled. Diuretic agents were prohibited during first 48 h after enrollment in the UF arm. The filtration rate and length of the procedure were adjusted by the physician up to 500 mL/h. Patients in the SC arm were treated with loop diuretics, according to the protocol, and the dose had to have been at least doubled in comparison to the pre-hospitalization dose. The primary endpoints were weight loss and dyspnea assessment at 48 h after randomization. At the time of the endpoint, patients enrolled in the UF group achieved greater weight and net fluid loss. Dyspnea scores were comparable across groups. The results of UNLOAD confirmed

the results of EUPHORIA and showed that UF patients at the 90 day follow-up had fewer rehospitalizations due to HF, rehospitalizations, rehospitalization days, and unscheduled visits. No sCr changes at 90 days and a lower incidence of episodes of hypokalemia were also observed in the study group. The authors suggested that the lack of an association between net fluid loss and sCr levels can imply a loop diuretics contribution to renal dysfunction, which propels HF progression.²⁷

One small, randomized study, ULTRADISCO, was performed by Giglioli et al.²⁸ Patients were assigned to UF and SC groups, and were monitored using PRAM²⁹ – a device that allows investigators to conduct noninvasive measurements of hemodynamic variables. The UF group received the procedure at a protocol-based rate, adjusted to SBP (SBP < 100 mm Hg meant an UF rate of 100 mL/h; 100 mm Hg < SBP < 110 mm Hg meant an UF rate of 200 mL/h; SBP > 110 mm Hg meant an UF rate of 300 mL/h). The duration of the procedure was left to the discretion of the physician. Patients treated with UF had a greater decrease in parameters such as N-terminal proBNP (NT-proBNP) and aldosterone. Arterial pressure parameters remained unchanged during the UF procedure and decreased significantly after diuretics infusion, suggesting a better hemodynamic stability with UF treatment. A number of cardiac parameters also showed greater improvement in the UF group (stroke volume index, cardiac index, cardiac power output, cardiac cycle efficiency, systemic vascular resistance).

The CARRESS-HF was the most concerning study published to date, and raised many doubts about the safety and efficacy of UF. One hundred and eighty-eight patients were enrolled in this study, equally distributed across the pharmacotherapy and UF arms. All of the participants were hospitalized because of HF, had worsened renal function (defined as increase of sCr \geq 0.3 mg/dL within 12 weeks before or 10 days after admission) and signs of hypervolemia. Diuretics were not administered during the UF treatment. The UF rate was configured to 200 mL/h in every patient; however, it could be slowed or discontinued by the physician. No protocol for implementing changes in UF was provided. Patients assigned to the pharmacotherapy arm were administered diuretics in doses adjusted to achieve production of 3–5 L of urine daily. The SCr change and weight loss at 96 h after randomization were the primary endpoints. A greater increase in sCr levels was observed in the UF group, but there were only non-significant differences seen in weight loss. In addition, a higher percentage of UF patients had serious adverse effects.²⁰

The results and methodology of the CARRESS-HF study raised major concerns. First, 39% of the UF group received diuretics instead of UF (9%), or received diuretics after the UF was stopped (30%). Clearly, these procedures can strongly impair the assessment of adverse effects in both groups. In addition, therapy in the diuretics group was titrated based on urine output, while the UF rate was mandated to be 200 mL/h for every patient in this group. Such

a rigid approach to UF without recalibrating the circuit to the clinical situation remains controversial.³⁰ A recent per-protocol analysis of the CARRESS-HF trial has shed additional light on the shortcomings of this study.³¹ This protocol analysis revealed that UF group patients, who actually received their randomized treatment, had a significantly higher net fluid loss and reduction of weight. The UF treatment was also associated with lower serum sodium levels. This analysis also confirmed a higher level of sCr in the UF group. However, recent studies have shown that a transient increase in sCr can be the result of better decongestion and a decrease in renal flow, and can even predict a better outcome.³² Moreover, 90% of the UF group was not properly decongested at the assessment of the primary endpoint.¹ At 96 h after start of the therapy, only 32% of UF patients were still included in the study compared to 80% in the diuretic group, and reasons for the withdrawal of patients from the UF group were likely not clinically driven.³³ Another problem with the trial was the adjustment of UF rates, which was primarily set at 200 mL/h. The per-protocol analysis showed that these rates were actually much lower and, more importantly, the timing of the adjustments is a matter of concern. Common consensus, stemming from the Frank–Starling law, suggests using high UF rates at the beginning of the procedure in order to achieve the highest possible transfer from the interstitial space and then reducing the rate in the case of hypotonia or other complications. The opposite approach can lead to suboptimal decongestion and deteriorate prognosis, which is what was observed in the CARRESS-HF study, where, in contrast to the results of UNLOAD, the 60-day outcome did not differ in both arms.¹

The results of the CARRESS-HF trial encouraged investigators to conduct another study where the UF rate would be adjustable. The CUORE trial was a small, single-center study where 56 patients were randomized into 2 arms – SC and UF. The participants were observed for 1 year and rehospitalization for CHF was the primary endpoint. The control group was treated with loop diuretics according to guideline recommendations, and the UF group received up to 2 sessions of UF, and up to a cumulative fluid removal >2 L. The physicians were encouraged not to exceed 75% of initial weight increase. An interesting observation in this study is that diuretic administration was maintained in both groups. The time and rate of UF was left to discretion of the treating physician. Peripheral and pulmonary edema, and the New York Heart Association Functional Classification (NYHA) stage improved similarly in both groups. Doses of furosemide, hospitalization time and absolute body weight reduction did not differ. At the six-month follow-up, average body weight, renal function and furosemide dose did not change compared to discharge in the UF group, while these variables worsened in the control group. The BNP levels were also reduced in the UF group, but remained unchanged in the control group. Four hospitalizations occurred in the UF group,

whereas 30 were observed in the control group.³⁴ The results of the CUORE trial are consistent with UNLOAD and indicate that a prolonged protective effect of UF can last for up to 6 months. The authors of the CUORE study also suggested that decongestion is not the only key to outcome improvement. As the amount of the fluid removed was similar in both groups, the improvement may be attributable to the quality of the withdrawn fluid.

The promising results of the CUORE study prompted researchers to carry out larger, randomized control trials with adjustable diuretic and UF doses.³⁵ The AVOID-HF is the most recent randomized multi-center study. This study was designed to randomize 810 HF hospitalized patients and was prematurely finished with 224 patients.³⁶ One hundred and sixty-five patients were observed until the end of follow-up. The study included ADHF patients who presented with symptoms of fluid overload.³⁷ Patients were evaluated at 30, 60 and 90 days following discharge. Doses of loop diuretic in the pharmacological arm and UF rates in the UF arm were established on the basis of a protocol prepared by the investigators.³⁷ The supply of diuretics was stopped during UF. The time to a HF-related event, defined as HF rehospitalization, unscheduled visits, or emergency treatment with intravenous loop diuretics or UF, was the primary endpoint. Due to the relatively short length of the study, significant differences in the survival curves were not observed. At 90 days post-treatment, 25% of the UF group and 35% of the pharmacotherapy group experienced a HF event. However, the suggested 37% risk reduction in HF events in the UF group did not reach statistical significance. The UF group also exhibited a greater net fluid loss. Weight loss at 72 h, total weight loss during hospitalization, time to freedom of congestion, and the percentage of patients free from congestion at discharge did not reach statistical significance, albeit greater improvement was noticed in the UF group. Within 30 days after discharge, patients in the UF group had, per day at risk, fewer rehospitalizations for HF, fewer HF rehospitalization days, lower rehospitalization rates due to a cardiovascular (CV) incident, fewer rehospitalization days due to a CV incident, and fewer rehospitalizations due to a CV incident. The findings of the AVOID-HD trial are consistent with the UNLOAD results and confirm that early UF, implemented before WRE, has a beneficial, prolonged effect on decongestion.³⁶

There were also several smaller and less known studies conducted. The first of them, conducted by Hanna et al.,¹⁹ included 36 patients. The primary endpoint for this study was a decrease in pulmonary artery wedge pressure less than 18 mm Hg for 4 consecutive hours. The results confirmed the findings from larger studies. The UF group tended to reach the primary endpoint faster than the pharmacotherapy group, achieved a greater weight reduction and a higher total volume was removed, and their hospitalization was shorter. Kidney function, biomarkers and adverse events did not differ.

Another study, conducted by Hu et al.,³⁸ enrolled 100 patients with ADHF. Patients were randomized into 2 groups: early UF (n = 40) or torsemide plus tolvaptan (n = 60). The UF rate and duration of the procedure was managed by the physician. The initial UF rate was set to 200–300 mL/h and then reduced. On the 4th day after initiation of the treatment, UF was terminated and UF patients received torsemide with tolvaptan at the same mean dose that was administered to the pharmacotherapy group. At day 3, UF patients exhibited greater weight loss and a urine increase. After 8 days, patients who received UF presented with increased weight loss and urine output, and decreased BNP levels, NYHA scores, jugular venous pulse scores, and inferior vena cava diameters. No differences in re-admissions and mortality at 1 and 3 months follow-up were observed; however, the three-month readmission rate was lower in the UF group, which may have reached statistical significance in a larger study.

Two meta-analyses were also conducted to evaluate the value of UF therapy among acute HF patients. The first included 7 articles and 771 patients,³⁹ and showed that UF leads to greater weight loss, fluid removal and better HF rehospitalization rates, with comparable effects on renal function. The UF, however, did not have impact on mortality. A more recent meta-analysis, carried out in 2020, included 8 trials and 801 participants. The results showed greater fluid removal and weight loss, and lower incidence of worsening HF and rehospitalizations for HF, without effects on renal function and all-cause mortality.⁴⁰ Regrettably, neither of these studies evaluated the incidence of adverse effects, such as catheter related infections, filter clotting, etc.

Proper time of initiation and selection of patients

Precisely distinguishing patients who will benefit from UF remains a challenge. The high cost and potential adverse effects restrict the use of UF as a global method for fluid management in HF patients. The current American and European cardiology guidelines do not provide clear information regarding who should undergo this procedure, suggesting that it should be restricted to patients with resistance to diuretics therapy.^{41,42} The American guidelines do indicate that UF may be considered to alleviate symptoms in patients with fluid overload (level of evidence B), while the European guidelines focus more on the aspect of renal failure and propose that UF should be considered in patients with congestion and AKI (level of evidence C). The aforementioned guidelines also suggest the following criteria to help qualify patients for UF: hyperkalemia >6.5 mmol/L, pH < 7.2, serum urea level >25 mmol/L, and sCr > 3.4 mg/dL.

The lack of a clear definition for diuretic resistance creates additional issues. Ter Maaten et al.¹⁴ have proposed

a three-part definition for diuretic resistance which includes persistent congestion despite administration of >80 mg of furosemide per day, amount of excreted sodium below 0.2% of filtered load, and failure to excrete at least 90 mmol of sodium within 72 h of 160 mg furosemide given twice daily. Notwithstanding this definition, persistent congestion with diuretic resistance implies a severe outcome and UF can serve as a rescue therapy.

Another issue is the time of the implementation of RRT in the context of renal function. The ELAIN trial compared early and delayed initiation of RRT in patients with stage 2 AKI. Patients were randomized to receive an immediate initiation of RRT (hemodiafiltration) or to wait until absolute indications occurred, or AKI progressed to stage 3. Patients in the early group had decreased all-cause mortality at 90 days compared to the delayed group (39.3% compared to 54.7%, $p = 0.03$).⁴³ However, the findings of this study have to be treated with caution because of the different RRT modality and the distinct population of patients. Nonetheless, the results suggest that RRT should be implemented sooner than later in diuretic-resistant renal worsening patients. Moreover, these studies did not include sufficient data about the use of UF in patients with different types of HF or valvular heart disease.

Choosing the most effective protocol

Selection of the most effective UF protocol and deciding its duration raises many doubts among clinicians. The cardiological, nephrological and intensive care medicine guidelines of European and American scientific associations do not propose a consistent protocol for UF, especially for patients with ADHF. The unique standards that have been recommended by Kidney Disease: Improving

Global Outcome and European Society of Intensive Care Medicine, are tailored for patients with AKI and suggest using an effluent volume of 20–25 mL/h/kg for post-dilution CRRT⁴⁴ and a 20 mL/kg/h clearance rate for small solutes.⁴⁵ Additional information about the recommendations proposed by these guidelines is shown in Table 3. Due to the different clinical constellations of ADHF patients in comparison to AKI group, these instructions need to be treated with caution.

Studies have clearly shown that UF parameters have to be tailored precisely for every patient. The CARRESS-HF trial, where same rate was used for all patients, manifested no difference in the weight loss and rehospitalizations, with a higher increase in sCr in the UF patients group. Conversely, the UNLOAD, ULTRADISCO, CUORE, and AVOID-HF studies, where parameters were adjusted by the physician or were protocol-based, showed that UF patients had fewer rehospitalizations or that their hemodynamic parameters were improved in comparison to SC group, with no difference in sCr. Interestingly, the mean UF rates used in the UNLOAD, CUORE and AVOID-HF trials were higher than in the CARRESS-HF study, suggesting that the outcome for sCr in these studies should be worse. This can be explained by the adjustment of the protocol; not tailoring procedure parameters can create a situation where some groups of patients are excessively dehydrated, leading to hypovolemia, and others remain congested due to lower than needed fluid removal.³³ Furthermore, protocol analysis of the CARRESS-HF study³¹ showed that the mean UF rates provided in the study were 83 mL/h, 140 mL/h, 107 mL/h, and 70 mL/h for every sequencing 24 h period, respectively. The UF rates should be maximized at the beginning of the procedure and then maintained or reduced. This conclusion stems from 2 rationales. The first derives directly from the Frank–Starling law. The process of refilling intravascular space from

Table 3. Guidelines-based recommendations from European, American, Canadian, and Japanese scientific associations on the fields of cardiology, nephrology and intensive care

Association	Information about UF in ADHF	Level of evidence
European Society of Cardiology	May be considered in refractory congestion/Should be considered in refractory volume overload and AKI	IIbB/IIaC
American College of Cardiology Foundation/American Heart Association	May be considered for fluid overload to alleviate symptoms/May be considered for refractory congestion	B/C
Canadian Cardiovascular Society	Not recommended for the routine use in intractable congestion	Weak recommendation, low-quality evidence
Japanese Circulation Society	Patients with renal dysfunction and refractory congestion should receive CRRT, all modalities have equal evidence level	IIbB/IIaC
European Renal Association – European Dialysis and Transplant Association; Kidney Disease Improving Global Outcome; Canadian Society of Nephrology; Japanese Society of Nephrology; European Society of Intensive Care Medicine; Society of Critical Care Medicine; Canadian Critical Care Society; The Japanese Society of Intensive Care Medicine	No guidelines for ADHF patients	–

UF – ultrafiltration; ADHF – acute decompensated heart failure; AKI – acute kidney injury; CRRT – continuous renal replacement therapy.

the interstitium decreases with the amount of removed fluid. Hence, the UF rate should be maintained or reduced during the procedure in order to allow the plasma refilling rate to keep up with the fluid removal rate. Proceeding in such a fashion preserves volume depletion and hypotension, and leads to better decongestion, which should be primary target of the treatment as the incomplete decongestion is associated with worse outcomes.^{32,46,47} Indeed, in the CARRESS-HF study, 90% of the patients were not properly decongested. In other studies, where dehydration was increased, improvement of the outcome, in the context of rehospitalizations, has been observed.^{27,34,36} Secondly, such low rates of UF can cause a higher incidence of filter clotting,⁴⁸ and the percentage (36% of patients) of filter clotting in the CARRESS-HF study was unprecedented in comparison to other studies.

At the time of the writing of this article, 1 randomized controlled trial had used loop diuretics during UF. The CUORE trial investigated UF patients with no diuretic gap, in a one-year follow-up, and reported a reduction in HF rehospitalizations and a non-significant trend towards lower mortality in comparison to the SC group. A diuretic holiday is suspected to reverse the braking phenomenon and to reduce diuretic-induced neurohormonal activity, thus making such an approach controversial.²⁶ Nevertheless, the process of the braking phenomenon is not fully understood. It is probable that some of its components, such as the proliferation of distal convoluted tubule, which is documented in rats,⁴⁹ can be irreversible or irreversible by the short period of time of the diuretic holidays. Future studies, like three-arm randomized control trials with SC, UF only and UF with diuretics, may be worth considering. Presuming that a diuretic holiday is beneficial for ADHF patients, the idea of implementing regular, preventive UF for patients with congestive HF should be investigated, especially given the potential reduction of hospitalizations shown in previous studies and the high cost of in-patient care.¹

Targets for decongestion

A number of different methods to evaluate the proper level of decongestion have been proposed. The most basic is the assessment of dry weight with an attempt to reach it exactly or a pre-specified percentage of it. This approach was used in the CUORE trial.³⁴ Increased central venous pressure, which was identified as threat for renal function, and is a neurohormonal, inflammatory and endothelial cell activator,³ can also constitute a target for a treatment. For obvious reasons, the invasive measurement of central venous pressure cannot be applied for every UF patient. However, it can be approximated using ultrasonography by measuring the collapsibility index of inferior vena cava.⁵⁰ It must be noted, however, that the reliability of this measurement can be limited by respiratory mechanics,

ventilation with positive pressure, elevated pulmonary artery pressure, valvular disease, and the skill of the physician performing the examination. The safety and efficacy of evaluating pulmonary artery pressure by the implantable wireless device CARDIOMEMS has been confirmed in a CHAMPION trial,⁵¹ and has been shown to reduce HF hospitalizations.

Monitoring therapy and preventing volume depletion

Online monitoring of hematocrit is the obvious method for preventing volume depletion during UF. This technique has been successfully used in the CUORE trial.³⁴ Limits that would automatically stop the UF procedure due to an excessive hematocrit increase can also be programmed. While hematocrit assessment can help estimate volume loss, many factors including position change or bleeding can interfere with measurement of this parameter. Attempts to use whole body bioimpedance to assess tissue hydration have also been successful,⁵² but this technique is not yet popular in clinical practice. A recent study has shown that the μ Cor system, which was tested on patients undergoing dialysis, part of whom suffered from HF, can assess thoracic fluid using radiofrequency.⁵³ Regrettably, none of the aforementioned methods are completely satisfactory.

Concerns about renal function during UF

The CARRESS-HF study reported a higher increase in sCr in the UF group compared to the diuretic group. Moreover, 16% of UF termination cases in this trial were caused by an increase in sCr. This finding seems to suggest that UF is associated with worsening renal function. However, there are many studies concluding that this approach can be justifiable in 2 dimensions. First, an increase in sCr in patients being decongested can be caused by number of different factors, and the increase should be judged in conjunction with the particular clinical constellation. The associations between increased sCr and renal tubular damage are also questionable. The ROSE-AHF trial examined the correlations between sCr and markers of tubular damage such as neutrophil gelatinase associated lipocalin (NGAL), N-acetyl- β -D-glucosaminidase (NAG) and kidney injury molecule-1 (KIM-1), and reported only low correlations.⁴⁷ Another study suggests that the evaluation of renal function through the prism of creatinine levels in decongested patients with ADHF can be misleading. Instead, this study proposed assessing spot urinary sodium levels, as decreases during the therapy were predictive of worse outcomes.¹² Furthermore, in the DOSE trial, an increase in sCr was found to be a predictor of better

outcomes in HF patients during decongestion.³² A possible explanation for this finding is that the increase of sCr is due to better decongestion. The ROSE-HF also showed that an increase in NGAL, NAG and KIM-1 was associated with improved survival. This finding suggests that some degree of tubular injury is acceptable in an endeavor to reach maximal decongestion. On the other hand, there are papers that suggest that a NGAL increase is not associated with volume depletion, so it could be more precise parameter than creatinine to evaluate kidney function during UF.⁵⁴ The essential thing about considering UF in ADHF in the context of renal function is to use a clinical-based approach. There is a major shortfall in evidence to prove beyond any reasonable doubt that transient WRF during the UF treatment is sufficient to abandon the therapy. Hence, the decision continue or discontinue therapy should be made individually in every case.

Conclusions

Ultrafiltration is a safe and effective method for decongestion in patients with ADHF. The effectiveness of this therapy for removing fluid, reducing HF events and decreasing the number of subsequent hospitalizations has been demonstrated in a number of clinical trials. The role of diuretic treatment as a standard therapy is unquestioned. However, UF can also serve as an alternative method for diuretic-resistant patients, without greater concern for a worsening of renal function.

Ultrafiltration obviously still needs to be carefully examined. An issue that is essential for future successful treatment with this method is the creation of precise algorithms for qualification and the selection of patients who will benefit from this procedure. Another issue that needs to be addressed is the timing of the implementation of UF in the context of renal function. Assessment of glomerular and tubular injury, and the use of specific biomarkers during UF, should also be further evaluated. There are also concerns regarding the best UF protocol to use for fluid overload patients and the role of diuretic use during the procedure needs more study. Ultrafiltration has multiple theoretical benefits such as not contributing to electrolyte abnormalities, diminishing neurohormonal and RAAS activation, and possibly reversing the “braking phenomenon”. The results of numerous trials show its safety and efficacy in fluid removal, and suggest a potential beneficial clinical effect in reducing the number of HF rehospitalizations. This trend requires further carefully designed trials to be confirmed. The prospects of implementing regular, preventive UF for HF congestive patients are distant, but worth imagining. The effects of this treatment on cardiovascular and all-cause mortality also have to be investigated in larger studies. In addition, the incidence, severity and management of adverse effects, such as thrombotic events, bleeding and filter clotting, require more precise investigation.

ORCID iDs

Szymon Urban  <https://orcid.org/0000-0002-5547-150X>
 Mikołaj Błaziak  <https://orcid.org/0000-0001-8207-1723>
 Jan Biegus  <https://orcid.org/0000-0001-9977-7722>
 Robert Zymliński  <https://orcid.org/0000-0003-1483-7381>

References

1. Costanzo MR. Ultrafiltration in acute heart failure. *Card Fail Rev.* 2019; 5(1):9. doi:10.15420/cfr.2018.29.2
2. Ronco C, Haapio M, House AA, Anavekar N, Bellomo R. Cardiorenal syndrome. *J Am Coll Cardiol.* 2008;52(19):1527–1539. doi:10.1016/j.jacc.2008.07.051
3. Colombo PC, Onat D, Harxhi A, et al. Peripheral venous congestion causes inflammation, neurohormonal, and endothelial cell activation. *Eur Heart J.* 2014;35(7):448–454. doi:10.1093/eurheartj/ehf456
4. Zymliński R, Sierpiński R, Metra M, et al. Elevated plasma endothelin-1 is related to low natriuresis, clinical signs of congestion, and poor outcome in acute heart failure. *ESC Hear Fail.* 2020;7(6):3536–3544. doi:10.1002/ehf2.13064
5. Metra M, Davison B, Bettari L, et al. Is worsening renal function an ominous prognostic sign in patients with acute heart failure? The role of congestion and its interaction with renal function. *Circ Hear Fail.* 2012;5(1):54–62. doi:10.1161/CIRCHEARTFAILURE.111.963413
6. Testani JM, Chen J, McCauley BD, Kimmel SE, Shannon RP. Potential effects of aggressive decongestion during the treatment of decompensated heart failure on renal function and survival. *Circulation.* 2010;122(3):265–272. doi:10.1161/CIRCULATIONAHA.109.933275
7. Damman K, Ng Kam Chuen MJ, MacFadyen RJ, et al. Volume status and diuretic therapy in systolic heart failure and the detection of early abnormalities in renal and tubular function. *J Am Coll Cardiol.* 2011;57(22):2233–2241. doi:10.1016/j.jacc.2010.10.065
8. Biegus J, Zymliński R, Sokolski M, et al. Impaired hepato-renal function defined by the MELD XI score as prognosticator in acute heart failure. *Eur J Heart Fail.* 2016;18(12):1518–1521. doi:10.1002/ejhf.644
9. Biegus J, Demissei B, Postmus D, et al. Hepatorenal dysfunction identifies high-risk patients with acute heart failure: Insights from the RELAX-AHF trial. *ESC Hear Fail.* 2019;6(6):1188–1198. doi:10.1002/ehf2.12477
10. Zymliński R, Ponikowski P, Biegus J. Looking at the heart failure through the prism of liver dysfunction. *Eur J Heart Fail.* 2020;22(9):1672–1674. doi:10.1002/ejhf.1932
11. Ronco C, Ricci Z, Bellomo R, Bedogni F. Extracorporeal ultrafiltration for the treatment of overhydration and congestive heart failure. *Cardiology.* 2001;96(3–4):155–168. doi:10.1159/000047399
12. Biegus J, Zymliński R, Sokolski M, et al. Serial assessment of spot urine sodium predicts effectiveness of decongestion and outcome in patients with acute heart failure. *Eur J Heart Fail.* 2019;21(5):624–633. doi:10.1002/ejhf.1428
13. Biegus J, Zymliński R, Testani J, et al. Renal profiling based on estimated glomerular filtration rate and spot urine sodium identifies high-risk acute heart failure patients. *Eur J Heart Fail.* Online ahead of print. doi:10.1002/ejhf.2053
14. Ter Maaten JM, Valente MAE, Damman K, Hillege HL, Navis G, Voors AA. Diuretic response in acute heart failure: Pathophysiology, evaluation, and therapy. *Nat Rev Cardiol.* 2015;12(3):184–192. doi:10.1038/nrcardio.2014.215
15. Miller WL, Mullan BP. Understanding the heterogeneity in volume overload and fluid distribution in decompensated heart failure is key to optimal volume management: Role for blood volume quantitation. *JACC Hear Fail.* 2014;2(3):298–305. doi:10.1016/j.jchf.2014.02.007
16. Zafar MR, Miller TW, Farrukh Mustafa S, Al-Khafaji N. Pharmacological and non-pharmacological strategies for volume overload in acute decompensated congestive heart failure: A review article. *Cureus.* 2020;12(2):e6952. doi:10.7759/cureus.6952
17. Marenzi GC, Lauri G, Grazi M, Assanelli E, Campodonico J, Agostoni PG. Circulatory response to fluid overload removal by extracorporeal ultrafiltration in refractory congestive heart failure. *J Am Coll Cardiol.* 2001;38(4):963–968. doi:10.1016/S0735-1097(01)01479-6
18. Agostoni PG, Marenzi GC, Pepi M, et al. Isolated ultrafiltration in moderate congestive heart failure. *J Am Coll Cardiol.* 1993;21(2):424–431. doi:10.1016/0735-1097(93)90685-T

19. Hanna MA, Wilson Tang WH, Teo BW, et al. Extracorporeal ultrafiltration vs conventional diuretic therapy in advanced decompensated heart failure. *Congest Hear Fail.* 2012;18(1):54–63. doi:10.1111/j.1751-7133.2011.00231.x
20. Bart BA, Goldsmith SR, Lee KL, et al. Ultrafiltration in decompensated heart failure with cardiorenal syndrome. *N Engl J Med.* 2012;367(24):2296–2304. doi:10.1056/nejmoa1210357
21. Nassiri AA, Ronco C, Kazory A. Resurgence of urgent-start peritoneal dialysis in COVID-19 and its application to advanced heart failure. *Cardiorenal Med.* 2021;11(1):1–4. doi:10.1159/000513496
22. Biegus J, Zymlinski R, Siwolowski P, et al. Controlled decongestion by reprieve therapy in acute heart failure: Results of the TARGET-1 and TARGET-2 studies. *Eur J Heart Fail.* 2019;21(9):1079–1087. doi:10.1002/ejhf.1533
23. Bart BA, Boyle A, Bank AJ, et al. Ultrafiltration versus usual care for hospitalized patients with heart failure: The relief for acutely fluid-overloaded patients with decompensated congestive heart failure (RAPID-CHF) trial. *J Am Coll Cardiol.* 2005;46(11):2043–2046. doi:10.1016/j.jacc.2005.05.098
24. Adams KF, Fonarow GC, Emerman CL, et al. Characteristics and outcomes of patients hospitalized for heart failure in the United States: Rationale, design, and preliminary observations from the first 100,000 cases in the Acute Decompensated Heart Failure National Registry (ADHERE). *Am Heart J.* 2005;149(2):209–216. doi:10.1016/j.ahj.2004.08.005
25. Costanzo MR, Saltzberg M, O'Sullivan J, Sobotka P. Early ultrafiltration in patients with decompensated heart failure and diuretic resistance. *J Am Coll Cardiol.* 2005;46(11):2047–2051. doi:10.1016/j.jacc.2005.05.099
26. Agostoni P, Marenzi G, Lauri G, et al. Sustained improvement in functional capacity after removal of body fluid with isolated ultrafiltration in chronic cardiac insufficiency: Failure of furosemide to provide the same result. *Am J Med.* 1994;96(3):191–199. doi:10.1016/0002-9343(94)90142-2
27. Costanzo MR, Guglin ME, Saltzberg MT, et al. Ultrafiltration versus intravenous diuretics for patients hospitalized for acute decompensated heart failure. *J Am Coll Cardiol.* 2007;49(6):675–683. doi:10.1016/j.jacc.2006.07.073
28. Giglioli C, Landi D, Cecchi E, et al. Effects of ULTRAFiltration vs. Diuretics on clinical, biohumoral and haemodynamic variables in patients with deCOMPensated heart failure: The ULTRADISCO study. *Eur J Heart Fail.* 2011;13(3):337–346. doi:10.1093/eurjhf/hfq207
29. Briganti A, Evangelista F, Centonze P, et al. A preliminary study evaluating cardiac output measurement using Pressure Recording Analytical Method (PRAM) in anaesthetized dogs. *BMC Vet Res.* 2018;14(1):1–10. doi:10.1186/s12917-018-1392-5
30. Costanzo MR, Ronco C, Abraham WT, et al. Extracorporeal ultrafiltration for fluid overload in heart failure: Current status and prospects for further research. *J Am Coll Cardiol.* 2017;69(19):2428–2445. doi:10.1016/j.jacc.2017.03.528
31. Grodin JL, Carter S, Bart BA, Goldsmith SR, Drazner MH, Tang WHW. Direct comparison of ultrafiltration to pharmacological decongestion in heart failure: A per-protocol analysis of CARRESS-HF. *Eur J Heart Fail.* 2018;20(7):1148–1156. doi:10.1002/ejhf.1158
32. Brisco MA, Zile MR, Hanberg JS, et al. Relevance of changes in serum creatinine during a heart failure trial of decongestive strategies: Insights from the DOSE Trial. *J Card Fail.* 2016;22(10):753–760. doi:10.1016/j.cardfail.2016.06.423
33. Costanzo MR, Kazory A. Better late than never: The true results of CARRESS-HF. *Eur J Heart Fail.* 2018;20(7):1157–1159. doi:10.1002/ejhf.1187
34. Marenzi G, Muratori M, Cosentino ER, et al. Continuous ultrafiltration for congestive heart failure: The CUORE trial. *J Card Fail.* 2014;20(1):9–17. doi:10.1016/j.cardfail.2013.11.004
35. Emani S. Ultrafiltration for the treatment of acute heart failure. *Heart Fail Clin.* 2018;14(4):517–524. doi:10.1016/j.hfc.2018.06.013
36. Costanzo MR, Negoianu D, Jaski BE, et al. Aquapheresis versus intravenous diuretics and hospitalizations for heart failure. *JACC Hear Fail.* 2016;4(2):95–105. doi:10.1016/j.jchf.2015.08.005
37. Costanzo MR, Negoianu D, Fonarow GC, et al. Rationale and design of the Aquapheresis Versus Intravenous Diuretics and Hospitalization for Heart Failure (AVOID-HF) trial. *Am Heart J.* 2015;170(3):471–482. doi:10.1016/j.ahj.2015.05.019
38. Hu J, Wan Q, Zhang Y, et al. Efficacy and safety of early ultrafiltration in patients with acute decompensated heart failure with volume overload: A prospective, randomized, controlled clinical trial. *BMC Cardiovasc Disord.* 2020;20(1):447. doi:10.1186/s12872-020-01733-5
39. Jain A, Agrawal N, Kazory A. Defining the role of ultrafiltration therapy in acute heart failure: A systematic review and meta-analysis. *Heart Fail Rev.* 2016;21(5):611–619. doi:10.1007/s10741-016-9559-2
40. Wobbe B, Wagner J, Kata Szabó D, et al. Ultrafiltration is better than diuretic therapy for volume-overloaded acute heart failure patients: A meta-analysis. 2021;26(3):577–585. doi:10.1007/s10741-020-10057-7
41. Ponikowski P, Voors AA, Anker SD, et al. 2016 ESC Guidelines for the diagnosis and treatment of acute and chronic heart failure. *Eur Heart J.* 2016;37(27):2129–2200. doi:10.1093/eurheartj/ehw128
42. Yancy CW, Jessup M, Bozkurt B, et al. 2013 ACCF/AHA guideline for the management of heart failure: A report of the American College of Cardiology Foundation/American Heart Association Task Force on Practice Guidelines. *J Am Coll Cardiol.* 2013;62(16):e147–e239. doi:10.1016/j.jacc.2013.05.019
43. Zarbock A, Kellum JA, Schmidt C, et al. Effect of early vs delayed initiation of renal replacement therapy on mortality in critically ill patients with acute kidney injury: The elain randomized clinical trial. *JAMA.* 2016;315(20):2190–2199. doi:10.1001/jama.2016.5828
44. Kellum JA, Lameire N, Aspelin P, et al. Kidney disease: Improving global outcomes (KDIGO) acute kidney injury work group. KDIGO clinical practice guideline for acute kidney injury. *Kidney Int Suppl.* 2012;2(1):1–138. doi:10.1038/kisup.2012.1
45. Brochard L, Abroug F, Brenner M, et al. An official ATS/ERS/ESICM/SCCM/SRLF statement: Prevention and management of acute renal failure in the ICU patient. An international consensus conference in intensive care medicine. *Am J Respir Crit Care Med.* 2010;181(10):1128–1155. doi:10.1164/rccm.200711-1664ST
46. Costanzo MR. Verdict in. Congestion guilty! *JACC Hear Fail.* 2015;3(10):762–764. doi:10.1016/j.jchf.2015.06.004
47. Ahmad T, Jackson K, Rao VS, et al. Worsening renal function in patients with acute heart failure undergoing aggressive diuresis is not associated with tubular injury. *Circulation.* 2018;137(19):2016–2028. doi:10.1161/CIRCULATIONAHA.117.030112
48. Brain M, Winson E, Roodenburg O, McNeil J. Non anti-coagulant factors associated with filter life in continuous renal replacement therapy (CRRT): A systematic review and meta-analysis. *BMC Nephrol.* 2017;18(1):1–27. doi:10.1186/s12882-017-0445-5
49. Kaissling B, Bachmann S, Kriz W. Structural adaptation of the distal convoluted tubule to prolonged furosemide treatment. *Am J Physiol Ren Fluid Electrolyte Physiol.* 1985;17(3):374–381. doi:10.1152/ajprenal.1985.248.3.f374
50. Stawicki SP, Braslow BM, Panebianco NL, et al. Intensivist use of hand-carried ultrasonography to measure IVC collapsibility in estimating intravascular volume status: Correlations with CVP. *J Am Coll Surg.* 2009;209(1):55–61. doi:10.1016/j.jamcollsurg.2009.02.062
51. Abraham WT, Adamson PB, Bourge RC, et al. Wireless pulmonary artery haemodynamic monitoring in chronic heart failure: A randomised controlled trial. *Lancet.* 2011;377(9766):658–666. doi:10.1016/S0140-6736(11)60101-3
52. Piccoli A. Whole body: Single frequency bioimpedance. *Contrib Nephrol.* 2005;149:150–161. doi:10.1159/000085478
53. Connaire JJ, Sundermann ML, Perumal R, Herzog CA. A novel radio-frequency device to monitor changes in pulmonary fluid in dialysis patients. *Med Devices Evid Res.* 2020;13:377–383. doi:10.2147/MDER.S277159
54. Xu K, Rosenstiel P, Paragas N, et al. Unique transcriptional programs identify subtypes of AKI. *J Am Soc Nephrol.* 2017;28(6):1729–1740. doi:10.1681/ASN.2016090974

Influence of SARS-CoV-2 infection on thyroid gland function: The current knowledge

Agata Czarnywojtek^{1,2,A–D}, Alicja Ochmańska^{1,2,A,F}, Małgorzata Zgorzalewicz-Stachowiak^{3,E,F},
Nadia Sawicka-Gutaj^{1,C,D,F}, Beata Matyjaszek-Matuszek^{4,C,F}, Magdalena Woźniak^{4,E,F}, Marek Ruchała^{1,E,F}

¹ Chair and Department of Endocrinology, Metabolism and Internal Medicine, Poznan University of Medical Sciences, Poland

² Department of Pharmacology, Poznan University of Medical Sciences, Poland

³ Department of Health Prophylaxis, Poznan University of Medical Sciences, Poland

⁴ Chair and Department of Endocrinology, Diabetology and Metabolic Diseases, Medical University of Lublin, Poland

A – research concept and design; B – collection and/or assembly of data; C – data analysis and interpretation;

D – writing the article; E – critical revision of the article; F – final approval of the article

Advances in Clinical and Experimental Medicine, ISSN 1899–5276 (print), ISSN 2451–2680 (online)

Adv Clin Exp Med. 2021;30(7):747–755

Address for correspondence

Małgorzata Zgorzalewicz-Stachowiak
E-mail: neuro@ump.edu.pl

Funding sources

None declared

Conflict of interest

None declared

Received on April 15, 2021

Reviewed on June 9, 2021

Accepted on June 30, 2021

Published online on July 20, 2021

Abstract

The paper summarizes the current knowledge about the influence of SARS-CoV-2 on the thyroid gland and benign thyroid diseases, with emphasis on the situation in Poland. Based on the latest scientific literature published up to May 1, 2021 and the PubMed, Google Scholar, EMBASE and Web of Science database searches, keywords related to SARS-CoV-2 and its impact on the thyroid gland and benign thyroid diseases were searched. COVID-19-related thyroid disorders include non-thyroid syndrome, hypothyroidism and thyrotoxicosis. The authors paid special attention to the treatment of thyroid disease during the pandemic. The emphasis was on radioiodine therapy, which is of high clinical value due to the lower risk of neutropenia or agranulocytosis. It is currently unknown whether COVID-19 may lead to de novo thyroid dysfunction or if it can aggravate an existing thyroid disease. Patients with uncontrolled thyrotoxicosis are in a risk group for complications (e.g., cytokine storm) from any infection (especially from SARS-CoV-2 infection). Moreover, this group of patients should receive more extensive care, bearing in mind the neutropenia from taking antithyroid drugs, which may mask the symptoms of COVID-19.

Key words: therapy, hyperthyroidism, hypothyroidism, autoimmune thyroid disease, COVID-19

Cite as

Czarnywojtek A, Ochmańska A, Zgorzalewicz-Stachowiak M, et al. Influence of SARS-CoV-2 infection on thyroid gland function: The current knowledge. *Adv Clin Exp Med.* 2021;30(7):747–755. doi:10.17219/acem/139622

DOI

10.17219/acem/139622

Copyright

© 2021 by Wrocław Medical University

This is an article distributed under the terms of the Creative Commons Attribution 3.0 Unported (CC BY 3.0) (<https://creativecommons.org/licenses/by/3.0/>)

Introduction

Coronavirus disease 2019 (COVID-2019) is an acute respiratory infectious disease caused by SARS-CoV-2 (severe acute respiratory syndrome corona virus 2). As evidenced, both SARS-CoV-2 and SARS-CoV spike (S) glycoproteins found on the envelope of the virus demonstrate affinity toward human angiotensin-converting enzyme 2 (ACE2). The carboxypeptidase ACE2 was identified as the entry host cell receptor for SARS-CoV-2.^{1,2} The world first heard of COVID-19 on January 3, 2020, when Chinese officials reported to the World Health Organization (WHO) about anomalous pneumonia affecting 44 patients in Wuhan (Hubei Province) and it was recognized as a “public health emergency of international concern”.³ The first cases were vendors in the Huanan seafood market. A series of illnesses initiated a pandemic of the disease, in which the so-called “cytokine storm” and, consequently, multi-organ damage occurs.⁴ COVID-19 has become a considerable threat, especially among the elderly, including those with chronic diseases (diabetes, heart diseases, respiratory diseases, cancer) and pregnant women. Despite the various precautions taken by people (face masks, face shields, self-isolation, zoning), the SARS-CoV-2 virus causing COVID-19 spread at a geometric rate.^{5–11} Because of the global increase in morbidity, coronavirus disease 2019 was recognized as a global pandemic by the WHO on March 11, 2020.¹² Severe acute respiratory syndrome (SARS) is an infectious condition caused by the SARS-CoV virus, belonging to the *Coronaviridae* family.^{8,13} SARS-CoV-2 has been found in the respiratory system (trachea, lungs), skeletal system (spine), digestive system (pancreas, liver, stomach, small intestine), distal convoluted renal tube, sweat glands, endocrine system (parathyroid, pituitary, adrenal gland), and central nervous system (cerebrum). It has not been detected in the heart, aorta, cerebellum, lymph node, bone marrow, esophagus, muscle, spleen, ovary, uterus, testis, and thyroid gland.^{14–16}

Objectives

The purpose of this article is to present the latest data on the impact of COVID-19 on the thyroid gland (with emphasis on benign thyroid disease) based on a review of the current literature.

Methodology

A literature search has been conducted with PubMed, Google Scholar, EMBASE, and Web of Science (most recent literature search: May 1, 2021) using the following search terms: “thyroid disease and COVID-19 (SARS-CoV-2)”, “autoimmune thyroid disease and coronavirus”, “antithyroid therapy and COVID-19”, “COVID-19 and hypothalamic-pituitary-adrenal axis”, and “COVID-19 and clinical implications”.

SARS-CoV-2 and the hypothalamic–pituitary–thyroid axis and thyroid hormones

It has been observed that an infection caused by SARS-CoV-2 impacts the nervous system by affecting the cranial nerves and resulting in the loss of the senses of smell and taste.¹⁶ A retrospective analysis by Chen et al.¹⁷ in 50 COVID-19 patients showed that the serum levels of thyroid-stimulating hormone (TSH) and total triiodothyronine (T3) were significantly lower compared to the control group (n = 54). The decrease in TSH levels observed in COVID-19 patients was caused by chronic stress with coexisting hypoxemia. Secondly, glucocorticoids were administered to 62% of patients at a dose of 57.3 mg of methylprednisolone per day. Moreover, the serum concentrations of T3 and TSH were lower in patients with more severe the course of COVID-19 (p < 0.001). However, no correlation was found between the severity of the disease and the concentration of total thyroxine (T4). No significant differences were found in the recovered patients between TSH and TH (thyroid hormones) levels in the control group, and affected by COVID-19.

Research by Wang et al.¹³ found that COVID-19 extensively damages the thyroid gland (follicular, epithelial, parafollicular cells). The observations of Wei et al. were conducted on the endocrine cells in the adenohypophysis of SARS-CoV-2-infected patients (autopsies, n = 5), where the reduced staining intensity of immunoreactivity and positive TSH cells (including growth hormone and adrenocorticotrophic hormone) were observed, while an increase in signal intensity was observed in the case of prolactin, luteinizing hormone, and follicle-stimulating hormone. It is likely that the COVID-19 infection changes TSH secreting cells in the pituitary (the endocrine cells of the adenohypophysis).¹⁸ Apart from destroying the thyroid cells, this inhibits the activity of deiodinase type I (DI1) (resulting from the euthyroid sick syndrome, ESS), and downregulation at the hypothalamic–pituitary–thyroid (HPT) axis level is observed.

It has been reported by Ur et al.¹⁹ that SARS-CoV-2 can spread through nerve axons (the facial nerve, the glossopharyngeal nerve, the vagus nerve) due to the high expression of ACE2 and the high levels of the virus that are present in the oropharyngeal region. These nerves are located in the nucleus tractus solitarius (NTS). They facilitate the spread of the infection to NTS and lead to a cytokine storm damaging the cholinergic transmitter of the cholinergic anti-inflammatory and hypothalamic–pituitary–adrenal (HPA) pathway. During the cytokine storm caused by SARS-CoV-2, increased levels of interleukin (IL)-6, IL-7, tumor necrosis factor (TNF), the soluble form of the α -chain of the IL-2 receptor, and inflammatory chemokines (CCL2, CCL3, CXCL10) are observed.²⁰

The impact of SARS-CoV-2 on TSH secreting cells is significant, leading to decreased concentrations of TSH and,

thus, the observed disturbance of the pituitary endocrine axis feedback loops. The changes to the TSH secreting cells could occur through 4 mechanisms: direct damage to the pituitary gland by SARS-CoV-2; an indirect mechanism – the influence of pro-inflammatory cytokines^{14,16–18,21,22} and the so-called “cytokine storm”;¹⁹ chronic stress caused by hypoxia; and the impact of the certain group of pharmaceuticals such as glucocorticoids (including methylprednisolone).^{21,22}

In addition, expression of the SARS-CoV-2 ACE 2 receptor in thyroid follicular cells was increased; it was observed in minimal amounts in the hypothalamus as well.^{22–26} The serum ACE level was directly correlated with 3,5,3'-T₃ and T₄,²⁶ which suggests it could be useful for exploring peripheral thyroid hormone action. Moreover, the study by Rotondi et al.²⁷ has shown that as the messenger RNA (mRNA) encoding for the ACE2 receptor is expressed in thyroid follicular cells, the thyroid then becomes a potential target for SARS-CoV-2 entry.

COVID-19 and euthyroid sick syndrome

Severe respiratory infection caused by SARS-CoV-2 is associated with ESS, known as low T₃ syndrome or non-thyroidal illness syndrome (NTIS),^{14,15} which disrupts the HPT axis, leading to hypothalamic (central hypothyroidism).^{16–18} The mechanism of the emergence of ESS as a severe systemic disease can be distinguished as 2 phases: phase I – acute (inhibition of the activity of D1 resulting in reduced conversion of T₄ to T₃, increased metabolism of TH and decreased production of TH-binding proteins (e.g., albumin and thyroid-binding globulin), reduction of pulsatile TSH secretion); and phase II – chronic, in which there is a decrease in thyrotropin-releasing hormone (TRH) secretion (which results in the lowering of TSH and an insufficient supply of calories) and TSH (an increase in the levels of IL-6 and IL-18 cytokines and TNF- α).^{15,17} In our opinion, neurological disorders (behavioral disorders, speech, olfactory disorders, taste disorders), which occur during the infection, but are nonetheless transient, can be compared to the “Polar T₃ Syndrome” which occurs among “long-term explorers” in Antarctica.²⁸ Indeed, in extreme cold, so much T₃ is required to regulate body temperature that the brain is left with a less than an adequate supply making it slow, forgetful, unfocused, and moody. One of the most significant effects that it is advisable to note is neurological functions, including Polar explorers’ speech, which tends to fail frequently.

Recent research by Lui et al.²⁹ demonstrated that NTIS may be present in patients with severe COVID-19 symptoms as well as in patients with mild or moderate cases, who do not always require intensive care. The same researchers have shown that patients with NTIS had lower

free triiodothyronine (fT₃)/free thyroxine (fT₄) and an indirect index of deiodinase activity converting T₄ to T₃.¹⁵ However, it was observed that the inflammatory markers (C-reactive protein (CRP) and erythrocyte sedimentation rate) and serum enzymatic markers of tissue damage (aspartate aminotransferase and lactate dehydrogenase) were increased, whereas cycle threshold values did not change. A previous retrospective study found that patients who died from COVID-19 had lower fT₃ on admission than those who survived.^{30,31}

COVID-19 and autoimmune thyroid disease

Nowadays, it is assumed that for the occurrence of autoimmune thyroid disease (AITD), including Graves’ disease (GD) and Hashimoto thyroiditis (HT), coexisting endogenous factors such as genetic, intrathyroidal and exogenous (environmental) play a pivotal role. Some of the factors that may induce an immune response typical of GD are: iodine overdose, pregnancy (especially in the postpartum period), certain medications, radioiodine (RAI) therapy, tobacco smoke, stress, and bacterial and viral infections (including Epstein–Barr, hepatitis C virus (HCV) and parvoviruses).^{32–35}

The AITD, which may manifest itself in the form of hypothyroidism or hyperthyroidism, does not require patients to mandatory self-isolate during the pandemic unless associated with idiosyncratic drug-induced neutropenia (IDIN) or post-antithyroid drugs (ATDs) – agranulocytosis.³⁵ In the case of IDIN, the help of an endocrinologist should be immediate, which, in the current situation in Poland, when healthcare professionals are involved in fighting the COVID-19 pandemic, might be significantly challenging. Therefore, nowadays, isotope therapy (which will be discussed in detail later) is highly appreciated by professionals. Also, the frequent checkups that the patients then need to undergo both in hospital and at the clinic additionally expose patients to potential SARS-CoV-2 infection. Moreover, as Dworakowska and Grossmann.³⁶ described, patients with IDIN belong to the high-risk group. In the UK, it has been reported that discussions with employers from various work environments are ongoing. This has a significant impact on employees who need to self-isolate (and possibly work from home) and those patients who have to continue to go to work, with the emphasis on warning patients taking antithyroid medications about the possible adverse effects of IDIN and recommending that they should seek immediate medical attention even for a fever or a sore throat.

It is now mandatory that patients with COVID-19 symptoms and coexisting GD and hyperthyroidism stay at home to self-quarantine for at least 10 days, which is no different to people with no coexisting thyroid dysfunction.

With decreasing numbers of healthcare professionals available in hospital facilities to help minimize the spread of the virus, one solution is to carry out online consultations using phone or video calls (telemedicine). European Thyroid Association (ETA)³⁷ and American Thyroid Association (ATA)³⁸ guidelines currently exist for the diagnosis and management of thyroid diseases; however, as Dworakowska and Grossmann³⁶ state, some analogies and helpful tips on how to treat patients can be drawn from the experience of rheumatologists; such analogies also apply to autoimmune diseases, including, for example, rheumatoid arthritis.³⁹ According to Figueroa-Parr et al.⁴⁰ and Dworakowska and Grossmann,³⁶ patients suffering from COVID-19 with coexisting AITD are not included in the high-risk group. There has been no evidence that patients with AITD are more likely to be infected by SARS-CoV-2 or are at risk of developing the more severe COVID-19 disease.^{25,36} However, according to Boelaert et al.,⁴¹ patients with Graves' ophthalmopathy (GO), who actively undergo active immunosuppressive therapy, may be particularly at risk.

Hypothyroidism

Treating hypothyroidism during the COVID-19 pandemic has not changed significantly. Therefore, substitution of levothyroxine (L-T4) at the same dose (the same as the usual treatment) is recommended.^{40,42} However, it should be noted that in the era of the COVID-19 outbreak in Poland, access to an endocrinologist and diagnostic tests may be difficult. In Poland and other European countries, patients with COVID-19 symptoms are recommended a new form of consultation, e.g., 1) online chat, 2) via email, 3) phone, and, from January 1, 2020, 4) electronic prescriptions.⁶

The problem of neonatal screening for congenital hypothyroidism is different, as these tests need to be carried out with special care, and any delays in performing them should be avoided.⁴³

Decreased serum TSH levels are observed among pregnant women of all populations. However, differences between ethnic and racial groups have been observed. A study conducted in Europe and the US showed that the upper reference limit for serum TSH concentration is 2.5 mU/L in the 1st trimester and 3.0 mU/L in the 2nd and 3rd trimester.^{44,45} However, a study conducted in China on 4800 women who were between 7 and 12 weeks pregnant, found that the upper reference limit only changed from 5.31 mU/L to 4.34 mU/L.⁴⁵ Thus, we can conclude that with the rise in COVID-19 cases, the therapy for hypothyroid disease for pregnant and postpartum women should be individualized, but according to the guidelines of the ATA, the L-T4 dose should be increased by 2 tables of the same dose weekly.⁴⁴ Thus, thyroid function tests should be measured according to the population-based and trimester-specific reference ranges.^{44,45}

Hyperthyroidism

A recent study (retrospective analysis) conducted by Lania et al.⁴⁶ in 287 consecutive patients (94 females and 193 males) showed a relationship between a high risk of thyrotoxicosis and the SARS-CoV-2 infection. Additional publications support an association between COVID-19 infection and overt and subclinical thyrotoxicosis, as well as with subacute thyroiditis.^{47,48} COVID-19 may exacerbate GD.^{17,49} A cohort study carried out by Khoo et al.⁵⁰ observed a small transient decrease in serum TSH and fT4 levels (which could also be considered to mimic hyperthyroidism) in patients with COVID-19 infection. However, the most likely explanation of this would be the nonthyroidal illness syndrome observed in some of the patients.

For the treatment of hyperthyroidism, antithyroid drugs (ATDs), including thiamazole (methimazole – MMI) and propylthiouracil (PTU), remain the first choice. In addition, RAI therapy is an alternative method, especially for multiple focal lesions, when a patient refuses to consent to strumectomy and agranulocytosis after ATDs. In exceptional circumstances, performing a strumectomy should be considered in the case of GO disease or in toxic nodular goiter after achieving euthyroidism when a malignant process is suspected. However, we must be aware of the adverse effect of ATDs, such as IDIN (neutrophil count of $<1.0 \times 10^9/L$) or agranulocytosis ($<0.5 \times 10^9/L$), which occurs in 0.2–0.5% of cases.^{46,51,52} Also, IDIN patients may have similar symptoms to patients with COVID-19 disease, such as a fever, mouth ulceration, a flu-like illness or a sore throat. Hence, it might be questionable whether, in view of this situation, patients should stay at home and undergo self-isolation or if they should visit an endocrinologist or general practitioner. Zhou et al.⁵³ found that 50% of patients who died of COVID-19 had neutropenia which exacerbated the severity of the disease. Additionally, the authors observed that advanced age, high d-dimer levels (greater than 1 $\mu g/mL$) and high Sequential Organ Failure Assessment (SOFA) scores may help clinicians with earlier identification of patients with a poor prognosis. Currently (and also before the global COVID-19 pandemic), an urgent full blood count measurement is recommended to check for IDIN and changing the drug, e.g., MMI to PTU, or discontinuing ATD treatment in neutropenic patients, as well as informing the patient about the results.⁵⁴ On the other hand, COVID-19 infection alone can often lead to lymphopenia and thrombocytopenia. Therefore, the additional problem arises of what to do with a COVID-19 patient who has also developed thyrotoxicosis? Can ATDs be started in the hospital setting or given at home when RAI cannot be used due to COVID-19 infection?^{50–54}

Pregnant women with hyperthyroidism

Pregnant women with hyperthyroidism should take special precautions against COVID-19, especially in later pregnancy, as the severe symptoms requiring hospital

admission are relatively uncommon in young women of reproductive age.⁵⁵ The standard therapy methods should be followed, i.e., PTU is recommended in the 1st trimester of pregnancy (through to 16 weeks), followed by a switch to MMI (a dose ratio of 1:20, i.e., MMI 5 mg/day = PTU 50 mg twice daily) using the lowest dose of ATD possible.⁴⁴ However, the physician should inform such patients about the potential teratogenic effects of MMI⁵³ and aplasia cutis,⁴³ as well as where methimazole/carbimazole embryopathy syndrome coexists with dysmorphic facies,^{57–60} channel or esophageal atresia, abdominal wall defects (e.g., umbilicocele) and other defects (i.e., of the urinary tract, eyes, and ventricular septum).^{61–64} It should be noted that while we can use block replace regimens (BRRs) in adults or children, this therapy method is prohibited in pregnant women. In pregnant women with COVID-19 infection, a higher susceptibility to both maternal and fetal immune complications has been observed.⁶⁵ It has been demonstrated that COVID-19 may exacerbate as well as trigger autoimmune thyroid diseases, especially GD.^{17,49}

Rules for treating hyperthyroidism during the pandemic

Antithyroid drugs

Titration therapy remains the treatment of choice (MMI or PTU). However, due to the COVID-19 pandemic and the lack of access to specialists in Poland and other countries, one of the recommended therapies is the BRR method introduced by Weetman et al. in 1994.⁶⁶ Until now, this therapy method, widely used in the UK, has not been so widespread in Poland but only used by older and more experienced endocrinologists. The BRRs are especially recommended for patients at baseline or with recurrent thyrotoxicosis (regardless of etiology, e.g., GD with or without GO, toxic multinodular goiter and amiodarone-induced thyrotoxicosis).^{66,67} For adults, when the serum fT4 concentration is at the upper normal limit of 30 pmol/L (fT4 ULN – 30 pmol/L), treatment should begin with 20 mg carbimazole or 15 mg methimazole. In the case of fT4 levels of 30–60 pmol/L or >60 pmol/L, the starting point should be a double dose (40 mg carbimazole/30 mg methimazole). At the same time, the patient must be informed about any side effects such as liver dysfunction, neutropenia, agranulocytosis, or congenital disabilities. After 4 weeks of the treatment, TH levels should be checked while continuing ATDs (40 mg carbimazole/30 mg methimazole) at the same dose for all patients. At the same time, L-T4 should be added (75 µg if body weight (BW) ≤55 kg, and 100 µg if BW > 55 kg). The exact algorithm for therapeutic management in both adults and children is presented in the publication by Boelaert et al.⁴¹

Thyroidectomy

The indications for performing surgery have not changed; only the pandemic itself, unfortunately, delays

the implementation of this procedure. A delay of a few months does not seem to be life-threatening for patients. Alternatively, RAI therapy could be another treatment option.

Radioiodine therapy

Oral administration of RAI therapy is used to treat benign thyroid disease, which includes autoimmune hyperthyroidism (GD, mild GO), solitary hyperfunctioning thyroid nodule, toxic multinodular goiter (Plummer's disease), toxic adenoma (Goetsch's disease), and non-toxic goiter (patients with a large retrosternal goiter).⁶⁸ In Poland, RAI deliveries to departments of endocrinology in Poznań and Lublin were only suspended for 3 weeks due to COVID-19, which did not negatively impact the wellbeing of patients. To date, these departments have been following the usual ways of working from before the global pandemic. However, to minimize risk for our patients, we have slightly modified our protocol. We have stopped performing radioiodine uptake (RAIU), both in 5 and 24-hour time point (which allowed us to shorten the waiting time for treatment and thus reduce the number of patients). Patients were admitted to hospital for 1 day, during which all required laboratory tests were performed, including those for thyroid-stimulating hormone (TSH), TH (fT4, fT3), and thyrotropin receptor autoantibodies (TRAb) titers, as well as ^{99m}Tc thyroid scintigraphy and thyroid ultrasound.

We followed the same practices from before the pandemic, excluding the RAI treatment, based on our 20 years of experience and the European Association of Nuclear Medicine guidelines, in line with the words of Stokkel et al.: “Uptake measurements are not absolutely required when fixed activities are used”.⁶⁹ It is noteworthy that our department (in Poznań) is the oldest center in Poland where RAI therapy is in use, being performed for the first time in 1956. We used the following fixed treatment regimen (fixed activity): from 5 (185 mBq) to 10 mCi (370 mBq) to treat GD or mild GO; 15 mCi (555 mBq) for toxic adenoma; from 10 (370 mBq) to 20 mCi (740 mBq) to treat toxic multinodular goiter; and in patients with large retrosternal goiter activity, 20 mCi (740 mBq) (3 times at intervals of 3 months – total activity 60 mCi = 2220 MBq) was administered.

However, the epidemic influenced the more frequent use of ablative rather than fixed activity. Fixed activity often requires repeated doses, which nowadays is inconvenient for both patients and physicians. It should be emphasized that in the pandemic era, hypothyroidism after RAI treatment is the goal of our therapy and not a complication (studies in preparation). Based on our experience, the use of RAI therapy is of increasing importance in the global COVID-19 era, for example, in the case of IDIN after ATDs. In patients with GD, increased morbidity and mortality is observed,^{69,70} although RAI itself does not increase the death rate.⁷¹ However, there are still concerns regarding the influence of RAI therapy on the risk of malignancy.⁷²

Currently (as already mentioned), we use RAI more frequently as the first-choice therapy, mostly because

of the common adverse effect of ATDs – neutropenia (which also occurs in patients infected with SARS-CoV-2) – and, due to the long waiting time to see a specialist. While hypothyroidism after RAI therapy is not an adverse effect but a therapeutic objective about which a family doctor can safely advise, IDIN after ATDs, however, is a difficult challenge even for an experienced endocrinologist and nuclear physician. There is currently no scientific evidence that patients after RAI therapy or thyroidectomy are more likely to become infected with any virus, including the SARS-CoV-2 virus.

Glucocorticoids and immunosuppressive and biological therapy

Patients with GO treated with immunosuppressants (mycophenolate, azathioprine), biological agents (teprotumumab, rituximab and tocilizumab) or glucocorticoids (GCs) belong to vulnerable populations, and are at particularly higher risk from coronavirus.⁷³ These patients are advised to self-isolate for as long as possible.^{74,75}

It is evidenced that GCs can affect serum TSH levels in humans. A study by Samuels and McDaniel⁷⁶ has shown that the physiological dose of hydrocortisone plays a pivotal role in the daily variations of serum TSH levels, with lower levels in the morning and higher levels at night.⁷⁷ The impact of GCs on TSH is still uncertain. One possible hypothesis is that GCs can directly inhibit TSH-releasing factor in the hypothalamus. John et al.⁷⁸ demonstrated that dexamethasone seems to suppress TSH release from thyrotropes in a protein kinase C-dependent manner through the protein annexin 1. The GS receptors are located in the TRH neurons of male rats.⁷² Moreover, a straightforward evidence shows that high-dose GCs may decrease TRH mRNA expression in the paraventricular nucleus of the hypothalamus in humans.⁷⁹ It is worth noting that the routine use of corticosteroids in COVID-19 patients complicates the diagnosis of thyroid function and the interpretation of some reports. As previously suggested, even low doses of corticosteroids can make interpretation of TSH levels much more difficult.⁸⁰

A British study performed by the RECOVERY Collaborative Group⁸¹ demonstrated that dexamethasone could increase survival rates among hospitalized COVID-19 patients receiving either invasive mechanical ventilation or oxygen alone. However, no change in the survival rates was observed among those receiving no respiratory support. Hence, in the most recent WHO guidelines on drugs for COVID-19,⁸² systemic corticosteroids were recommended in patients with acute and critical COVID-19 but not in patients with mild COVID-19 symptoms.

Rituximab is an anti-CD20 antibody which depletes B cells and became a second-line therapy for people with GO.⁸³ Whereas the risk of opportunistic infections is higher in the long term, follow-up trials of rituximab in rheumatoid arthritis show that the risk is likely to be minimal in those patients with GO who are receiving

low doses of this drug.⁸⁴ Teprotumumab (an insulin-like growth factor1 (IGF1) receptor inhibitor) has recently been approved as a therapy for moderate-to-severe GO. Preliminary data have shown that no significant increase in the rate of infections was observed in patients on teprotumumab.⁸⁴ It could be an interesting alternative to GCs during the COVID-19 pandemic, but unfortunately, the high costs and low availability can limit the number of patients who may take advantage of this therapy.

To reduce the signs of ophthalmopathy, especially in times of a global pandemic, it is essential and advisable to strictly discontinue cigarette smoking and reinforce recommendations, including selenium supplementation.⁸⁵ Patients with GO may be more susceptible to developing symptomatic forms of COVID-19 (where SARS-CoV mRNA expression has been found).⁸⁶

Limitations

The main limitation of our study is that no follow-up data were available to analyze the effects of COVID-19 specifically on the thyroid gland. Secondly, the mechanism by which COVID-19 affects thyroid gland function is not well understood and requires further investigation at the molecular level. Thirdly, it is necessary to observe the disease for a longer period to determine whether it increases the incidence of autoimmune diseases of the thyroid gland (GD and HT). However, there are already preliminary meta-analyses that deal with this issue.

Conclusion


In conclusion, COVID-19 can be called the plague of the 21st century, and we may have to live with it until the end of our existence; perhaps, it will be the norm to take precautionary measures. It is currently unknown whether COVID-19 may lead to de novo thyroid dysfunction or at least aggravate an existing thyroid disease. There is no scientific evidence that people with poorly controlled thyroid disease are at higher risk of viral infections. However, it is likely that patients with uncontrolled thyroid dysfunction, especially those with thyrotoxicosis, may be at higher risk of complications (e.g., cytokine storm) from any infection. It should be noted that this group of patients should receive more extensive care, bearing in mind the neutropenia after ATDs, which may mask the symptoms of COVID-19 infection. The COVID-19 pandemic has slightly changed our approach to the BRRs method, which is not commonly used in Poland. As already noted, the role of RAI therapy in the global pandemic has become of greater importance, especially when taking neutropenia into account – the adverse effect of ATDs, which may mask the symptoms of COVID-19 disease caused by SARS-CoV-2. It should be emphasized that special precautions

during the global COVID-19 pandemic should be taken for patients with GO undergoing immunosuppressive medication and pregnant women with hyper- and hypothyroidism.


The COVID-19 pandemic has changed health provision drastically. The use of telemedicine could, in certain situations, lead to improved access to care, shortening waiting times to see a specialist as well as minimalizing the risk of person-to-person transmission of COVID-19. As a result, the burden on healthcare systems could be reduced, but we must remember that this solution is not ideal and there can be a risk of misdiagnosis.

ORCID iDs

Agata Czarnywojtek  <https://orcid.org/0000-0003-3595-8449>

Alicja Ochmańska  <https://orcid.org/0000-0001-7892-6135>


Małgorzata Zgorzalewicz-Stachowiak

 <https://orcid.org/0000-0001-9260-3674>

Nadia Sawicka-Gutaj  <https://orcid.org/0000-0003-1510-4702>

Beata Matyjaszek-Matuszek  <https://orcid.org/0000-0001-7386-8087>

Magdalena Woźniak  <https://orcid.org/0000-0003-0442-7899>

Marek Ruchała  <https://orcid.org/0000-0002-6296-7220>

References

- Gorbalenya AE, Baker SC, Baric RS, et al. Severe acute respiratory syndrome-related coronavirus. The species and its viruses: A statement of the Coronavirus Study Group. *Nat Microbiol.* 2020;5:536–544. doi:10.1038/s41564-020-0695-z
- Hossain MF, Hasana S, Mamun AA, et al. COVID-19 outbreak: Pathogenesis, current therapies, and potentials for future management. *Front Pharmacol.* 2020;16(11):563478. doi:10.3389/fphar.2020.563478
- WHO: Coronavirus disease (COVID-19) pandemic. <https://www.who.int/emergencies/diseases/novel-coronavirus-2019>. Accessed December 23, 2021.
- Hui DS, Azhar EI, Madani TA, et al. The continuing 2019-nCoV epidemic threat of novel coronaviruses to global health: The latest 2019 novel coronavirus outbreak in Wuhan, China. *Int J Infect Dis.* 2020;91:264–266. doi:10.1016/j.ijid.2020.01.009
- Mehta P, McAuley DF, Brown M, Sanchez E, Tattersall RS, Manson JJ; HLH Across Speciality Collaboration, UK. COVID-19: Consider cytokine storm syndromes and immunosuppression. *Lancet.* 2020;395(10229):1033–1034. doi:10.1016/S0140-6736(20)30628-0
- Art. 96a Pf. <https://www.lexlege.pl/prawo-farmaceutyczne/art-96a/> <https://lexlege.pl/prawo-farmaceutyczne/art-96a/>. Accessed February 1, 2021.
- Studdert DM, Hall MA. Disease control, civil liberties, and mass testing: Calibrating restrictions during the Covid-19 pandemic. *N Engl J Med.* 2020;9:383(2):102–104. doi:10.1056/NEJMp2007637
- Guo Y, Korteweg C, McNutt MA, Gu J. Pathogenetic mechanisms of severe acute respiratory syndrome. *Virus Res.* 2008;133(1):4–12. doi:10.1016/j.virusres.2007.01.022.
- Guo YR, Cao QD, Hong ZS, et al. The origin, transmission and clinical therapies on coronavirus disease 2019 (COVID-19) outbreak: An update on the status. *Mil Med Res.* 2020;13(7):11. doi:10.1186/s40779-020-00240-0
- Docea AO, Tsatsakis A, Albulescu D, et al. A new threat from an old enemy: Reemergence of coronavirus. *Int J Mol Med.* 2020;45(6):1631–1643. doi:10.3892/ijmm.2020.4555
- Albano F, Bertagna M, Bertolia G, et al. Incidental findings suggestive of Covid-19 in asymptomatic patients undergoing nuclear medicine procedures in a high prevalence region. *J Nucl Med.* 2020;61(5):632–636. doi:10.2967/jnumed.120.246256
- World Health Organization. WHO Timeline – COVID-19. <https://www.who.int/news-room/detail/27-04-2020-who-timeline-covid-19>. Accessed January 15, 2021.
- Wang W, Ye YX, Yao H. Evaluation and observation of serum thyroid hormone and parathyroid hormone in patients with severe acute respiratory syndrome. *J Chin Antituberculous Assoc.* 2003;25:232–234.
- Ding Y, He L, Zhang Q, et al. Organ distribution of severe acute respiratory syndrome (SARS) associated coronavirus (SARSCoV) in SARS patients: Implications for pathogenesis and virus transmission pathways. *J Pathol.* 2004;203(2):622–630. doi:10.1002/path.1560
- Fliers E, Bianco AC, Langouche L, Boelen A. Thyroid function in critically ill patients. *Lancet Diabetes Endocrinol.* 2015;3(10):816–825. doi:10.1016/S2213-8587(15)00225-9
- Gu J, Gong E, Zhang B, et al. Multiple organ infection and the pathogenesis of SARS. *J Exp Med.* 2005;202(3):415–424. doi:10.1084/jem.20050828
- Chen M, Zhou W, Xu W. Thyroid function analysis in 50 patients with COVID-19: A retrospective study. *Thyroid.* 2021;31(1):8–11. doi:10.1089/thy.2020.0363
- Wei L, Sun S, Zhang J, et al. Endocrine cells of the adenohypophysis in severe acute respiratory syndrome (SARS). *Biochem Cell Biol.* 2010;88(4):723–730. doi:10.1139/O10-022
- Ur A, Verma K. Cytokine storm in COVID-19: A neural hypothesis. *ACS Chem Neurosci.* 2020;11(13):1868–1870. doi:10.1021/acscchemneuro.0c00346
- Merad M, Martin JC. Pathological inflammation in patients with COVID-19: A key role for monocytes and macrophages. *Nat Rev Immunol.* 2020;20:355–362. doi:10.1038/s41577-020-0331-4
- Lechien JR, Chiesa-Estomba CM, De Siaty DR, et al. Olfactory and gustatory dysfunctions as a clinical presentation of mild-to-moderate forms of the coronavirus disease (COVID-19): A multicenter European study. *Eur Arch Otorhinolaryngol.* 2020;277(8):2251–2261. doi:10.1007/s00405-020-05965-1
- Pal R. COVID-19, hypothalamo-pituitary-adrenal axis and clinical implications. *Endocrine.* 2020;68(2):251–252. doi:10.1007/s12020-020-02325-1
- Pal R, Banerjee M. COVID-19 and the endocrine system: Exploring the unexplored. *J Endocrinol Invest.* 2020;43(7):1027–1031. doi:10.1007/s40618-020-01276-8
- Lazartigues E, Qadir MMF, Mauvais-Jarvis F. Endocrine significance of SARS-CoV-2's reliance on ACE2. *Endocrinology.* 2020;161(9):bqaa108. doi:10.1210/endo/bqaa108
- Li MY, Li L, Zhang Y, Wang XS. Expression of the SARS-CoV-2 cell receptor gene ACE2 in a wide variety of human tissues. *Infect Dis Poverty.* 2020;9(1):45. doi:10.1186/s40249-020-00662-x
- Smallridge RC, Rogers J, Verma PS. Serum angiotensin-converting enzyme: Alterations in hyperthyroidism, hypothyroidism, and subacute thyroiditis. *JAMA.* 1983;250(18):2489–2493. doi:10.1001/jama.250.18.2489
- Rotondi M, Coperchini F, Ricci G, et al. Detection of SARSCoV-2 receptor ACE-2 mRNA in thyroid cells: A clue for COVID-19-related subacute thyroiditis. *J Endocrinol Invest.* 2020;44(5):1085–1090. doi:10.1007/s40618-020-01436-w
- Reed HL, Silverman ED, Shakir KM, Dons R, Burman KD, O'Brian JT. Changes in serum triiodothyronine (T3) kinetics after prolonged Antarctic residence: The polar T3 syndrome. *J Clin Endocrinol Metab.* 1990;70(4):965–974. doi:10.1210/jcem-70-4-965
- Lui DTW, Lee CH, Chow WS, et al. Thyroid dysfunction in relation to immune profile, disease status and outcome in 191 patients with COVID-19. *J Clin Endocrinol Metab.* 2020;3:dgaag813. doi:10.1210/clinem/dgaa813
- Chen T, Wu D, Chen H, et al. Clinical characteristics of 113 deceased patients with coronavirus disease 2019: Retrospective study [published correction appears in *BMJ*. 2020;368:m1295]. *BMJ.* 2020;368:1–12. doi:10.1136/bmj.m1091
- Gao W, Guo W, Guo Y, et al. Thyroid hormone concentrations in severely or critically ill patients with COVID-19. *J Endocrinol Invest.* 2020;44(5):1031–1040. doi:10.1007/s40618-020-01460-w
- Tomer Y, Huber A. The etiology of autoimmune thyroid disease: A story of genes and environment. *J Autoimmun.* 2009;32(3–4):231–239. doi:10.1016/j.jaut.2009.02.007
- Tomer Y. Genetic susceptibility to autoimmune thyroid disease: Past, present, and future. *Thyroid.* 2010;20(7):715–725. doi:10.1089/thy.2010.1644
- Antonelli A, Ferrari SM, Ragusa F, et al. Graves' disease: Epidemiology, genetic and environmental risk factors and viruses. *Best Pract Res Clin Endocrinol Metab.* 2020;34(1):101387. doi:10.1016/j.beem.2020.101387
- Brancatella A, Ricci D, Viola N, Sgrò D, Santini F, Latrofa F. Subacute thyroiditis after SARS-COV-2 infection. *J Clin Endocrinol Metab.* 2020;105(7):dgaag276. doi:10.1210/clinem/dgaa276

36. Dworakowska D, Grossman AB. Thyroid disease in the time of COVID-19. *Endocrine*. 2020;68(3):471–474. doi:10.1007/s12020-020-02364-8
37. European Thyroid Association. COVID-19: Information for patients with thyroid diseases. <https://www.eurothyroid.com/news/covid19-thyroid-diseases.html>. Accessed February 1, 2021.
38. American Thyroid Association. Novel coronavirus (COVID-19) and the thyroid: Resources. <https://www.thyroid.org/covid-19>. Accessed February 1, 2021.
39. Conigliaro P, D'Antonio A, Pinto, et al. Autoimmune thyroid disorders and rheumatoid arthritis: A bidirectional interplay. *Autoimmun Rev*. 2020;19(6):102529. doi:10.1016/j.autrev.2020.102529
40. Figueroa-Parra GM, Aguirre-Garcia CM, Gamboa-Alonso CM, Camacho-Ortiz A, Galarza-Delgado DA. Are my patients with rheumatic diseases at higher risk of COVID-19? *Ann Rheum Dis*. 2020;79(6):839–840. doi:10.1136/annrheumdis-2020-217322.
41. Boelaert K, Visser W, Taylor P, Moran C, Léger J, Persani L. Endocrinology In the time of COVID-19: Management of hyperthyroidism and hypothyroidism. *Eur J Endocrinol*. 2020;183(1):G33–G39. doi:10.1530/EJE-20-0445
42. Chaker L, Bianco AC, Jonklaas J, Peeters RP. Hypothyroidism. *Lancet*. 2017;390(10101):1550–1562. doi:10.1016/S0140-6736(17)30703-1
43. Art. 96a Pf. <https://www.lexlege.pl/prawo-farmaceutyczne/art-96a/>.
44. Stagnaro-Green A, Abalovich M, Alexander EK, et al; American Thyroid Association Taskforce on Thyroid Disease During Pregnancy and Postpartum. Guidelines of the American Thyroid Association for the diagnosis and management of thyroid disease during pregnancy and postpartum. *Thyroid*. 2011;21(10):1081–1125.
45. De Groot L, Abalovich M, Alexander EK, et al. Management of thyroid dysfunction during pregnancy and postpartum: An Endocrine Society clinical practice guideline. *J Clin Endocrinol Metab*. 2012;97(8):2543–2565. doi:10.1210/jc.2011-2803
46. Lania A, Sandri MT, Cellini M, Mirani M, Lavezzi E, Mazziotti G. Thyrotoxicosis in patients with COVID-19: The THYRCOV study. *Eur J Endocrinol*. 2020;183(4):381–387. doi:10.1530/EJE-20-0335
47. Brancatella A, Ricci D, Cappellani D, Sgrò VD, Santini F, Latrofa F. Is subacute thyroiditis an underestimated manifestation of SARS-CoV-2 infection? Insights from a case series. *J Clin Endocrinol Metab*. 2020;105(10):dgaa537. doi:10.1210/clinem/dgaa537
48. Sohrabpour S, Heidari F, Karimi E, Ansari R, Tajdini A, Heidari F. Subacute thyroiditis in COVID-19 patients. *Eur Thyroid J*. 2020;9(6):321–323. doi:10.1159/000511707
49. Mateu-Salat M, Urgell E, Chico A. SARS-CoV-2 as a trigger for autoimmune disease: Report of two cases of Graves' disease after COVID-19. *J Endocrinol Invest*. 2020;43(10):1527–1528. doi:10.1007/s40618-020-01366-7
50. Khoo B, Tan T, Clarke SA, et al. Thyroid function before, during and after COVID-19. *J Clin Endocrinol Metab*. 2020;106(2):e803–e811. doi:10.1210/clinem/dgaa830
51. De Leo S, Lee SY, Braverman LE. Hyperthyroidism. *Lancet*. 2016;388(10047):906–918. doi:10.1016/S0140-6736(16)00278-6
52. Burch HB, Cooper DS. Antithyroid drug therapy: 70 years later. *Eur J Endocrinol*. 2018;179(5):R261–R274. doi:10.1530/EJE-18-0678
53. Zhou F, Yu T, Du R, et al. Clinical course and risk factors for mortality of adult in patients with COVID-19 in Wuhan, China: A retrospective cohort study. *Lancet*. 2020;395(10229):1054–1062. doi:10.1016/S0140-6736(20)30566-3
54. Ross DS, Burch HB, Cooper DS, et al. American Thyroid Association guidelines for diagnosis and management of hyperthyroidism and other causes of thyrotoxicosis. *Thyroid*. 2016;26(10):1343–1421.
55. Terpos E, Ntanasis-Stathopoulos I, Elalamy I, et al. Hematological findings and complications of COVID-19. *Am J Hematol*. 2020;95(7):834–847. doi:10.1002/ajh.25829.
56. Royal College of Obstetricians and Gynaecologists. Coronavirus (COVID-19). Infection in Pregnancy. <https://www.rcog.org.uk/globalassets/documents/guidelines/2020-04-17-coronavirus-covid-19-infection-in-pregnancy.pdf>.
57. Li C, Shan Z, Mao J, et al. Assessment of thyroid function during first-trimester pregnancy: What is the rational upper limit of serum TSH during the first trimester in Chinese pregnant women? *J Clin Endocrinol Metab*. 2014;99(1):73–79. doi:10.1210/jc.2013-1674
58. Anderson SL, Olsen J, Laurberg P. Antithyroid drug side effects in the population and in pregnancy. *J Clin Endocrinol Metab*. 2016;101(4):1606–1614.
59. Milham SJ, Elledge W. Maternal methimazole and congenital defects in children. *Teratology*. 1972;5:125–126. doi:10.1002/tera.1420050117
60. Clementi M, Di Gianantonio E, Cassina M, Leoncini E, Botto LD, Mastroiaco P; SAFE-Med Study Group. Treatment of hyperthyroidism in pregnancy and birth defects. *J Clin Endocrinol Metab*. 2010;95(11):E337–E341. doi.org/10.1210/jc.2010-0652
61. Foulds N, Walpole I, Elmslie F, Mansour S. Carbimazole embryopathy: An emerging phenotype. *Am J Med Genet*. 2015;132A(2):130–135. doi:10.1002/ajmg.a.30418
62. Yoshihara A, Noh J, Yamaguchi T, et al. Treatment of Graves' disease with antithyroid drugs in the first trimester of pregnancy and the prevalence of congenital malformation. *J Clin Endocrinol Metab*. 2012;97(7):2396–2403. doi:10.1210/jc.2011-2860
63. Andersen SL, Olsen J, Wu CS, et al. Birth defects after early pregnancy use of antithyroid drugs: A Danish nationwide study. *J Clin Endocrinol Metab*. 2013;98(11):4373–4381. doi:10.1210/jc.2013-2831
64. Andersen SL, Laurberg P. Antithyroid drugs and congenital heart defects: Ventricular septal defect is part of the methimazole/carbimazole embryopathy. *Eur J Endocrinol*. 2014;171(5):C1–C3. doi:10.1530/EJE-14-0524
65. Liu H, Wang LL, Zhao SJ, Kwak-Kim J, Mor G, Liao AH. Why are pregnant women susceptible to COVID-19? An immunological viewpoint. *J Reprod Immunol*. 2020;139:103122. doi: 10.1016/j.jri.2020.103122
66. Weetman AP, Pickerill AP, Watson P, Chatterjee VK, Edwards OM. Treatment of Graves' disease with the block-replace regimen of antithyroid drugs: The effect of treatment duration and immunogenetic susceptibility on relapse. *Q J Med*. 1994;87(6):337–334. PMID:7913766.
67. National Institute for Health and Care Excellence. Thyroid disease: Assessment and management. <https://www.nice.org.uk/guidance/ng145>. Accessed January 14, 2021.
68. Abraham P, Avenell A, McGeoch S, et al. Antithyroid drug regimen for treating Graves' hyperthyroidism. *Cochrane Database Syst Rev*. 2010;2010:CD003420. doi:10.1002/14651858
69. Stokkel MPM, Handkiewicz-Junak D, Lassmann JM, Clark LF, Bevan JS. EANM procedure guidelines for therapy of benign thyroid disease. *Eur J Nucl Med Mol Imaging*. 2020;37(11):2218–2228. doi:10.1007/s00259-010-1536-8
70. Brandt F, Thvilum M, Almind D, et al. Graves' disease and toxic nodular goiter are both associated with increased mortality but differ with respect to the cause of death: A Danish population-based register study. *Thyroid*. 2013;23(4):408–413. doi:10.1089/thy.2012.0500
71. Schwensen CF, Brandt F, Hegedus L, Brix TH. Mortality in Graves' orbitopathy is increased and influenced by gender, age and pre-existing morbidity: A nationwide Danish register study. *Eur J Endocrinol*. 2017;176(6):669–676. doi:10.1530/eje-16-0954
72. Kitahara CM, Berrington de Gonzalez A, Bouville A, et al. Association of radioactive iodine treatment with cancer mortality in patients with hyperthyroidism. *JAMA Intern Med*. 2019;179(8):1034–1042. doi:10.1001/jamainternmed.2019.0981
73. Bonnema SJ, Hegedus L. Radioiodine therapy in benign thyroid diseases: Effects, side effects, and factors affecting therapeutic outcome. *Endocr Rev*. 2012;33(6):920–980. doi:10.1210/er.2012-1030
74. Taylor PN, Zhang L, Lee RWJ, et al. New insights into the pathogenesis and nonsurgical management of Graves orbitopathy. *Nat Rev Endocrinol*. 2020;16(2):104–116. doi:10.1038/s41574-019-0305-4
75. UK Government, Department of Health & Social Care. Guidance on shielding and protecting people who are clinically extremely vulnerable from COVID-19. <https://www.gov.uk/government/publications/guidance-on-shielding-and-protecting-extremely-vulnerable-persons-from-covid-19/guidance-on-shielding-and-protecting-extremely-vulnerable-persons-from-covid-19>. Accessed February 1, 2021.
76. Samuels MH, McDaniel PA. Thyrotropin levels during hydrocortisone infusions that mimic fasting-induced cortisol elevations: A clinical research center study. *J Clin Endocrinol Metab*. 1997;82(11):3700–3704. doi:10.1210/jcem.82.11.4376
77. Samuels MH. Effects of variations in physiological cortisol levels on thyrotropin secretion in subjects with adrenal insufficiency: A clinical research center study. *J Clin Endocrinol Metab*. 2000;85(4):1388–1393. doi:10.1210/jcem.85.4.6540
78. John CD, Christian HC, Morris JF, Flower RJ, Solito E, Buckingham JC. Kinase-dependent regulation of the secretion of thyrotrophin and luteinising hormone by glucocorticoids and annexin 1 peptides. *J Neuroendocrinol*. 2003;15(10):946–957. doi:10.1046/j.1365-2826.2003.01081

79. Cintra A, Fuxe K, Wikström AC, Visser T, Gustafsson JA. Evidence for thyrotropin-releasing hormone and glucocorticoid receptor-immunoreactive neurons in various preoptic and hypothalamic nuclei of the male rat. *Brain Res.* 1990;506(1):139–144. doi:10.1007/BF02686119
80. Alkemade A, Unmehopa UA, Wiersinga WM, Swaab DF, Fliers E. Glucocorticoids decrease thyrotropin-releasing hormone messenger ribonucleic acid expression in the paraventricular nucleus of the human hypothalamus. *J Clin Endocrinol Metab.* 2005;90(1):323–327.
81. Horby P, Lim WS, Emberson JR, et al; RECOVERY Collaborative Group. Dexamethasone in hospitalised patients with Covid-19: Preliminary report. *N Engl J Med.* 2021;384(8):693–704. doi:10.1056/NEJMoa2021436
82. Lamontagne F, Agoritsas T, Macdonald H, et al. A living WHO guideline on drugs for Covid-19. *BMJ.* 2020;370:m3379. doi:10.1136/bmj.m3379
83. Bartalena L, Baldeschi L, Boboridis K, et al. The 2016 European Thyroid Association/European Group on Graves' orbitopathy guidelines for the management of Graves' orbitopathy. *Eur Thyroid J.* 2016;5:9–26. doi:10.1159/000443828
84. van Vollenhoven RF, Emery P, Bingham CO, et al. Long-term safety of rituximab in rheumatoid arthritis: 9.5-year follow-up of the global clinical trial programme with a focus on adverse events of interest in RA patients. *Ann Rheum Dis.* 2013;72(9):1496–1502. doi:10.1136/annrheumdis-2012-201956
85. Kahaly GJ, Bartalena L, Hegedus L, Leenhardt L, Poppe K, Pearce SH. 2018 European Thyroid Association guideline for the management of Graves' hyperthyroidism. *Eur Thyroid J.* 2018;7(4):167–186. doi:10.1159/000490384
86. Xia J, Tong J, Liu M, Shen Y, Guo D. Evaluation of coronavirus in tears and conjunctival secretions of patients with SARS-CoV-2 infection. *J Med Virol.* 2020;92(6):589–594. doi:10.1002/jmv.25725

Analysis and comparison of autologous platelet-rich plasma preparation systems used in the treatment of enthesopathies: A preliminary study

Maciej Dejne^{1,2,A–F}, Helena Moreira^{3,A–C}, Sylwia Płaczowska^{4,B}, Piotr Morasiewicz^{5,A,E}, Ewa Barg^{3,A,E}, Jarosław Witkowski^{1,2,D,E}, Paweł Reichert^{1,A,E,F}

¹ Department of Trauma and Hand Surgery, Wrocław Medical University, Poland

² Department of Sports Medicine, Wrocław Medical University, Poland

³ Department of Basic Medical Sciences, Wrocław Medical University, Poland

⁴ Diagnostic Laboratory for Teaching and Research, Department of Laboratory Diagnostics, Wrocław Medical University, Poland

⁵ Department of Orthopaedic and Trauma Surgery, Institute of Medical Sciences, University of Opole, Poland

A – research concept and design; B – collection and/or assembly of data; C – data analysis and interpretation;

D – writing the article; E – critical revision of the article; F – final approval of the article

Advances in Clinical and Experimental Medicine, ISSN 1899–5276 (print), ISSN 2451–2680 (online)

Adv Clin Exp Med. 2021;30(7):757–764

Address for correspondence

Maciej Dejne

E-mail: maciejdejnek@gmail.com

Funding sources

This research was financially supported by the Ministry of Health subvention according to number of STM.E067.20.112 from the IT Simple system of Wrocław Medical University.

Conflict of interest

None declared

Received on December 30, 2020

Reviewed on February 6, 2021

Accepted on March 26, 2021

Published online on June 11, 2021

Cite as

Dejne M, Moreira H, Płaczowska S, et al. Analysis and comparison of autologous platelet-rich plasma preparation systems used in the treatment of enthesopathies:

A preliminary study. *Adv Clin Exp Med.* 2021;30(7):757–764.

doi:10.17219/acem/135045

DOI

10.17219/acem/135045

Copyright

© 2021 by Wrocław Medical University

This is an article distributed under the terms of the Creative Commons Attribution 3.0 Unported (CC BY 3.0)

(<https://creativecommons.org/licenses/by/3.0/>)

Abstract

Background. Autologous platelet-rich plasma (PRP) injection is an alternative but widely accepted method for the treatment of degenerative changes in tendon attachments known as enthesopathies. The PRP is considered a safe source for high concentrations of the growth factors involved in the healing process. Despite initial promising outcomes, many recent studies report conflicting results for this treatment. This may be due to differences in the concentrations of platelets and growth factors in PRPs obtained using different methods.

Objectives. The aim of this study was to compare PRP preparation systems in terms of morphotic components and selected growth factors to find the most appropriate procedure for the treatment of enthesopathies.

Materials and methods. Whole blood samples from 6 healthy male volunteers were collected. Using different commercial kits (Mini GPS III System, Arthrex ACP, and Xerthra, Dr. PRP), 4 PRPs were prepared from the blood of each participant. All samples were analyzed for the content of morphotic components and the following growth factors: transforming growth factor- β 1 (TGF- β 1), epidermal growth factor (EGF), vascular endothelial growth factor (VEGF), and platelet-derived growth factor AA (PDGF-AA).

Results. The Mini GPS III produced PRP with the highest concentration of platelets and white blood cells (WBC) compared to the other systems included in the study. Significant differences in the levels of EGF and PDGF-AA were found only between the Mini GPS III and Arthrex ACP. There was positive correlation between the content of platelets and the levels of PDGF-AA and EGF. The red blood cells (RBC) concentration positively correlated with PDGF-AA, EGF and VEGF.

Conclusions. This study showed differences between the morphotic components and levels of selected growth factors in PRP obtained with the different preparation methods. Due to insufficient data, we cannot argue for or against any of the studied protocols for the treatment of enthesopathy. Further studies on a larger population are required to validate our results.

Key words: platelet-rich plasma, growth factors, platelet-derived growth factor, enthesopathy

Background

Enthesopathies are degenerative changes in the site of tendon attachment to the bone. This disease can affect many different sites in the human body. The most common and best described are changes in the attachment of wrist extensors or flexors to humeral epicondyles, the Achilles tendon, patellar tendon, suprascapular tendon, or plantar fascia.¹ The main symptoms reported by patients include local pain and limitations in sport, work and daily activities. The cause of the disease still remains unclear. However, the most widely accepted theory is the accumulation of microinjuries resulting from repeated overloads that exceed the body's compensatory capacity. The change in the dogma of the inflammatory nature of this disease was the result of numerous histopathological studies that found disorganized tissue and neovessels within the involved tendon, but only few inflammatory cells. In many cases, symptoms resolve spontaneously and properly selected exercises help prevent them in the future. Unfortunately, some cases turn into a chronic condition that is very difficult to treat, and sometimes only surgical excision of the affected tissue can lead to improvement.

Due to the lack of effective therapy, many different methods have been proposed, and autologous platelet-rich plasma (PRP) is one of the most promising treatments.¹⁻³ For this procedure, the patient's blood is collected and centrifuged to isolate the platelet-rich part of the plasma. This plasma is then administered into the affected tissue, typically by local injection. The α -granules of platelets contain significant amounts of cytokines involved in tissue healing.⁴ It is expected that PRP containing a platelet concentration above the baseline will contain a significantly higher concentration of important cytokines, chemokines and growth factors.⁵ Numerous *in vitro* studies have shown that these biologically active components play a key role in tissue repair by stimulating proliferation, chemotaxis, cell differentiation, and angiogenesis.^{4,6,7}

The acceleration of natural tissue healing processes by PRP administration was expected to revolutionize the treatment of injuries and chronic degenerative diseases like enthesopathy. Other diseases in which the natural balance between anabolic and catabolic processes is disrupted are also candidates for PRP treatment. Positive clinical outcomes have been reported for various conditions including bone nonunions, osteonecrosis, difficult-to-heal wounds, osteoarthritis, and sports injuries.⁸⁻¹²

The enthusiastic adoption of this method began to wane with the increasing appearance of studies showing conflicting results.¹²⁻¹⁴ A major problem with this body of research is the lack of a standardized definition for PRP. Many manufacturers have released commercially available kits for the easy preparation of PRP in an outpatient setting.^{8,15} These kits differ from each other in various parameters, such as the amount of material collected from the patient, the type of anticoagulant used, the structure

of the separator, the length and speed of centrifugation, the method of extraction and activation, the assumed concentration of platelets and leukocytes in final product, and its consistency.¹⁶⁻¹⁹ These differences have made it almost impossible to compare the results of studies where PRP was prepared according to different protocols.

The answer to the above problem should be a reliable classification system for PRP. One of the classification systems designed to standardize the nomenclature is based on the content of fibrin and leukocytes in the PRP. In this system, 4 main classes of autologous PRPs are identified — PRP with a low content of leukocytes (P-PRP), PRP with a high content of leukocytes (L-PRP), platelet-rich fibrin with a low content of leukocytes (P-PRF), and platelet-rich fibrin with a high content of leukocytes (L-PRF).²⁰ However, these divisions do not include the concentration or the absolute number of platelets. Another classification system proposed to improve the comparison of results from different publications is the PAW system. This system is based on the 3 most important components of PRP: the absolute number of platelets, the method of their activation and the leukocyte content.²¹

The classification systems mentioned above do not solve all the problems connected with studies on PRP. The multiplicity of variables still makes it almost impossible to predict the content of different growth factors in PRP.

Objectives

The main goal of this study is to compare the PRP preparation systems available on the local market in terms of morphotic components and selected growth factors.

The results of such an analysis are essential for selecting the most appropriate procedure for daily clinical practice and for further research on the treatment of degenerative conditions. Regarding legal issues, only those systems that are officially registered for the treatment of enthesopathy were included in the study. However, our results can be helpful in decision-making for all conditions treated with PRP.

Materials and methods

Study design and setting

This controlled laboratory study was conducted at Wrocław Medical University, Poland, in the Diagnostic Laboratory for Teaching and Research by clinicians and laboratory researchers. All procedures on human participants were conducted in accordance with the ethical standards of Wrocław Medical University (Poland) and with the 1964 Helsinki Declaration and its later amendments. The study was approved by the local bioethics committee (Ethics Committee of Wrocław Medical University, 30.03.2020, approval No. KB 163/2020).

Participants

Six healthy male volunteers similar in age were asked for a whole blood donation. The number of participants included reflects the preliminary nature of the study. Criteria for inclusion in the study were an age of 27–28 years, absence of significant disease and conditions that could affect the blood morphotic components, at least 2 weeks without taking any drug that may interfere with the function of platelets, and a non-smoking status.

Data sources and measurement

Approximately 75 mL of whole blood was collected from each participant under aseptic conditions and immediately divided into 5 samples. First, ~2 mL was transferred to a tube with ethylenediaminetetraacetic acid (EDTA) and then analyzed for morphotic components using an automatic laboratory analyzer (Mindray BC-5150; Shenzhen Mindray Bio-Medical Electronics Co., Ltd, Shenzhen, China). The 4 remaining blood samples from each participant were used to prepare 4 different PRPs according to the protocols provided by the manufacturers. Four commercial PRP systems that were available on the local medical market were chosen as they are frequently used for the treatment of orthopedic conditions. The systems used included the Arthrex Autologous Conditioned Plasma (ACP) Double Syringe system (Arthrex Inc., Naples, USA), the Mini GPS III Platelet Concentration system (Biomet Inc., Warsaw, USA), the Xerthra PRP kit (Biovico Sp. z o.o., Gdynia, Poland), and Dr. PRP (Rmedica, Seoul, South Korea).

The Arthrex ACP Double Syringe system required 13.5 mL of whole blood collected into a specially designed double-syringe system within 1.5 mL ACD-A added as an anticoagulant. The samples were spun at 1500 rpm for 5 min in a dedicated centrifuge provided by the local distributor. After centrifugation, conditioned plasma in a volume of 4 mL was transferred to the inner syringe in the double-syringe system and was ready to use.

The Mini GPS III Platelet Concentration system has a specially designed valve for automatic PRP separation. After mixing 27 mL of whole blood with 3 mL of ACD-A anticoagulant, the samples were placed in a separator and spun at 3200 rpm for 15 min in a dedicated centrifuge provided by the local distributor. The platelet-poor plasma was then removed and about 3 mL of leukocyte-rich (LR)-PRP was collected into a new sterile syringe.

The Xerthra PRP kit required 13.5 mL of whole blood that was mixed with 1.5 mL of 3.13% sodium citrate as an anticoagulant. The samples were spun at 3500 rpm for 5 min in a dedicated centrifuge provided by the local distributor, transferring plasma into the neck of the tube and removing platelet poor plasma 1.5 mL of leukocyte-poor (LP)-PRP was then collected into a new sterile syringe.

Whole blood in a volume of 18 mL mixed with 2 mL of 3.13% sodium citrate was transferred into the Dr. PRP

tube. The samples were then spun for 4 min at 3100 rpm in a dedicated centrifuge provided by the local distributor. Following this, the piston in the device was used to separate the plasma from the red blood cells (RBC) by moving it into the neck of the tube. After removing platelet poor plasma, LP-PRP in a volume of 3 mL was collected into a new sterile syringe.

All 24 samples of prepared plasma were analyzed for the content of morphotic components using an automatic laboratory analyzer (Mindray BC-5150). The count and concentration of white blood cells (WBC), RBC and platelets were evaluated immediately after collection of the samples. Platelet capture efficiency (PCE) was calculated using the following formula:

$$\text{obtained PRP volume [mL]} \times \text{platelets concentration in PRP (G/L)/whole blood collected volume [mL]} \times \text{platelets concentration in whole blood (G/L)}$$

Following collection, 1 mL of each PRP sample was placed into an Eppendorf polypropylene tube and went through the platelet activation process developed by Zimmermann et al.²² The activation procedure involved freezing at -80°C for 30 min, followed by thawing to room temperature for another 30 min and freezing for a second time at -80°C . The samples were then stored at -80°C until further analysis.

Before cytokine measurement, the PRP samples were thawed completely at room temperature and spun for 5 min at 2.5 rpm using a Micro Star 17 centrifuge (VWR International Company, ThermoElectron LED, Langensfeld, Germany). A custom-designed bead-based multiplex immunoassay that uses fluorescence-encoded beads and flow cytometry (LEGENDplex™; BioLegend, San Diego, USA) was used to quantify the following platelet growth factors: transforming growth factor- β 1 (TGF- β 1, free active), epidermal growth factor (EGF), vascular endothelial growth factor (VEGF), and platelet-derived growth factor-AA (PDGF-AA). The concentration of a particular cytokine was determined by means of a standard curve generated during the performance of the test. The analyses were done according to the manufacturer's instructions. The samples were acquired on CyFlow SPACE and a CyFlow CUBE flow cytometer (Sysmex-Partec, Görlitz, Germany) by applying a 488 nm laser with a 536/40 (BP) filter for the PE fluorochrome, and a 638 nm laser with a 675/20 (BP) filter for the APC fluorochrome. The results were analyzed with LEGENDplex™ Data Analysis Software v. 8.0 (Vigene Tech Inc., Carlisle, USA).

All data obtained and analyzed in this study are quantitative. To avoid bias in the obtained results, all PRP samples were made with the same great care.

Statistical methods

All data were analyzed using STATISTICA v. 13.3 software (StatSoft Inc., Tulsa, USA). Due to the lack of confirmation of to a normal distribution, as assessed with

the Shapiro–Wilk test, nonparametric methods were used (Kruskal–Wallis one-way analysis of variance (ANOVA) with Dunn's post hoc test and Spearman's correlation). Statistical significance was established at the level of $p < 0.05$.

Results

Study participants

Six volunteers, aged 27.8 ± 0.4 years, met the criteria for inclusion and were enrolled in the study. The average body mass index (BMI) of the volunteers was $25.82 \pm 2.12 \text{ kg/m}^2$. Each participant signed an informed consent form.

Main results

Whole blood count

The distribution of the cellular components of whole blood samples collected from all participants are included in Table 1. All results were in the range of normal physiological values.

Concentration of platelets

The platelet concentrations for the PRP samples are illustrated in Fig. 1. Only 1 single sample of PRP delivered by Xerthra PRP kit had a lower concentration of platelets than baseline. The highest platelet concentration was produced with the Mini GPS III System ($1266.33 \pm 347.96 \times 10^9/\text{L}$), and the lowest with Arthrex ACP ($395 \pm 110.15 \times 10^9/\text{L}$). Statistical analysis showed a significant difference between the 2 systems mentioned above ($p = 0.003$), and between the Mini GPS III and Xerthra PRP kits ($513.67 \pm 255.99 \times 10^9/\text{L}$; $p = 0.04$). There was no significant difference when compared to Dr. PRP ($504.83 \pm 106.29 \times 10^9/\text{L}$; $p > 0.05$).

PCE

The PCE results are illustrated in Fig. 2. The highest PCE score was obtained from the Mini GPS III system ($53.76 \pm 6.66\%$), and the lowest from the Xerthra PRP kit

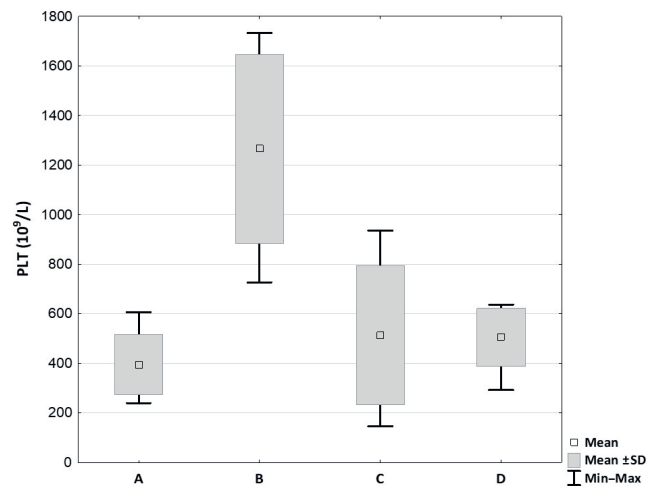


Fig. 1. Platelet concentration in PRP obtained using different systems

A – Arthrex ACP; B – Mini GPS III System; C – Xerthra PRP kit; D – Dr. PRP.

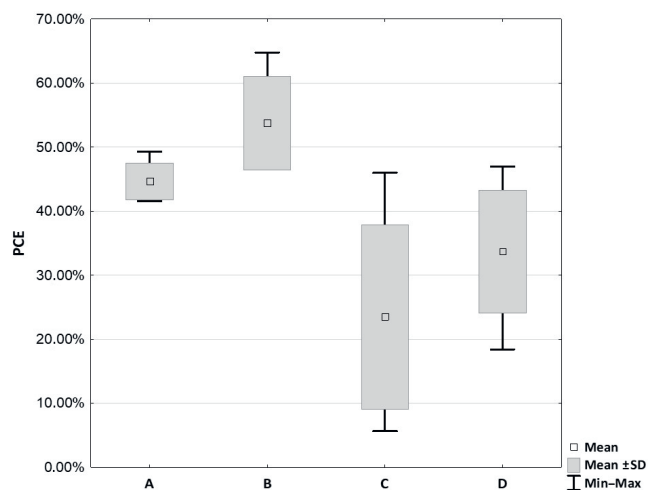


Fig. 2. Platelet capture efficiency in PRP obtained using different systems

A – Arthrex ACP; B – Mini GPS III System; C – Xerthra PRP kit; D – Dr. PRP.

($23.50 \pm 13.13\%$). The Mini GPS III System provided a significantly higher PCE than the Xerthra PRP kit ($p = 0.001$) and Dr. PRP ($33.68 \pm 8.78\%$; $p = 0.02$). Although the PCE

Table 1. Whole blood characteristics from all participants (NR 1–6)

Blood parameter	Participant						Mean
	NR1	NR2	NR3	NR4	NR5	NR6	
RBC [$10^{12}/\text{L}$]	4.69	4.47	4.97	5.82	5.5	5.04	5.08 ± 0.46
Platelets [$10^9/\text{L}$]	171	288	244	226	364	264	259.5 ± 59.09
WBC [$10^9/\text{L}$]	4.79	5.62	7.22	6.5	7.64	6.19	6.33 ± 0.95
Neutrophils [$10^9/\text{L}$]	2.52	3.01	4.13	3.34	4.37	2.97	3.39 ± 0.66
Lymphocytes [$10^9/\text{L}$]	1.79	1.83	2.41	2.44	2.53	2.53	2.26 ± 0.32
Monocytes [$10^9/\text{L}$]	0.34	0.4	0.53	0.49	0.54	0.45	0.46 ± 0.07
Eosinophils [$10^9/\text{L}$]	0.11	0.34	0.11	0.18	0.17	0.21	0.19 ± 0.08
Basophils [$10^9/\text{L}$]	0.03	0.04	0.04	0.05	0.03	0.03	0.04 ± 0.01

RBC – red blood cells; WBC – white blood cells.

obtained from the Arthrex ACP kit ($44.66 \pm 2.65\%$) was lower than that for the Mini GPS III and higher than that for the Xerthra PRP and Dr. PRP kits, the differences were not statistically significant ($p = 0.061$, $p = 0.22$, $p = 1$, respectively).

Concentration of WBC

The WBC concentrations for the PRP samples are illustrated in Fig. 3. The highest concentrations of WBC were obtained with the Mini GPS III system ($34.81 \pm 9.59 \times 10^9/L$), and it was the only system that produced a WBC concentration above the whole blood baseline level. Statistical analysis showed significant differences when comparing Mini GPS III to Arthrex ACP ($0.78 \pm 0.73 \times 10^9/L$; $p = 0.02$) and Dr. PRP ($0.50 \pm 0.59 \times 10^9/L$; $p = 0.001$), but not to the Xerthra PRP kit ($1.91 \pm 1.87 \times 10^9/L$; $p = 0.16$).

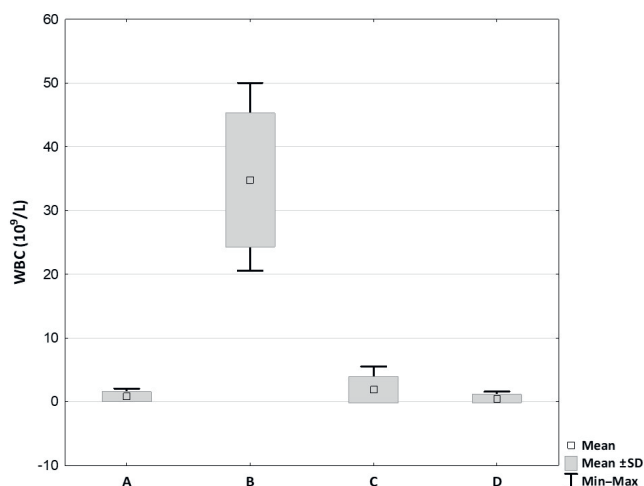


Fig. 3. White blood cells concentration in PRP obtained using different systems

A – Arthrex ACP; B – Mini GPS III System; C – Xerthra PRP kit; D – Dr. PRP.

Concentration of RBC

The RBC concentrations for the PRP samples are illustrated in Fig. 4. One of the goals of producing PRP is to separate it from plasma containing RBC. Hence, the RBC concentration in PRP can be treated as a measure of purification. The Mini GPS III System delivered PRP with the highest concentration of RBC ($1.48 \pm 0.88 \times 10^{12}/L$), which was significantly higher than

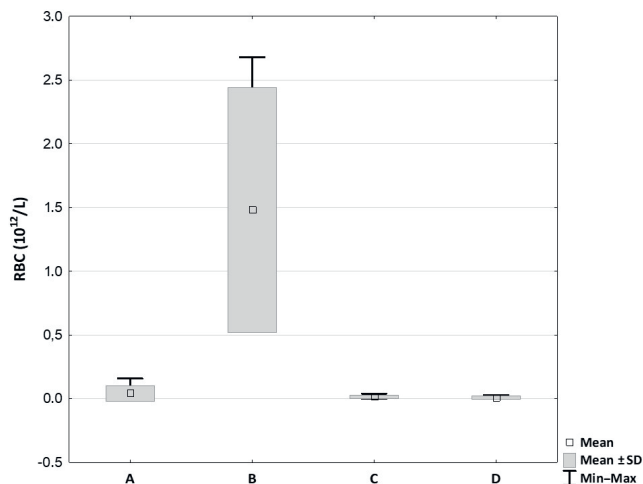


Fig. 4. Red blood cells concentration in PRP obtained using different systems

A – Arthrex ACP; B – Mini GPS III System; C – Xerthra PRP kit; D – Dr. PRP.

Arthrex ACP ($0.04 \pm 0.06 \times 10^{12}/L$; $p = 0.045$), the Xerthra PRP kit ($0.02 \pm 0.01 \times 10^{12}/L$; $p = 0.04$) and Dr. PRP ($0.01 \pm 0.01 \times 10^{12}/L$; $p = 0.004$). No significant differences were found between the other systems.

Concentration of growth factors

All obtained growth factor concentrations are included in Table 2. Statistical analysis showed that the Mini GPS III System compared to Arthrex ACP delivered PRP with significantly higher levels of EGF (364.1 ± 180.16 pg/mL compared to 107.37 ± 95.12 pg/mL; $p = 0.04$) and PDGF-AA ($98,698 \pm 23,843.58$ pg/mL compared to $33,172.5 \pm 13,266.38$ pg/mL; $p = 0.02$). There were no significant differences among the other systems and growth factors.

Correlation between growth factors and morphotic components

All Spearman’s correlations are presented in Fig. 5. There was a significant positive correlation between platelet concentration and both EGF and PDGF-AA (Spearman’s R values 0.46 and 0.58, respectively). A significant positive correlation was also observed between the WBC concentration and PDGF-AA (Spearman’s R value 0.51). The RBC concentration was also significantly positively correlated

Table 2. Concentration of growth factors in PRP obtained using different systems

System	Growth factor			
	TGF-β1 [pg/mL]	EGF [pg/mL]	VEGF [pg/mL]	PDGF-AA [pg/mL]
Arthrex ACP	58.12 ± 76.92	107.37 ± 95.12	138.88 ± 189.52	33172.5 ± 13266.38
Mini GPS III System	31.72 ± 17.26	364.1 ± 180.16	456.06 ± 301.51	98698 ± 23843.58
Xerthra PRP kit	45.97 ± 59.60	161.20 ± 125.34	288.61 ± 364.54	54565.43 ± 43241.12
Dr. PRP	30.18 ± 25	223.48 ± 173.63	187.58 ± 134.90	41400.6 ± 18537.8

TGF-β1 – transforming growth factor-β1; EGF – epidermal growth factor; VEGF – vascular endothelial growth factor; PDGF-AA – platelet-derived growth factor-AA.

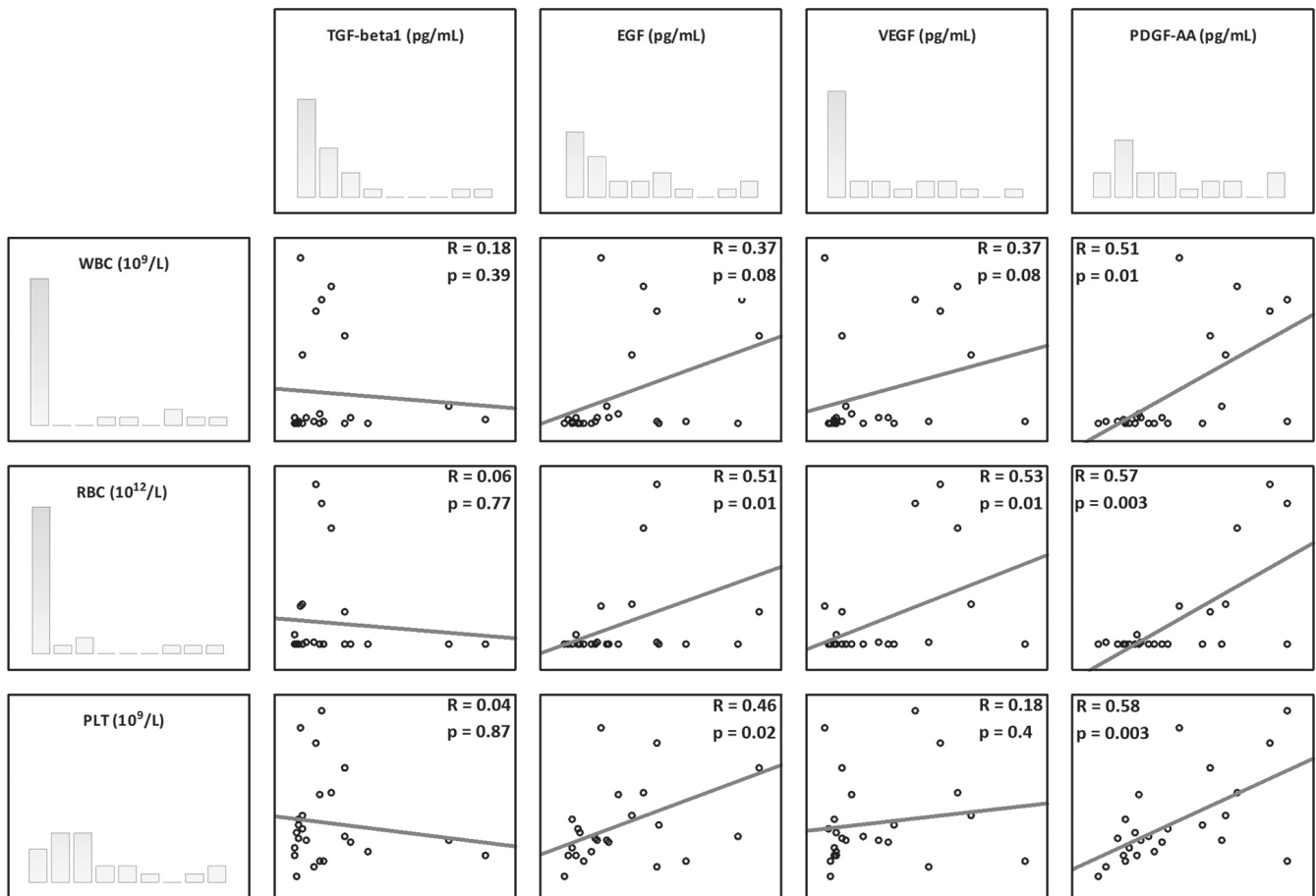


Fig. 5. Spearman correlations between morphotic components and growth factors in PRP samples

with the levels of EGF, VEGF and PDGF-AA (Spearman's R values 0.51, 0.53 and 0.57, respectively). No significant correlation was found between TGF- β 1 and any PRP morphotic component.

Discussion

As expected, the current study showed differences between PRP produced with the use of various commercial kits. These findings confirm the results of other studies that have been summarized in a recent systemic review.¹⁹ However, it is important to point out that these differences do not determine the possible clinical superiority of any of the described systems.

All kits used in the current study produced PRP with an average platelet concentration above the whole blood baseline level. For unexplained reasons, 1 PRP sample obtained using the Xerthra PRP system had a platelet concentration below the baseline level. The Mini GPS III System produced the highest platelet concentration in relation to the whole blood baseline level ($\times 4.84 \pm 0.6$), while the lowest concentration was generated with the Arthrex ACP system ($\times 1.51 \pm 0.09$). These 2 systems are among the most studied and others have reported similar results

for platelet concentrations.^{17,19,23,24} The Xerthra PRP kit and Dr. PRP were able to concentrate platelets in similar manner ($\times 2.11 \pm 1.18$ and $\times 2.02 \pm 0.53$, respectively).

Both too low and too high a platelet concentration can reduce the chances of a good therapeutic response. Platelet levels below the baseline are not sufficient to induce a significant response and a concentration above $\times 6$ may slow down the repair processes.²¹ Graziani et al. concluded that platelet concentrations of approx. 2.5 times greater than native blood achieved a maximum effect on osteoblast and fibroblast proliferation in vitro. In addition, higher dosages 3.5 times above baseline could lead to some adverse events.²⁵ Various studies have also reported different ideal therapeutic platelet concentrations. While some authors recommend a platelet concentration of about $1000 \times 10^3/mL$, others consider a number $>200 \times 10^3/mL$ as sufficient.^{26,27} According to this latter definition of PRP, all samples included in this study met the criteria.²⁸

In the current study, there were significant correlations observed between platelet concentration and both EGF and PDGF-AA, but no correlations with VEGF and TGF- β 1. These results are somewhat different from what has been reported previously. For example, Magalon observed significant correlations between platelet dose and all growth factors examined (VEGF, EGF, PDGF-AB, and

TGF- β 1).¹⁷ Similarly, Sundman also reported positive significant correlations between platelets and both TGF- β 1 and PDGF-AB.²⁹

Significantly higher concentrations of WBC were delivered by the Mini GPS III system as it is designed for LR-PRP production. The mean concentration of WBC produced by this system was 5.55 ± 1.65 times above the baseline in whole blood. The mean content of neutrophils and leukocytes were distributed almost equally ($15.72 \pm 8.11 \times 10^9/L$ and $15.99 \pm 2.96 \times 10^9/L$, respectively). Similar results have been observed in previous studies.^{17–19,23,24,29} Arthrex ACP, Xerthra PRP kit and Dr. PRP delivered LP-PRP with a WBC concentration much lower than the baseline level. According to the literature, the presence of leukocytes in PRP could affect the levels of important growth factors such as VEGF and EGF, and may also have antibacterial or immune-regulating effects.^{17,18,30} While we did not observe a correlation between WBC and both VEGF and EGF, a positive correlation with PDGF-AA was found. This finding has not been reported in previous research, likely because PDGF-AA is not a frequently analyzed cytokine. In vitro studies have shown a potential negative effect on the healing of tendon structures due to the high content of proteinases and hydrolases in WBC, especially in neutrophils.^{29,31–33} In vivo studies do not confirm this effect; however, when planning the therapy for enthesopathies, one should take into consideration the possible stimulation of catabolic processes by a high content of leukocytes.^{15,21}

An efficient PRP preparation procedure should remove RBC as much as possible, as their presence is considered as the sign of impurity. This is likely the reason why the most studies do not analyze the correlation between RBC and growth factors. Our results showed a significant correlation between RBC concentration and levels of growth factors such as EGF, VEGF and PDGF-AA. The strength of correlation was moderate (Spearman's R value between 0.51 and 0.57) but still worthy of further analysis in a larger population. Among the tested PRP preparation kits, the Mini GPS III System produced a significantly higher RBC contamination compared to other systems. This may be one of the factors behind the higher growth factor content in PRP obtained by the Mini GPS III System in other studies.^{17,19} Arthrex ACP, Xerthra PRP kit and Dr. PRP delivered PRP with an almost undetectable RBC concentration.

Limitations

To date, numerous studies have already shown the diversity in the morphotic components and growth factor content in PRP obtained various using methods. However, systems such as the Xerthra PRP kit and Dr. PRP were tested here for the first time. There are many more commercially available systems for PRP preparation than those included in the study. Even if we chose the most popular systems, it does not allow the results to be transferred to other systems, and they have to be evaluated separately.

As this is a preliminary study, we decided to examine only a few selected growth factors. Many other cytokines, chemokines and growth factors released by platelets are also involved in tissue healing. The task for future research is to study all of the cytokines that play a key role in regenerative processes. On the other hand, even a precise determination of the cytokine content does not allow one to predict clinical effects in vivo. Therefore, it will be necessary to evaluate how differences in PRP characteristics affect living tissues.


Due to the lack of confirmation to a normal distribution for most of the data, nonparametric methods were used for statistical analyses. This lack of confirmation was likely due to the small sample size used, and extension to a larger group of participants may provide more reliable results.


Conclusions


The current study showed a wide heterogeneity in the characteristics of autologous PRPs produced by various commercial kits. Based on the obtained results and previous studies, the correlation between the concentration of desired growth factors and morphotic components remains unclear. Due to insufficient data, we cannot argue for or against use of any of the mentioned protocols for the treatment of enthesopathy. Further studies on a larger population that examine a wider variety of cytokines are required to validate our results. Future research should also focus on both the in vitro and in vivo biological effects of PRP produced by different preparation protocols to establish the effects of different concentrations of the various growth factors on tissue healing.

ORCID iDs


Maciej Dejneki  <https://orcid.org/0000-0002-6675-0256>


Helena Moreira  <https://orcid.org/0000-0002-8084-3686>

Sylwia Płaczowska  <https://orcid.org/0000-0002-1466-3820>

Piotr Morasiewicz  <https://orcid.org/0000-0002-7587-666X>

Ewa Barg  <https://orcid.org/0000-0002-7069-5026>

Jarosław Witkowski  <https://orcid.org/0000-0002-2754-1339>

Paweł Reichert  <https://orcid.org/0000-0002-0271-4950>

References

1. Fitzpatrick J, Bulsara M, Zheng MH. The effectiveness of platelet-rich plasma in the treatment of tendinopathy. *Am J Sports Med.* 2017;45(1):226–233. doi:10.1177/0363546516643716
2. Mi B, Liu G, Zhou W, et al. Platelet rich plasma versus steroid on lateral epicondylitis: Meta-analysis of randomized clinical trials. *Phys Sportsmed.* 2017;45(2):97–104. doi:10.1080/00913847.2017.1297670
3. Królikowska A, Sikorski Ł, Czamara A, Reichert P. Are the knee extensor and flexor muscles isokinetic parameters affected by the duration of postoperative physiotherapy supervision in patients eight months after ACL reconstruction with the use of semitendinosus and gracilis tendons autograft? *Acta Bioeng Biomech.* 2018;20(4):89–100. doi:10.5277/ABB-01149-2018-02
4. Sánchez-González DJ, Méndez-Bolina E, Trejo-Bahena NI. Platelet-rich plasma peptides: Key for regeneration. *Int J Pept.* 2012;2012:532519. doi:10.1155/2012/532519.
5. Creaney L, Hamilton B. Growth factor delivery methods in the management of sports injuries: the state of play. *Br J Sports Med.* 2008;42(5):314–320. doi:10.1136/bjism.2007.040071

6. Werner S, Grose R. Regulation of wound healing by growth factors and cytokines. *Physiol Rev.* 2003;83(3):835–870. doi:10.1152/physrev.2003.83.3.835
7. Molloy T, Wang Y, Murrell GAC. The roles of growth factors in tendon and ligament healing. *Sport Med.* 2003;33(5):381–394. doi:10.2165/00007256-200333050-00004
8. Alsousou J, Thompson M, Hulley P, Noble A, Willett K. The biology of platelet-rich plasma and its application in trauma and orthopaedic surgery: A review of the literature. *J Bone Joint Surg Br.* 2009;91(8):987–996. doi:10.1302/0301-620X.91B8.22546
9. Tenore G, Zimbalatti A, Rocchetti F, et al. Management of medication-related osteonecrosis of the jaw (MRONJ) using leukocyte- and platelet-rich fibrin (L-PRF) and photobiomodulation: A retrospective study. *J Clin Med.* 2020;9(11):3505. doi:10.3390/jcm9113505
10. Suthar M, Gupta S, Bukhari S, Ponemone V. Treatment of chronic non-healing ulcers using autologous platelet rich plasma: A case series. *J Biomed Sci.* 2017;24(1):16. doi:10.1186/s12929-017-0324-1
11. Tietze DC, Geissler K, Borchers J. The effects of platelet-rich plasma in the treatment of large-joint osteoarthritis: A systematic review. *Phys Sportsmed.* 2014;42(2):27–37. doi:10.3810/psm.2014.05.2055
12. Moraes VY, Lenza M, Tamaoki MJ, Faloppa F, Belloti JC. Platelet-rich therapies for musculoskeletal soft tissue injuries. *Cochrane Database Syst Rev.* 2013;12:CD010071. doi:10.1002/14651858.CD010071.pub2
13. Scott A, LaPrade RF, Harmon KG, et al. Platelet-rich plasma for patellar tendinopathy: A randomized controlled trial of leukocyte-rich PRP or leukocyte-poor PRP versus saline. *Am J Sports Med.* 2019;47(7):1654–1661. doi:10.1177/0363546519837954
14. Navani A, Li G, Chrystal J. Platelet rich plasma in musculoskeletal pathology: A necessary rescue or a lost cause? *Pain Physician.* 2017;20(3):E345–E356. doi:10.36076/ppj.2017.e356
15. Wasterlain AS, Braun HJ, Dragoo JL. Contents and formulations of platelet-rich plasma. *Oper Tech Orthop.* 2012;22(1):33–42. doi:10.1053/j.oto.2011.11.001
16. Kushida S, Kakudo N, Morimoto N, et al. Platelet and growth factor concentrations in activated platelet-rich plasma: A comparison of seven commercial separation systems. *J Artif Organs.* 2014;17(2):186–192. doi:10.1007/s10047-014-0761-5
17. Magalon J, Bausset O, Serratrice N, et al. Characterization and comparison of 5 platelet-rich plasma preparations in a single-donor model. *Arthroscopy.* 2014;30(5):629–638. doi:10.1016/j.arthro.2014.02.020
18. Castillo TN, Pouliot MA, Kim HJ, Dragoo JL. Comparison of growth factor and platelet concentration from commercial platelet-rich plasma separation systems. *Am J Sports Med.* 2011;39(2):266–271. doi:10.1177/0363546510387517
19. Oudelaar BW, Peerbooms JC, Huis In 't Veld R, Vochteloo AJH. Concentrations of blood components in commercial platelet-rich plasma separation systems: A review of the literature. *Am J Sports Med.* 2019;47(2):479–487. doi:10.1177/0363546517746112
20. Dohan Ehrenfest DM, Rasmusson L, Albrektsson T. Classification of platelet concentrates: From pure platelet-rich plasma (P-PRP) to leukocyte- and platelet-rich fibrin (L-PRF). *Trends Biotechnol.* 2009;27(3):158–167. doi:10.1016/j.tibtech.2008.11.009
21. Delong JM, Russell RP, Mazzocca AD. Platelet-rich plasma: The PAW classification system. *Arthroscopy.* 2012;28(7):998–1009. doi:10.1016/j.arthro.2012.04.148
22. Zimmermann R, Arnold D, Strasser E, et al. Sample preparation technique and white cell content influence the detectable levels of growth factors in platelet concentrates. *Vox Sang.* 2003;85(4):283–289. doi:10.1111/j.0042-9007.2003.00361.x
23. Oh JH, Kim WOO, Park KU, Roh YH. Comparison of the cellular composition and cytokine-release kinetics of various platelet-rich plasma preparations. *Am J Sports Med.* 2015;43(12):3062–3070. doi:10.1177/0363546515608481
24. Mazzocca AD, McCarthy MB, Chowaniec DM, et al. Platelet-rich plasma differs according to preparation method and human variability. *J Bone Joint Surg Am.* 2012;94(4):308–316. doi:10.2106/JBJS.K.00430
25. Graziani F, Ivanovski S, Cei S, Ducci F, Tonetti M, Gabriele M. The in vitro effect of different PRP concentrations on osteoblasts and fibroblasts. *Clin Oral Implants Res.* 2006;17(2):212–219. doi:10.1111/j.1600-0501.2005.01203.x
26. Marx RE. Platelet-rich plasma (PRP): What is PRP and what is not PRP? *Implant Dent.* 2001;10(4):225–228. doi:10.1097/00008505-200110000-00002
27. Mazzucco L, Balbo V, Cattana E, Guaschino R, Borzini P. Not every PRP-gel is born equal. Evaluation of growth factor availability for tissues through four PRP-gel preparations: Fibrinet[®], RegenPRP-Kit[®], Plateltex[®] and one manual procedure. *Vox Sang.* 2009;97(2):110–118. doi:10.1111/j.1423-0410.2009.01188.x
28. Królikowska A, Reichert P, Czamara A, Krzemińska K. Peak torque angle of anterior cruciate ligament-reconstructed knee flexor muscles in patients with semitendinosus and gracilis autograft is shifted towards extension regardless of the postoperative duration of supervised physiotherapy. *PLoS One.* 2019;14(2):e0211825. doi: 10.1371/journal.pone.0211825
29. Sundman EA, Cole BJ, Fortier LA. Growth factor and catabolic cytokine concentrations are influenced by the cellular composition of platelet-rich plasma. *Am J Sports Med.* 2011;39(10):2135–2140. doi:10.1177/0363546511417792
30. Cieślak-Bielecka A, Reichert P, Skowroński R, Królikowska A, Bielecki T. A new aspect of in vitro antimicrobial leukocyte- and platelet-rich plasma activity based on flow cytometry assessment. *Platelets.* 2019;30(6):728–736. doi:10.1080/09537104.2018.1513472
31. Kobayashi Y, Saita Y, Nishio H, et al. Leukocyte concentration and composition in platelet-rich plasma (PRP) influences the growth factor and protease concentrations. *J Orthop Sci.* 2016;21(5):683–689. doi:10.1016/j.jos.2016.07.009
32. McCarrel TM, Minas T, Fortier LA. Optimization of leukocyte concentration in platelet-rich plasma for the treatment of tendinopathy. *J Bone Joint Surg Am.* 2012;94(19):e143(1). doi:10.2106/JBJS.L.00019
33. Zhang L, Chen S, Chang P, et al. Harmful effects of leukocyte-rich platelet-rich plasma on rabbit tendon stem cells in vitro. *Am J Sports Med.* 2016;44(8):1941–1951. doi:10.1177/0363546516644718

Effects of calcium electroporation, electrochemotherapy, and irreversible electroporation on quality of life and progression-free survival in patients with pancreatic cancer: IREC clinical study

Julia Rudno-Rudzińska^{1,A–E}, Wojciech Kielan^{2,A,B,F}, Maciej Guziński^{1,B}, Julita Kulbacka^{3,A,E,F}

¹ 2nd Department of General and Oncological Surgery, Wrocław Medical University, Poland

² Department of Radiology, Wrocław Medical University, Poland

³ Department of Molecular and Cellular Biology, Wrocław Medical University, Poland

A – research concept and design; B – collection and/or assembly of data; C – data analysis and interpretation; D – writing the article; E – critical revision of the article; F – final approval of the article

Advances in Clinical and Experimental Medicine, ISSN 1899–5276 (print), ISSN 2451–2680 (online)

Adv Clin Exp Med. 2021;30(7):765–770

Address for correspondence

Julia Rudno-Rudzińska

E-mail: julia.rudno-rudzinska@umed.wroc.pl

Funding sources

This study was supported by the Medical Research Agency, Poland, Study No. 2020/ABM/01/00098/P/02 (PI: Prof. Wojciech Kielan).

Conflict of interest

None declared

Received on July 1, 2021

Accepted on July 5, 2021

Published online on July 27, 2021

Cite as

Rudno-Rudzińska J, Kielan W, Guziński M, Kulbacka J. Effects of calcium electroporation, electrochemotherapy, and irreversible electroporation on quality of life and progression-free survival in patients with pancreatic cancer: IREC clinical study. *Adv Clin Exp Med.* 2021;30(7):765–770. doi:10.17219/acem/139917

DOI

10.17219/acem/139917

Copyright

© 2021 by Wrocław Medical University

This is an article distributed under the terms of the Creative Commons Attribution 3.0 Unported (CC BY 3.0) (<https://creativecommons.org/licenses/by/3.0/>)

Abstract

Background. According to the National Cancer Registry, 3486 people (1744 men and 1742 women) were diagnosed with pancreatic adenocarcinoma in Poland in 2018, resulting in 4908 deaths (2396 men and 2512 women). The only chance of successful treatment is through surgical resection, which is possible in only 20–30% of patients (stage I, II and some stage III cases). The remaining 70–80% of patients are those with stage III and IV disease, for whom resection is not possible. Mean survival in these patients is approx. 10.4 months (stage III). In the recent decade, an innovative method called electroporation, which involves destabilization of the cell membrane, has been established. This process can be reversible (RE) or irreversible (IRE), and leads to cell death. The ability to change membrane permeability has led to the development of novel methods involving electrochemotherapy (ECT) and calcium electroporation (CaEP) to treat solid tumors.

Objectives. In this study, both ECT and CaEP will be used to treat pancreatic cancer patients with poor prognosis. For each patient, the best “therapeutic moment” for the procedure will be selected based on the therapeutic protocol.

Materials and methods. Patients will receive reversible and irreversible electroporation (control arm-group A), CaEP (active arm-group B), or ECT with intravenous and intratumoral administration of bleomycin (active arm-group C) randomized 1:1:1.

Results. The primary endpoints will be progression-free survival (PFS) and patients’ quality of life (QOL) assessed using the EORTC-PAN 26 scale. Secondary endpoints will be patient overall survival (OS), body weight, pain level, and levels of biomarkers such as Ca 19-9.

Conclusions. The Irreversible Electroporation, Electrochemotherapy and Calcium electroporation (IREC) study is necessary to examine the safety and efficiency of irreversible electroporation, electrochemotherapy and calcium electroporation in pancreatic cancer treatment.

Key words: pancreatic cancer, electroporation, electrochemotherapy, calcium electroporation

Introduction

Pancreatic cancer is a global problem with increasing incidence, high mortality-to-incidence ratio, lack of screening tools, and few effective forms of treatment.^{1–3} The five-year survival rate does not exceed than 7–8% and most patients are diagnosed at stage III or above, which means the tumor cannot be resected.¹ As a result, this diagnosis is practically a death sentence for the patient. Contemporary treatment regimens for patients with stage III or IV pancreatic cancer are based on systemic treatment with the FOLFIRINOX regimen or regimens based on nab-paclitaxel and gemcitabine.^{4–7} These regimens have been shown to be more effective than the previous regimens in terms of overall survival (OS) by several weeks, and on this basis they are considered superior and registered for clinical use.

Due to the anatomical location of the pancreas, the use of conventional local ablative therapy has not proven effective due to the thermal effect and the possibility of damaging large vessels and bile ducts. One method that has begun to be used in pancreatic cancer treatment is electroporation.^{8,9} This involves the placement of electrodes and the administration of short electrical pulses (up to 100 μ s) with electric field strengths in the range of 1500–3000 V/cm. The cell membrane is either reversibly rearranged, which potentially increases its permeability to drugs, including chemotherapeutics (reversible electroporation – RE), or cell death occurs due to apoptosis (irreversible electroporation – IRE).^{10–13} This method has started to be used in pancreatic,¹⁴ liver¹⁵ and prostate cancer treatments.¹⁶ The IRE has been shown to be effective in palliative treatment of pancreatic cancer.¹⁷ Notably, it has proved so effective that it has found its way into the British National Institute for Health and Clinical Excellence (NICE) standards for the treatment of melanoma and head and neck cancers. A protocol for its use, in combination with chemotherapy (CTH), is also described in the European Standard Operating Procedures of Electrochemotherapy (ESCOPE) for the treatment of cutaneous and subcutaneous lesions.¹⁸

In investigations of electroporation, this method has begun to be combined with chemotherapeutics. The efficacy of this method has been demonstrated both in vitro and in vivo, even reducing drug toxicity to healthy cells.^{19–25} This has led to the emergence of the new field of electrochemotherapy (ECT). The drugs used in ECT include bleomycin and cisplatin, which can be administered intravenously or intratumorally.²⁶ It has been calculated that the cytotoxicity of chemotherapeutics to tumor cells increases 700–1000 times when used with IRE, along with a reduction in toxicity to the patient.^{27–33}

Calcium ion electroporation (CaEP) is another recent advance in the treatment of solid tumors. Calcium is internalized into tumor cells in excessive amounts due to regulatory mechanisms being disrupted by electroporation, resulting in cell necrosis through an adenosine triphosphate (ATP)

deficit, which fails to be replenished.^{34–40} It has also been demonstrated that ECT induces an immune response.³² Treatment with CaEP and ECT stimulate the immune system to such an extent that it induces an “abscopal effect”, i.e., remission of distant lesions not treated with ECT or IRE.^{22,27–32} Moreover, ECT “breaks” chemo-resistance in solid tumors by using a vascular effect and “trapping” the chemotherapeutic agent in the region of the tumor.^{25,33} This concept has been shown to be efficacious and is used as a standard treatment of skin and subcutaneous cancers. In addition, there is currently a study underway to apply this method to colorectal cancers. In the course of our research, we have applied this method to patients with pancreatic cancer, which was published as the first application of its kind in the world.⁴¹

Bleomycin was selected as the most active chemotherapeutic agent. Originally, bleomycin in ECT was used for treatment of head and neck cancer, melanoma, basal cell carcinoma (BCC) skin lesions, squamous cell carcinoma (SCC), and breast cancer. It has since become the standard of care for skin diseases with bleomycin as the recommended chemotherapeutic agent.^{42–46} Other chemotherapeutic agents that have been tested for efficacy in vitro include daunorubicin, doxorubicin, etoposide, paclitaxel, gemcitabine, 5-fluorouracil, carboplatin, and cisplatin. While daunorubicin, etoposide, and paclitaxel were reported to be ineffective in vitro, cisplatin and bleomycin were found to be the most effective.^{31,47} Bleomycin was also found to be the most effective drug in ECT for pancreatic cancer in vitro while also increasing the immune response of the body.^{38,48,49} Furthermore, in an animal model, ECT with bleomycin was shown to be effective in the treatment of pancreatic cancer.^{21,50} The results of studies involving patients with stage III pancreatic cancer are encouraging; however, the number of procedures performed is small,⁵¹ and the results are similar to studies on the efficacy of ECT for metastatic liver lesions.^{42,52,53}

The ECT and CaEP are evolving therapies for which there are few studies involving only a small number of recruited patients. However, these treatments enable personalized medicine, are feasible for older patients, and offer hope of treatment to patients whose prognosis is already poor upon diagnosis. Since 2018, a project entitled “Electrochemotherapy of solid tumors of the gastrointestinal tract: research on the application of electrochemotherapy in pancreatic cancer with unresectable or oligometastatic lesions” has been conducted at the Wrocław Medical University, Poland, after receiving approval from the Bioethics Committee (approval No. KB-330/2018).

IREC project assumptions

The project entitled “Effects of calcium electroporation, electrochemotherapy and irreversible electroporation

(CaEP, ECT and IRE) on quality of life and progression-free survival in patients with pancreatic cancer” aims to answer questions about the efficacy of electroporation (group A) compared with CaEP (group B) and ECT with bleomycin (group C) in patients with unresectable pancreatic cancer. The safety of these 3 treatments will be compared, as well as their efficacy measured as progression-free survival (PFS) and OS. Another important factor being investigated is patients’ quality of life (QOL) after surgery, which will be assessed using the EORTC-PAN 26 scale.

If a patient is qualified for the treatment, their data will be entered into the Case Report Form (CRF) system and the procedures will be performed at the 2nd Department of General Surgery and Surgical Oncology of Wrocław Medical University or at a partner center possessing the required equipment and levels of staff experience on a referral basis. Data on the treatment and hospital stay will be entered into the system. Data will include information regarding both the procedure and hospital stay. The inclusion and exclusion criteria are listed in Table 1. Patients will receive follow-up at the center where the procedure was performed for consultation and imaging examination at 1 month, 3 months and 6 months after treatment, and then every 6 months thereafter. Examinations are permitted as part of the drug program, as well as measurement of hemoglobin (Hb) [g/dL], Ca 19-9 [U/mL], protein levels [g/L], and albumin [mg/mL]. Patients will be assessed as part of a clinical trial, with examinations ending upon patient death or the end of the project.

In order to jointly implement the planned project, collaboration has been established with Dr. Julie Gehl (Department of Clinical Oncology and Palliative Care, Zealand University Hospital, Roskilde, Denmark), who is a pioneer and specialist in CaEP. Doctor Gehl will contribute human and organizational resources to the project under the conditions specified in the agreement or partnership contract.

Study eligibility and IREC inclusion and exclusion criteria

The study group (Table 1) includes non-pregnant patients over the age of 18 years with unresectable pancreatic cancer (stage III), which represents the largest population

at the time of diagnosis, as well as patients who have undergone resection but have had local recurrence. Histo-pathological confirmation of the malignancy is required, although intraoperative examination is permissible. A lesion infiltrating the superior mesenteric vein exceeding 180% of the circumference of the celiac artery, superior mesenteric artery, hepatic artery, or aorta is considered unresectable. Furthermore, patients require computed tomography (CT) scans not more than 30 days prior to joining the study. Patients with cardiac arrhythmias or pacemakers/defibrillators are disqualified due to potential device failure and synchrony of the NanoKnife device with the P wave of the electrocardiogram (ECG). Patients allergic to bleomycin or with pulmonary fibrosis are also excluded due to bleomycin administration in group C.

Patients with stage IV disease will not be eligible for the program due to the previous experience of the center and latent frailty syndrome.

Project implementation

After providing informed consent to participate in this study, patients will be randomized to 3 groups:

- group A: patients undergoing IRE;
- group B: patients undergoing CaEP. After electroporation, patients will be administered an appropriate dose of intratumoral calcium ions (CaCl₂) calculated with relation to tumor volume; or
- group C: patients undergoing electrochemotherapy with intravenous and intratumoral administration of bleomycin at a dose of 15,000 IU/m² as a bolus over 30–60 s, approx. 8–28 min before the electroporation procedure, and simultaneously intratumorally at 1000 IU/mL at a dose of 1000 UI/cm² in lesions less than 1 cm and 250 UI/cm² in lesions larger than 1 cm³.

All procedures will be performed under general anesthesia and following the administration of muscle relaxants to negate potential muscle spasm when the pulse is administered. A single dose of intravenous antibiotics will also be given perioperatively. The procedure will be carried out using the conventional percutaneous method. Due to complaints of postoperative pain, patients will be administered additional epidural anesthesia during the procedure, which

Table 1. Inclusion and exclusion criteria for the IREC project

Inclusion criteria	Exclusion criteria
<ul style="list-style-type: none"> • age over 18 years • histopathologically confirmed adenocarcinoma of the pancreas (intraoperative examination possible) • WHO performance status (ECOG) 0, 1 or 2 • written informed consent • lesion defined as unresectable (infiltration of mesenteric vein or portal vein exceeding 180 degrees or its thrombosis, infiltration of the hepatic artery, celiac artery or superior mesenteric artery) on abdominal CT not older than 30 days (stage III), or patients after resection with local recurrence of the neoplastic process • tumor size not larger than 6 cm on a CT scan not older than 30 days • patients undergoing chemotherapy or patients with a “de novo” diagnosis of pancreatic cancer 	<ul style="list-style-type: none"> • pregnant women • patients with pacemakers • patients with rhythms other than sinus rhythm on ECG • patients allergic to bleomycin • patients with pulmonary fibrosis

WHO – World Health Organization; ECOG – Eastern Cooperative Oncology Group; CT – computed tomography.

will be maintained for 72 h. In the case of patients with gastrointestinal obstruction or hyperbilirubinemia, palliative procedures (by-pass) will be performed at the same time.

During the hospital stay, patients will be monitored daily for any deterioration in condition by analyzing morphology and Ca19-9, amylase and lipase levels. Patients will be treated with analgesics, anticoagulants and fluid therapy according to the recognized standards and individual patient's needs. Discharge will take place when their clinical condition stabilizes. Following hospital discharge, all patients will be referred to a clinical oncologist for systemic treatment in accordance with the guidelines.

Patient monitoring

Patients will be assessed as part of the clinical trial for 12 months. Each follow-up examination will consist of:

- physical examination (body weight, body mass index – BMI);
- health assessment according to World Health Organization (WHO);
- pain assessment according to visual analogue scale (VAS);
- QOL according to European Organization for Research and Treatment of Cancer (EORTC) QLQ-PAN 26 scale;
- Hb level;
- total protein level;
- serum albumin level;
- Ca19-9 marker level.

Imaging examinations utilizing abdominal CT or magnetic resonance imaging (MRI) will be performed at 1 month, 3 months, 6 months, and 1 year following treatment. Patient assessment schedule is presented in Table 2. As the majority of systemically treated patients in the drug programs already have imaging examinations scheduled, these can be used as follow-up examinations. If they are not scheduled, imaging will be prescribed by the examiner.

Analysis of the obtained results and conclusions of the IREC study

The results obtained in this non-commercial clinical trial will be compared with the results of patients who did not receive electroporation for the treatment of pancreatic cancer. Retrospective analyses will be allowed for comparison, but only for the group treated with the same chemotherapeutic regimens used as part of the current standard of care, namely, FOLFIRINOX, gemcitabine and nab-paclitaxel regimens. The PFS and QOL will be compared. One interesting result will be the OS of both groups. At present, the mean OS for stage III pancreatic cancer patients is 8–10 months from the time of diagnosis. Treatment with electroporation, CaEP or ECT has been performed in the 2nd Department of General Surgery and Surgical Oncology at Wrocław Medical University in 15 patients at various stages, achieving a mean survival of 26 months from diagnosis; notably, 7 of these patients are still alive.

Three of the primary outcomes are: 1) assessment of improvements in QOL using the EORTC QOL-PAN26 scale; 2) reduction of pain on the VAS; and 3) increases in body weight and protein and albumin levels as indications of patient well-being. Quality of life will be compared between patients who have undergone ablation and those who have not.

A number of secondary studies will be included as part of this project, including the determination of the Ca19-9 marker for predicting the best “therapeutic moment” and the efficacy of electroporation, CaEP and ECT. Groups A, B and C will be compared to each other in terms of safety of use and routes of administration of bleomycin and Ca²⁺ ions. The comparison will include administration safety and dose. Secondary studies will also include any relevant postoperative complications measured on the Clavien–Dindo scale and the length of hospitalization.

On the basis of data concerning malignant progression (stage, tumor size and tumor location) and co-morbidities

Table 2. Patient assessment chart for the IREC project

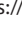
Parameter	1 month	3 months	6 months	12 months
Clinical examination	X	X	X	X
BMI	X	X	X	X
Body weight [kg]	X	X	X	X
Health according to WHO	X	X	X	X
Pain according to VAS	X	X	X	X
EORTC QLQ-PAN 26	X	X	X	X
Hb level [mg/dL]	X	X	X	X
Protein level [g/dL]	X	X	X	X
Albumin level [g/dL]	X	X	X	X
Ca 19-9 market level [U/mL]	X	X	X	X
CT/MRI	X	X	X	X

BMI – body mass index; WHO – World Health Organization; VAS – visual analogue scale; CT – computed tomography; MRI – magnetic resonance imaging; EORTC – European Organization for Research and Treatment of Cancer.

using the Charlson Comorbidity Index, we will select a group of patients from those we believe will benefit most from the treatments. Patients will be individually analyzed in terms of the best “therapeutic moment” which, in the future, may be important in relation to new standards of management and the inclusion of this method as part of the treatment regimen for pancreatic cancer.

The effectiveness of the method will be assessed using abdominal MR and/or abdominal CT. The control methods will be compared and the most effective will be selected. The characteristic changes after IRE and their predictive value for OS and PFS will also be assessed. Overall, this study will evaluate the effectiveness and safety of IRE, CaEP and ECT with bleomycin in the treatment of non-resectable pancreatic cancer. It will also address the question of which of these methods is the safest and most effective, and at which point during treatment a patient should be qualified for this procedure. The IREC project may contribute to the inclusion of a new therapeutic method in the treatment regimen for pancreatic cancer.

ORCID iDs

Julia Rudno-Rudzińska  <https://orcid.org/0000-0002-4619-7510>
 Wojciech Kielan  <https://orcid.org/0000-0001-6116-6504>
 Maciej Guziński  <https://orcid.org/0000-0002-9781-2114>
 Julita Kulbacka  <https://orcid.org/0000-0001-8272-5440>

References

- Siegel RL, Miller KD, Jemal A. Cancer statistics, 2018. *CA Cancer J Clin*. 2018;68(1):7–30. doi:10.3322/caac.21442
- Rahib L, Smith BD, Aizenberg R, Rosenzweig AB, Fleshman JM, Matrisian LM. Projecting cancer incidence and deaths to 2030: The unexpected burden of thyroid, liver, and pancreas cancers in the United States. *Cancer Res*. 2014;74(11):2913–2921. doi:10.1158/0008-5472.CAN-14-0155
- Quante AS, Ming C, Rottmann M, et al. Projections of cancer incidence and cancer-related deaths in Germany by 2020 and 2030. *Cancer Med*. 2016;5(9):2649–2656. doi:10.1002/cam4.767
- Klaiber U, Leonhardt CS, Strobel O, Tjaden C, Hackert T, Neoptolemos JP. Neoadjuvant and adjuvant chemotherapy in pancreatic cancer. *Langenbecks Arch Surg*. 2018;403(8):917–932. doi:10.1007/s00423-018-1724-8
- Raufi AG, Manji GA, Chabot JA, Bates SE. Neoadjuvant treatment for pancreatic cancer. *Semin Oncol*. 2019;46(1):19–27. doi:10.1053/j.seminoncol.2018.12.002
- Murphy JE, Wo JY, Ryan DP, et al. Total neoadjuvant therapy with FOLFIRINOX in combination with losartan followed by chemoradiotherapy for locally advanced pancreatic cancer: A phase 2 clinical trial. *JAMA Oncol*. 2019;5(7):1020–1027. doi:10.1001/jamaoncol.2019.0892
- Venkatesulu BP, Hsieh CE, Sanders KL, Krishnan S. Recent advances in radiation therapy of pancreatic cancer. *F1000Res*. 2018;7:F1000 Faculty Rev-1931. doi:10.12688/f1000research.16272.1
- Daniels C, Rubinsky B. Electrical field and temperature model of non-thermal irreversible electroporation in heterogeneous tissues. *J Biomech Eng*. 2009;131(7):071006. doi:10.1115/1.3156808
- Lee EW, Chen C, Prieto VE, Dry SM, Loh CT, Kee ST. Advanced hepatic ablation technique for creating complete cell death: Irreversible electroporation. *Radiology*. 2010;255(2):426–433. doi:10.1148/radiol.10090337
- Lee EW, Thai S, Kee ST. Irreversible electroporation: A novel image-guided cancer therapy. *Gut Liver*. 2010;4(Suppl 1):S99–S104. doi:10.5009/gnl.2010.4.S1.S99
- Maor E, Rubinsky B. Endovascular nonthermal irreversible electroporation: A finite element analysis. *J Biomech Eng*. 2010;132(3):031008. doi:10.1115/1.4001035
- Thompson CB. Apoptosis in the pathogenesis and treatment of disease. *Science*. 1995;267(5203):1456–1462. doi:10.1126/science.7878464
- Susin SA, Lorenzo HK, Zamzami N, et al. Molecular characterization of mitochondrial apoptosis-inducing factor. *Nature*. 1999;397(6718):441–446. doi:10.1038/17135
- Lambert L, Horejs J, Krska Z, et al. Treatment of locally advanced pancreatic cancer by percutaneous and intraoperative irreversible electroporation: General hospital cancer center experience. *Neoplasma*. 2016;63(2):269–273. doi:10.4149/213_150611N326
- Thomson KR, Cheung W, Ellis SJ, et al. Investigation of the safety of irreversible electroporation in humans. *J Vasc Interv Radiol*. 2011;22(5):611–621. doi:10.1016/j.jvir.2010.12.014
- Onik G, Mikus P, Rubinsky B. Irreversible electroporation: Implications for prostate ablation. *Technol Cancer Res Treat*. 2007;6(4):295–300. doi:10.1177/153303460700600405
- Martin RCG, McFarland K, Ellis S, Velanovich V. Irreversible electroporation in locally advanced pancreatic cancer: Potential improved overall survival. *Ann Surg Oncol*. 2013;20(3 Suppl):S443–S449. doi:10.1245/s10434-012-2736-1
- Campana LG, Edhemovic I, Soden D, et al. Electrochemotherapy: Emerging applications technical advances, new indications, combined approaches, and multi-institutional collaboration. *Eur J Surg Oncol*. 2019;45(2):92–102. doi:10.1016/j.ejso.2018.11.023
- Gehl J. Electroporation: Theory and methods, perspectives for drug delivery, gene therapy and research. *Acta Physiol Scand*. 2003;177(4):437–447. doi:10.1046/j.1365-201X.2003.01093.x
- Mir LM, Orłowski S, Belehradek J, Paoletti C. Electrochemotherapy potentiation of antitumor effect of bleomycin by local electric pulses. *Eur J Cancer Clin Oncol*. 1991;27(1):68–72. doi:10.1016/0277-5379(91)90064-K
- Girelli R, Prejanò S, Cataldo I, et al. Feasibility and safety of electrochemotherapy (ECT) in the pancreas: A pre-clinical investigation. *Radiol Oncol*. 2015;49(2):147–154. doi:10.1515/raon-2015-0013
- Falk H, Lambaa S, Johannesen HH, Wooler G, Venzo A, Gehl J. Electrochemotherapy and calcium electroporation inducing a systemic immune response with local and distant remission of tumors in a patient with malignant melanoma: A case report. *Acta Oncol*. 2017;56(8):1126–1131. doi:10.1080/0284186X.2017.1290274
- Zhang Z, Li W, Procissi D, Tyler P, Omary RA, Larson AC. Rapid dramatic alterations to the tumor microstructure in pancreatic cancer following irreversible electroporation ablation. *Nanomedicine*. 2014;9(8):1181–1192. doi:10.2217/nnm.13.72
- Serša G, Jarm T, Kotnik T, et al. Vascular disrupting action of electroporation and electrochemotherapy with bleomycin in murine sarcoma. *Br J Cancer*. 2008;98(2):388–398. doi:10.1038/sj.bjc.6604168
- Serša G, Beravs K, Čemažar M, Miklavčič D, Demsar F. Contrast enhanced MRI assessment of tumor blood volume after application of electric pulses. *Electromagn Biol Med*. 1998;17(2):299–306. doi:10.3109/15368379809022574
- Serša G, Cemazar M, Miklavčič D, Chaplin DJ. Tumor blood flow modifying effect of electrochemotherapy with bleomycin. *Anticancer Res*. 1999;19(5B):4017–4022. PMID:10628347
- Postow MA, Callahan MK, Barker CA, et al. Immunologic correlates of the abscopal effect in a patient with melanoma. *N Engl J Med*. 2012;366(10):925–931. doi:10.1056/NEJMoa112824
- Caracò C, Mozzillo N, Marone U, et al. Long-lasting response to electrochemotherapy in melanoma patients with cutaneous metastasis. *BMC Cancer*. 2013;13:564. doi:10.1186/1471-2407-13-564
- Kunte C, Letulé V, Gehl J, et al. Electrochemotherapy in the treatment of metastatic malignant melanoma: A prospective cohort study by InspECT. *Br J Dermatol*. 2017;176(6):1475–1485. doi:10.1111/bjd.15340
- Mir LM, Orłowski S, Poddevin B, Belehradek JJ. Electrochemotherapy tumor treatment is improved by interleukin-2 stimulation of the host's defenses. *Eur Cytokine Netw*. 1992;3(3):331–334. PMID:1379837
- Serša G, Čemažar M, Menart V, Gaberc-Porekar V, Miklavčič D. Anti-tumor effectiveness of electrochemotherapy with bleomycin is increased by TNF- α on SA-1 tumors in mice. *Cancer Lett*. 1997;116(1):85–92. doi:10.1016/S0304-3835(97)00170-5
- Gerlini G, Di Gennaro P, Borgognoni L. Enhancing anti-melanoma immunity by electrochemotherapy and in vivo dendritic-cell activation. *Oncoimmunology*. 2012;1(9):1655–1657. doi:10.4161/onci.21991

33. Kos B, Voigt P, Miklavcic D, Moche M. Careful treatment planning enables safe ablation of liver tumors adjacent to major blood vessels by percutaneous irreversible electroporation (IRE). *Radiol Oncol*. 2015;49(3):234–241. doi:10.1515/raon-2015-0031
34. Carafoli E, Santella L, Branca D, Brini M. Generation, control, and processing of cellular calcium signals. *Crit Rev Biochem Mol Biol*. 2001;36(2):107–260. doi:10.1080/20014091074183
35. Berridge MJ, Bootman MD, Roderick HL. Calcium signaling: Dynamics, homeostasis and remodelling. *Nat Rev Mol Cell Biol*. 2003;4(7):517–529. doi:10.1038/nrm1155
36. Frandsen SK, Gissel H, Hojman P, Tramm T, Eriksen J, Gehl J. Direct therapeutic applications of calcium electroporation to effectively induce tumor necrosis. *Cancer Res*. 2012;72(6):1336–1341. doi:10.1158/0008-5472.CAN-11-3782
37. Frandsen SK, Gehl J. Effect of calcium electroporation in combination with metformin in vivo and correlation between viability and intracellular ATP level after calcium electroporation in vitro. *PLoS One*. 2017;12(7):e0181839. doi:10.1371/journal.pone.0181839
38. Hansen EL, Sozer EB, Romeo S, Frandsen SK, Vernier PT, Gehl J. Dose-dependent ATP depletion and cancer cell death following calcium electroporation, relative effect of calcium concentration and electric field strength. *PLoS One*. 2015;10(4):e0122973. doi:10.1371/journal.pone.0122973
39. Calvet CY, Famin D, André FM, Mir LM. Electrochemotherapy with bleomycin induces hallmarks of immunogenic cell death in murine colon cancer cells. *Oncoimmunology*. 2014;3:e28131. doi:10.4161/onci.28131
40. Plaschke CC, Gehl J, Johannesen HH, et al. Calcium electroporation for recurrent head and neck cancer: A clinical phase I study. *Laryngoscope Invest Otolaryngol*. 2019;4(1):49–56. doi:10.1002/lio2.233
41. Rudno-Rudzińska J, Kielan W, Guziński M, Płochocki M, Kulbacka J. The first study of irreversible electroporation with calcium ions and chemotherapy in patients with locally advanced pancreatic adenocarcinoma. *Appl Sci*. 2020;10(15):5163. doi:10.3390/app10155163
42. Mir LM, Gehl J, Sersa G, et al. Standard operating procedures of the electrochemotherapy: Instructions for the use of bleomycin or cisplatin administered either systemically or locally and electric pulses delivered by the Cliniporator TM by means of invasive or non-invasive electrodes. *EJC Suppl*. 2006;4(4):14–25. doi:10.1016/j.ejcsup.2006.08.003
43. Campana LG, Mocellin S, Basso M, et al. Bleomycin-based electrochemotherapy: Clinical outcome from a single institution's experience with 52 patients. *Ann Surg Oncol*. 2009;16(1):191–199. doi:10.1245/s10434-008-0204-8
44. Gargiulo M, Papa A, Capasso P, Moio M, Cubicciotti E, Parascandolo S. Electrochemotherapy for non-melanoma head and neck cancers: Clinical outcomes in 25 patients. *Ann Surg*. 2012;255(6):1158–1164. doi:10.1097/SLA.0b013e31824f68b2
45. National Institute for Health and Care Excellence (NICE). Electrochemotherapy for primary basal cell carcinoma and primary squamous cell carcinoma. <https://www.nice.org.uk/guidance/ipg478>. Published February 26, 2014.
46. National Institute for Health and Care Excellence (NICE). Electrochemotherapy for metastases in the skin from tumours of non-skin origin and melanoma. <https://www.nice.org.uk/guidance/ipg446>. Published March 27, 2013.
47. Schmidt G, Juhasz-Böss I, Solomayer EF, Herr D. Electrochemotherapy in breast cancer: A review of references. *Geburtshilfe Frauenheilkd*. 2014;74(6):557–562. doi:10.1055/s-0034-1368538
48. Miklavčič D, Mali B, Kos B, Heller R, Serša G. Electrochemotherapy: From the drawing board into medical practice. *Biomed Eng Online*. 2014;13(1):29. doi:10.1186/1475-925X-13-29
49. Bimonte S, Leongito M, Granata V, et al. Electrochemotherapy in pancreatic adenocarcinoma treatment: Pre-clinical and clinical studies. *Radiol Oncol*. 2016;50(1):14. doi:10.1515/raon-2016-0003
50. Jaroszeski MJ, Illingworth P, Pottinger C, Hyacinthe M, Heller R. Electrically mediated drug delivery for treating subcutaneous and orthotopic pancreatic adenocarcinoma in a hamster model. *Anticancer Res*. 1999;19(2A):989–994. PMID:10368643
51. Granata V, Fusco R, Piccirillo M, et al. Electrochemotherapy in locally advanced pancreatic cancer: Preliminary results. *Int J Surg*. 2015;18:230–236. doi:10.1016/j.ijsu.2015.04.055
52. Tafuto S, von Arx C, De Divitiis C, et al. Electrochemotherapy as a new approach on pancreatic cancer and on liver metastases. *Int J Surg*. 2015;21(Suppl 1):S78–S82. doi:10.1016/j.ijsu.2015.04.095
53. Edhemovic I, Gadzijev EM, Breclj E, et al. Electrochemotherapy: A new technological approach in treatment of metastases in the liver. *Technol Cancer Res Treat*. 2011;10(5):475–485. doi:10.7785/tcrt.2012.500224